

# **Bubbles, Thin Films and Ion Specificity**

by

**Christine Louise Henry**

B.Sc.(Hons) LL.B. (Hons), ANU

*A thesis submitted for the degree of Doctor of Philosophy  
of  
The Australian National University*



January 2009



---

## Preface

---

This thesis is an account of research undertaken within the Department of Applied Mathematics, Research School of Physical Sciences and Engineering, within the Australian National University.

This thesis comprises my original work; however some aspects of the work were undertaken in collaboration with others. In Chapter 2, on bubble coalescence and surface tension in mixed electrolytes, the surface tension measurements were carried out by Lehoa Scruton and some of the bubble coalescence data were obtained by Casuarina Dalton. The work in Chapter 5 on thin films was done in the laboratories of, and in collaboration with, colleagues at the University of Queensland Professor Anh Nguyen, Dr Stoyan Karakashev and Mr Phong Nguyen. Mr Phong Nguyen assisted in experimental set-up and instrument use, and Dr Karakashev carried out the theoretical analysis. The bubble terminal rise measurements in Chapter 6 were carried out at the Ian Wark Research Institute, University of South Australia, in collaboration with Mr Luke Parkinson and Professor John Ralston. Luke Parkinson designed and built the bubble rise instrument, and assisted with its use.

This thesis contains no material which has been accepted for the award of any other degree or diploma in any university. To the best of my knowledge, it contains no material previously published or written by another person, except where due reference is made in the text.

---

Christine Henry

---

## Acknowledgements

---

First, many thanks to my supervisor, Vince Craig, for all the support, help, ideas and editing. Thanks especially for your drive and belief in the work, which kept it going forwards when I had doubts. You were right!

The Department of Applied Maths has been a great place to work, and I thank everyone who made my time here so enjoyable. Tim Sawkins and Anthony Hyde provided technical assistance and advice, and Margo Davies and Jan James kept everything running smoothly. Tim Senden was a great friend, advisor and editor, always willing to offer suggestions. Chiara Neto was an advisor, and helped me get started in research. Toen Castle, my officemate for most of the PhD, was a steady source of friendship, music, unfamiliar words and fun conversation. Many others gave social support in the tearoom and the beer garden – an incomplete list: Anna Carnerup, Drew Evans, Shaun Howard, Steve Hyde, Stu Ramsden, Vanessa Robins, and Adrian Sheppard.

Every conference I went to provided a fresh charge of scientific inspiration and energy, and some great friendships – thanks to people I talked with (and bodysurfed with) at ACSSSC '06 and '08, Cancun '06, ECIS '07, and all the Kioloa trips. Thanks also to collaborators and to everyone at the University of Melbourne, the University of Queensland and the Ian Wark Research Institute who helped out when I visited. CRC SmartPrint provided scholarship assistance throughout the PhD.

Canberra is my hometown, and the nature, geography and weather are part of my life. As I move on (literally and figuratively) I acknowledge that these years wouldn't have been the same anywhere else.

My family offered unwavering support. All the Canberra friends provided a life outside uni, especially with the increasingly luxurious coast trips. Paul Barnsley, among other things, fed me a steady supply of comics. I couldn't have got through without various other cultural and pop-cultural distractions – Salon, The Daily Show, the Colbert Report and Wired all assisted. A PhD involves much more than just science, and I've had the

freedom over the past four years to meet a lot of cool people, read a lot, learn a lot, and develop my interests in all directions. Thanks to everyone who helped.

---

## Abstract

---

Bubbles in water are stabilised against coalescence by the addition of salt. The white froth in seawater but not in freshwater is an example of salt-stabilised bubbles. A range of experiments have been carried out to investigate this simple phenomenon, which is not yet understood.

The process of thin film drainage between two colliding bubbles relates to surface science fields including hydrodynamic flow, surface forces, and interfacial rheology. Bubble coalescence inhibition also stands alongside the better known Hofmeister series as an intriguing example of ion specificity: While some electrolytes inhibit coalescence at around 0.1M, others show no effect. The coalescence inhibition of any single electrolyte depends on the combination of cation and anion present, rather than on any single ion.

The surfactant-free inhibition of bubble coalescence has been studied in several systems for the first time, including aqueous mixed electrolyte solutions; solutions of biologically relevant non-electrolytes urea and sugars; and electrolyte solutions in nonaqueous solvents methanol, formamide, propylene carbonate and dimethylsulfoxide. Complementary experimental approaches include studies of terminal rise velocities of single bubbles showing that the gas-solution interface is mobile; and measurement of thin film drainage in inhibiting and non-inhibiting electrolyte solution, using the microinterferometric thin film balance technique.

The consolidation of these experimental approaches shows that inhibiting electrolytes act on the non-equilibrium dynamic processes of thin film drainage and rupture between bubble surfaces – and not via a change in surface forces, or by ion effects on solvent structure. In addition, inhibition is driven by osmotic effects related to solute concentration gradients, and ion charge is not important.

A new model is presented for electrolyte inhibition of bubble coalescence via changes to surface rheology. It is suggested that thin film stabilisation over a lifetime of seconds,

is caused by damping of transient deformations of film surfaces on a sub-millisecond timescale. This reduction in surface deformability retards film drainage and delays film rupture. It is proposed that inhibiting electrolyte solutions show a dilational surface viscosity, which in turn is driven by interfacial concentration gradients. Inhibiting electrolytes have two ions that accumulate at the surface or two ions that are surface-excluded, while non-inhibiting electrolytes have more evenly distributed interfacial solute. Bubble coalescence is for the first time linked through this ion surface partitioning, to the ion specificity observed at biological interfaces and the wider realm of Hofmeister effects.

---

## Publications

---

Aspects of the work presented in this thesis have been, or will be, presented in the following journal articles.

1. Henry, C. L.; Dalton, C. N.; Scruton, L.; Craig, V. S. J., Ion-specific coalescence of bubbles in mixed electrolyte solutions. *J. Phys. Chem. C* **2007**, 111, 1015-1023.
2. Henry, C. L.; Craig, V. S. J., Ion-specific influence of electrolytes on bubble coalescence in nonaqueous solvents. *Langmuir* **2008**, 24, 7979-7985.
3. Henry, C. L.; Parkinson, L.; Ralston, J. R.; Craig, V. S. J., A mobile gas-water interface in electrolyte solutions. *J. Phys. Chem. C* **2008**, 112, 15094-15097.
4. Craig, V. S. J.; Henry, C. L., Specific ion effects at the air-water interface - experimental studies. In *Specific Ion Effects*, Kunz, W., Ed. World Scientific Publishing: *Submitted for publication*.
5. Henry, C. L.; Craig, V. S. J., Bubble coalescence inhibition by sugars and urea. *In Preparation*.
6. Henry, C. L.; Nguyen, P.; Karakashev, S. I.; Nguyen, A. V.; Craig, V. S. J., Electrolyte effects on lifetime, rupture and drainage kinetics of surfactant-free nonaqueous thin films. *In Preparation*.
7. Henry, C. L.; Honig, C. D. F.; Ducker, W. A.; Craig, V. S. J., Cantilever-dependent hydrodynamic forces in the AFM. *In Preparation*.
8. Henry, C. L.; Craig, V. S. J., Specific ion effects in bubble coalescence: Quantitative determination of  $\alpha$  and  $\beta$  and the link to the Hofmeister series. *In Preparation*.



Publications associated with earlier work are listed below:

9. Henry, C. L.; Neto, C.; Evans, D. R.; Biggs, S.; Craig, V. S. J., The effect of surfactant adsorption on liquid boundary slippage. *Physica A* **2004**, 339, 60-65.
10. Kourie, J. I.; Henry, C. L., Ion channel formation and membrane-linked pathologies of misfolded hydrophobic proteins: The role of dangerous unchaperoned molecules. *Clin. Exp. Pharmacol. P.* **2002**, 29, 741-753.
11. Kourie, J. I.; Culverson, A. L.; Farrelly, P. V.; Henry, C. L.; Laohachai, K.N., Heterogeneous amyloid-formed ion channels as a common cytotoxic mechanism - Implications for therapeutic strategies against amyloidosis. *Cell Biochem. Biophys.* **2002**, 36, 191-207.
12. Kourie, J.I.; Farrelly, P.V.; Henry, C. L., Channel activity of deamidated isoforms of prion protein fragment 106-126 in planar lipid bilayers. *J. Neurosci. Res.* **2001**, 66, 214-220.
13. Kourie, J.I.; Henry, C. L.; Farrelly, P.V., Diversity of amyloid beta protein fragment [1-40]-formed channels. *Cell. Mol. Neurobiol.* **2001**, 21, 255-284.
14. Kourie, J.I.; Hanna, E.A.; Henry, C. L., Properties and modulation of alpha human atrial natriuretic peptide (alpha-hANP)-formed ion channels. *Can. J. Physiol. Pharmacol.* **2001**, 79, 654-664.
15. Kourie, J.I.; Henry, C. L., Protein aggregation and deposition: implications for ion channel formation and membrane damage. *Croat. Med. J.* **2001**, 42, 359-374.

---

# Contents

---

<b>Preface</b> .....	<b>i</b>
<b>Acknowledgements</b> .....	<b>ii</b>
<b>Abstract</b> .....	<b>iv</b>
<b>Publications</b> .....	<b>vi</b>
<b>Contents</b> .....	<b>viii</b>
<b>Chapter 1 Bubble Coalescence and Electrolyte Inhibition</b> .....	<b>1</b>
1.1 Introduction.....	1
1.2 Collision, Drainage and Rupture.....	3
1.3 Bubble Coalescence in Electrolyte Solutions .....	15
1.4 Methods in Coalescence Inhibition.....	22
1.5 Hypotheses of Electrolyte Coalescence Inhibition .....	31
1.6 Summary .....	38
1.7 Thesis Outline .....	39
<b>Chapter 2 Bubble Coalescence Inhibition in Mixed Electrolytes</b> .....	<b>41</b>
2.1 Preamble.....	41
2.2 Bubble Column Apparatus.....	41
2.3 Mixed Electrolyte Experiments .....	46
2.4 Conclusions.....	64
<b>Chapter 3 Bubble Coalescence Inhibition by Sugars and Urea</b> .....	<b>66</b>
3.1 Introduction.....	66
3.2 Osmolytes and Bubble Coalescence: Sucrose, Urea and Electrolytes.....	73
3.3 Coalescence Inhibition in Sugars.....	82
<b>Chapter 4 Bubble Coalescence Inhibition by Electrolytes in Nonaqueous Solvents</b> .....	<b>95</b>
4.1 Introduction.....	95

4.2	Materials and Methods .....	97
4.3	Results .....	98
4.4	Discussion .....	108
4.5	Conclusions .....	116
<b>Chapter 5</b>	<b>Thin Film Drainage in Nonaqueous Electrolyte Solutions.....</b>	<b>118</b>
5.1	Introduction .....	118
5.2	Materials and Methods .....	121
5.3	Results and Discussion.....	125
5.4	Conclusions .....	144
<b>Chapter 6</b>	<b>Surface Mobility of Bubbles in Electrolyte Solutions .....</b>	<b>145</b>
6.1	Introduction .....	145
6.2	Methods and Materials .....	147
6.3	Results .....	149
6.4	Discussion .....	150
6.5	Conclusion .....	153
<b>Chapter 7</b>	<b>Electrolyte Coalescence Inhibition: A New Model.....</b>	<b>154</b>
7.1	Overview of findings .....	154
7.2	Electrolyte Inhibition and Surface Partitioning.....	158
7.3	Ions at the Interface and Surface Rheology .....	166
7.4	Surface Partitioning, Bubble Coalescence Inhibition and Hofmeister Effects ... .....	177
7.5	Conclusions .....	179
<b>Chapter 8</b>	<b>Summary .....</b>	<b>182</b>
<b>References</b>	<b>.....</b>	<b>186</b>
<b>Appendix</b>	<b>Surface Tension in Single Electrolytes .....</b>	<b>205</b>



**Bubbles, Thin Films  
and  
Ion Specificity**



---

# Chapter 1 Bubble Coalescence and Electrolyte Inhibition

---

## 1.1 INTRODUCTION

The problem I set out to investigate in this thesis is readily observed. Take three flasks: one contains pure water; the second contains salty water (at such levels as might be found in the sea, or in blood); and the third contains water with a surfactant. Shaking each flask creates bubbles, and ceasing to shake allows one to observe the qualitative difference in bubble lifetimes. In pure water the bubbles coalesce with each other and with the liquid surface, and disappear almost immediately. A small amount of surfactant stabilises the bubbles and produces a froth or foam that may last for minutes, or even days. The effect of the salt is somewhere in between – bubbles are stabilised for several seconds before they merge with the liquid free surface. The mechanism behind this electrolyte inhibition of bubble coalescence is unknown.

The aim of this project has been to elucidate the mechanism behind electrolyte inhibition of bubble coalescence.

### 1.1.1 Applications

Many systems contain both salt and bubbles. Bubble coalescence is inhibited in seawater by the presence of electrolytes,<sup>1</sup> and the resulting fine spray and extra surface area is important for oxygen dissolution and for mass transfer of ions to the atmosphere.<sup>2,3</sup> Froth flotation as used in mineral extraction requires an understanding of bubble coalescence,<sup>4</sup> while some bioreactors rely on a bubble stream with a large interfacial surface area to diffuse oxygen.<sup>5</sup> Bubbles in electrochemical cells can affect electrode performance.<sup>6,7</sup>

More generally, the drainage of a thin liquid film confined between two surfaces is a process at the heart of colloid and interface science. Examples of cases where film stability and drainage kinetics are important include emulsions, foams, biological systems, mineral flotation and capillary flow. Hence, the electrolyte stabilisation of the thin film between bubbles has parallels in other colloidal systems like emulsions, where electrolyte will also play a part.<sup>8</sup>

Importantly, bubble coalescence inhibition is found to display ion specific effects – the degree of inhibition depends on the identity of the cation and anion present, and cannot be predicted from valency or from the identity of a single ion.<sup>9, 10</sup> The bubble system can thus act as both a model and a powerful and simple test of general theories of ion specificity. Specific ion effects are ubiquitous at high salt concentrations and fundamental to many biological processes,<sup>11</sup> and in complex fluids<sup>12</sup> and slurries<sup>13</sup>. Current explanations are largely empirical and system-specific.<sup>14</sup> If the reasons for the ion specificity in bubble coalescence are determined, the implications may be wide-ranging.

### **1.1.2 Chapter outline**

The next section of this chapter (Section 1.2) describes theories of bubble coalescence via thin film drainage and rupture, as applied to surfactant systems. Surfactant thin films are well-studied and generally have formed the basis for existing theories of film stabilisation and rupture. The theories are applied to predict thin film stability in pure liquids, surfactants and electrolyte solutions.

In section 1.3 a review of literature on bubble coalescence inhibition in electrolyte solutions is presented. I summarise the early research into the phenomenon, and the importance of the finding of ion specificity and ion combining rules.

Section 1.4 contains a summary of experimental techniques to investigate the gas-solution system, and I also consider the relevance of related systems including electrolyte films on solid surfaces and in emulsions.



---

In section 1.5, a range of hypotheses about electrolyte bubble coalescence inhibition are described. Some of these form the basis of the experiments described in this thesis, while others can be dismissed on the basis of previous work. I have investigated a range of hypotheses touching upon interfacial forces, surface deformation, solvent structure, drainage dynamics, and surface mobility. The focus in this chapter is on theories and hypotheses from before the commencement of this project. More recent findings and results from this thesis are consolidated in the general discussion in Chapter 7.

## **1.2 COLLISION, DRAINAGE AND RUPTURE**

Bubble coalescence is the joining together of two bubbles in a fluid, to form one larger bubble. As it involves the reduction of surface area, coalescence is always an overall energetically-favoured process.<sup>15</sup> However coalescence can be inhibited kinetically or in the presence of a local energy minimum.<sup>16, 17</sup> Coalescence can be described as a three-step process: bubble approach and creation of a thin film; film drainage; and film rupture.<sup>18</sup> Coalescence is inhibited when the steps are not completed over the lifetime of a collision. The processes are of course interrelated: film drainage hydrodynamics are affected by collision velocity, and rupture occurs only when the film has drained to within a certain critical thickness. Each step is here discussed separately. This section briefly lays out models of film drainage and film rupture that have been applied successfully to pure liquid films and to surfactant-stabilised thin films.

### **1.2.1 Collision**

The rate at which two bubbles approach (as well as the angle of approach, and the bubble size) will affect whether they coalesce during a collision lifetime.<sup>19</sup> Ribeiro and Mewes have shown that whether a collision results in bouncing or coalescence is determined by the relative rate of approach, with coalescence occurring only below a critical approach velocity.<sup>20</sup> This velocity is related to the interface deformability, and is affected by surfactant or electrolyte additives as well as by bubble size. The question may arise whether turbulence in a bubble flow can affect coalescence and thin film

drainage. Lee and Hodgson note that in inviscid water, the smallest turbulent eddies are on the order of  $25\mu\text{m}$ ,<sup>21</sup> and thus flow in the much smaller-scale thin film is laminar. However turbulence will affect bubble collision incidence and velocity, as well as more complex formation and break-up processes, in some bubble column and stirred vessel experiments.<sup>22</sup>

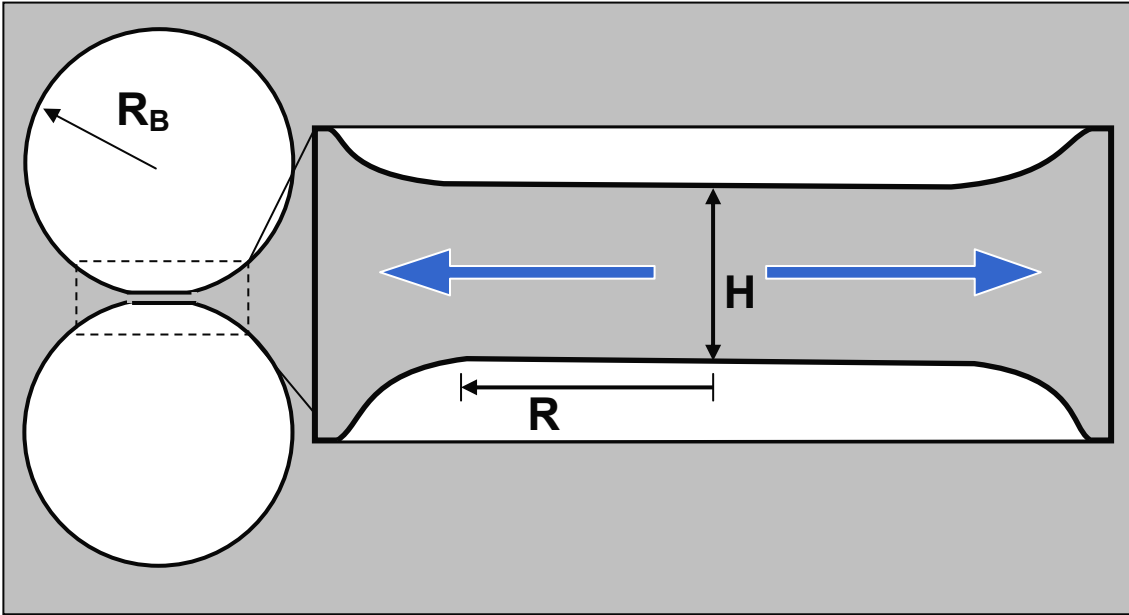


**Figure 1.1.** A planar thin film of mean thickness  $H$ , with radius  $R$ , is formed between two approaching spherical bubbles with radius  $R_B$  approaching through a fluid. The film drainage at values of  $H > 100\text{nm}$  is driven by capillary pressure.

### 1.2.2 Hydrodynamic drainage

Thin film drainage at large separations is driven by hydrodynamic pressure. The bubbles deform from sphericity under hydrodynamic pressure, and the thin film can be treated as planar.<sup>23</sup> For a circular planar film, the drainage pressure between the film and the bulk is given by:<sup>24</sup>

$$\Delta P = \frac{2\gamma R_B}{(R_B^2 - R^2)} \quad (1.1)$$

This is a version of the Young-Laplace equation for the pressure within a flattened bubble, where  $\gamma$  is surface tension,  $R_B$  is the radius of the bubble contributing to pressure

outside the thin film, and  $R$  is the radius of the planar film (see Figure 1.1). This capillary pressure creates a laminar flow from the thin film interior to the surrounding fluid.<sup>25</sup> This purely pressure-driven flow slows rapidly as the volume of the thin film decreases.<sup>26</sup> In pure liquids the film generally thins below the critical rupture thickness very rapidly: no pure liquid has been observed to support a stable film.<sup>27</sup>

During initial bubble deformation, a “dimple” may be created in the film (Figure 1.2). The hydrodynamic pressure in the film is largest at closest bubble separations, and this can drive the central film region to invert.<sup>28</sup> At large separations the rims around the dimple will subsequently thin more slowly and the film will eventually flatten. However the dimple can persist if the rim forms a barrier to drainage.<sup>23</sup> Dimpling occurs more readily in larger bubbles with lower Laplace pressure and greater interfacial deformability.

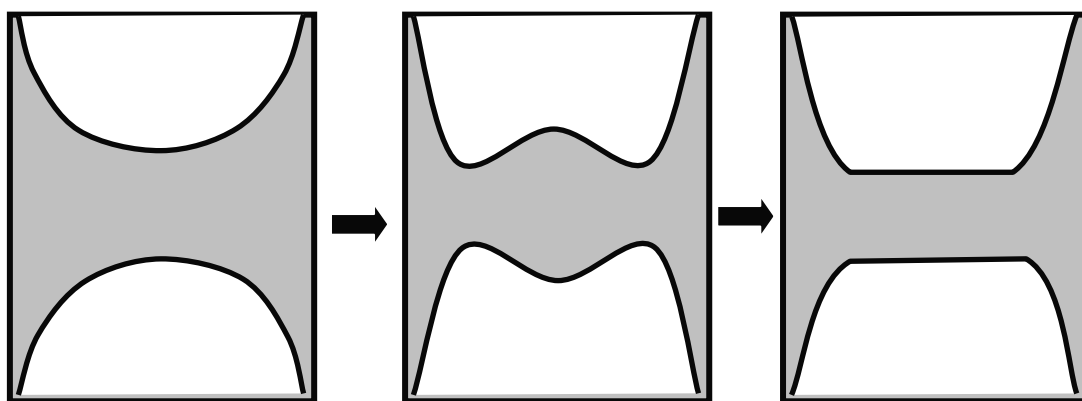


**Figure 1.2** Dimpling and flattening process during thin film drainage between two spherical bubbles.

#### 1.2.2.1 *Hydrodynamic drainage in the presence of surfactant*

Capillary flow can be retarded when another component is present in solution. Surface adsorption changes the interfacial flow at the gas-liquid surface. As liquid is carried away from the centre of a planar film during drainage, any surfactant at the interface is transported towards the edges of the film (see Figure 1.3). The Gibbs adsorption

isotherm describes how the surface tension is related to the surface excess  $\Gamma$ . For a single component system,

$$\Gamma = \frac{-c}{kT} \frac{d\gamma}{dc} \quad (1.2)$$

where  $c$  is concentration,  $d\gamma/dc$  is the change in surface tension as a function of concentration,  $k$  is Boltzmann's constant and  $T$  is temperature. A *local* variation in surface excess across the surface of the film drives a *local* variation in surface tension.<sup>17</sup>

The consequent restoring force against non-equilibrium surface concentration gradients is known as the Marangoni effect, and acts to retard film drainage.

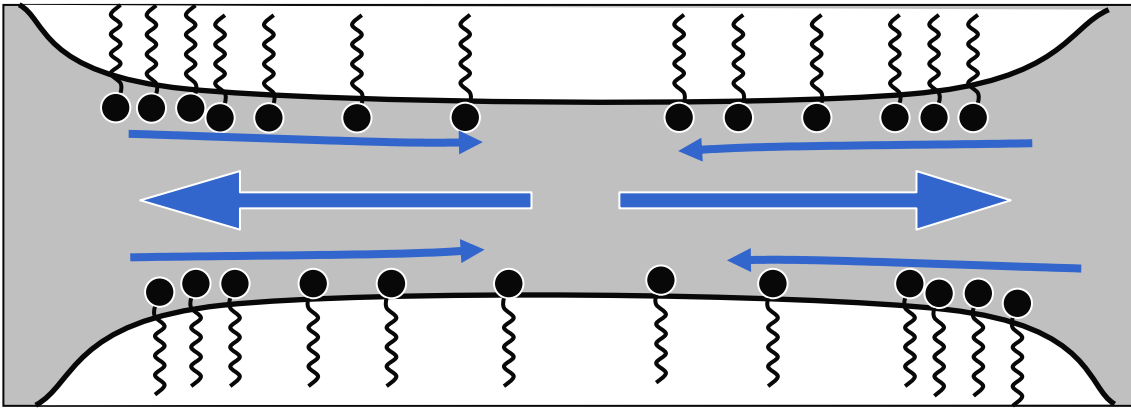


**Figure 1.3** The Marangoni effect in surfactant. Film drainage reduces surface concentration in the film centre and sets up a non-equilibrium surface tension gradient that restores surfactant and opposes hydrodynamic film drainage. At some concentrations the interfaces can be immobilised.

The surface tension gradient is restored, in the case of surfactants, predominantly by surface diffusion.<sup>23</sup> The interfacial flux towards the film centre opposes film drainage and can effectively immobilize the fluid layer at the interface (Figure 1.4). In the presence of immobile, planar interfaces the film thinning velocity is given by the well-known Reynolds equation:<sup>17</sup>

$$V_{\text{Re}} = \frac{2H^3 \Delta P}{3\eta R^2} \quad (1.3)$$

where  $V_{Re}$  is Reynolds velocity of film thinning,  $H$  is film thickness,  $\Delta P$  is the driving pressure (which is purely capillary pressure at  $H > 100\text{nm}$ ),  $\eta$  is liquid viscosity and  $R$  is film radius. In water the gas-water interface is fully mobile, as it cannot support a shear stress without the presence of a third component; surface mobility is required to correctly model drainage in pure liquids.<sup>27</sup>

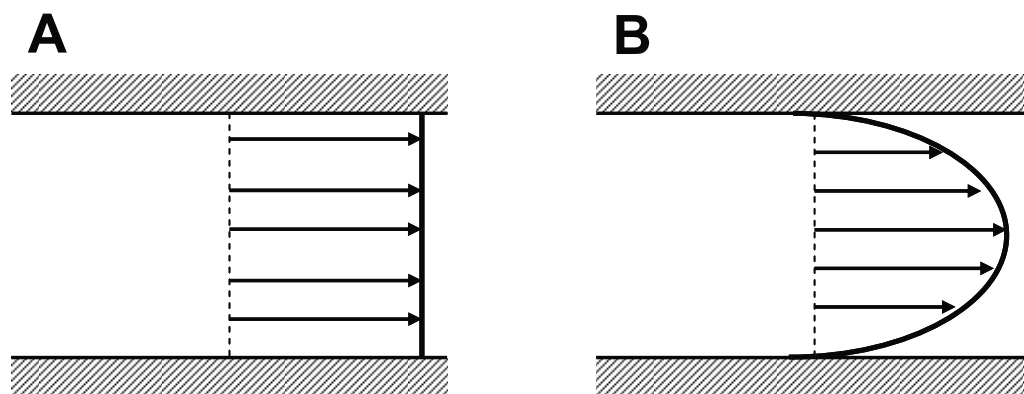


**Figure 1.4** Capillary flow between mobile (A) and immobilised (B) bubble surfaces. Surface immobilisation in the presence of surfactant reduces thin film flow and slows film drainage.

### 1.2.3 Surface forces and film drainage

As a thin film drains, the surfaces begin to interact and the system can no longer be treated as purely hydrodynamic.<sup>29</sup> *Surface forces* is the term used to refer to the distant-dependent interactions between macroscopic interfaces across a fluid, derived from the sum of intermolecular forces. The forces are generally assumed to be at equilibrium, and independent of any dynamic interactions in the system.<sup>30</sup> The surface forces between two like surfaces are generally repulsive; formation of a stable liquid film in surfactant (a foam) can occur when at a given film thickness attractive hydrodynamic and surface forces are balanced by the repulsive components of the force.<sup>31</sup>

The sum of surface forces across a thin film is also known as the “disjoining pressure”,  $\Pi$ . In this case the disjoining pressure is the positive (or negative) external pressure required to equalise the repulsive (or attractive) interaction between the film surfaces, and stabilise the thin film. (For a review of disjoining pressure in foams, the reader is

directed to Bergeron.<sup>16)</sup> The disjoining pressure can be described as the sum of components that are (variously) distance-dependent.<sup>32</sup> In general,

$$\Pi(h) = \Pi_{vdW} + \Pi_{edl} + \Pi_{steric} + \dots \quad (1.4)$$

where  $\Pi(h)$  signifies the disjoining pressure dependence on local film thickness  $h$  and the subscripts are defined: *vdW* is the van der Waals interaction; *edl* is the electrical double layer force; and *steric* refers to structural forces associated with the solvent and adsorbed molecules and may include surface solvation. There may also be other contributions such as the hydrophobic force (discussed below, in Section 1.5.1.3, in the context of electrolyte solutions).<sup>33</sup>

### 1.2.3.1 *van der Waals interactions*

van der Waals interactions arise from the totality of molecular interactions between interfaces across the thin film (excluding the electrostatic component). The major contribution to disjoining pressure is the dispersion force, arising from interaction between instantaneous molecular multipoles.<sup>30</sup> The dispersion force between two like surfaces interacting across a thin film is always attractive, and the attraction can become significant at surface separations of 100nm and less.<sup>25</sup> van der Waals interaction is distance dependent, with a first approximation of the disjoining pressure given by:<sup>30</sup>

$$\Pi_{vdW} = \frac{A}{6\pi h^3} \quad (1.5)$$

where  $A$  is the Hamaker constant for the air-liquid-air system and  $h$  is the local film thickness, as distinct from the mean film thickness  $H$ . This local interaction means that for a non-planar film the surface attraction may be non-uniform across the film surface. For the air-water-air system  $A$  has a value of approximately  $3.7 \times 10^{-20}$  J.<sup>30</sup> At larger separations the retardation effects can become important and  $\Pi_{vdW}$  scales with  $1/h^4$ . Retardation is due to the finite time required for a dipole to be induced through a thin film, which increases with distance.<sup>30</sup> van der Waals effects are discussed in more detail in Section 1.2.4 below, in the context of their contribution to film rupture.

### 1.2.3.2 *Double layer repulsion*

A charged surface attracts counterions from solution, and these counterions attract a second, more diffuse layer enhanced in co-ions. This is the electric double layer,

distinguished from the bulk solution. The electric double layers at like surfaces will have a like charge and their overlap exerts an osmotic repulsion between the interfaces, because the excess concentration of counterions is entropically unfavourable.<sup>30</sup> The distance into solution at which the electrostatic double layer repulsion can still exert an effect is dependent upon the concentration of ions. In weak solutions the ions are diffuse and the double layer will be large; in strong electrolyte the double layer is compressed and the surfaces are “screened” from each other.<sup>34</sup> The characteristic length of influence is known as the Debye length,  $\kappa_D^{-1}$ . It is determined by the Poisson-Boltzmann theory, and for a univalent electrolyte is given by:<sup>35, 36</sup>

$$\kappa_D^{-1} = \sqrt{\frac{\varepsilon k T}{8 \pi e^2 n^0}} \approx c^{-1/2} \quad (1.6)$$

Here  $\varepsilon$  is the solvent permittivity,  $k$  is Boltzmann’s constant,  $T$  is the temperature,  $e$  is proton charge,  $n^0$  is the number density of ions in bulk and  $c$  is ion concentration. The Debye length in a  $10^{-5}$ M solution of ionic surfactant is around 100nm, while in a 0.1M salt solution the Debye length is <1nm.

#### 1.2.3.3 Steric interactions

Interfacial repulsion can arise due to steric confinement effects at very small surface separations. The solvation force arising from confinement and layering of solvent molecules, is observed only within 5nm of the surface. Confinement of surfactant molecules on each film surface can stabilize very thin “Newton black” films even when nearly all solvent has been squeezed from the film, as observed in some foam systems.<sup>32</sup> Another repulsion may arise due to “undulations” or thermomechanical fluctuations of deformable interfaces.<sup>37</sup> This force, known as the Helfrich force, effectively expands the range of interaction of some bilayers and membrane films and it can be long-range, with a  $1/h^3$  distance dependence.<sup>30</sup>

#### 1.2.3.4 DLVO theory

The steric interaction between surfaces becomes apparent only at very small surface separations (5nm or less), and so for thicker films only the van der Waals and electrostatic double layer forces are important.<sup>16</sup> These two components of the

disjoining pressure together are described by DLVO theory. DLVO theory was developed by Derjaguin and Landau, and Verwey and Overbeek, in the 1940s.<sup>35, 36</sup> It is a powerful tool of colloid science for predicting surface interactions. The basis of DLVO theory is that surface interaction can be modeled by summing van der Waals attraction and electrostatic repulsion (obtained from Poisson-Boltzmann equations). DLVO theory works very well to model forces in the circumstances for which it was designed – that is, dilute solutions of symmetrical electrolyte and low surface potentials.<sup>38</sup> Fundamental assumptions within the theory are that the solvent can be treated as a continuum characterized by a dielectric constant, and that ions can be treated as point charges. It also assumes that van der Waals and electric double layer forces can be treated as independent and additive – though later work showed that this is not strictly correct.<sup>39</sup> DLVO theory begins to break down at concentrations greater than  $10^{-3}$  M as ion size and solvent structure become important.<sup>40</sup>

#### 1.2.4 Film rupture

Rupture occurs rapidly and dynamically, and it is consequently difficult to observe and to characterize. In fact the exact process of rupture, even in pure liquids, is unknown.<sup>41</sup> The mechanism in surfactant foam films is usually considered to be rupture via a growth of capillary waves at each interface.<sup>42</sup> It is supposed that deformations at each film surface can come into contact across a thin film of much greater mean thickness, and that rupture at one such contact point leads to very rapid coalescence and formation of a larger bubble.<sup>15, 43</sup>

This model requires that the film be treated as non-uniform in thickness. There are observed fluctuations in film thickness because of mechanical disturbances, the movement of fluid and the shear stresses (See Figure 1.5).<sup>31</sup> There are, in addition, small thermal fluctuations due to the movement of molecules at the interface; these are generally on the order of  $5\text{\AA}$  in amplitude.<sup>44</sup>

At large separations the film thinning is dominated by the capillary pressure, which is largely independent of film thickness. If fluctuations arise in the film at that stage, thick



---

areas will tend to drain more quickly and the planar condition will be restored.<sup>23</sup> When the surfaces approach within about 100nm, surface attraction arising from van der Waals dispersion force (described above) becomes important. This attraction scales with  $1/h^3$  where  $h$  is the local film thickness (see equation (1.5)), and increases with smaller surface separation. In a non-uniform film, the van der Waals attraction is greater in those parts of the film that are thinner. Under this force the hydrodynamic waves will continue to grow in amplitude until a critical mean film thickness  $H$  is reached. At this point the thermal fluctuations at the narrowest parts of the film (those with smallest local film thickness,  $h$ ) can produce osculation (literally, “kissing”) of the two interfaces, and film rupture. The amplitude of fluctuations grows with the radius of the thin film, and in large films with immobile interfaces it can be around 25nm, and lead to a critical mean film thickness  $H$  (at which rupture is possible) of 50nm.<sup>44</sup>

Rupture will be favoured when capillary waves are minimally damped and have had time to grow in size.<sup>45</sup> The theory assumes that electrostatic repulsion is highly screened and that there is no effect due to non-DLVO disjoining force components. It is also assumed that surfaces are immobile. These conditions are met experimentally in the presence of surfactant with screening electrolyte, and here the theories for film drainage velocity and rupture thickness would seem to agree well with observations.<sup>31, 42</sup> It is noted that the time of wave growth is on the order of tens to hundreds of seconds on immobile surfaces. At mobile film surfaces, as found in surfactant-free liquid, surface waves grow rapidly. Ruckenstein and Jain give the theoretical lower bound for rupture time by surface wave growth in pure liquid to be on the order of microseconds.<sup>46</sup>

Hole nucleation is an alternative model of film rupture.<sup>47</sup> Such a mechanism has been observed in polymer and supported surfactant films.<sup>48</sup> While it has been suggested that film thicknesses on the order of 25Å would be required for hole formation, Lee and Hodgson conclude that at a rapid rate of approach the precise local film thickness is unimportant.<sup>21</sup> Hole formation is predicted to occur only between surfaces separated by a few nanometres or less, and so will require a similar local approach of surfaces to the thermal wave osculation mechanism described above.<sup>43</sup>

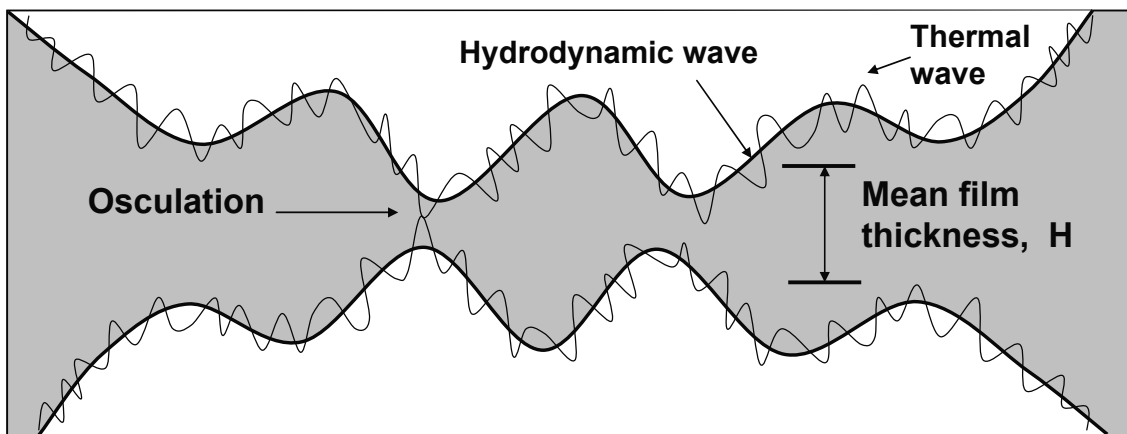


**Figure 1.5** Surface fluctuation model of film rupture between two bubbles. A large wavelength hydrodynamic wave grows via van der Waals forces, and at a thin point thermal fluctuations of each interface meet and osculate, causing rupture across a film of mean thickness  $H$ . Diagram based on work by Sharma and Ruckenstein.<sup>44</sup>

### 1.2.5 Coalescence in pure liquid

In pure water no stable film is formed and coalescence takes only a few milliseconds.<sup>27, 49, 50</sup> The film surfaces are mobile and capillary drainage to within the critical rupture thickness is not impeded.<sup>51</sup> The rupture thickness in pure liquid is difficult to measure because it is hard to avoid contamination and because the film ruptures quickly, but films have been observed to rupture at around 100nm bulk bubble separation.<sup>52, 53</sup> The timescale of thin film drainage is very short and theories modeling drainage in pure water are subject to various constraining assumptions (for a helpful summary see Ribeiro and Mewes<sup>54</sup>). Thus, the complete process of bubble coalescence in pure liquid remains obscure.

### 1.2.6 Coalescence inhibition in surfactant

Surfactants stabilise bubbles against coalescence, leading to foam lifetimes from seconds to days.<sup>17</sup> Surfactants, as the name implies, adsorb to the interface, and from this property derive many of their effects. Some of the ways in which added surfactant affects the thin film relative to pure liquid are:

- 
- Surface tension. The direct effect of surface tension reduction is to reduce the capillary pressure driving thin film drainage, as shown by equation (1.1).
  - Immobilisation of the interface via Marangoni effects driven by surface tension gradients across the film surface (arising from concentration gradients). Although much attention has been paid to this factor in development of drainage velocity models (see for example Marrucci<sup>25</sup>), Ivanov and co-workers suggest that surface immobilisation is often unimportant in controlling rupture and coalescence.<sup>23</sup> In particular, at high surfactant concentrations, surface diffusion is rapid and mobility may again increase.<sup>55</sup>
  - The deformation of the film surface during drainage leads to increased interfacial elasticity. Gibbs Elasticity of an interface,  $E$ , is a measure of the response of the interface to mechanical disturbance. It is proportional to the square of surface tension gradient,  $(d\gamma/dc)^2$ :<sup>56</sup>

$$E = \frac{4c[d\gamma/dc]^2}{kTD} \quad (1.7)$$

Here  $c$  is concentration,  $(d\gamma/dc)$  is the change in surface tension with concentration,  $k$  is Boltzmann's constant,  $T$  is temperature and  $D$  is a measure of interfacial thickness related to the shearing of the interface.<sup>56</sup> Increased surface elasticity acts to damp the growth of capillary waves.<sup>55</sup> This in turn will reduce the rupture probability over the timescale of a collision. Changes in surface elasticity in electrolyte solution are discussed further in Chapter 2.

- The surfactant will affect disjoining pressure. In ionic surfactants or with added electrolyte, the presence of ions in solution and the change in surface potential with surfactant adsorption will alter the electrical double layer and induce repulsion largely absent in pure liquids.<sup>55</sup>
- Steric effects. A short-range repulsive interaction between surfactant layers at opposite interfaces may stabilise a very thin Newton black film when much of the solvent has been drained.<sup>16, 17</sup>

In summary, the effect of surfactant is to reduce the rate of film drainage and increase the repulsive disjoining pressure across the thin film. Surfactants can also produce a

---

film that is stable to lower thicknesses, due to repulsive electrostatic forces or to steric effects.<sup>17</sup>

### 1.2.7 Coalescence in electrolyte solution - according to theory

One can take the models of thin film stabilisation, drainage and rupture derived from the case of surfactant, and predict the stability of thin films between bubbles in surfactant-free electrolyte solution. Of course the models do not predict experimental data, because had they done so then this project would have been exceedingly brief and devoid of interest – but this is a useful exercise to highlight the anomalies associated with bubble coalescence inhibition by electrolytes.

- The electrolyte effect on surface tension is too small to affect capillary drainage substantially. The relevant concentration range of electrolyte is approximately 0.01-0.5M. The surface tension of pure water is  $72.75\text{mN m}^{-1}$  at  $20^\circ\text{C}$ ,<sup>57</sup> and electrolytes tend to change surface tension by  $<3\text{ mN m}^{-1}\text{ M}^{-1}$ .<sup>58-60</sup> Therefore the relative change of surface tension at the relevant concentrations of electrolyte is  $\leq 2\%$ . This change can be positive or negative – many electrolytes increase the surface tension relative to pure liquid, which would if anything drive more rapid capillary drainage (see equation (1.1)).
- The surface tension gradient across the thin film, which creates Marangoni effects in the presence of surfactant, is very small in electrolyte solution. Because of high ion concentrations (rapid equilibration) and low dependence of surface tension on concentration, it is predicted that the surface tension gradient is too low to stabilise the thin film via interface immobilisation.<sup>60</sup> The same arguments apply with respect to the surface tension gradient with film deformation, which drives Gibbs elasticity in surfactant films and so damps film deformation and prevents rupture.
- Electrostatic repulsion is not predicted to stabilise thin films in these electrolyte solutions. At a typical inhibiting concentration of 0.1M 1:1 electrolyte, the

---

Debye length of the electric double layer is on the order of 1nm (see equation (1.6), while thin films rupture at 50-100nm.<sup>18, 53</sup> The bubble interfaces are effectively screened from each other and are expected to experience no repulsive disjoining pressure during drainage.

The models that adequately predict surfactant film stabilisation, via surface forces from repulsive electric double layer and steric interactions and dynamic effects related to surface tension gradients at the film surfaces, predict no such stability in electrolyte solutions. Rather, a rapid coalescence of bubbles might be expected, as observed in pure liquid. However, it has been known for decades that some electrolytes at sufficiently high concentration, do inhibit bubble coalescence relative to pure water.<sup>61-63</sup> A review of the literature on this phenomenon is presented in the next section.

### **1.3 BUBBLE COALESCENCE IN ELECTROLYTE SOLUTIONS**

#### **1.3.1 An example of electrolyte inhibition**

Before a review of the different studies of electrolyte bubble coalescence inhibition, it is as well to demonstrate the phenomenon. An example of typical bubble coalescence inhibition by electrolyte is given in Figure 1.6. This particular data is based on laser scattering turbidity measurements of bubbles in a bubble column (see Chapter 2 for a full description), and is consistent with a range of other experimental techniques. The percentage coalescence scale used on the y-axis was first developed by Lessard and Zieminski in their work on two-bubble collisions, where the percentage refers to the tallied number of collisions resulting in coalescence.<sup>63</sup> In bulk measurements the percentage coalescence is obtained by setting the pure water measurement as 100% coalescence, and the stable low coalescence value obtained in inhibiting salts as 0% coalescence.<sup>9</sup> The NaCl data shown are typical of a monovalent inhibiting salt. At a concentration of around 0.01M coalescence inhibition begins, and coalescence reduces over a narrow concentration range before reaching a constant low value, defined as 0% coalescence. The concentration required is high relative to surfactant effects: electrolytes generally show inhibition at  $10^{-2}$ M and above,<sup>9, 63, 64</sup> while surfactant may require as little as  $10^{-6}$ M.<sup>65</sup>

Electrolytes may be compared using the transition concentration (or critical concentration), which is defined as the concentration at which coalescence is 50% of the maximum. For the sodium chloride data shown here, transition concentration is 0.093M. This concentration depends on bubble size<sup>66</sup> and interaction time<sup>67</sup> and so is not completely uniform across all systems and experimental techniques; however within a given technique the transition concentration provides a useful comparison between electrolytes.

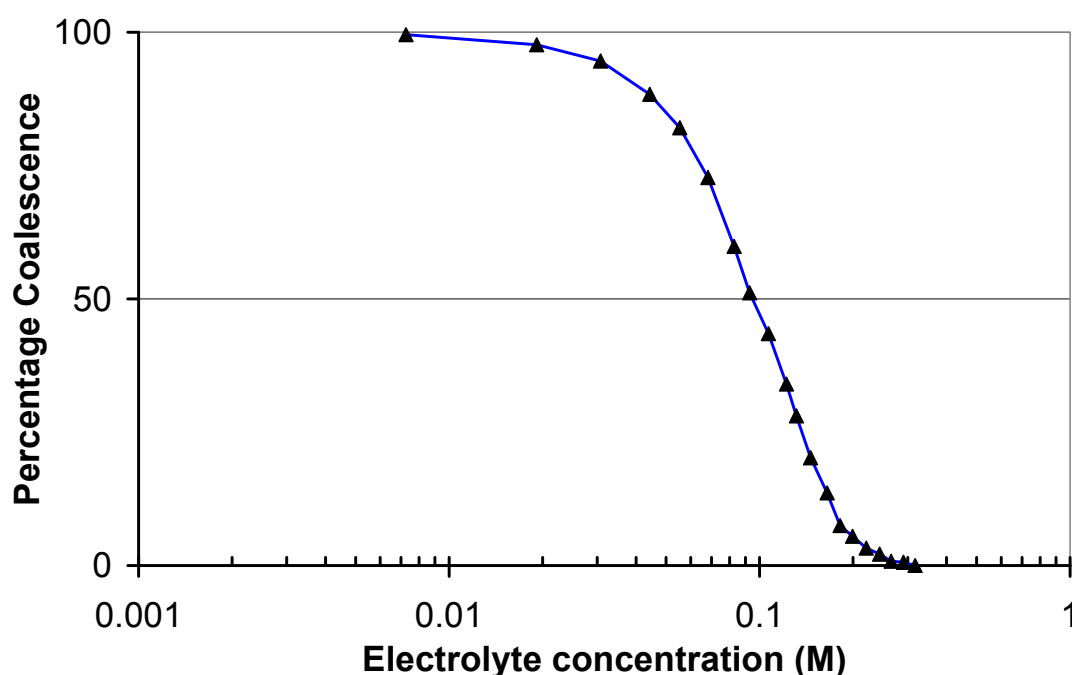


**Figure 1.6** Effect of NaCl on bubble coalescence in water. Percentage coalescence (where 100% is value in pure water and 0% is a stable low value of coalescence) is plotted against the log of concentration. Transition concentration, measured at 50% coalescence, is 0.093M.

### 1.3.2 Historical studies of bubbles in electrolytes

#### 1.3.2.1 Early experimental studies on bubble coalescence in electrolytes

The earliest work on the topic of bubble stabilisation in salt solutions is a series of papers by Foulk (with Miller, in one case).<sup>61, 68, 69</sup> In his 1924 article, Foulk deplors the poor state of the science of foams. He further states that sodium salts are known to cause foaming, but cannot find the original reference for this widely-held view – and

---

neither can I. Foulk's experiments in boiling sodium salt solutions indicate no foaming, but this is possibly due either to the temperature conditions, or to the definition of "foaming" requiring a white froth, rather than the transient stabilisation of bubbles commonly observed in electrolyte solution.<sup>68</sup> Foulk and Miller in their 1931 paper (which I strongly recommend) have covered a lot of the ground concerning bubble stabilisation in electrolytes: bubble column experiments (using measurement of froth height to indicate degree of coalescence inhibition); two-bubble experiments in which thin film lifetime is measured; a range of electrolytes that includes non-inhibiting salts; electrolyte mixtures; and measurements of surface tension and dynamic surface tension.<sup>69</sup> They even consider coalescence in the nonelectrolyte sucrose – on which little further had been done before my experiments (see Chapter 3). Foulk and Miller attribute thin film stabilisation to surface adsorption of solute, which might be positive or negative (corresponding to decreased or increased surface tension, respectively, as per Gibbs adsorption isotherm (equation (1.2) above)). It was suggested that such variation in solute concentration leads to osmotic resistance against mixing of surface layers such as is required at coalescence.

The 1960s and 1970s brought the next major forays into the study of bubbles in coalescence inhibition. Marrucci and Nicodemo measured gas hold-up and bubble size in a bubble column, in a range of inhibiting electrolytes.<sup>62</sup> They also report the importance of varying surface tension gradient, and were the first to note a correlation of bubble size (related to coalescence inhibition) and the square of surface tension gradient,  $(d\gamma/dc)^2$ . This correlation is still considered important, and is still unexplained. Chapter 2 describes experiments to investigate it further. Lessard and Zieminski obtained results consistent with Marrucci using two-bubble experiments, and defined percentage coalescence as the number of bubble pairs (on twin capillaries) that coalesce at a given concentration.<sup>63</sup> The transition concentration is defined as that at which 50% coalescence occurs. An inverse correlation between transition concentration and ionic strength of electrolyte was also noted – that is, electrolytes of higher ionic strength require a lower concentration to elicit coalescence inhibition.<sup>63, 70</sup> Other workers also studied two-bubble coalescence<sup>29, 71</sup> and bubble column measurements,<sup>71</sup> although these

---

investigations tended to concentrate on the same handful of known inhibiting electrolytes.

Cain and Lee used the technique of thin film interferometry to measure the film thickness between two bubbles in KCl at varying concentrations as a function of time, in order to determine film drainage kinetics and rupture thickness.<sup>18</sup> This is the first attempt to quantitatively study these film properties in the absence of surfactant. This study also provided early proof that deformation of the bubble interfaces was in fact leading to formation of a planar thin film. No stable film was observed at low electrolyte concentrations. In 0.5M KCl the film thickness at rupture was from 75-95nm, with drainage lifetime of 420ms, while the film thickness in 1.0M KCl was 55-75nm (with a lifetime of 600ms). It was shown that neither Reynolds drainage (which assumes planar immobile interfaces, see equation (1.3)) nor the Radoev model<sup>72</sup> (which allows diffusional relaxation and partial surface mobility) correctly predicted the film thinning rate.<sup>18</sup> This study was important in showing that electrostatic repulsion does not drive bubble coalescence inhibition, as the Debye length of  $\leq 1$ nm is much less than the film rupture thickness. The disagreement with Reynolds drainage also showed that planar immobile interfaces are a poor model for the thin liquid film between bubbles. This posed a challenge for the dominant theory of bubble coalescence inhibition of the time.

#### 1.3.2.2 *Early theory of bubble coalescence inhibition: Marangoni effects*

The dominant model in the literature up until at least 1990 was that electrolytes exert their effect by changing the thin film drainage of solution from the viscous to the elastic regime – that is, the electrolyte surface tension gradient was believed to immobilise the gas-liquid interface at sufficiently high concentration via Marangoni effects.<sup>25</sup> This theory had the advantage of covering electrolytes that increase and decrease the surface tension of solution – the surface tension gradient can be positive or negative, so long as it exists.<sup>69</sup>

It is well accepted that if a solute is surface active and adsorbed to the interface, Marangoni effects can reduce surface mobility.<sup>21, 25</sup> Stretching of the film surface during



---

drainage lowers the surfactant concentration at the centre of the film and raises its surface tension, leading to restoring surface flow in opposition to film drainage. It is perhaps less clear that there will be such a Marangoni effect during drainage of films containing electrolytes that are depleted from the interface. Lee and co-workers showed that there is indeed an increase in surface tension in the film centre even if the solute raises the surface tension relative to pure liquid.<sup>21, 73</sup> As the film thins, surface flow of depleted layers means that local electrolyte concentration increases in the thin film, causing a non-equilibrium increase in surface tension relative to the surrounding surface.<sup>18</sup> This (small) increase will oppose film drainage, and so can potentially stabilise the film. The change in surface tension in electrolyte solutions is inversely related to film thickness.<sup>60, 73</sup>

Marrucci produced a model of film drainage as driven by capillary drainage between mobile interfaces, that were immobilised at the electrolyte transition concentration leading to quasi-equilibrium thinning under van der Waals attraction.<sup>25</sup> This theory leads to the relationship:  $c_t \propto (dy/dc)^{-2}$ .<sup>74</sup> That is, transition concentration is inversely correlated with the square of surface tension gradient for inhibiting electrolytes, as observed in experiments.<sup>29, 62</sup> A great many variations on empirical formulae were produced to enable prediction of the transition concentration, depending on the precise assumptions employed.<sup>29, 71, 74</sup> It was always acknowledged that some inhibiting electrolytes (particularly KCl) failed to agree with predictions. The Marrucci model and its variations were really challenged, though, by the existence of non-inhibiting electrolytes.

### 1.3.3 Bimodal ion specificity in bubble coalescence inhibition

A resurgence of interest in bubble coalescence inhibition by electrolytes can be said to have begun with the work of Craig et al. in 1993,<sup>9, 10</sup> along with the measurements of Hofmeier et al.<sup>2</sup> Coalescence inhibition was measured in a bubble column for a range of electrolytes. Notably, it was found that some electrolytes show no effect on coalescence inhibition relative to pure water, up to a concentration of 0.5M. These electrolytes were defined as “non-inhibiting”.

The observation that some electrolytes fail to inhibit bubble coalescence in water, at moderate concentrations, was reported several decades ago by Foulk and Miller.<sup>69</sup> However Craig et al. were the first to rigorously probe the ion specific nature of the phenomenon. They showed that the combination of cation and anion is important, and grouped cations and anions each into two categories, with  $\alpha$  and  $\beta$  cations and  $\alpha$  and  $\beta$  anions having different effects with a given counterion.<sup>9, 10</sup> The  $\alpha$  and  $\beta$  designations are purely empirical, and need not have the same physical meaning in cations and anions. The ion assignments are presented in Table 1.1. No exceptions have been found to the rules here presented.

**Table 1.1**  $\alpha$  and  $\beta$  ion assignments of single electrolytes in water<sup>a</sup>

Ions	Li <sup>+</sup>	Na <sup>+</sup>	K <sup>+</sup>	Cs <sup>+</sup>	Mg <sup>2+</sup>	Ca <sup>2+</sup>	NH <sub>4</sub> <sup>+</sup>	H <sup>+</sup>	(CH <sub>3</sub> )NH <sub>3</sub> <sup>+</sup>	(CH <sub>3</sub> ) <sub>2</sub> NH <sub>2</sub> <sup>+</sup>	(CH <sub>3</sub> ) <sub>3</sub> NH <sup>+</sup>	(CH <sub>3</sub> ) <sub>4</sub> N <sup>+</sup>
Assignment	$\alpha$	$\alpha$	$\alpha$	$\alpha$	$\alpha$	$\alpha$	$\alpha$	$\beta$	$\beta$	$\beta$	$\beta$	$\beta$
OH <sup>-</sup>	$\alpha$	✓	✓					✗				
F <sup>-</sup>	$\alpha$	✓										
Cl <sup>-</sup>	$\alpha$	✓	✓		✓	✓		✗	✗	✗	✗	✗
Br <sup>-</sup>	$\alpha$		✓	✓				✗				✗
I <sup>-</sup>	$\alpha$	✓	✓	✓								
NO <sub>3</sub> <sup>-</sup>	$\alpha$	✓	✓	✓		✓		✗				
SO <sub>4</sub> <sup>2-</sup>	$\alpha$	✓	✓	✓	✓			✗				
(COO <sub>2</sub> ) <sup>2-</sup>	$\alpha$			✓				✗				
IO <sub>3</sub> <sup>-</sup>	$\alpha$		✓									
ClO <sub>3</sub> <sup>-</sup>	$\beta$		✗									
ClO <sub>4</sub> <sup>-</sup>	$\beta$		✗		✗		✗	✓				
CH <sub>3</sub> COO <sup>-</sup>	$\beta$		✗	✗	✗	✗	✗	✓				✓
SCN <sup>-</sup>	$\beta$		✗				✗					

✓=inhibit coalescence  
 $\alpha\alpha, \beta\beta = \checkmark$   
✗=no inhibition  
 $\alpha\beta, \beta\alpha = \times$

<sup>a</sup> Based on Craig et al.<sup>9</sup> with additional results.

An example of the importance of ion combination is given in Figure 1.7. At concentrations below 0.5M, sodium chloride substantially inhibits bubble coalescence relative to pure water, while sodium perchlorate has no effect. Conversely, in this concentration range hydrochloric acid does not affect coalescence but perchloric acid acts as a strong inhibitor. It is neither the cation nor the anion alone that determines coalescence inhibition, but the combination that is important.

There are two meanings of “ion specificity” that have relevance in bubble coalescence. The first is simply the general definition, referring to any difference of behaviour in salts containing different ions of the same charge. This would include, for example, variations in transition concentrations and surface tensions amongst inhibiting electrolytes. The second type of ion specificity is that described by the  $\alpha$  and  $\beta$  assignments, grouping electrolytes into two groups of “inhibiting” and “non-inhibiting” based on their effect on bubble coalescence. Where the meaning is unclear this ion specificity will be described as “bimodal ion specificity” because it groups the electrolytes into two categories.

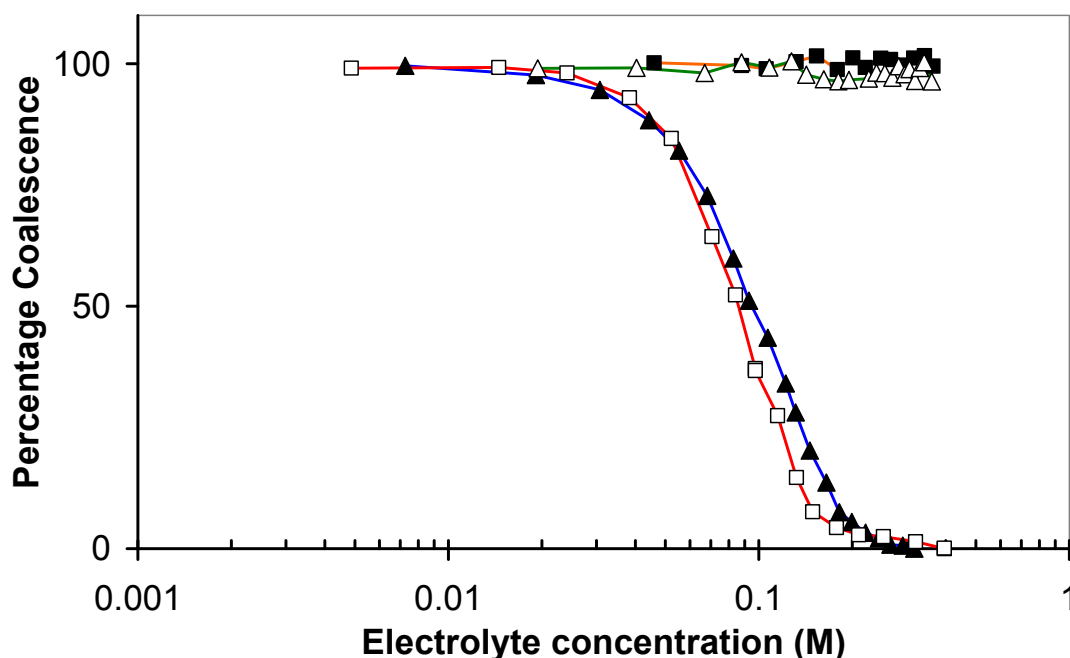


**Figure 1.7** Ion specificity and combining rules in electrolyte bubble coalescence inhibition. Coalescence is plotted as a function of electrolyte concentration on a log scale. Electrolytes NaCl ( $\alpha\alpha$ ) ( $\blacktriangle$ ) and HClO<sub>4</sub> ( $\beta\beta$ ) ( $\square$ ) inhibit at 0.1M, while their ‘cross-products’ NaClO<sub>4</sub> ( $\alpha\beta$ ) ( $\blacksquare$ ) and HCl ( $\beta\alpha$ ) ( $\triangle$ ) have no effect up to 0.5M concentration. 100% coalescence is defined in pure water, 0% is a stable low value in inhibiting electrolytes.

## 1.4 METHODS IN COALESCENCE INHIBITION

Before going on to discuss hypotheses to explain ion specificity in electrolyte inhibition of bubble coalescence in Section 1.5, I will here describe some of the experimental techniques that have been used to garner information about the phenomenon. The results of the studies are remarkably consistent, whether using multiple bubbles in columns or stirred vessels, two bubbles approaching on side-by-side or facing capillaries, or a single thin film. The same patterns of ion specificity and concentration dependence are observed in each case. This suggests that the bubble coalescence inhibition phenomenon is an example of a universal effect at gas-solution interfaces. The limits of this universality are considered in a comparison of two related systems: the liquid-liquid system of emulsions in salt solution, and the stability of a thin liquid film on a solid surface.

### 1.4.1 Experimental techniques in bubble coalescence inhibition

#### 1.4.1.1 *Two-bubble experiments*

Two-bubble experiments are the most direct way of observing electrolyte effects on coalescence, as they are minimally affected by formation and break-up contributions to bubble stability. These experiments involve observing the interaction between two bubbles produced on adjacent capillaries. The capillaries may be side by side as in Figure 1.8,<sup>29, 63, 64, 66</sup> or facing so that the bubbles encounter each other “head-on”.<sup>18, 67, 69</sup> Foulk and Miller coined the term “two-bubble experiments”,<sup>69</sup> while Lessard and Zieminski defined the transition concentration at 50% coalescing pairs.<sup>63</sup>

In general the head-on encounters enable greater control over the pressure used and the thin film lifetime.<sup>75</sup> However at large surface approach velocities for trapped bubbles the behaviour can be anomalous – for instance, Tse et al. observed no rapid coalescence even at high concentrations of inhibiting electrolyte  $\text{MgSO}_4$  when large bubbles were rapidly pushed together, though inhibition did occur at slower surface approach rates.<sup>67</sup> Bubbles at parallel capillaries better mimic collision lifetimes and flow conditions in a multiple bubble system.

A variation of the two-bubble experiments is measurement of the coalescence time of a small bubble with a free gas-solution surface, which can be thought of as a bubble of infinite radius. Under such conditions bubble bouncing against the interface can sometimes be observed.<sup>51, 76, 77</sup> Inhibiting electrolyte increases bubble lifetime against the free surface.<sup>78, 79</sup>

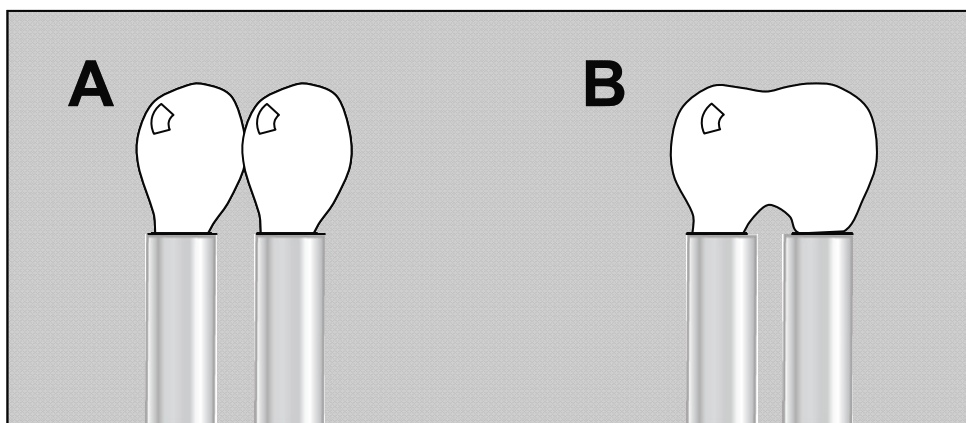


**Figure 1.8** Two-bubble experiment. Bubbles are produced at two neighbouring capillaries, with outcomes (A) non-coalescence and (B) coalescence.

One of the inherent problems in two-bubble experiments is the possibility of contamination whenever a stagnant liquid is used and there is minimal fresh interface created – as with two small bubbles with moderate lifetime. Any surface active material typically controls drainage and rupture behaviour as the effect is much stronger than electrolyte film stabilisation.<sup>63</sup> Cleaning is thus more important in these experiments than in bubble column or stirrer experiments where freshly created interface will take some time to accumulate contaminant in a purified solution.

#### 1.4.1.2 *Bubble column experiments*

I used a bubble column for many of the investigations performed in this thesis. A more detailed description of this particular apparatus is given in Chapter 2, below. There is generally a sparger or frit at the base of the column releasing gas into a solution through capillary pores. The bubbles then rise through the column under their own buoyancy and the effect of turbulence induced by the bubbly flow.

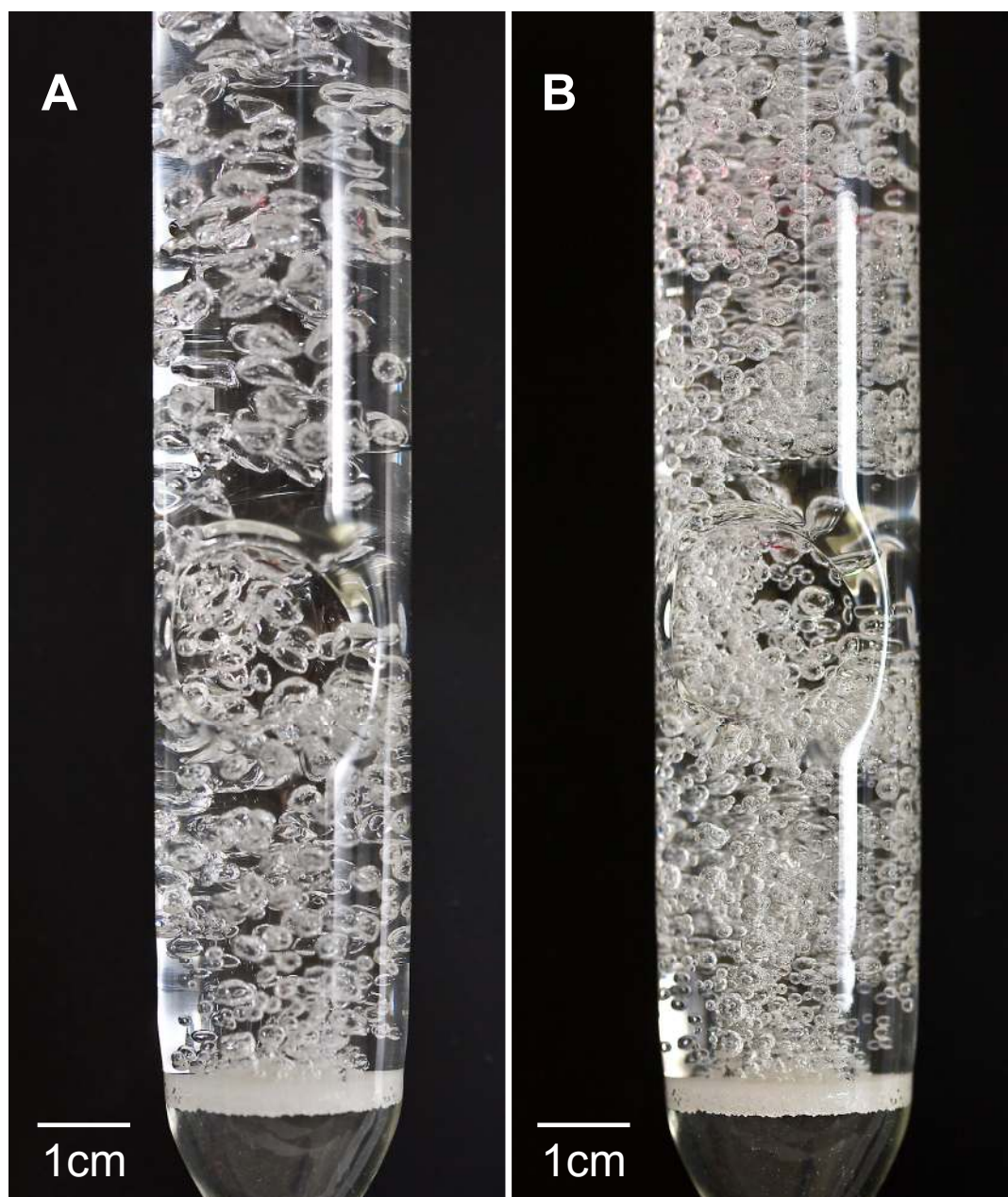


**Figure 1.9** Bubble column used in coalescence inhibition experiments. Bubbles in (A) pure water and (B) 0.3M NaCl. Nitrogen flow is  $12\text{mL s}^{-1}$ . The flattened part of the column disrupts laminar flow and promotes coalescence. The red near the top of the column in each photo is due to laser scattering; transmitted laser light provides a measure of turbidity and hence bubble coalescence.

Hofmeier et al. showed that bubble size in columns is influenced not only by collisions during rise, but by the coalescence that can occur during bubble formation at neighbouring pores in the frit.<sup>2</sup> The outcome of any particular collision will depend on a

range of factors including velocity and angle of approach,<sup>19, 20</sup> and bubble size.<sup>66</sup> Coalescence in multi-bubble or turbulent systems is a stochastic phenomenon.

There are several ways to analyse bubble column data. Bubble size, and hence coalescence, can be determined using visual analysis of bubbles in static images or high speed video.<sup>62</sup> This method is very accurate and can provide information about the kinetics of bubble coalescence. However analysis is very time-consuming, and a large amount of data must be collected to observe coalescence events.<sup>49</sup> Our group uses laser scattering to measure solution turbidity across the diameter of the column (see Figure 1.9).<sup>9, 58</sup> Scattering is greater in the presence of more, smaller bubbles. This method provides an average across a large number of bubble collisions and sizes, and enables one rapidly to collect a large amount of data in a range of solution conditions. Foulk and Miller in early experiments, measured foam height above the liquid as an indicator of froth formation.<sup>69</sup> However, the foam stability is expected to be influenced by liquid viscosity and density as well as coalescence inhibition. The column height at which bubbles of a certain size (indicative of coalescence) is observed, is the chosen analysis method of Deschenes et al.<sup>80</sup> This method may be more sensitive to very small changes in coalescence inhibition, but it is limited by the size of the column used. It is also possible to measure gas hold-up at various heights in the column.<sup>71</sup> Gas hold-up,  $\varepsilon$ , is the proportion of gas volume in total volume:<sup>22</sup>

$$\varepsilon = \frac{V - V_L}{V} \quad (1.8)$$

where  $V$  is volume of mixture in the column (gas + liquid) and  $V_L$  is liquid volume. Gas hold-up tends to increase with smaller bubbles and so may increase with added electrolyte; however it is also strongly influenced by sparger design and gas velocity.<sup>71,</sup>

81

#### 1.4.1.3 *Stirred vessel experiments*

This group of experiments is closely related to the work in bubble columns, because multiple bubbles are produced at a porous plate. They have been distinguished in part because of historical circumstance – the work in bubble stirrers or beds was concerned with bubble size distribution and with gas hold-up because of the industrial applications,

---

and these measures were rarely referenced by the theoreticians and fundamental researchers studying bubble coalescence as a phenomenon; and in part because of the use of baffles or stirrers to further impose turbulence on the bubble stream and so encourage break-up of bubbles.<sup>82</sup>

In turbulent bubble flow, bubble size is influenced by formation, coalescence and break-up phenomena, and it may be hard to differentiate the effects, if any, of electrolyte at each of these stages.<sup>1</sup> Nevertheless there is general consensus that the action of electrolyte in such system is predominantly on coalescence.<sup>22, 83</sup> Machon et al., among others, also find that electrolyte lowers the incidence of bubble breakup.<sup>22</sup> Later Tse et al.<sup>49</sup> developed a hypothesis based on highspeed video images to attribute very small bubbles seen in pure water as “daughters” of coalescence events. The incidence of such bubbles is reduced on addition of salt. This is attributed in part to decrease in coalescence and in part to a qualitatively observed increase in bubble wall rigidity, and lessening of annular capillary waves that cut off the daughter bubble.

#### 1.4.1.4 *Thin film interferometry*

In thin film interferometry experiments, a free-standing thin liquid film is formed, and its thinning is recorded using CCD video. Reflective interference fringes are obtained in white light, as shown in Figure 1.10. Interferometry is used to quantitatively measure the thickness of the film, and analysis of results yields the film drainage kinetics as well as the rupture thickness.<sup>84</sup> This technique has long been used to study surfactant-stabilised films.<sup>32, 84, 85</sup> However to date few studies have been carried out in surfactant-free electrolyte solution. The exposed film surface is highly susceptible to contamination, and without coalescence inhibition the thin film lifetime is too short, and the rupture thickness too high, for the method to be yield useful data. However at sufficient concentrations of inhibiting electrolyte, and in noncontaminated solutions, the interferometric method can yield valuable data about the mechanics of bubble coalescence and inhibition. I used a thin-film technique to study films in nonaqueous electrolyte solutions, and this method is therefore described in greater detail in Chapter 5.



Cain and Lee produced an early study using two captive bubbles on the ends of capillaries in KCl solutions, and pushing them together, measuring the change in film thickness with time using interferometry.<sup>18</sup> Recently Karakashev et al. have used microinterferometry to measure film lifetime and rupture thickness in aqueous inhibiting and non-inhibiting electrolytes over a range of concentrations.<sup>86</sup> The results show more stable films in inhibiting electrolytes, consistent with the results from bulk bubble coalescence.

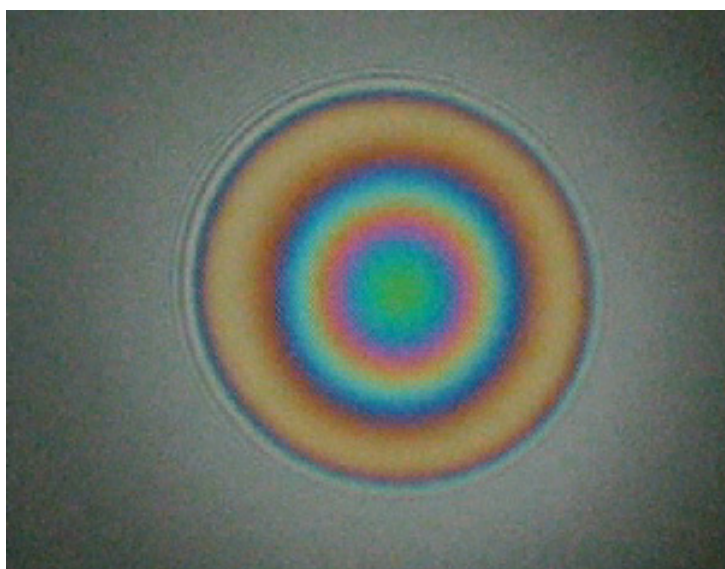


**Figure 1.10** Reflective interference fringes in a thin liquid film in air. This film shows increased thickness in the centre, indicative of a “dimple” during drainage. Beyond the boundaries of the film the liquid interfaces are curved rather than planar, and no interference pattern is seen. This is one frame of a 30 frames-per-second recording of film drainage.

#### 1.4.1.5 Atomic force microscopy

The use of atomic force microscopy (AFM) for force measurement at deformable surfaces is a recent development.<sup>87</sup> The technique can now be used to measure interaction between a bubble attached to the AFM cantilever tip, and another attached to a substrate.<sup>88</sup> In general the longer bubble lifetimes required for transfer of a bubble of suitable size to an AFM cantilever tip, and consistent force measurements, have limited the technique’s usefulness to surfactant-stabilised bubbles. Manor et al. have recently measured interactions in surfactant-free 1mM electrolyte (too low to exhibit coalescence

inhibition effects) and found dynamics equivalent to a partially mobile gas-water interface, that they attribute to some low-level surfactant contamination.<sup>89</sup> However, this technique holds promise for future measurements in surfactant-free and high electrolyte systems.

### **1.4.2 Electrolyte thin films at solid and liquid surfaces**

The gas-solution system of bubble coalescence is only one example of thin film formation in electrolyte solution. Other systems that contain surfactant-free electrolyte solutions may also exhibit ion specificity and thin film stabilisation, and it has been suggested that the study of such systems might be of use in bubble coalescence inhibition.<sup>41</sup> I here briefly summarise experiments in surfactant-free emulsions (liquid-liquid systems) featuring aqueous electrolyte as the continuous or the droplet phase, and thin films at solid surfaces (solid-liquid-gas systems). The solid-liquid-solid system in colloidal suspensions is another example of a solution thin film. However, no evidence of stabilisation of colloidal solids at high salt has been found. Rather, salt increase leads to increased attraction and coalescence in accordance with a decrease in electrostatic repulsion.<sup>30</sup> Therefore this system is not considered in any detail.

#### *1.4.2.1 Surfactant-free emulsions*

Some oil droplets may be stabilised in some very low electrolyte systems. Even in pure water, hydroxyl ions can adsorb at the oil-water interface, producing negatively-charged surfaces and an electrostatic barrier to coalescence of emulsion droplets.<sup>90</sup> (The same mechanism is believed to account for the negative potential of the gas-water interface, although this is a somewhat controversial topic.<sup>91</sup>) Relatively few studies have been carried out in surfactant-free emulsions sufficiently high in salt to compare with bubble coalescence results.

Oil droplets may be stabilised or destabilised by high electrolyte concentrations. Neumann et al. show convincingly that a surfactant-free monodisperse emulsion of poly(dimethylsiloxane) (PDMS) coalesces over two days in 0.1M NaCl solution but not at lower concentrations, suggesting an electrostatic repulsion that is screened at sufficiently high salt.<sup>92</sup> 0.1M NaCl was also found to lower the turbidity of squalane-

---

water mixtures – that is, salt reduced the initial formation of oil droplets from a bulk oil phase.<sup>93</sup> The authors attribute this to lower electrostatic repulsion at the interface, which makes droplet detachment less likely.

In contrast to these results, Nandi et al. report that a 5% NaCl solution (~0.9M) in the presence of glycerol stabilises oil-in-water emulsions against coalescence, but has no effect for the inverted water-in-oil system. This is attributed to a surface tension gradient in electrolyte thin films, and is consistent with results of bubble coalescence inhibition.<sup>94</sup>

An inhibiting effect at high salt concentrations is confirmed by Stevens et al. in the case of polar organic liquids but not nonpolar hydrocarbons.<sup>95</sup> They observed an increase in coalescence time (inhibition of coalescence) with increasing electrolyte from  $10^{-4}$ M to 1.0M, which is a larger concentration range than the bubble coalescence effects. Only bubble coalescence-inhibiting ( $\alpha\alpha$ -type) electrolytes were used in this study. Chen et al. considered the inverse system of dispersed aqueous droplets in an oil continuous phase.<sup>96</sup> Aqueous electrolyte droplets coalesce more rapidly with increasing electrolyte concentration for the most part, although at  $10^{-1}$ M there may be an increased droplet lifetime. There was no correlation with the electrolyte ionic strength, and the electrolyte effect varied depending on the polarity of the oil phase.<sup>96</sup>

As Stevens et al. found, the electrolyte effect in surfactant-free emulsions is dependent on the nature of the dispersed hydrophobic phase.<sup>95</sup> Neumann et al. also saw some low-salt stabilisation of PDMS but not of other oils,<sup>92</sup> while Clasohm et al. observed different stability of hydrocarbon and fluorocarbon droplets using the AFM, in the presence of 0.1M NaNO<sub>3</sub>.<sup>97</sup>

The results of surfactant-free emulsion studies do in some cases correlate with bubble coalescence measurements. In particular, Stevens et al.<sup>95</sup> and Nandi et al.<sup>94</sup> both report the possibility of stabilisation of oil droplets in water at high salt concentrations. However in many surfactant-free emulsions, electrolyte effects follow standard DLVO theory with electrostatic repulsion observed at larger Debye lengths (lower electrolyte

---

concentration). Therefore the coalescence inhibition is affected by the properties of the organic phase and the nature of the liquid-liquid interface. There is currently little information on ion specificity in oil-water systems, and so while the electrolyte inhibition mechanism may be related to that in bubble coalescence, the liquid-liquid system is not for the moment considered any further.

#### 1.4.2.2 *Thin aqueous films between a solid and a gas*

As with the surfactant-free emulsion system described above, few studies of thin films on solid surfaces exist that use electrolytes at sufficiently high concentration to compare with bubble coalescence experiments.

It has been found that surface hydrophobicity is an important determinant of water film stability on solids, even in cases of equal surface potential.<sup>98, 99</sup> Pure water<sup>100</sup> and electrolyte solution<sup>99</sup> films are stable on a hydrophilic substrate. The equilibrium film thickness decreases with increased ionic strength and screening of the electric double layer, in accordance with DLVO theory.<sup>101</sup>

Films that are stable in pure water and at all electrolyte concentrations do not provide a good analogy for the bubble coalescence system, which features the rupture of thin films between air-water surfaces. The air-water surface is highly hydrophobic<sup>102</sup> and so comparison with hydrophobic solids may be more productive. A pure water film between two hydrophobic surfaces or between a hydrophobic surface and a bubble is not stable and will rupture at sufficiently low thickness. Yoon and Yordan observe rupture on hydrophobic surfaces at around 200nm,<sup>100</sup> but other authors observe thinner films (down to tens of nanometres) even in non-wetting, low salt conditions.<sup>98, 99</sup> At hydrophobic methylated silica surfaces Blake and Kitchener find the film thickness to decrease with increasing electrolyte in accordance with DLVO theory, and at high electrolyte ( $\sim 10^{-1}$ M) no stable film can be formed.<sup>98</sup> Diakova et al. changed the surface treatment of silicon carbide and showed that at hydrophobic surfaces films with  $>0.01$ M electrolyte are unstable, while at hydrophilic surfaces wetting films are produced even at 1M salt.<sup>99</sup> These results are in direct contrast to the increased film stability seen at high concentrations in bubble systems.<sup>10</sup> In addition, no difference is observed between

---

the films in KCl, KOH and HCl on methylated silica, suggesting that ion specificity does not play a role in this case.<sup>98</sup>

It can be concluded that the available studies of surfactant-free electrolyte thin films at solid interfaces are not comparable to the system of bubbles in electrolyte solution. Thin film stabilisation occurs at low electrolyte concentrations, and film thickness is consistent with DLVO theory. Increased electrolyte destabilises films on hydrophobic surfaces, and the nature of the solid surface seems to control film properties to a far greater extent than the added electrolyte. Hence, no further study of films at solid surfaces is made in this thesis.

## **1.5 HYPOTHESES OF ELECTROLYTE COALESCENCE INHIBITION**

Any proposed mechanism for bubble coalescence inhibition should describe why some electrolytes inhibit coalescence at  $\sim 0.1\text{M}$ , while others have no effect – and why ion specificity depends upon the combination of ions.<sup>9, 10</sup> This section describes and evaluates some of the hypotheses that have been put forward concerning bubble coalescence inhibition. The reader is asked to bear in mind that some of the models and ideas are very much tied up with the work presented in this thesis, and these mechanisms are discussed in greater detail in the relevant experimental chapters and in the general discussion in Chapter 7.

### **1.5.1 Disjoining pressure and electrolyte bubble coalescence inhibition**

Electrolytes may change the equilibrium surface forces present in the thin film between bubbles by enhancing a repulsive component of the disjoining pressure, or by removing an attraction between surfaces that exists in pure water.

#### *1.5.1.1 Electric double layer repulsion*

At the concentrations of electrolyte at which coalescence is observed, the Debye length is on the order of one nanometre and electrostatic repulsion is therefore highly screened.<sup>9</sup> Miklavcic has proposed that increased coalescence inhibition in high salt can be explained by an increased double layer repulsion at higher salt concentrations, based

on a charge-reversal constant potential model of the gas-water interface.<sup>103</sup> However the maximum electrolyte considered is  $10^{-3}\text{M}$ , well below the  $10^{-1}\text{M}$  electrolyte at which bubble coalescence is observed. There is also no explanation given for ion specificity.<sup>103, 104</sup> Inhibiting electrolyte transition concentrations are found to scale with the inverse of a solution's ionic strength.<sup>63</sup> However Weissenborn and Pugh observe that ionic strength influences not only double layer forces, but also solution properties such as surface tension, ion hydration and solvent structural effects.<sup>60</sup> Therefore electrolyte bubble coalescence inhibition is not achieved via an increase in electric double layer repulsion.

#### *1.5.1.2 Hydration force*

As well as electric double layer forces, various other repulsive components of the disjoining pressure have been suggested as contributing to coalescence inhibition in electrolytes. One of these is the surface hydration force. This is a short-range steric repulsion in excess of that predicted by DLVO theory. It is attributed to structuring of solvent at a surface, and to the hydration shells of adsorbed ions.<sup>105</sup> It has been observed, for example, between mica surfaces at concentrations of electrolyte above  $10^{-3}\text{M}$ .<sup>106</sup> This force has not been observed to extend beyond 5nm into solution, the range of the first few layers of water molecules.<sup>106</sup> Therefore hydration force can only contribute to bubble stability at portions of the films approach that closely, while the average overall film separation is on the order of tens of nanometres.<sup>18</sup> If this were the stabilization mechanism one might expect the whole film eventually to thin down to the repulsion distance ( $\sim 10\text{nm}$ ) as observed in Newton black film formation in surfactants<sup>16</sup> – but this does not occur. In addition, while a hydration force has been observed at deformable bilayer and membrane surfaces, it is not known whether such a force exists at the air-solution interface.<sup>30</sup>

#### *1.5.1.3 Hydrophobic attraction*

The hydrophobic force (or forces) is an attraction between hydrophobic surfaces across a water thin film, that is greater than the van der Waals attraction.<sup>30</sup> Air-water interfaces are highly hydrophobic, and it has been suggested that a hydrophobic attraction is present between bubbles across a pure water film. Thus, under this hypothesis inhibiting

---

electrolytes work by reducing the hydrophobic attraction that would otherwise drive the bubbles to coalesce.<sup>9, 107</sup>

It was suggested by Craig<sup>41</sup> that a reduction in the hydrophobic attraction could be discounted as a coalescence inhibition mechanism because the long-range attraction between hydrophobic solid surfaces had been found to be unchanged by addition of electrolytes.<sup>108</sup> However such certainty was misplaced. There are now reckoned to be at least two hydrophobic attractive forces. The long-range one mentioned above as being undiminished by salt is now attributed to surface nanobubbles.<sup>109</sup> There yet remains a short-range “true hydrophobic” force observed between hydrophobic surfaces in water at surface separations  $\leq 10\text{nm}$ , the origin of which is as yet unexplained.<sup>109</sup> This means that a hydrophobic attraction may still be relevant to bubble coalescence in electrolyte solutions. The length scale of this force, however, makes it unlikely that it can drive the surface attraction and rupture of bubbles in pure water where coalescence takes place at mean surface separations on the order of  $100\text{nm}$ .<sup>52</sup> The short-range hydrophobic force has also not been observed at the air-water interface.

For completeness I mention the work of Wang and Yoon on hydrophobic forces in surfactant foam systems.<sup>110, 111</sup> It appears that the hydrophobic force to which they refer is a fitting parameter for adjusting drainage kinetics predicted by Reynolds theory (equation (1.3)) to align with experiment. The Reynolds model of thin film drainage assumes immobile, planar interfaces, and there are many theories that provide alternatives to Reynolds drainage without invoking a changing hydrophobic attraction. For instance, allowing partially mobile surfaces, deformability and a changing surface viscosity with solute concentration can all improve theoretical modeling of foam drainage.<sup>31, 112</sup> Therefore this work is not seen as strong evidence of a hydrophobic attraction between foam surfaces.

### 1.5.2 Hypotheses of ion specificity and bubble coalescence inhibition

Ion specificity is concerned with any differences in effects caused by ions of identical charge - any system where treatment of ions as point charges breaks down.<sup>11, 14</sup> Ion

---

specificity is often found to control behaviour at interfaces, such as biological membranes and proteins (for reviews see Kunz et al.<sup>14, 113</sup>). Different salts also change bulk solution properties such as viscosity, osmotic pressure, and activity coefficient.<sup>114</sup>

One of the earliest studies of specific-ion effects was made by Hofmeister (for an English translation, see Kunz et al.<sup>115</sup>). He arranged the anions in a “Hofmeister series” according to their ability to precipitate, or salt out, proteins from solution. For this reason specific-ion effects are sometimes known as Hofmeister effects. It is often the case that ion specificity is controlled by either the anion or the cation in solution, and findings are commonly presented as a series of increasingly effective anions or cations in the presence of a given counterion.<sup>116</sup> While the combining rules determined by Craig et al.<sup>9, 10</sup> do not align with Hofmeister series of anions or cations, it is thought possible that there may be some ion property/s that relates to both bubble coalescence inhibition and more traditional specific ion effects in solution. This relationship is explored in Chapter 7.

#### 1.5.2.1 *Surface tension gradient*

Solutions of different electrolytes at the same concentration will have different surface tensions. The surface tension gradient,  $(d\gamma/dc)$ , of electrolytes is therefore a fundamental example of ion specificity in solution.<sup>11</sup>

Weissenborn and Pugh determined surface tension gradient,  $(d\gamma/dc)$ , in electrolyte solutions, and compared the results to bubble coalescence inhibition data.<sup>59, 60</sup> Surface tension gradient itself shows no correlation with bubble coalescence inhibition – some inhibiting electrolytes increase and some decrease the surface tension of solution. There is an inverse correlation between  $(d\gamma/dc)^2$  and transition concentration,<sup>62</sup> although the correlation is only moderate.<sup>60</sup> Weissenborn and Pugh showed that the surface tension gradient in active concentrations of inhibiting electrolytes, was insufficient to cause Marangoni effects and drive surface immobilisation, as occurs in surfactant films.<sup>60</sup> However, surface tension gradient is related to several other solution and interfacial properties, and so the correlation with transition concentration may indicate some other



---

inhibition mechanism. Experiments to investigate the correlation between  $(d\gamma/dc)^2$  and coalescence inhibition are described in Chapter 2.

Bubble coalescence inhibition via changes in solution surface tension is a dynamics-related mechanism, as electrolytes act on the drainage and rupture processes of the thin film in a non-equilibrium state. This mechanism is therefore distinct from those outlined in section 1.5.1 above, that propose a change in quasistatic surface forces in the presence of inhibiting electrolyte. During film drainage the gas-water interface is stretched and deformed, leading to non-equilibrium variations in solute concentration across the interface, and between the interface and the bulk solution.<sup>17</sup> These variations in concentration drive variations in surface tension. Changes in surface tension may act on the film drainage process by creating a force in opposition to film drainage (Marangoni effects);<sup>25</sup> alternatively (or additionally) the surface tension variation may affect surface elasticity and so inhibit capillary wave growth and thin film rupture.<sup>56</sup>

#### 1.5.2.2 *Bulk solvent structure*

Dissolved ions change the solvent structure in their immediate vicinity when they insert into the solvent and are surrounded by a hydration shell.<sup>117</sup> The solvent interactions depend upon such factors as solvent affinity, charge, polarisability and ion size.<sup>118</sup> There is a notion that ions may have an effect on solution structure at distances beyond the solvation shell, by disrupting the hydrogen-bonding network of water.<sup>119</sup> Ions may be placed along a continuum from structure-breakers to structure-makers.

It was originally suggested by Lessard and Zieminski that inhibiting electrolytes may impose structure on the water in the thin film between bubbles to restrict drainage and inhibit coalescence.<sup>63</sup> They correlated transition concentrations of inhibiting electrolytes with indicators of solvent structure – molar entropy of solvation; and the self-diffusion coefficient of water. A decrease in entropy indicates an increase in solvent ordering, while self-diffusion of water is retarded in the presence of greater structure. These correlations do not hold up when a wider range of electrolytes is considered, including non-inhibiting salts. For example, the molar entropy of hydration of nitrate and chlorate anions is almost identical (+95 and +99 J K<sup>-1</sup> mol<sup>-1</sup>, respectively<sup>120</sup>) yet in the presence

of a given cation they have very different effects on bubble coalescence, with  $\text{NO}_3^-$  being classified as  $\alpha$  and  $\text{ClO}_3^-$  as a  $\beta$  anion (see Table 1.2).

**Table 1.2**  $\alpha$  and  $\beta$  ion assignments of single electrolytes in water. Anions ordered from structure-breaking (top) to structure-making (bottom) and cations ordered from structure-breaking (left) to structure-making (right).<sup>a</sup>

Ions	$\text{Ca}^{2+}$	$\text{Mg}^{2+}$	$\text{H}^+$	$\text{Li}^+$	$\text{Na}^+$	$\text{K}^+$	$\text{Cs}^+$	$\text{NH}_4^+$	$(\text{CH}_3)\text{NH}_3^+$	$(\text{CH}_3)_2\text{NH}_2^+$	$(\text{CH}_3)_3\text{NH}^+$	$(\text{CH}_3)_4\text{N}^+$
Assignment	$\alpha$	$\alpha$	$\beta$	$\alpha$	$\alpha$	$\alpha$	$\alpha$	$\alpha$	$\beta$	$\beta$	$\beta$	$\beta$
$\text{SCN}^-$	$\beta$				x			x				
$\text{ClO}_4^-$	$\beta$	x	✓		x			x				
$\text{I}^-$	$\alpha$			✓	✓	✓						
$\text{ClO}_3^-$	$\beta$				x							
$\text{NO}_3^-$	$\alpha$	✓	x	✓	✓	✓						
$\text{Br}^-$	$\alpha$		x		✓	✓	✓					x
$\text{Cl}^-$	$\alpha$	✓	✓	x	✓	✓	✓		x	x	x	x
$\text{CH}_3\text{COO}^-$	$\beta$		x	✓	x	x	x	x				✓
$\text{IO}_3^-$	$\alpha$				✓							
$\text{OH}^-$	$\alpha$				✓	✓						
$\text{F}^-$	$\alpha$				✓							
$\text{SO}_4^{2-}$	$\alpha$		✓	x	✓	✓						
$(\text{COO}_2)^{2-}$	$\alpha$		x			✓						

✓=inhibit coalescence  
 $\alpha\alpha, \beta\beta = \checkmark$   
x=no inhibition  
 $\alpha\beta, \beta\alpha = \times$

<sup>a</sup> Ion series taken from various sources.<sup>14, 116, 121</sup>

Table 1.2 reproduces the  $\alpha$  and  $\beta$  assignments in Table 1.1, but lists anions and cations in order of their effect on protein solubility, from salting-in (structure-breaking) to salting-out (structure-making). It can be seen that the  $\alpha$  and  $\beta$  designations do not coincide with the effect of the ions on water structure. The importance of water structure in bubble coalescence inhibition is discussed further in Chapter 3.

### 1.5.2.3 Solution viscosity

Changes in bulk viscosity have been considered as a mechanism by which electrolytes in solution can inhibit bubble coalescence. Increased viscosity will reduce the rate of thin film drainage, and may also affect the diffusion and adsorption of ions at the interface.<sup>60</sup> Craig et al. showed convincingly that there is no relationship between transition concentration and solution viscosity – indeed, both increases and decreases in viscosity are observed on addition of inhibiting electrolyte.<sup>9</sup>

---

#### 1.5.2.4 *Gas solubility*

Electrolytes change the solubility of gas molecules in solution; most electrolytes lower the concentration of dissolved gas with the degree of “salting-out” depending upon the identity of the electrolyte.<sup>60</sup> Qualitatively gas dissolution can be viewed as the creation of a single-molecule cavity in the water network, and the electrolyte effect can hence be related to both changes in surface tension and changes in bulk water structure in the presence of ions.

A number of explanations have been advanced for how a reduction in dissolved gas may decrease coalescence. It is thought that dissolved gas may affect the gas-solution interfacial properties.<sup>80, 122</sup> Alternatively, higher concentrations of dissolved gas may lead to nucleation of ‘microbubbles’ in the thin film, as part of a proposed rupture mechanism.<sup>60</sup> The long-range hydrophobic attraction between hydrophobic solid and oil surfaces in water has been found to depend upon the presence of dissolved gas to create surface nanobubbles (section 1.5.1.3 above), and so a reduction in dissolved gas in the presence of inhibiting electrolytes could reduce the surface attraction and so inhibit coalescence.

Weissenborn and Pugh showed that the inhibiting electrolytes with the greatest effect on dissolved gas also have the lowest transition concentrations.<sup>60</sup> Craig et al. measured the transition concentration in inhibiting salts using different gases in a bubble column apparatus. Even when solubility changed substantially the effect on transition concentration was only small.<sup>9</sup> However, because the transition concentration in a bubble column experiment is defined relative to values in pure water and at high salt, there is no comparison between absolute coalescence in different gases. There is some correlation with the gas diffusivity rather than solubility,<sup>122</sup> and it was hypothesised that reduction in gas diffusivity might hinder the growth and bridging of interfacial capillary waves. Sagert and Quinn showed that some gases can act as surface active species that change bubble stability through monolayer formation; N<sub>2</sub>, which was used for the studies conducted in this thesis, does not interact with the surface.<sup>50</sup>

The role of dissolved gas in bubble coalescence inhibition is still uncertain. Gas solubility studies are complex, time-consuming and require special equipment that was not available.<sup>123</sup> Gas solubility is related to many other electrolyte effects in solution (such as surface tension gradient and electrolyte solvation), so a correlation between gas solubility and coalescence inhibition does not necessarily point to a mechanism involving dissolved gas.

#### *1.5.2.5 Ions at the interface*

Traditionally, the gas-solution interface has been modelled as devoid of ions in electrolytes that increase surface tension – in accordance with the Gibbs adsorption isotherm (equation (1.2)). Recently it has been shown, however, that some ions can in fact accumulate at the air-water interface, and have lower concentrations in the subsurface region so that overall interfacial depletion is still observed.<sup>124, 125</sup> It has been hypothesised that surface ions may influence bubble coalescence inhibition – possibly by changing local solvent structure and dynamics within a few angstroms of the interface, or by creating a surface repulsion.<sup>126</sup> The relationship between ions at the interface and bubble coalescence inhibition is considered in Chapter 2.

## **1.6 SUMMARY**

Bubble coalescence is inhibited by some electrolytes at concentrations in the range of 0.01-0.5M. This is not consistent with standard theories of thin film drainage, which predict that thin films will not be stable in electrolyte solution.

The general characteristics of ion specific bubble coalescence inhibition are:

- Coalescence takes place at moderate to high electrolyte concentrations. Some electrolytes inhibit bubble coalescence in the concentration range 0.01M – 0.5M, with transition concentration in univalent electrolytes on the order of 0.1M. At this concentration the Debye length is on the order of 1nm and surface double layer repulsions are highly screened.
- The thin film between bubbles ruptures in inhibiting electrolyte at thicknesses of tens of nanometres, and film lifetimes are on the order of 1 second.

- 
- Coalescence inhibition is ion specific. Some electrolytes show no effect relative to pure water, up to 0.5M concentration. The ion specificity depends on both the cation and the anion, and is described by empirical combining rules.

A range of mechanisms have been proposed to explain bubble coalescence inhibition in electrolytes. However none of them has fully explained all of the experimental observations. The major categories of proposals are:

- Inhibiting electrolytes increase the repulsive component of the disjoining pressure. Electric double layer repulsion, hydration forces and a reduction in hydrophobic attraction have all been considered as possibilities.
- Inhibiting electrolytes affect the drainage and rupture of the dynamic (non-equilibrium) thin film. Variations in interfacial concentration during film drainage can change interfacial mobility and deformability. This would lead to retardation of drainage or inhibition of the film rupture process.
- Inhibiting electrolytes change the solution properties. By altering such solution properties as bulk water structure and gas solubility, electrolytes affect the thin film drainage or the surface interaction sufficiently to inhibit coalescence over the lifetime of a bubble collision.

These mechanisms are not mutually exclusive – surfactants, for example, are known to alter disjoining pressure as well as surface rheology during dynamic drainage.<sup>17</sup>

## 1.7 THESIS OUTLINE

The five following chapters (Chapter 2 to Chapter 6) describe a range of experiments designed to investigate bubble coalescence inhibition by electrolytes.

*Chapter 2* describes a series of bubble column experiments was carried out in mixed electrolytes. Surface tension measurements in the mixtures were also made, enabling us to test a possible correlation between bubble coalescence inhibition and surface tension gradient. The mixed electrolyte data also provides a basic test of theories concerning ion

separation at the interface and bubble coalescence. This chapter contains a description of the bubble column apparatus for measuring coalescence inhibition.

*Chapter 3* looks at bubble coalescence in non-electrolyte solutions, including urea, sucrose and other sugars. Such solutes, like Hofmeister ions, can increase or decrease protein solubility, and so we investigated their effect in the bubble coalescence system where ion specificity is also found.

*Chapter 4* moves to a consideration of nonaqueous electrolyte systems, in order to determine the importance of solvent structure and surface forces in bubble coalescence inhibition.

In *Chapter 5*, I describe further experiments in nonaqueous electrolyte solutions, using a thin film balance to study drainage kinetics and rupture of a single film between gas interfaces.

*Chapter 6* reports a study on interfacial mobility at the gas-solution interface. We tested the effect of electrolytes on bubble interfacial mobility by measuring the single bubble terminal rise velocity, and comparing it to models for a mobile and an immobile interface.

In each of the above chapters the discussion and conclusions are limited only to what may be drawn from that particular set of results (and previous literature), without attempting to reconcile data from the other experiments. *Chapter 7* brings all of the results together in a general discussion, and also presents a hypothesis for the mechanism of bubble coalescence inhibition that arises out of consolidation of my experimental results and recent developments in the literature.

A final summary of the results and conclusions reached in this thesis is presented in *Chapter 8*.

---

## Chapter 2 Bubble Coalescence Inhibition in Mixed Electrolytes

---

### 2.1 PREAMBLE

This chapter describes a series of experiments on bubble coalescence in mixed electrolytes. Section 2.2 describes in some detail the bubble column instrument used in this and later experimental studies. Following this, I present the results of coalescence measurements in mixed electrolytes. Many real-world systems (for example, sea water) comprise bubbles in electrolyte mixtures, so it is useful to test whether the empirical  $\alpha$  and  $\beta$  cation and anion designations from single electrolytes, have any predictive value. The mixture bubble coalescence inhibition results are compared with surface tension gradient data. By comparing the surface tension gradient and coalescence inhibition in mixed electrolytes, we could test the hypothesis that coalescence inhibition correlates with the square of surface tension gradient,  $(d\gamma/dc)^2$  (where  $\gamma$  is surface tension and  $c$  is electrolyte concentration).<sup>56</sup> Coalescence in mixed electrolyte solutions is also considered in the context of recent hypotheses concerning ion positioning within the interfacial region. Many of the results reported in this chapter have been published elsewhere.<sup>58</sup>

### 2.2 BUBBLE COLUMN APPARATUS

Many of my studies on bubble coalescence were carried out using a purpose-built bubble column apparatus (see Figure 2.1 for a schematic, and Figure 1.9 in the previous chapter for a photograph). This apparatus was first used by Craig et al.<sup>9, 10</sup> and was improved by Dalton.<sup>127</sup> The general principle of the bubble column is that bubbles are produced at a frit in the base of the column, and undergo collisions that may result in coalescence. The degree of coalescence is detected in our method as a difference in

solution turbidity, with increased turbidity (small non-coalesced bubbles) causing greater scattering of a laser beam passed through the column.

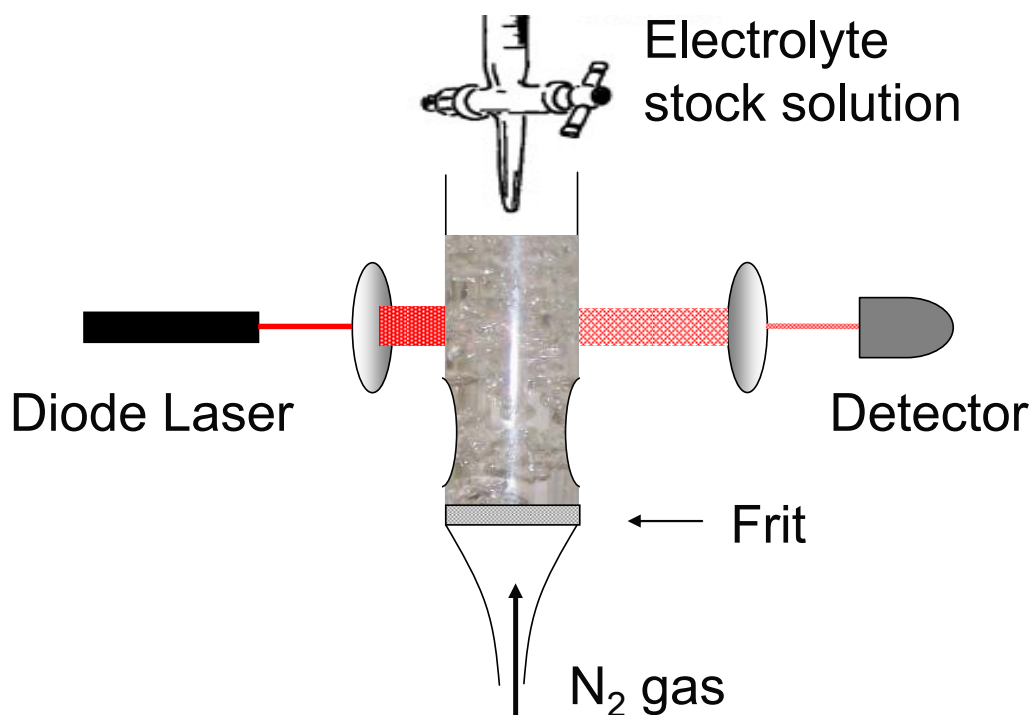


**Figure 2.1** Schematic of bubble coalescence apparatus. Small bubbles are produced at the frit and rise in the column, passing through the constriction that promotes bubble collisions. In pure water they rapidly coalesce such that the bubbles breaking the laser beam are large and few in number. In this case, most of the light is transmitted and strikes the photodiode detector. When coalescence is inhibited, the bubbles remain small and numerous, resulting in a large amount of scattering and low light intensity at the detector.

### 2.2.1 Technique choice

The bubble column turbidity technique has a number of advantages over other experimental methods. Compared to two-bubble experiments and video analysis, it is simple and fast to collect a large amount of data and to monitor the effect of changing the concentration of any component. The average outcome of many bubble collisions is produced by the nature of the technique, so the results are statistically rigorous. A great



---

advantage is that the system is self-cleaning: many bubbles are sent through the solution and collect any surface-active material present, transporting it to the glass above the solution interface. Indeed, it is possible to see the top of the bubble column become non-wetting after adding a contaminated electrolyte. In many other instruments, an interface may be exposed for some time and so accumulate any contamination present. It is less ideal that bubble size and interaction time are not known exactly, and the technique is perhaps best utilised as one of a suite, highlighting trends that would repay closer study.

## 2.2.2 Instrument details

### 2.2.2.1 *Laser scattering*

At the air-water interface there is a large, rapid change in refractive index, leading to scattering and reflection of light from the bubble surfaces. For a given gas flow, multiple small bubbles will scatter more light than fewer, larger bubbles. A 670nm solid state diode laser beam is used as the light source. It is passed through a collimating lens (6cm diameter) to expand the beam to interact with many bubbles (see Figure 2.2). The transmitted beam is condensed by a similar lens, and falls onto a photodiode detector, after which the signal is converted to a voltage and sent to the analysis computer. The photodiode is covered by a narrow-band filter to prevent ambient light from affecting the collected signal.

### 2.2.2.2 *Column and gas flow*

Dry nitrogen gas obtained as boiloff from a liquid N<sub>2</sub> tank is run through Teflon and glass tubing, and introduced to the bubble column via a sintered glass frit (type 2) in the base of a cylindrical column of 25mm internal diameter, and 220mm height. The column sides are flattened at a height of 50mm; this irregularity disrupts laminar flow and promotes bubble collision. The column is housed in a larger Perspex box with small openings, and the solution is thus in a continually replenished clean nitrogen environment. Changes to solute concentration are made by introducing stock solution from a burette into the column, and allowing time for mixing. Gas flow into the bubble column was measured by the rising soap film method, whereby the rate of rise of a soap

film through a burette, driven by the gas, is timed. The flow was on the order of  $10\text{mLs}^{-1}$  for all experiments in the bubble column. It can be altered to check the dependence of the transition concentration on gas flow. The transition concentration between full coalescence and minimum coalescence, remained essentially constant with changing gas flow, confirming the results of Craig et al.<sup>9</sup>

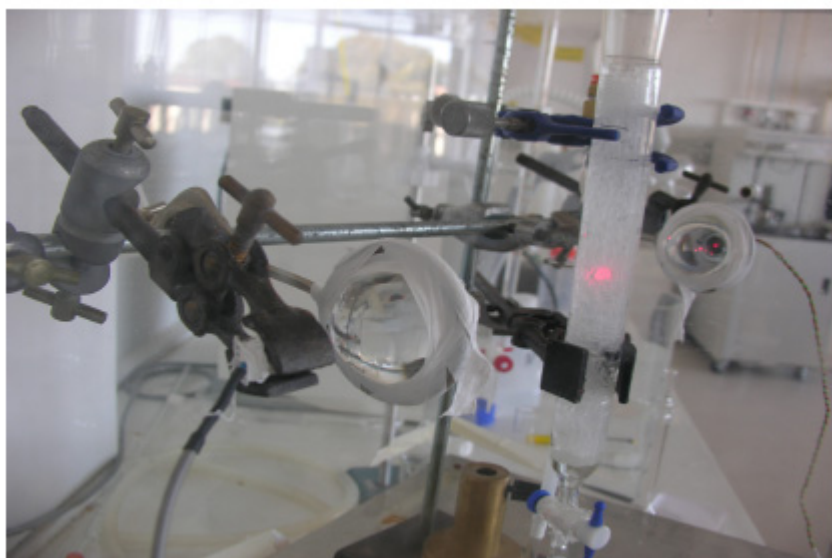


**Figure 2.2** Bubble column showing laser and collimating lens on the right, and condensing lens and photodiode collector on the left. Photo from Dalton.<sup>127</sup>

The system is sensitive to bubble column positioning. It was most important to keep the column position constant during the course of an experiment, as slight changes to its position could, for example, leave the column slightly off-vertical and so alter the gas flow rate, bubble stream and collision frequency, as well as the path travelled by the laser beam. Markings on the outside of the column were used to keep positioning, and in each experiment bubble coalescence is first measured in pure solvent to ensure that the coalescence signal was constant; however between experiments done years apart there may be variations in electrolyte transition concentration.

### 2.2.2.3 *Data analysis*

The analysis program used was created by Craig and Dalton in the LabVIEW graphical programming environment.<sup>127</sup> The data recorded by the program consists of (i) the photodiode signal read as a voltage through an amplifier; and (ii) the nitrogen gas flow rate just prior to its introduction into the bubble column, using a flow meter that

---

recorded flow as a voltage. The photodiode raw signal varies with time, as it depends on the bubbles passing through the laser beam at any instant. The signal is collected at 60kHz, and an average data point is recorded every three seconds (180000 samples). A further average is generally taken over 30-40 data points (90-120 seconds). The time course of coalescence can be monitored by eye, and is generally stable well within 60 seconds of a concentration change. Longer term stability was also checked in some samples by taking two, 90 second averages at different times. The coalescence was found to be stable over  $\geq 2$  hours.

### **2.2.3 Experimental protocol**

The cleaning, set-up and data collection steps followed in a typical experiment are here outlined. Where changes were made (as, for instance, when nonaqueous solvents are used in Chapter 4) they are described in the appropriate section.

#### *2.2.3.1 Cleaning*

The column is cleaned by leaving in 10% w/w NaOH solution, overnight. It is then rinsed with copious water, rinsed again with distilled ethanol and dried with a stream of N<sub>2</sub> gas. Drying is necessary because varying moisture below the frit could affect the gas flow during bubble coalescence measurements. In between experiments on the same day, it was found sufficient to rinse the column with copious water, so long as the water was not left to percolate through the frit and into the column base.

#### *2.2.3.2 Experiments*

A bubble column measurement begins with addition of 41.0mL of pure solvent into the column, with gas flowing. At this liquid volume the laser detection is far enough above the flattened region of the glass column that it is insensitive to the induced turbulence, and far enough below the interface that the signal is not prone to “edge effects” – where the froth and bubble bursting at the top of the liquid can change the bubble sizes present. The photodiode signal is checked in pure solvent; an anomalous record indicates contamination or improper alignment of the bubble column and gas tubing, and the cleaning and column setup steps are repeated until a satisfactory result is obtained.

Stock electrolyte solution is made up and added in small aliquots via burette. At least 60 seconds is allowed for mixing, though generally the coalescence signal has stabilised within ten seconds. Stock solution is added until a stable coalescence value is attained (high inhibition), or the top of the column is reached.

## 2.3 MIXED ELECTROLYTE EXPERIMENTS

### 2.3.1 Introduction

#### 2.3.1.1 *Surface tension gradient*

A correlation between the transition concentration of inhibiting electrolytes and the inverse square of surface tension gradient,  $(d\gamma/dc)^{-2}$ , was first noted by Marrucci and Nicodemo in 1967.<sup>62</sup> In single electrolytes that inhibit bubble coalescence, Weissenborn and Pugh found a moderate correlation ( $R=0.74$ ) between transition concentration and  $(d\gamma/dc)^{-2}$ . These authors further noted that noninhibiting electrolytes all have a small effect on surface tension, with  $(d\gamma/dc)^2 \leq 1 \text{ mN}^2 \text{ m}^{-2} \text{ M}^{-2}$ . However, and as Weissenborn and Pugh amply demonstrate, surface tension gradient also shows moderate correlation with many other properties of electrolyte solutions, including ionic strength, gas solubility, electrolyte activity, viscosity, and hydration entropy.<sup>59, 60</sup> Therefore the importance of surface tension gradient per se has been disputed. Measuring the correlation in electrolyte mixtures is a simple and powerful way to expand the number of systems that can be tested.

Supposing that surface tension gradient in electrolyte solutions drives bubble coalescence inhibition, there have been a number of mechanisms proposed by which  $(d\gamma/dc)^2$  can exert an effect. Christenson et al.<sup>56</sup> showed that the addition of electrolytes results in an increase in the Gibbs Elasticity,  $E$ , of an interface and that this elasticity is proportional to  $(d\gamma/dc)^2$ :

$$E = \frac{4c(d\gamma/dc)^2}{kTD} \quad (2.1)$$

---

Here  $k$  is Boltzmann's constant,  $T$  is temperature and  $D$  is a measure of interfacial thickness related to the shearing of the interface.<sup>56</sup> Higher values of  $E$  should be associated with increased damping of capillary waves in a solution, and so this was proposed as a means by which electrolytes can inhibit the rupture event during a bubble collision.<sup>41</sup> However it has long been thought that in electrolyte the small gradient in surface tension and hence minor changes in elasticity are insufficient to confer stability.<sup>128</sup>

More recently, Stoyanov and Denkov<sup>129</sup> argued that the drainage and the hydrodynamic stability of thin liquid films are related to surface deformation and mobility more generally, and showed that these properties depend upon diffusion of solute – which is also proportional to  $(dy/dc)^2$ .

In early models for electrolyte coalescence inhibition it was proposed that at the transition concentration the gas-solution interface is immobilised via Marangoni effects, in a way comparable to surfactant coalescence inhibition.<sup>25</sup> This theory also leads to a correlation between transition concentration and  $(dy/dc)^{-2}$ ; <sup>74</sup> however the small surface tension gradient in electrolytes is now believed to be insufficient to immobilise the interface.<sup>60</sup>

Electrolytes are known to reduce the solubility of dissolved gases in solution and it has been suggested that dissolved gas plays an important role in the coalescence of bubbles.<sup>10, 60</sup> The solubility of gas in solution is related to the energy of producing a cavity for the gas molecule, which depends upon the intermolecular forces within the liquid and therefore is also expected to be related to the interfacial tension.

We investigated bubble coalescence in mixed electrolytes to determine the rigour of the correlation between coalescence inhibition and surface tension, by expanding the range of systems tested. It was also of interest to determine whether ion assignments from single electrolytes can be used to predict coalescence in mixtures. (These mixed electrolyte experiments were also used to evaluate an hypothesis concerning ion interfacial positioning and bubble coalescence inhibition;<sup>38</sup> because the scientific

---

background is lengthy and complex and because this evaluation was carried out after the fact, it is relegated to Section 2.3.4.)

### 2.3.1.2 *Ion assignments in mixed electrolytes*

The mixed electrolyte experiments are also used to further investigate the ion  $\alpha$  and  $\beta$  assignments. Bubble coalescence behaviour in single electrolytes is determined by the combination of *both* ions and any particular ion can participate in bubble coalescence inhibition or bubble coalescence, depending on the ion with which it is partnered. For example a  $\alpha\alpha$  electrolyte such as NaCl or a  $\beta\beta$  electrolyte such as perchloric acid prevent coalescence, but the electrolytes made from the cross combination of the above electrolytes are NaClO<sub>4</sub> ( $\alpha\beta$ ) and HCl ( $\beta\alpha$ ), which have no effect on bubble coalescence. This raises the question, if the ions Na<sup>+</sup>, Cl<sup>-</sup>, H<sup>+</sup> and ClO<sub>4</sub><sup>-</sup> are all added in equal numbers what behaviour results? Is bubble coalescence inhibited? We aimed to determine if the empirical assignments developed for single electrolyte systems provide a means to characterise mixed electrolyte systems: if combinations having the same mixture of  $\alpha$  and  $\beta$  cations and anions exhibit a consistent and predictable effect on bubble coalescence, then the  $\alpha$  and  $\beta$  designations have a meaning beyond single electrolyte systems.

### 2.3.2 **Methods and materials**

Analytical Grade electrolytes were used and roasted to remove organic contaminants wherever possible, and freeze-dried to remove excess water when necessary. Roasting was carried out at temperatures up to 600°C and sustained for more than four hours. Acids and some salts were used as provided. All water used in the bubble coalescence studies was purified using a Milli-Q gradient system. Water used in the surface tension studies was purified by filtering through a coarse filter, charcoal and a reverse osmosis membrane before distillation and a final purification using a Milli-Q system.

The surface tension of electrolyte solutions were determined by the maximum bubble pressure method<sup>130</sup> using a custom built device (for a full description see Henry et al.<sup>58</sup>) The radius of the capillary was calibrated from the measurement of maximum bubble

---

pressure in pure water using the value of  $72.75 \text{ mN m}^{-1}$  for the surface tension. The average of the maximum pressure values recorded for each bubble was used to determine the surface tension of the solution using the Laplace equation.

The bubble column was used as set out in Section 2.2 above. The flow rate of nitrogen for mixed electrolyte experiments was  $14 \text{ mL s}^{-1}$ . When equimolar electrolyte mixtures were being investigated, a mixture was made up as stock solution (between 0.5M and 3.0M in each salt) and added to an initial amount of pure water. Experiments were only run when initial detector voltage in pure water showed that the system was correctly aligned and free from contamination.

### 2.3.3 Coalescence inhibition and surface tension gradient

#### 2.3.3.1 *Surface tension gradient and inhibition in single electrolytes*

The surface tensions of 28 different electrolytes in water at a range of concentrations were measured. Despite the high level of internal consistency in our data and in the data of Weissenborn and Pugh<sup>59, 60</sup> we find that the measurements do not agree within experimental error ( $\pm 0.1 \text{ mN m}^{-1} \text{ M}^{-1}$  in  $d\gamma/dc$ ) in about a third of the cases. If the error in the measurement of  $d\gamma/dc$  is taken as 10% we find agreement between our data and the results of Weissenborn and Pugh in all cases other than those with acetate ions, which generally give non-linear plots and therefore do not have a constant surface tension gradient. As our interpretation of surface tension data for electrolyte systems does not depend on a precision in measuring  $d\gamma/dc$  of better than 10%, such interpretation can be made with confidence. We find that the electrolytes are naturally separated into those that inhibit bubble coalescence (large values of  $(d\gamma/dc)^2$ ) and those that do not (small values of  $(d\gamma/dc)^2$ ). In all cases when  $(d\gamma/dc)^2 < 1.0 \text{ mN}^2 \text{ m}^{-2} \text{ M}^{-2}$  no effect on bubble coalescence is observed. However the correlation between  $(d\gamma/dc)^2$  and the transition concentration for an inhibiting electrolyte, shown in Figure 2.3, is only moderate ( $R=0.71$ ). A list of single electrolyte surface tension measurements can be found in the Appendix.

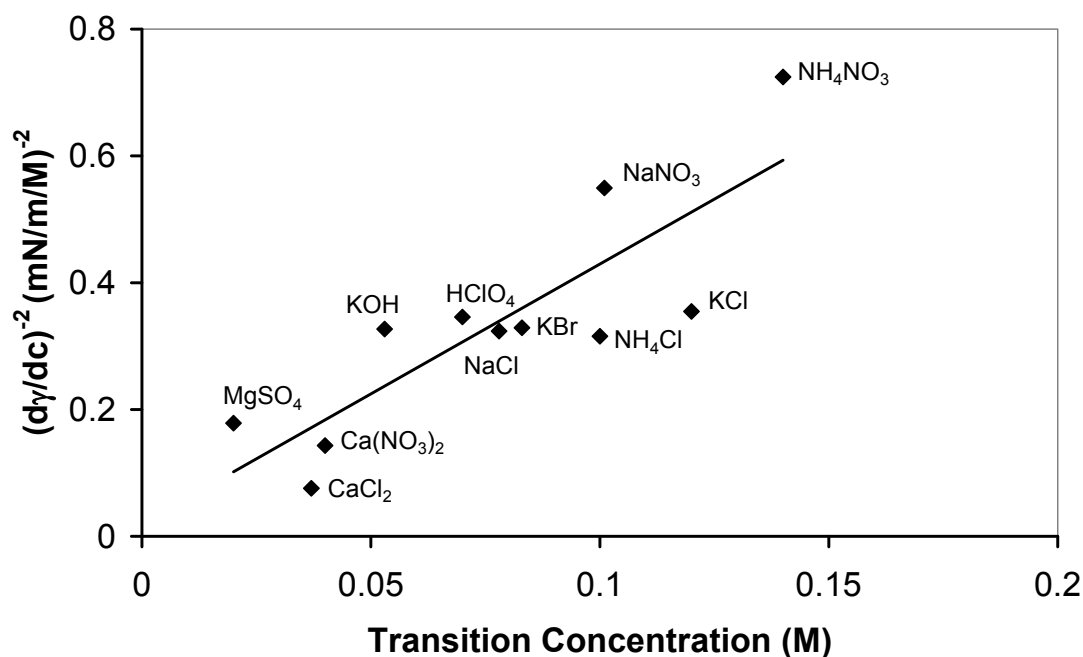


**Figure 2.3** Correlation between  $(d\gamma/dc)^2$  and transition concentration of inhibiting single electrolytes. Correlation coefficient  $R = 0.71$ . Some of the transition concentrations are taken from Craig et al.<sup>9</sup> The transition concentration is defined at 50% coalescence.

### 2.3.3.2 Surface tension and bubble coalescence inhibition in mixed electrolytes

We tested the correlation between  $(d\gamma/dc)^2$  and bubble coalescence in mixed electrolyte systems. Electrolyte systems were chosen to represent different possible combinations of  $\alpha$  and  $\beta$  ions. For most combinations at least two mixtures, featuring either three or four ionic species, were studied. In all cases the same combination of  $\alpha$  and  $\beta$  ions led to the same effect on bubble coalescence, and similar values for  $(d\gamma/dc)$  (see Table 2.1). It was not possible to test all combinations. For instance, any combination of  $H^+$  and  $CH_3COO^-$  produces undissociated acetic acid which is surface active and causes foaming even at low concentrations. A mixture of two different  $\beta\beta$  electrolytes was not used, because any combination of four currently identified and available  $\beta$  ions would involve formation of either acetic acid or the insoluble tetramethylammonium perchlorate.



**Table 2.1** Coalescence inhibition and  $(d\gamma/dc)^2$  in mixed electrolytes grouped in  $\alpha$  and  $\beta$  ion combinations

Mixture of Ions	Electrolytes	$d\gamma/dc$ (mN/m/M)	$(d\gamma/dc)^2$ (mN/m/M) <sup>2</sup>	Prediction <sup>a</sup> (✓=inhibit if $(d\gamma/dc)^2 \geq 1$ )	Coalescence Inhibition	Transition Conc. (M)
$\alpha\alpha, \alpha\alpha$	KOH+NaCl	1.6	2.49	✓	✓	0.05
	NaCl + Ca(NO <sub>3</sub> ) <sub>2</sub>				✓	0.041
$\alpha\alpha, \alpha\beta$	KCl+CH <sub>3</sub> COONa	1.01	1.02	✓		
	KCl+NaClO <sub>3</sub>	1.2	1.46	✓		
	NaCl+NaClO <sub>4</sub>				✓	0.103
	NaClO <sub>4</sub> +Ca(NO <sub>3</sub> ) <sub>2</sub>				✓	0.084
	NaCl+NaClO <sub>3</sub>				✓	0.105
	NaNO <sub>3</sub> + Ca(ClO <sub>4</sub> ) <sub>2</sub>				✓	0.16
$\alpha\alpha, \beta\alpha$	NaCl + HCl	0.45	0.21	✗	✓	0.083
	NaNO <sub>3</sub> + HCl	0.28	0.079	✗	✓	0.070
$\alpha\alpha, \beta\beta$ or $\alpha\beta, \beta\alpha$	NaCl+HClO <sub>4</sub> (Equivalent to) NaClO <sub>4</sub> +HCl	-0.23	0.055	✗	✓	0.053
	KClO <sub>3</sub> +HNO <sub>3</sub>	-0.23	0.052	✗	✓	0.071
	NaClO <sub>3</sub> +HCl	-0.18	0.033	✗		
	KCl+HClO <sub>4</sub>	-0.17	0.027	✗		
	Ca(ClO <sub>4</sub> ) <sub>2</sub> + HCl	-0.32 <sup>b</sup>	0.10 <sup>b</sup>	✗		
	Ca(ClO <sub>4</sub> ) <sub>2</sub> + HNO <sub>3</sub>				✓	0.040
	Ca(NO <sub>3</sub> ) <sub>2</sub> + HClO <sub>4</sub>				✓	0.038
	NaOH+HClO <sub>4</sub> <sup>c</sup>	0.33	0.11	✗		
	NaOH+CH <sub>3</sub> COOH <sup>c</sup>	0.72	0.52	✗		
	CH <sub>3</sub> COONa+HCl <sup>d</sup>	6.9	48.25	✓		
KCl+CH <sub>3</sub> COOH <sup>d</sup>	8.0	64.04	✓			
$\alpha\beta, \alpha\beta$	CH <sub>3</sub> COOK+NaClO <sub>3</sub>	0.66	0.44	✗	✗	NI
	NaClO <sub>3</sub> +NaClO <sub>4</sub>				✗	NI
	CH <sub>3</sub> COONa+CH <sub>3</sub> COONH <sub>4</sub>				✗	NI
	CH <sub>3</sub> COONa + Ca(ClO <sub>4</sub> ) <sub>2</sub>	0.49 <sup>b</sup>	0.24 <sup>b</sup>	✗		
$\alpha\beta, \beta\beta$	NaClO <sub>3</sub> +HClO <sub>4</sub>	-0.69	0.48	✗	✓	0.054
	CH <sub>3</sub> COONa+HClO <sub>4</sub> <sup>d</sup>	6.3	39.66	✓		
	NaClO <sub>3</sub> +CH <sub>3</sub> COOH <sup>d</sup>	9.0	80.85	✓		
$\beta\alpha, \beta\alpha$	HNO <sub>3</sub> +(CH <sub>3</sub> ) <sub>4</sub> NCl				✗	NI
	HCl+HNO <sub>3</sub>				✗	NI
$\beta\alpha, \beta\beta$	HCl+HClO <sub>4</sub>	-0.94	0.89	✗	✓	0.06
	(CH <sub>3</sub> ) <sub>4</sub> NCl+CH <sub>3</sub> COO N(CH <sub>3</sub> ) <sub>4</sub>				✓	0.084
$\beta\beta, \beta\beta$	[Untested] <sup>e</sup>					

NI = no inhibition (up to > 0.15M in each electrolyte)

<sup>a</sup> Following single-electrolyte data no coalescence is predicted for  $(d\gamma/dc)^2 \leq 1 \text{ mN}^2 \text{ m}^{-2} \text{ M}^{-2}$ .

<sup>b</sup> The concentration used to determine the gradient was the concentration of positive (or negative) charges in solution.

<sup>c</sup> Formation of water and single electrolyte solution.

<sup>d</sup> Incomplete dissociation results in uncharged species that are surface active.

<sup>e</sup> No nonreactive combination of two  $\beta\beta$  salts was available.

In the results presented, electrolytes were mixed in equal amounts and their influence on bubble coalescence was evaluated. The influence of selected mixed electrolytes on bubble coalescence as a function of concentration is shown in Figure 2.4. As with single electrolytes two dramatically different types of behaviour are observed. Some combinations of ions inhibit bubble coalescence whereas others have little or no effect on bubble coalescence up to concentrations of 0.2M in each electrolyte. Where coalescence inhibition occurs, the electrolyte mixtures exhibit transition concentrations similar to those seen for single electrolytes. Therefore mixed electrolytes show bubble coalescence behaviour consistent with single electrolyte experiments.

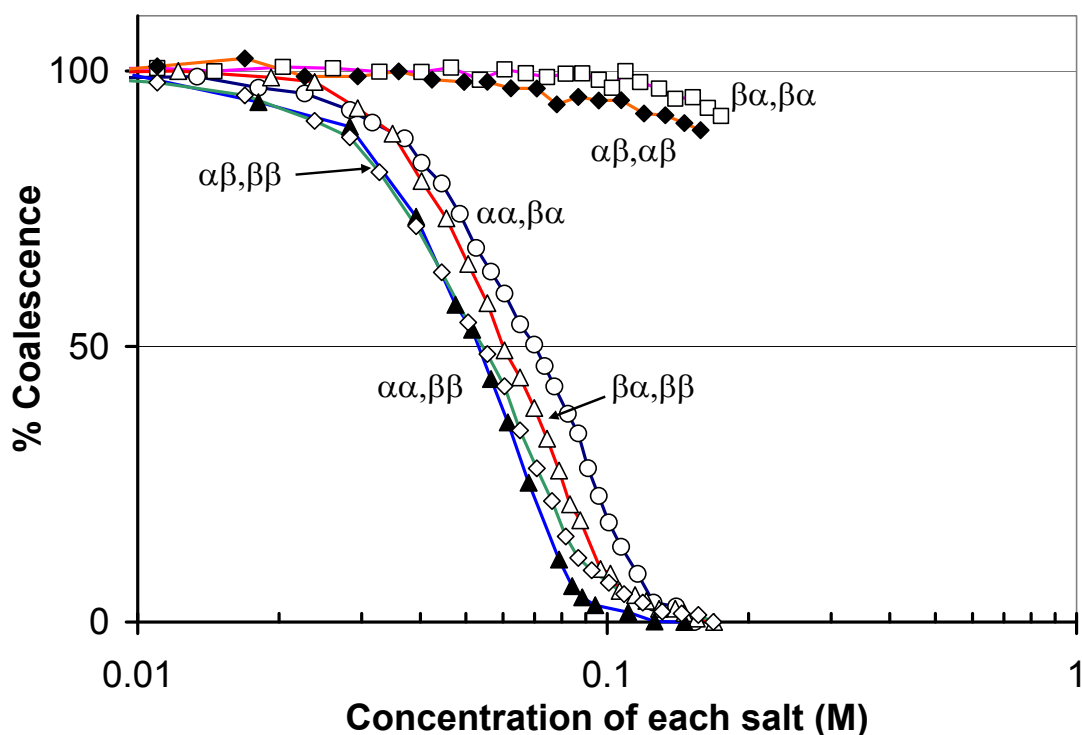


**Figure 2.4** Bubble coalescence in a selection of mixed 1:1 electrolytes as a function of log of concentration of each electrolyte. Mixtures shown are HCl + HNO<sub>3</sub> (□), CH<sub>3</sub>COONa + KClO<sub>3</sub> (◆), HCl + NaNO<sub>3</sub> (○), HCl + HClO<sub>4</sub> (△), NaClO<sub>3</sub> + HClO<sub>4</sub> (◇), and NaCl + HClO<sub>4</sub> (▲). Percentage coalescence is defined as 100% in pure water and 0% at a stable lower voltage in coalescence-inhibiting systems. The empirical assignments used in the combining rules for single electrolytes are shown for each electrolyte combination. As with single electrolyte systems, some combinations exhibit a sharp transition to bubble coalescence inhibition and others do not.

In Table 2.1 the measured surface tension and the calculated values of  $d\gamma/dc$  and  $(d\gamma/dc)^2$  are compared with the measured bubble coalescence behaviour of a range of electrolyte combinations. There is no correlation between coalescence inhibition and  $(d\gamma/dc)^2$ . For single electrolyte systems we noted that in all cases when  $(d\gamma/dc)^2 < 1.0 \text{ mN}^2 \text{ m}^{-2} \text{ M}^{-2}$ , no effect on bubble coalescence is observed. This is not the case for mixed electrolyte systems. In inhibiting electrolyte mixtures there is no correlation between transition concentration and  $(d\gamma/dc)^2$ , as shown in Figure 2.5.

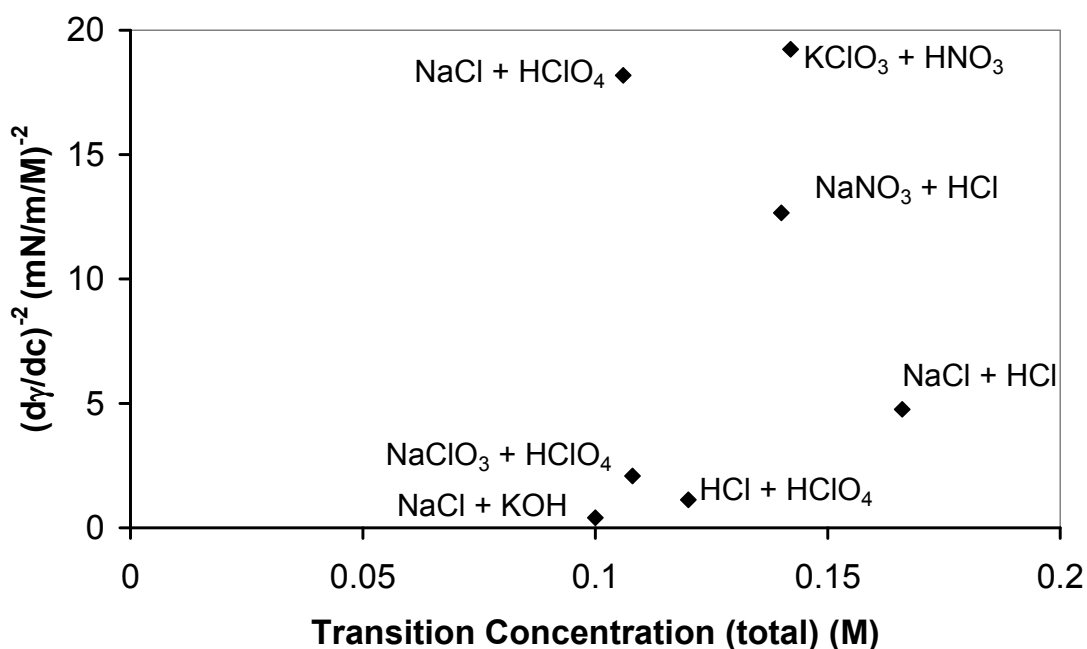


**Figure 2.5** Lack of correlation between  $(d\gamma/dc)^2$  and transition concentration of inhibiting 1:1 electrolyte mixtures. Transition concentration is defined at 50% coalescence, and is given as total concentration of cations or anions.

### 2.3.4 Coalescence inhibition and ions at the interface

#### 2.3.4.1 Ions at the interface: Surface enhancement

Many, though not all, of the electrolytes that inhibit bubble coalescence, raise solution surface tension relative to pure water.<sup>58-60</sup> The Gibbs adsorption isotherm gives the surface excess  $\Gamma$  of species in solution as a function of surface tension and concentration.

---

A raised surface tension corresponds to depletion of solute in the interfacial region. For a single component system,

$$\Gamma = \frac{-c d\gamma}{kT dc} \quad (2.2)$$

The interfacial region is commonly defined by the boundary at which  $\Gamma_{\text{H}_2\text{O}} = 0$  (the water concentration in the whole interfacial region is equal to that in bulk).<sup>60, 131</sup>

Ion depletion at the interface is justified physically using the theory of Onsager and Samaras,<sup>132</sup> which states that an image-charge repulsion makes interfacial ions energetically unfavourable: there is an equivalent ‘charge’ in the low-dielectric vapour region repulsing ions. The ions attract water molecules and so make the surface less energetically favourable than in the pure liquid.<sup>60</sup>

However, the Gibbs adsorption isotherm indicates solute depletion in the interfacial region, while telling us nothing about the distribution of ions within that region.<sup>133</sup> Consequently solutions may contain surface-partitioning species and still show a rise in surface tension relative to water.<sup>125</sup> Early indications that some ions do populate the liquid surface came from atmospheric chemistry studies, which indicated that some ions in aerosol drops were more readily available for reaction with the vapour phase than theories of depletion had indicated.<sup>134</sup>

Simulation work<sup>124, 135, 136</sup> and surface-selective spectroscopic techniques<sup>137-139</sup> confirmed that asymmetric or large, polarisable ions such as the larger halides and hydronium may be enhanced at the solution surface, and depleted in the “subsurface” to maintain overall depletion in the interfacial layer. The modelling of such non-uniform interfacial concentration gradients relies upon using polarisable potentials for water – if traditional non-polarisable potentials are used, then ions are all found to be depleted from the interface.<sup>140</sup> Other ions, including the smaller, harder cations like sodium, are found to show no surface enhancement. A qualitative picture of ion concentrations at the solution interface is given in Figure 2.6.

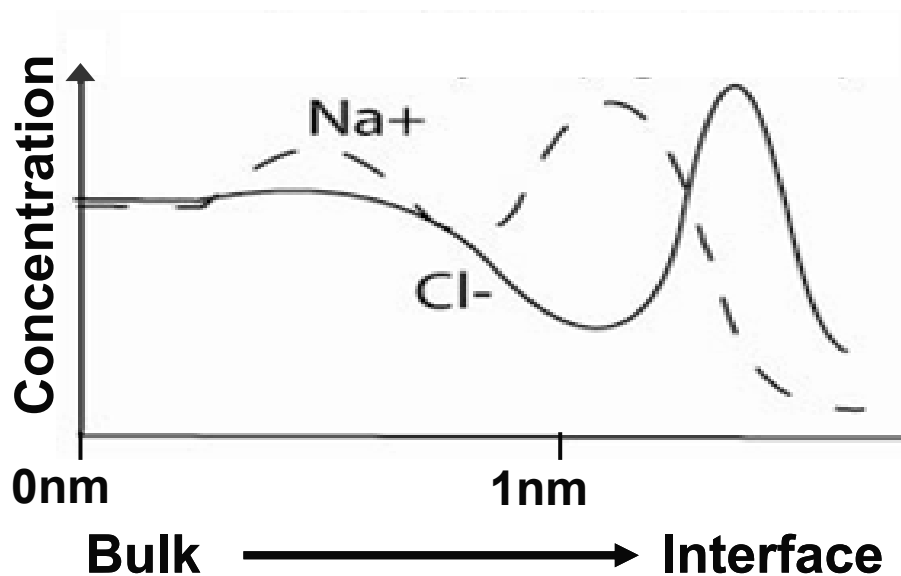


**Figure 2.6** Ions at the interface of aqueous NaCl solution. Chloride (—) has surface enhancement and subsurface depletion, while sodium (---) shows no surface propensity. The solute is overall depleted in the interface relative to bulk, as it has a positive surface tension gradient. This concentration profile is drawn from calculations by Marcelja based on a method of effective potentials.<sup>126</sup>

The observed difference in affinities of ions for the solution surface inspired Marcelja to suggest that an ion's surface or subsurface preference might align with  $\alpha$  and  $\beta$  designations from bubble coalescence (not respectively).<sup>38</sup> In particular, based on some reported ion surface propensities it was suggested that  $\alpha$  anions (like  $\text{Cl}^-$ ) have a surface preference and  $\alpha$  cations (like  $\text{Na}^+$ ) prefer the fully-solvated subsurface, while  $\beta$  anions (like  $\text{ClO}_4^-$ ) exist subsurface and  $\beta$  cations ( $\text{H}_3\text{O}^+$ ) show surface enhancement. It is hypothesised that ion separation at the interface is required for coalescence inhibition. This proposal implies a natural combining law where the influence of an ion is dependent upon the nature of the other ions present. A calculation of the electrostatic interaction between free surfaces of NaCl and HCl solutions found a significant short-range repulsion in the former case but not in the latter that is associated with the locations of the ions within the interfacial region.<sup>126</sup>

### 2.3.4.2 Ions at the interface: Electrolyte mixtures

It was hypothesized that  $\alpha$  anions and  $\beta$  cations have an affinity for the gas-water interface, whereas  $\alpha$  cations and  $\beta$  anions exist preferentially in the subsurface region. Further, it was hypothesized that interfacial ion separation is required for coalescence inhibition – possibly due to creation of an electrostatic repulsion.<sup>126</sup> Thus any combination of ions that includes an  $\alpha$  cation and  $\alpha$  anion or a  $\beta$  cation and a  $\beta$  anion should inhibit bubble coalescence. Therefore, as shown in Table 2.2, it is predicted that coalescence inhibition will occur in all electrolyte mixtures except combinations  $\alpha\beta/\alpha\beta$  and  $\beta\alpha/\beta\alpha$  (all surface and all subsurface species, respectively). All bubble coalescence inhibition results obtained in mixtures are consistent with this prediction.

**Table 2.2** Coalescence inhibition and the interfacial ion separation hypothesis

Mixture of Combinations	Prediction from Ion Separation Hypothesis ( $\checkmark$ = inhibit)	Coalescence Inhibition
$\alpha\alpha, \alpha\beta$	$\checkmark$	$\checkmark$
$\alpha\alpha, \alpha\beta$	$\checkmark$	$\checkmark$
$\alpha\alpha, \beta\alpha$	$\checkmark$	$\checkmark$
$\alpha\alpha, \beta\beta$ or $\alpha\beta, \beta\alpha$	$\checkmark$	$\checkmark$
$\alpha\beta, \alpha\beta$	$\times$	$\times$
$\alpha\beta, \beta\beta$	$\checkmark$	$\checkmark$
$\beta\alpha, \beta\alpha$	$\times$	$\times$
$\beta\alpha, \beta\beta$	$\checkmark$	$\checkmark$
$\beta\beta, \beta\beta$	$\checkmark$	(untested) <sup>a</sup>

<sup>a</sup>  $\beta\beta, \beta\beta$  mixtures currently cannot be tested as no suitable combination is stable in solution. See section 2.3.3.

### 2.3.4.3 Ions at the interface: Varying ion ratios

The possible electrostatic effect of ions at the interface was investigated by varying electrolyte ratio. If interfacial ions inhibit coalescence via charge separation, then it is possible that the effect can be “switched off” or neutralised if a cation and an anion are present at the surface (or the subsurface) in the same concentration. By varying the bulk concentration ratio of two species believed to be surface enhanced,  $H^+$  and  $Cl^-$ , I aimed to find whether this switching-off point exists by looking for a sudden jump to lower

coalescence inhibition (higher coalescence). The results are shown in Figure 2.7. Two different acids were added (separately) to NaCl, and in neither case is there evidence of surface charge neutralisation. When HCl was added, nothing suggesting a charge neutralisation was observed. There is a slight decrease in coalescence inhibition at larger added volumes of HCl, attributed to a decrease in concentration of sodium cation. In that experiment, the  $\text{Cl}^-$  concentration was always greater than the  $\text{H}^+$  concentration, because molecular dynamics simulations suggested  $\text{H}^+$  had a greater surface affinity.<sup>126</sup> In a second experiment  $\text{HClO}_4$  was added to NaCl solution and the  $\text{H}^+/\text{Cl}^-$  ratio was varied over a larger range. Here again no coalescence spike is seen, and the coalescence reaches a stable low level.

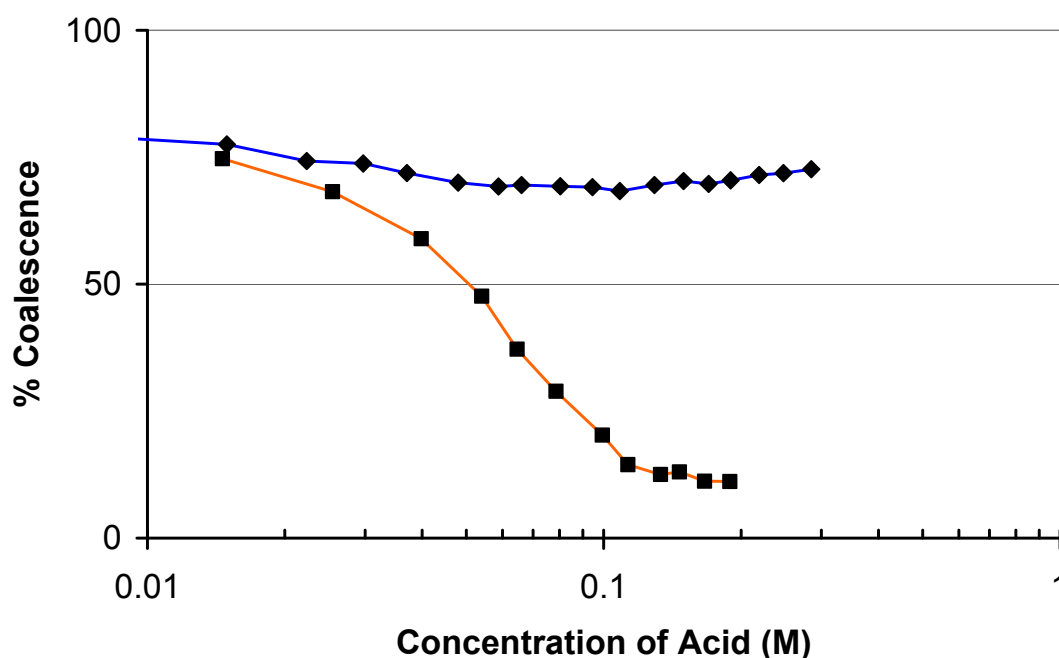


**Figure 2.7** Acids HCl (◆) and  $\text{HClO}_4$  (■) are added to 0.078M NaCl. In added HCl, the bulk concentration of  $\text{Cl}^-$  always exceeds that of  $\text{H}^+$ , while in the  $\text{HClO}_4$  measurement  $\text{H}^+$  concentration becomes greater than  $\text{Cl}^-$  concentration. There is no “switching off” or anomaly in the coalescence inhibition, indicating that these ions do not cancel out each other’s effects, in any combination.

In varying the ion ratio we are able to reject the early hypothesis of Foulk and Miller,<sup>69</sup> who suggested that surface tension gradient of two electrolytes having opposite effects on surface tension, would at some point cancel out and lead to no coalescence

inhibition. They claim to have observed this for the NaCl and NaSCN case. However HClO<sub>4</sub> and NaCl (and HCl and NaCl) have opposite effects on surface tension and we observe no variation in coalescence inhibition curve with varying electrolyte ratio. It is interesting that adding a small amount of HCl does decrease the inhibition, and then it levels out. This perhaps indicates that there is an optimal ratio of the ions Na<sup>+</sup> and Cl<sup>-</sup>, and that after this point the Na<sup>+</sup> is exhausted. It is consistent with the equimolar mixture of NaCl and HCl being more effective than either of these electrolytes alone, as shown in Figure 2.10.

#### 2.3.4.4 Ions at the interface: Alkali metal halides

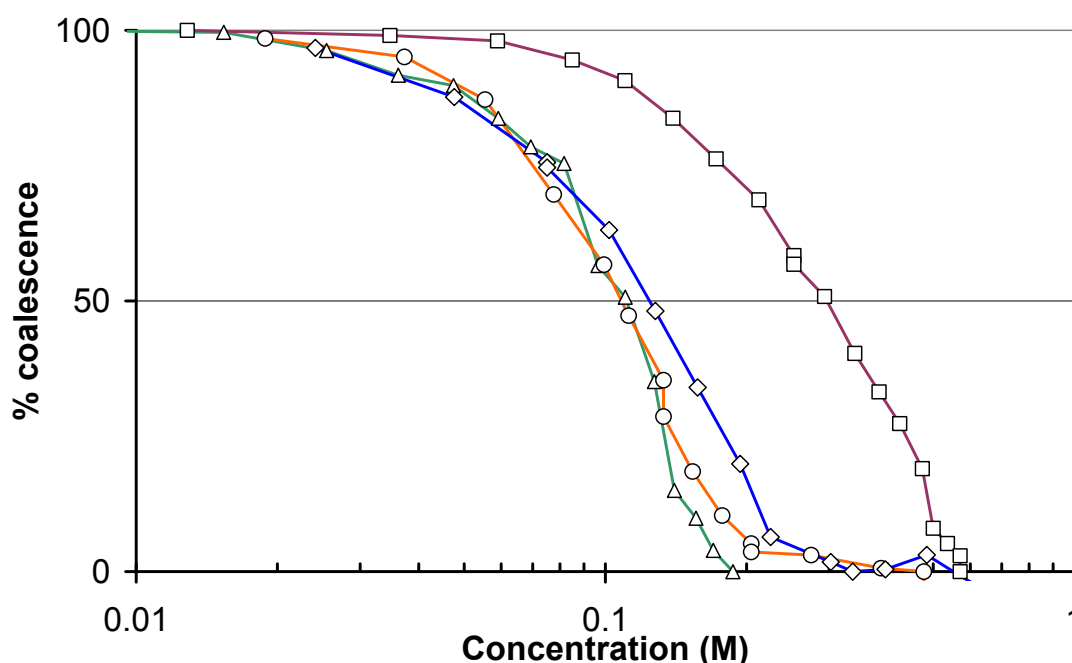


**Figure 2.8** Coalescence inhibition in sodium halides: fluoride ( $\Delta$ ), chloride ( $\circ$ ), bromide ( $\diamond$ ) and iodide ( $\square$ ). Percentage coalescence is plotted against the log of concentration. 100% coalescence occurs in pure water, 0% coalescence is defined at a stable low signal in inhibiting electrolytes. Transition concentration occurs at 50% coalescence.

Many of the studies of ion position at the surface use alkali metal halides as their examples.<sup>141, 142</sup> Molecular dynamics simulations and spectroscopic techniques alike show that the large and polarisable iodide is strongly enhanced at the surface; bromide



and chloride are less enhanced; and fluoride shows no surface propensity.<sup>124, 137</sup> This is difficult to reconcile with the classification of all of the halides as  $\alpha$  anions, if ion interfacial position is related to bubble coalescence inhibition. I measured bubble coalescence inhibition in the sodium salts of each of these halides, with a view to determining whether any correlation with proposed surface enhancement exists. The results are presented in Figure 2.8. There is a difference between the coalescence in iodide and that in the other halides, with iodide being a much less powerful inhibitor. A similar trend is observed in lithium and potassium halides. The transition concentrations are reported in Table 2.3. It is worth noting that the greater transition concentration for sodium iodide is predicted reasonably well by  $(d\gamma/dc)$  (or by  $(d\gamma/dc)^2$ ). (The values from Weissenborn and Pugh<sup>60</sup> are used because we made no measurements in some of these salts.)

**Table 2.3** Transition concentrations of sodium halides

Electrolyte	Transition Concentration (M)	$(d\gamma/dc)^a$ (mN/m/mol)
NaF	0.11	$1.83 \pm 0.06$
NaCl	0.095	$2.08 \pm 0.08$
NaBr	0.13	$1.83 \pm 0.05$
NaI	0.30	$1.23 \pm 0.06$

<sup>a</sup> From Weissenborn and Pugh<sup>60</sup>.

### 2.3.5 Transition concentrations in mixtures

The major part of this investigation of mixed electrolyte bubble coalescence has been concentrated on dividing mixtures into two categories only: those that inhibit bubble coalescence (at 0.2M concentration in each electrolyte), and those that show no effect. It is natural to consider whether the transition concentration in inhibiting mixtures can be predicted from the identity of the contributing ions – this would be helpful for those working in applications of mixed electrolyte solutions who might wish to know to what degree a particular mixture *at a given concentration*, will stabilise bubbles. While it is possible to make statements about minimum required concentrations for coalescence

inhibition in mixed electrolytes, we have found no simple predictable trend for transition concentrations based on ion assignments.

### 2.3.5.1 Univalent electrolyte mixtures

A range of transition concentrations is observed in mixtures containing only univalent ions – from 0.05M in NaCl + KOH, to 0.105M in NaCl + NaClO<sub>3</sub> – in both cases this value is the concentration of each electrolyte at 50% coalescence (see Figure 2.9).

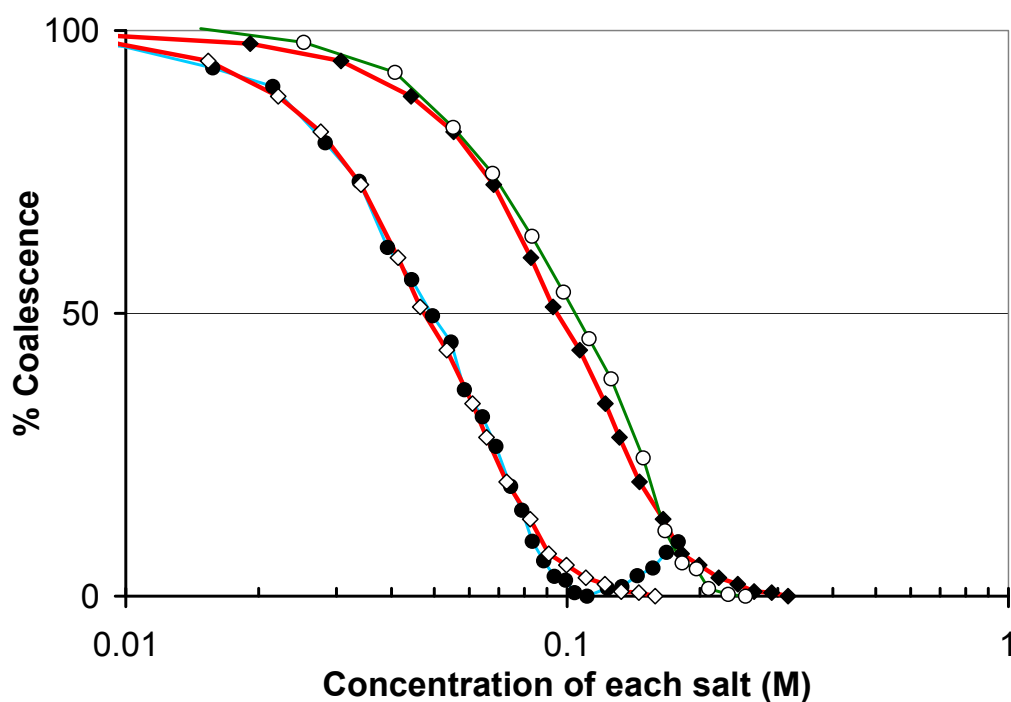


**Figure 2.9** Range of possible bubble coalescence inhibition effects on adding a 1:1 electrolyte to NaCl. NaCl as a single salt (◆) and the equivalent of a NaCl+NaCl mixture (◇) are shown. When inhibiting  $\alpha\alpha$  electrolyte KOH is added, NaCl+KOH (●) shows an additive effect. When noninhibiting  $\alpha\beta$  salt NaClO<sub>3</sub> is added, it has no effect and coalescence inhibition is similar to NaCl alone in NaCl+NaClO<sub>3</sub> (○).

The full range of effects for mixtures containing both Na<sup>+</sup> and Cl<sup>-</sup> is shown in Figure 2.10. When another 1:1 electrolyte is added the effect may be additive (equivalent to doubling the concentration of NaCl), no effect at all (coalescence in the mixture is approximately equivalent to coalescence in NaCl alone), or somewhere in between. It is possible that a much larger number of mixtures would produce a reliable trend of transition concentration based on ion  $\alpha$  and  $\beta$  assignments, but with the available data

we are not able to predict in advance what any mixture's transition concentration will be. It is particularly unwise to attempt any predictions given the complex and confusing results when divalent, as well as univalent, ion mixtures are considered in the next section.

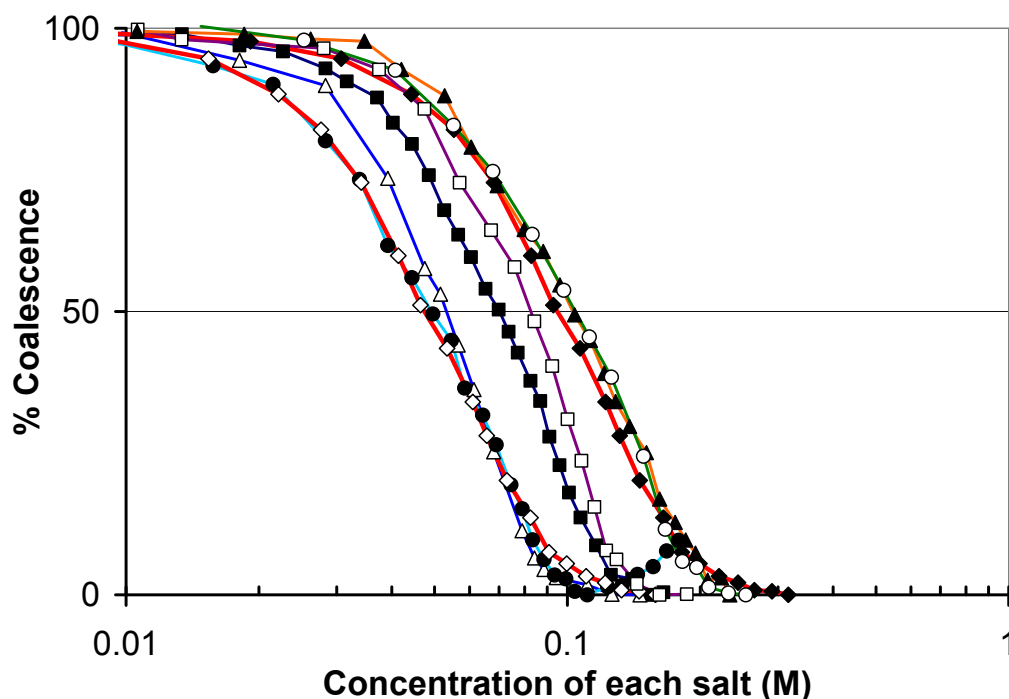


**Figure 2.10** Range of transition concentrations in mixtures containing  $\text{Na}^+$  and  $\text{Cl}^-$ . Presented as reference are  $\text{NaCl}$  ( $\blacklozenge$ ) and the equivalent of a  $\text{NaCl}+\text{NaCl}$  mixture ( $\diamond$ ). Mixtures are  $\text{NaCl}+\text{KOH}$  ( $\bullet$ ) ( $\alpha\alpha+\alpha\alpha$ ),  $\text{NaCl}+\text{HClO}_4$  ( $\triangle$ ) ( $\alpha\alpha+\beta\beta$ ),  $\text{NaNO}_3+\text{HCl}$  ( $\blacksquare$ ) ( $\alpha\alpha+\beta\alpha$ ),  $\text{NaCl}+\text{HCl}$  ( $\square$ ) ( $\alpha\alpha+\beta\alpha$ ),  $\text{NaCl}+\text{NaClO}_4$  ( $\blacktriangle$ ) ( $\alpha\alpha+\alpha\beta$ ) and  $\text{NaCl}+\text{NaClO}_3$  ( $\circ$ ) ( $\alpha\alpha+\alpha\beta$ ). The inhibiting strength of the mixture is not easily predictable.

### 2.3.5.2 Mixtures involving the calcium cation

Consider the two equimolar electrolyte mixtures ( $\text{Ca}(\text{NO}_3)_2 + \text{HClO}_4$ ) and ( $\text{Ca}(\text{ClO}_4)_2 + \text{HNO}_3$ ). The species present are the same in each case, but the first solution has a ratio of 2:1 in nitrate:perchlorate anions, while in the second solution the ratio is 1:2. Nitrate is an  $\alpha$  anion and perchlorate is a  $\beta$  anion. Thus, by using a combination of divalent and univalent ions in mixtures, it is possible to vary only the ratio of the  $\alpha$  and  $\beta$  anion (or cation) while keeping other species constant. It was hoped that such experiments might reveal more about how the amounts of various ions present affect the bubble

coalescence inhibition and transition concentration; however the results are perhaps more confusing than helpful at this stage. Figure 2.11 shows the results in the mixtures described,  $(\text{Ca}(\text{NO}_3)_2 + \text{HClO}_4)$  and  $(\text{Ca}(\text{ClO}_4)_2 + \text{HNO}_3)$ .  $\text{Ca}^{2+}$  is an  $\alpha$  cation and  $\text{H}^+$  is a  $\beta$  cation, so it was hypothesised that changing the anion ratio might lead to some difference in coalescence inhibition. However, both mixtures have an identical effect on bubble coalescence. The mixtures are more powerful inhibitors than calcium nitrate alone.

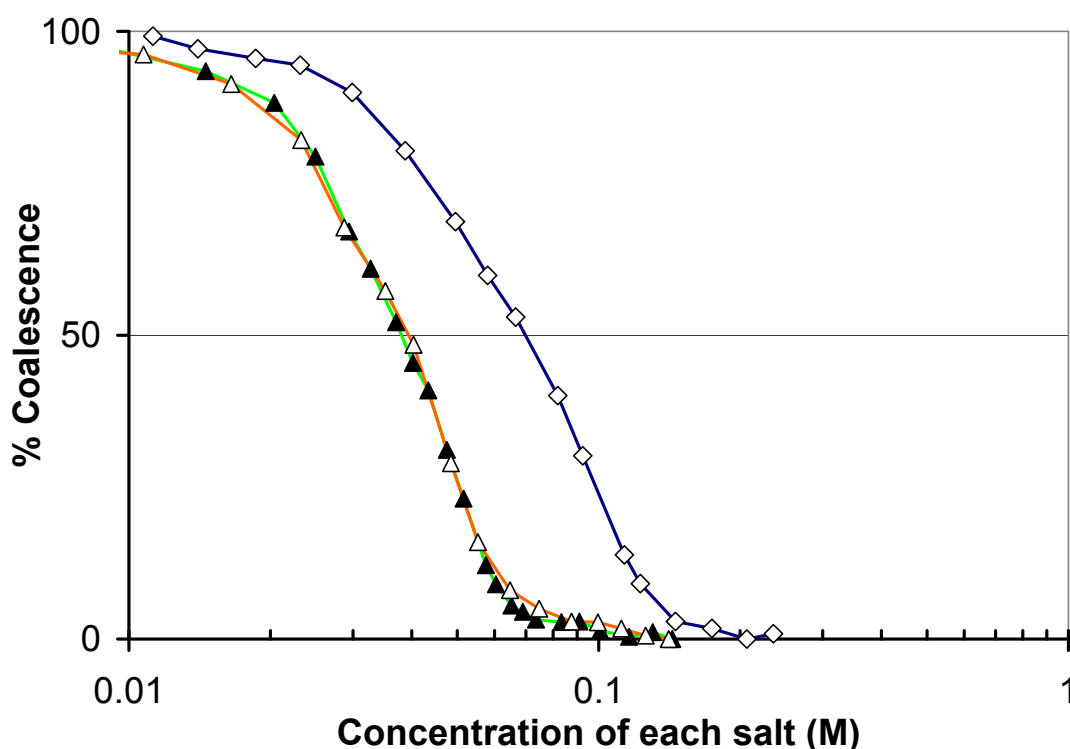


**Figure 2.11** Varying anion ratio in calcium and hydrogen electrolyte mixtures.  $\alpha\alpha$  electrolyte  $\text{Ca}(\text{NO}_3)_2$  ( $\diamond$ ) as a single salt is shown as a reference ( $\alpha\beta$  salt  $\text{Ca}(\text{ClO}_4)_2$  does not inhibit coalescence). Mixtures  $\text{Ca}(\text{NO}_3)_2 + \text{HClO}_4$  ( $\blacktriangle$ ) (nitrate:perchlorate ratio is 2:1) and  $\text{Ca}(\text{ClO}_4)_2 + \text{HNO}_3$  ( $\triangle$ ) (nitrate:perchlorate ratio is 1:2) have identical effects on bubble coalescence. Both mixtures have greater power than calcium nitrate alone.

In order to check the impact of the cation  $\alpha$  or  $\beta$  assignment, I repeated the experiment using mixtures  $(\text{Ca}(\text{NO}_3)_2 + \text{NaClO}_4)$  and  $(\text{Ca}(\text{ClO}_4)_2 + \text{NaNO}_3)$  – replacing univalent  $\beta$  cation  $\text{H}^+$  with univalent  $\alpha$  cation  $\text{Na}^+$ . The results, presented in Figure 2.12, are easily distinguishable from the previous data.

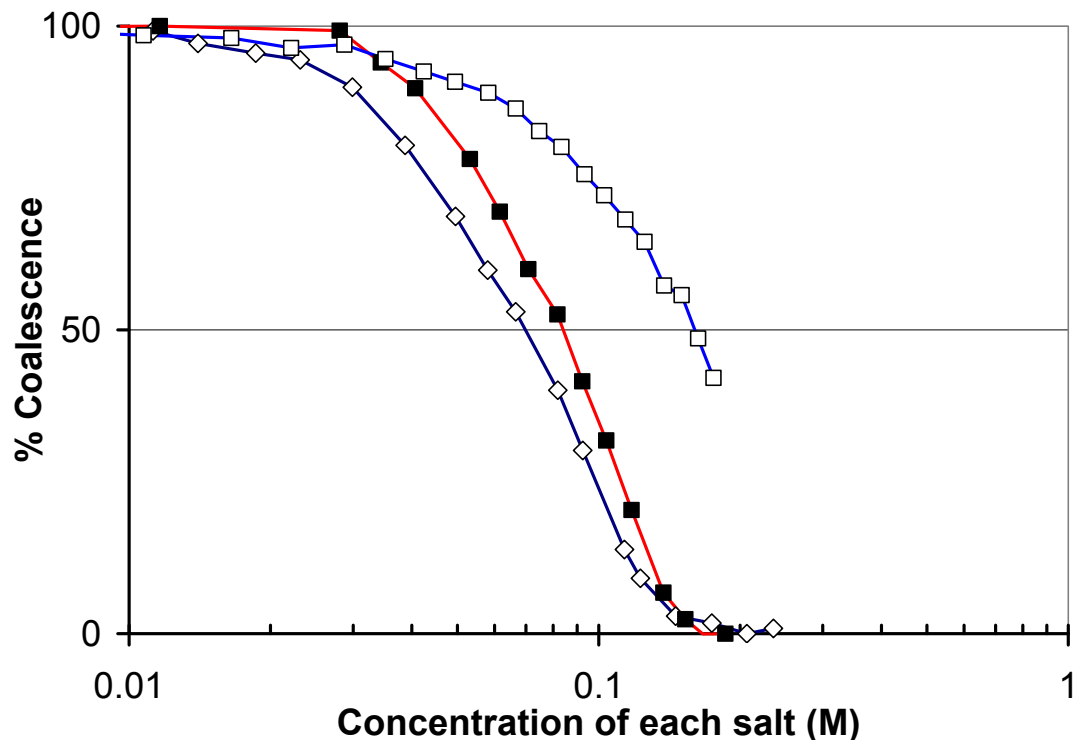


**Figure 2.12** Varying anion ratio in calcium and sodium electrolyte mixtures.  $\alpha\alpha$  electrolyte  $\text{Ca}(\text{NO}_3)_2$  ( $\diamond$ ) as a single salt is shown as a reference ( $\alpha\beta$  salt  $\text{Ca}(\text{ClO}_4)_2$ , which is not shown, does not inhibit coalescence). Mixtures  $\text{Ca}(\text{NO}_3)_2 + \text{NaClO}_4$  ( $\blacksquare$ ) (nitrate:perchlorate ratio is 2:1) and  $\text{Ca}(\text{ClO}_4)_2 + \text{NaNO}_3$  ( $\square$ ) (nitrate:perchlorate ratio is 1:2) have different effects on bubble coalescence. Both mixtures are less powerful inhibitors than calcium nitrate alone.

It is found that the effect of changing anion ratio depends upon the univalent cation. This is an unexpected result. In the case of  $\text{Ca}^{2+}$  and  $\text{H}^+$  as the cations, coalescence inhibition is not affected by whether the ratio of nitrate:perchlorate is 1:2 or 2:1. This could be taken to indicate that the concentration of each anion is not important. However when calcium and sodium are the cations, coalescence inhibition is greater when the nitrate:perchlorate ratio is 2:1, in the  $\text{Ca}(\text{NO}_3)_2 + \text{NaClO}_4$  case. Interestingly this inhibition is slightly less than occurs in  $\text{Ca}(\text{NO}_3)_2$  alone. Inhibition is still poorer when the anion ratio is reversed in the presence of  $\text{Ca}^{2+}$  and  $\text{Na}^+$ .

Transition concentrations in ion mixtures suggest a complex behaviour that depends strongly on the identity of all of the individual ions present. While these observations do

---

not at present reveal the mechanism of coalescence inhibition, they are expected to be an invaluable test of any hypotheses concerning the ion-specific effects observed in bubble coalescence.

## 2.4 CONCLUSIONS

Bubble coalescence inhibition in mixed electrolyte systems depends upon the combination of ions present in a way consistent with  $\alpha$  and  $\beta$  assignments of cations and anions as determined in single electrolytes. This result indicates that these assignments can be generalized to multi-electrolyte systems. Consequently we are now able to predict the bubble coalescence behaviour of both single and mixed electrolyte systems using the  $\alpha$  and  $\beta$  empirical assignments – without any known exceptions. All mixtures inhibit bubble coalescence at concentrations below 0.2M in each species, except those mixtures containing matched non-inhibiting electrolytes – two  $\alpha\beta$  or two  $\beta\alpha$  species.

We measured bubble coalescence in, and surface tensions of, solutions of electrolyte mixtures. It was shown that inhibition of coalescence does not correlate with the square of surface tension gradient,  $(d\gamma/dc)^2$ , for mixed electrolyte systems as it does for single electrolyte systems. This indicates that Gibbs elasticity does not provide an explanation for the influence of electrolyte on bubble coalescence. In contrast to single electrolyte data, mixtures with a small effect on surface tension will inhibit bubble coalescence. We also note that surface tension gradient is not independent of ion  $\alpha$  and  $\beta$  assignments because mixtures featuring the same  $\alpha/\beta$  ion combinations have surface tension gradients that are similar in sign and in magnitude (if the anomalies such as undissociated  $\text{CH}_3\text{COOH}$  are excluded). It is suggested that the correlation between  $(d\gamma/dc)^2$  and coalescence inhibition in single electrolytes is a secondary effect, in that the surface tension gradient may be related to the true controlling parameter of bubble coalescence inhibition.

Coalescence inhibition in equimolar mixed electrolytes is consistent with the proposal by Marcelja that inhibition depends upon ion separation within the interfacial region. All mixtures inhibit coalescence except those featuring ions that are assigned as all

---

surface ( $\beta\alpha/\beta\alpha$  mixtures) or all subsurface ( $\alpha\beta/\alpha\beta$  mixtures). Coalescence inhibition in single sodium halide salts is not consistent with a simple ion separation hypothesis. In the presence of subsurface sodium, the anion with the greatest surface propensity, iodide, shows weakest coalescence inhibition, while near-identical coalescence inhibition is seen in solutions featuring bromide, chloride and fluoride – which differ in their surface enhancement. Therefore the role of ion surface enhancement in bubble coalescence inhibition remains uncertain.

---

## Chapter 3 Bubble Coalescence Inhibition by Sugars and Urea

---

### 3.1 INTRODUCTION

The ion specificity seen in the inhibition of bubble coalescence is a special case amongst specific ion systems. Ion specificity is commonly studied in the interaction of electrolytes with proteins and other macromolecules.<sup>113</sup> Series of cations and anions can be ordered from salting-in to salting-out for any protein, depending on whether the ion increases or decreases the protein solubility. Ion-specificity also encompasses a myriad of other effects.<sup>11</sup> The ion-combining rules observed in bubble coalescence inhibition do not correlate in any clear way with such series. However protein dissolution and bubble coalescence inhibition are not entirely dissimilar processes- in fact, ion affinity for the air-water interface has recently been linked to protein solvation and dissolution, through a similar affinity of ions for hydrophobic regions on the protein surface.<sup>143</sup> This chapter concerns some attempts to find links between traditional ion specific systems and bubble coalescence.

In Section 3.2 I report investigations of bubble coalescence in solutions of other common cosolutes of proteins, urea and sucrose. Such species are commonly known as osmolytes because of their biological roles.<sup>144</sup> Urea and sucrose typically have opposite effects on protein solvation, with urea acting as a denaturant and enhancing solvation and dissolution, while sucrose (and other sugars) constricts solvent and excludes hydrophobic proteins.<sup>145</sup> In the past the action on protein solubility of urea, sucrose and Hofmeister ions has been described in terms of their supposed effect on solvent structure, but there is growing evidence for the importance of local interactions with waters of solvation and with the protein interface.<sup>117</sup> Analogously, it was hypothesised that osmolytes might affect bubble stability via their local interactions with water and



---

with the gas-water interface. Determining how these solutes affect bubble coalescence may give further information about the mechanism of thin film stabilisation. The solvent structure is further discussed in Section 3.1.1 below.

The effects of several mono- and disaccharides on bubble coalescence are reported in Section 3.3. These small sugars generally are non-surface active. We investigated whether these non-electrolyte non-surfactants might also inhibit bubble coalescence in water. This study originated with and further extended results from Craig et al. showing differences in coalescence inhibition between glucose, fructose, and the disaccharide sucrose.<sup>9</sup> It was hypothesised that differences in coalescence inhibition between sugars might be traced back to some solution parameter such as surface tension gradient, or to structural differences in the sugars themselves. Such a result concerning “molecular specificity” might in turn elucidate the bubble coalescence inhibition mechanism in electrolyte solutions, and the reason for the ion-specific combining rules.

### 3.1.1 Solvent structure and Hofmeister effects

The dissolution of a hydrophobic protein can be considered as consisting of the two processes of cavity creation in the solvent; and solvation of the protein.<sup>146</sup> Hofmeister ion specificity has been linked to ion effects on solvent structure.<sup>147, 148</sup> “Salting out” species that reduce solubility are, under this interpretation, considered as constricting water, attracting a solvation shell and strengthening the wider hydrogen-bond network so that the protein can not squeeze in to be dissolved.<sup>63</sup> In contrast “salting in” species are weakly hydrated, disrupt the water hydrogen bond network, show stronger preference for the interface and generally make it easy for proteins to find a place.<sup>149</sup>

It is now generally accepted that this bulk water structure mechanism is *not* how ions affect protein solubility.<sup>117</sup> Instead of a single ion inserting into and disrupting a large-scale water network, an ion’s effects are seen as very local.<sup>118, 121</sup> Ions are solvated by a hydration shell, the size and character of which depends upon the characteristics (size, charge, polarisability) of that individual ion.<sup>150</sup> There is broad (although not universal<sup>149</sup>) agreement that bulk water structure is little affected by small solute

---

molecules or ions<sup>151, 152</sup> – even in the extreme case of 8M urea, where almost all the water molecules are bound up in solvation.<sup>153</sup> Similarly, protein salting out will be driven by how the ion (or other osmolyte) interacts directly with the exposed protein surface.<sup>154, 117, 155, 156</sup> Ions may be accumulated at or excluded from different surface regions.<sup>145</sup>

I would argue that the persistence of the solvent structure idea is due in part to the language in much of the Hofmeister and ion specificity literature. Species are still referred to by their effect on solvent structure. The cations and anions are described as “structure-makers” or “structure-breakers”.<sup>157</sup> The terms kosmotrope (or cosmotrope) and chaotrope (order-maker and disorder-maker) are also used to suggest an increase or decrease in order in the solvent.<sup>119</sup> Structure-breakers, in the traditional narrative, tend to be weakly solvated and to increase hydrophobe solubility by associating with (or allowing solvent to associate with) the protein surface. Structure-makers, in contrast, attract a water solvation shell (which may disrupt the hydrogen-bonding network in the vicinity<sup>119</sup>) and stabilise protein structure against denaturing and dissolution.<sup>157</sup> Thus, the cation and anion series derived from various protein solubility (and other) studies are still meaningful, but the kosmotrope and chaotrope definitions must be accepted as referring only to the strength of the local solvation shell.<sup>118</sup>

### 3.1.2 Hofmeister ions and bubble coalescence inhibition

As in the case of Hofmeister ion specificity, changes to bulk water structure have in the past been invoked as a possible mechanism of bubble coalescence inhibition,<sup>63</sup> in part because this offers a solution to the problem of how ions can affect film drainage and rupture across films of 40nm thickness or greater.<sup>18</sup> Lessard and Zieminski found correlations between transition concentration of inhibiting ions and the two parameters entropy of hydration and water self-diffusion, both of which are related to solvent structure.<sup>63</sup> However these correlations do not hold up once a wider range of electrolytes is considered (see Section 1.5.2.2). Ions and osmolytes in the gas-solution system of bubble coalescence are now expected to interact locally, with the waters of hydration or with the gas interface.

Figure 3.1 shows the cations and anions arranged in order from most destabilising (salting-in, or chaotropic) of proteins to most stabilising (salting-out, or kosmotropic), along with their  $\alpha$  and  $\beta$  assignments. The order does not align. This is perhaps expected, as it is quite difficult to extend the ion specificity of chaotropes and kosmotropes to the combination-dependent ion specific effects observed in bubble coalescence inhibition, if ion effects are only upon the immediate vicinity of the ion.

### A

Most Destabilising											Most Stabilising	
$\text{SCN}^-$	$\text{ClO}_4^-$	$\text{I}^-$	$\text{ClO}_3^-$	$\text{NO}_3^-$	$\text{Br}^-$	$\text{Cl}^-$	$\text{CH}_3\text{COO}^-$	$\text{IO}_3^-$	$\text{OH}^-$	$\text{F}^-$	$\text{SO}_4^{2-}$	$(\text{COO})_2^{2-}$
$\beta$	$\beta$	$\alpha$	$\beta$	$\alpha$	$\alpha$	$\alpha$	$\beta$	$\alpha$	$\alpha$	$\alpha$	$\alpha$	$\alpha$

### B

Most Destabilising											Most Stabilising	
$\text{Ca}^{2+}$	$\text{Mg}^{2+}$	$\text{H}^+$	$\text{Li}^+$	$\text{Na}^+$	$\text{K}^+$	$\text{Cs}^+$	$\text{NH}_4^+$	$(\text{CH}_3)\text{NH}_3^+$	$(\text{CH}_3)_2\text{NH}_2^+$	$(\text{CH}_3)_3\text{NH}^+$	$(\text{CH}_3)_4\text{N}^+$	
$\alpha$	$\alpha$	$\beta$	$\alpha$	$\alpha$	$\alpha$	$\alpha$	$\alpha$	$\beta$	$\beta$	$\beta$	$\beta$	

**Figure 3.1** Anions (A) and cations (B) arranged in order from most destabilising of proteins to most stabilising or kosmotropic. The ion positions are approximate and may change a little with protein, counterion and pH. The  $\alpha$  and  $\beta$  assignments are from bubble coalescence inhibition studies. The protein stability sequence is taken from various sources.<sup>14, 116, 121</sup>

Collins has proposed a “Law of Matching Water Affinities” to explain Hofmeister effects.<sup>118, 158</sup> The potential attraction of a link between this hypothesis and the bubble coalescence inhibition is that Collins’ law also features a combining rule whereby an ion’s effect changes depending on the counterion present. Collins argues that two weakly hydrated (chaotrope) ions will form contact ion pairs in solution (or go to the interface) as this releases water to participate in the bulk network. Likewise, two kosmotropes will stay as an ion pair because they interact strongly with each other, releasing energy. However one kosmotrope and one chaotrope will tend to form individual ions in solution because the energy gained from excluding water from the

---

chaotrope is less than is lost by dehydrating a hydrogen-bond strengthening kosmotrope.<sup>158</sup>

The ion water affinities do not match with bubble coalescence ion assignments, and so this model cannot be an explanation for bubble coalescence ion specificity. In particular, the water affinities are based on monotonically increasing charge density from chaotrope to kosmotrope, and this is strongly size-dependent.<sup>158</sup> In bubble coalescence inhibition, it was found in Chapter 2 that sodium fluoride, chloride and bromide all have much the same effect on bubble coalescence, but the large change in anion charge density would put these ions in different categories in the Collins model.

### 3.1.3 Water structure and coalescence inhibition

Two minor experiments are reported here that were done to investigate the importance of structural changes in the solvent.

#### 3.1.3.1 *Coalescence inhibition in heavy water*

The bubble column was used to compare the action of a coalescence-inhibiting electrolyte in H<sub>2</sub>O and D<sub>2</sub>O. There are differences in the H-bonding network between these two solvents, as shown in a recent simulation study by Soper and Benmore.<sup>159</sup> They found that the H-bonding changes in length, symmetry and average number around each molecule (3.62 in H<sub>2</sub>O versus 3.76 in D<sub>2</sub>O). Thus, a difference observed between these two solvents might indicate the importance of solvent structure in electrolyte coalescence inhibition. D<sub>2</sub>O also is around 10% denser than H<sub>2</sub>O, and it has a 25% higher viscosity,<sup>57</sup> and these properties might also affect bubble coalescence and thin film drainage.

D<sub>2</sub>O was obtained from SigmaAldrich (99.9% deuterated), and a 5 molal stock solution of oven-roasted NaBr (SigmaAldrich) was made up in each solvent. This high concentration was used to minimise the amount of solvent required, as my stock of D<sub>2</sub>O was limited. The greater density and viscosity of D<sub>2</sub>O led to few bubbles being produced at the frit. In the pure solvent, lower turbidity was observed than in water, as indicated by an increased photodiode detector voltage in our laser scattering data. The

gas flow was therefore increased in order that collision behaviour should be the same before salt was added, as determined by an equal initial photodiode voltage in water and heavy water.

No significant difference in the electrolyte effect was observed for NaBr (Figure 3.2). This indicates that minor changes to bulk water structure do not greatly affect bubble coalescence inhibition by electrolytes.

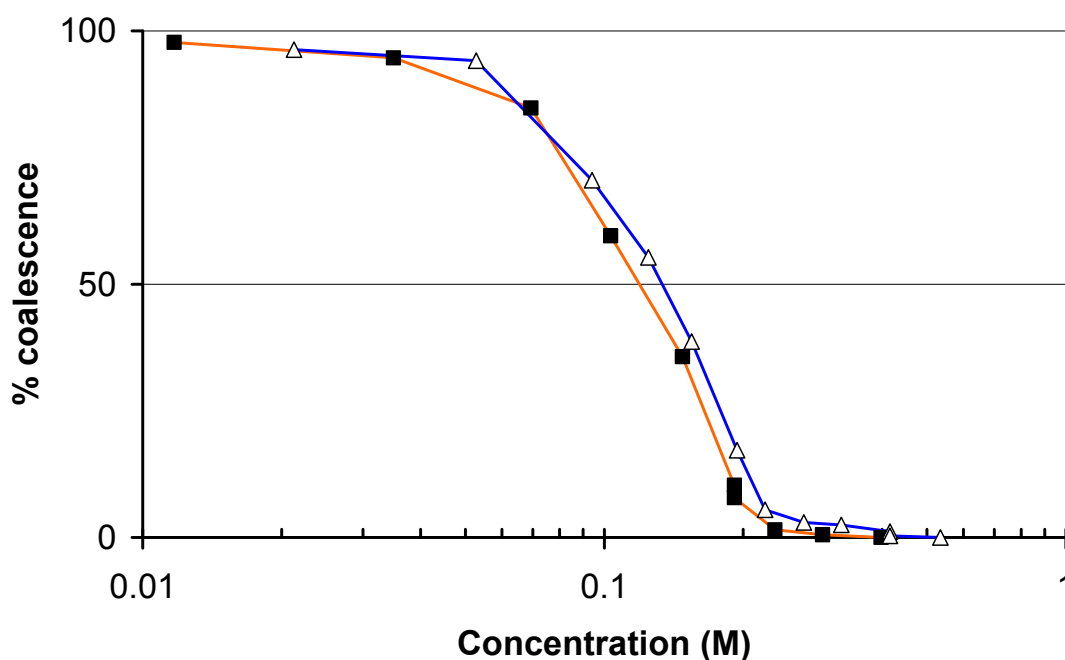


**Figure 3.2** Comparison of coalescence inhibition by NaBr in H<sub>2</sub>O ( $\Delta$ ) and D<sub>2</sub>O ( $\blacksquare$ ) as a function of concentration. There is no significant difference in inhibition between the two solvents.

### 3.1.3.2 Temperature and Bubble Coalescence

The effect of temperature on coalescence inhibition was investigated in the bubble column. Craig et al. showed that there was a small increase in coalescence *inhibition* (decrease of percentage coalescence) for a given concentration of inhibiting electrolyte, over a 40K temperature range.<sup>9</sup> They note, however, that water viscosity decreases with increasing temperature and this should instead tend towards faster drainage and increased coalescence. Ribeiro and Mewes studied the critical velocity for coalescence

or bouncing from 10°C to 40°C, in single-collision experiments.<sup>20</sup> They report increased *coalescence* at increased temperature, both in pure water and in the presence of constant electrolyte concentration. They attribute the increased coalescence to increased vaporisation of interfacial water, which may play a part in film rupture by changing the surface properties.<sup>20</sup> Therefore the effect of temperature on coalescence inhibition by electrolyte is uncertain.

The hydrogen-bonding in water is reduced at higher temperatures, with the average number of hydrogen bonds per molecule found to drop from 3.59 at 25°C to 3.24 at 100°C (using molecular dynamics simulations).<sup>160</sup> I therefore aimed to investigate the effect of changed water structure on bubble coalescence by heating water and salt solutions to  $\geq 90^\circ\text{C}$  and observing bubble coalescence.

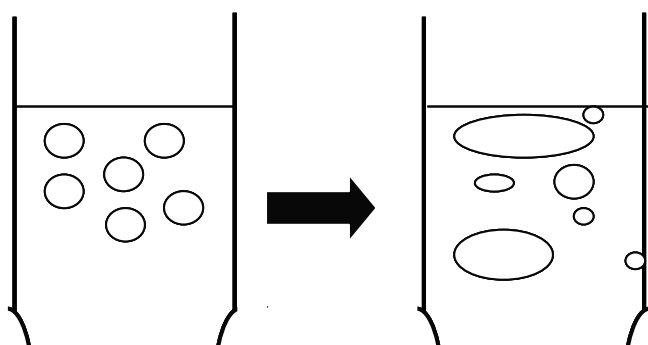


**Figure 3.3** Effect of heating on bubbles in the bubble column. From roughly uniform size, the bubbles when the column is heated from 20°C towards 90°C become highly non-uniform in size and shape. The laser scattering data is then difficult to interpret.

It was found that the bubble column method is not suitable for studies of temperature effects without serious modification – at least for temperatures close to boiling. Temperature gradients between gas and liquid in the column could not equilibrate, and produced “hot spots” due to the turbulent and uneven flow required for bubble collisions. The net result was that the bubbles produced differed in size, some being very large at the point of the laser scattering measurement, and others very small (see the cartoon in Figure 3.3). This made the bulk turbidity essentially meaningless as a measure of coalescence. The experiments were not reproducible, even for temperature

---

ramps run within the same solution. Condensation of the solvent on the optics was another issue that arose with the current instrument design. A serious drawback was that at the high temperatures rapid evaporation of the liquid meant that electrolyte concentration was not accurately known, and care had to be taken or the interface dropped to the level of the laser detector. This list of difficulties led to the abandonment of this experiment.

## **3.2 OSMOLYTES AND BUBBLE COALESCENCE: SUCROSE, UREA AND ELECTROLYTES**

### **3.2.1 Introduction**

Ion-specificity in Hofmeister systems arises from ions' varying effects on protein solubility. Sucrose and urea are non-ionic cosolutes that in general have different effects on the solubility of hydrophobic species, with urea acting to denature hydrophobic proteins and relax their structure in solution, while sucrose acts to stabilise aggregates and reduce solubility.<sup>155</sup> I investigated the effects of sucrose and urea on bubble coalescence, to determine if they could be related to the protein stabilising effects of these solutes and of electrolytes.

### **3.2.2 Materials and Methods**

The bubble column apparatus was used for coalescence inhibition measurements, as described in Section 2.2, above. All water used in the bubble coalescence studies was purified using a Milli-Q gradient system. Electrolyte NaClO<sub>4</sub> was used as received; NMe<sub>4</sub>Br was dried at 250°C for several hours to drive off moisture and NaCl and KCl were roasted at 500°C for several hours to remove organic contaminants (all electrolytes from SigmaAldrich). Urea (BDH, AnalaR grade) was freeze-dried before use, and sucrose (SigmaAldrich) was used as received. Stock solutions were added to 41.0mL purified water. In the experiments where the ratio of cosolutes was varied, one component was added first before introducing a stock solution of the second solute; otherwise equimolar mixtures were used.

### 3.2.3 Coalescence inhibition in sucrose and electrolytes

Sucrose is a disaccharide of glucose and fructose, with structure as shown in Figure 3.4.

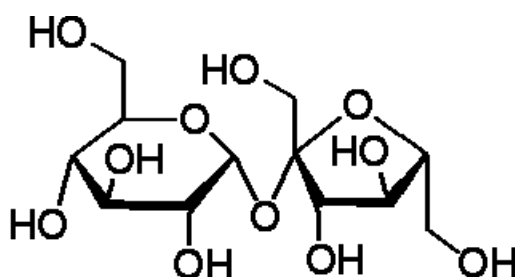


**Figure 3.4** The structure of sucrose. Sucrose is a disaccharide of fructose and glucose, that “salts out” or reduces the solubility of hydrophobic species in aqueous solution.<sup>161</sup>

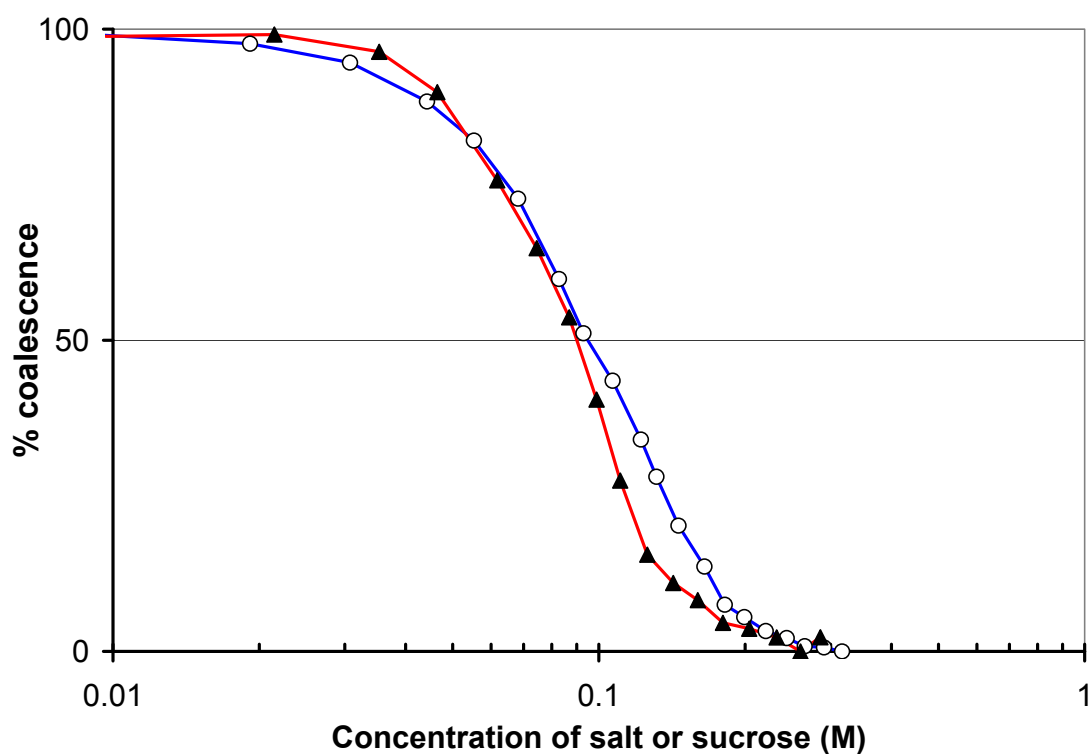


**Figure 3.5** Coalescence inhibition by sucrose (▲) as a function of concentration, shown on a log scale. Typical inhibiting  $\alpha\alpha$  electrolyte NaCl (O) is shown for comparison. The inhibition effect is very similar. 100% coalescence is defined in pure water; 0% is a stable low value in inhibiting solutions.



Sucrose acts to inhibit bubble coalescence, in a way comparable to an inhibiting electrolyte – as shown in Figure 3.5. This finding is consistent with the earlier results of Craig et al.<sup>9</sup> The transition concentration is in the region of 0.075-0.09M. Equimolar mixtures of sucrose and electrolytes were also studied, to determine how this “structure-maker” might change bubble coalescence in the presence of ions. The results are presented in Figure 3.6 for inhibiting electrolyte NaCl and in Figure 3.7 for the two noninhibiting electrolytes NaClO<sub>4</sub> and (CH<sub>3</sub>)<sub>4</sub>NBr.

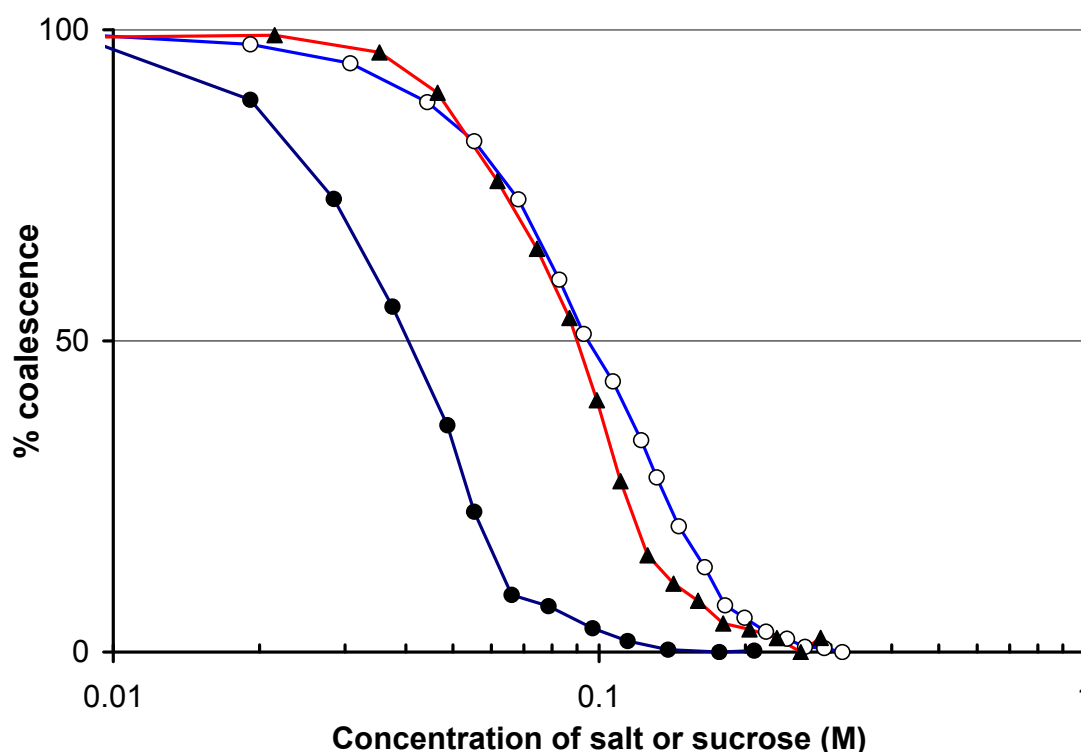


**Figure 3.6** Sucrose and coalescence inhibition in the presence and absence of inhibiting electrolyte. Sucrose (▲),  $\alpha\alpha$  salt NaCl (○), and an equimolar mixture of NaCl + sucrose(●). Sucrose and NaCl are cooperative in effect, with the mixture inhibiting at lower concentrations than the sum of both contributions would produce. 100% coalescence is defined in pure water; 0% is a stable low value in inhibiting electrolytes.

We observe a cooperative effect between sucrose and electrolytes. Equimolar mixtures of sucrose and both inhibiting and non-inhibiting salts show lower coalescence (greater inhibition) than the sum of their individual contributions at a given concentration (Figure 3.6 and Figure 3.7). This is perhaps most clearly observed in the case of non-inhibiting salts, with mixtures of NaClO<sub>4</sub> or (CH<sub>3</sub>)<sub>4</sub>NBr and sucrose showing bubble

coalescence inhibition greater than that in sucrose alone. The inhibition in the NaCl+sucrose mixture is also greater than the sum of the individual contributions. An equimolar mix of sucrose and KCl (not shown) also demonstrates this cooperative effect.

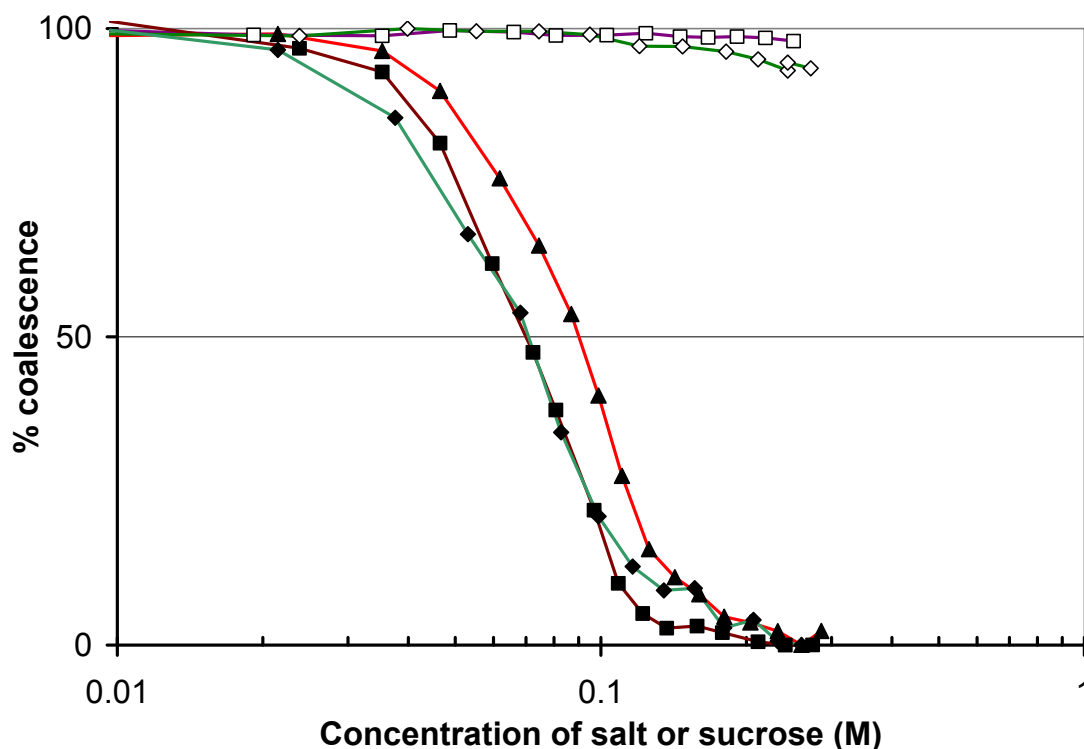


**Figure 3.7** Sucrose effect on coalescence inhibition in the presence and absence of noninhibiting electrolytes. Sucrose (▲),  $\alpha\beta$  salt  $\text{NaClO}_4$  (□), and  $\beta\alpha$  salt  $(\text{CH}_3)_4\text{NBr}$  (◇); and equimolar mixtures of  $\text{NaClO}_4$  + sucrose (■) and  $(\text{CH}_3)_4\text{NBr}$  + sucrose (◆). Sucrose and electrolytes are cooperative in effect. 100% coalescence is defined in pure water; 0% is a stable low value in inhibiting solutions.

The importance of the component ratio was tested by adding sucrose to the bubble column to around its transition concentration and then introducing either NaCl or  $\text{NaClO}_4$ , as shown in Figure 3.8. The results replicated what is seen in equimolar mixtures, with no strong dependence on ratio. In the case of  $\text{NaClO}_4$  there is a small decrease in coalescence inhibition that rapidly levels out, and additional salt leads to no extra change. On adding NaCl to sucrose solution there is immediate sharp increase in coalescence inhibition, before a stable low value is reached.

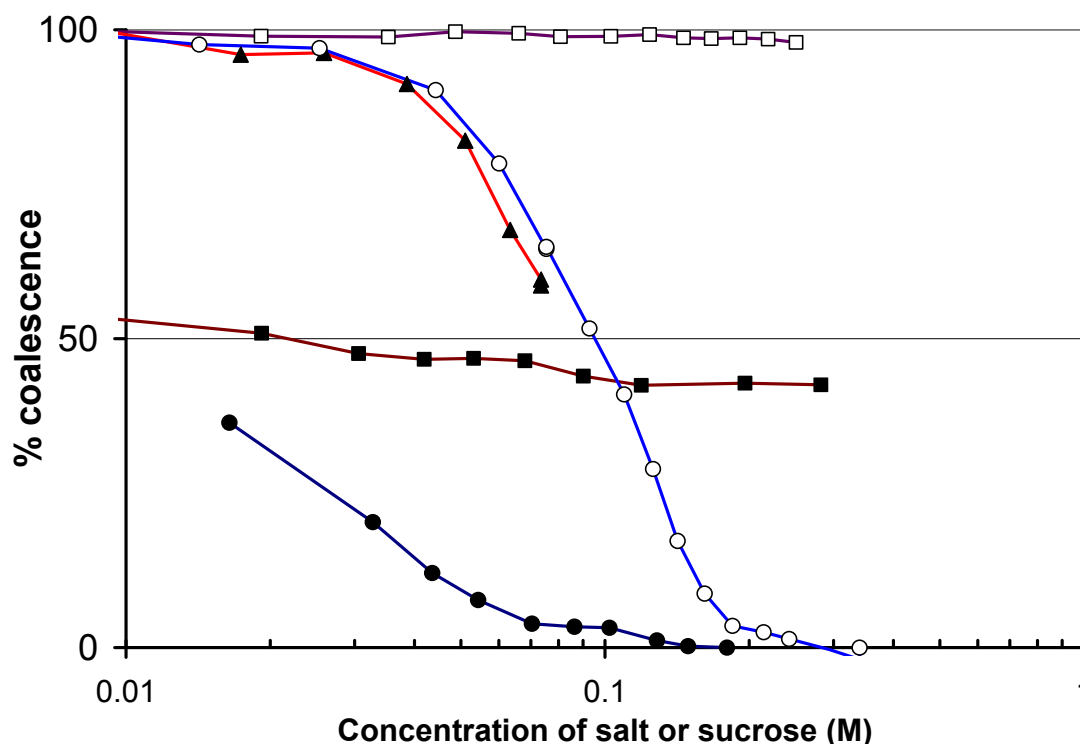


**Figure 3.8** Changing ratio of sucrose and electrolyte. After sucrose ( $\blacktriangle$ ) is added to water to 0.07M, coalescence inhibition in (0.07M sucrose + NaCl) ( $\bullet$ ) and (0.07M sucrose + NaClO<sub>4</sub>) ( $\blacksquare$ ) is greater than in NaCl (O) and NaClO<sub>4</sub> ( $\square$ ) in the absence of sucrose.

### 3.2.4 Coalescence inhibition in urea and electrolytes

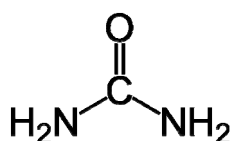


**Figure 3.9** The structure of urea. Urea is found to fit quite easily into the water hydrogen bonding network.<sup>162</sup>

Urea has the structure shown in Figure 3.9. Urea slightly raises the surface tension of solution relative to pure water.<sup>163</sup> It is described as a structure-breaker, and increases hydrophobe solubility; it also denatures proteins. Urea exerts its denaturing (and solubilising) effect on proteins at concentrations above 3M,<sup>164</sup> although in some cases 6M may be required for an effect on protein to be observed.<sup>165</sup> Rezus and Bakker used

IR pumped-probe spectroscopy and saw no major change to bulk water structure up to 8M urea concentration.<sup>153</sup> I measured coalescence inhibition in urea to a concentration of 3.10M. The concentration was not increased beyond this because of the necessity for a stock solution to be added to pure water in the bubble column, to obtain a baseline signal. As shown in Figure 3.10, urea has no effect on bubble coalescence much below 1M, after which bubble coalescence decreases slowly with increasing concentration.

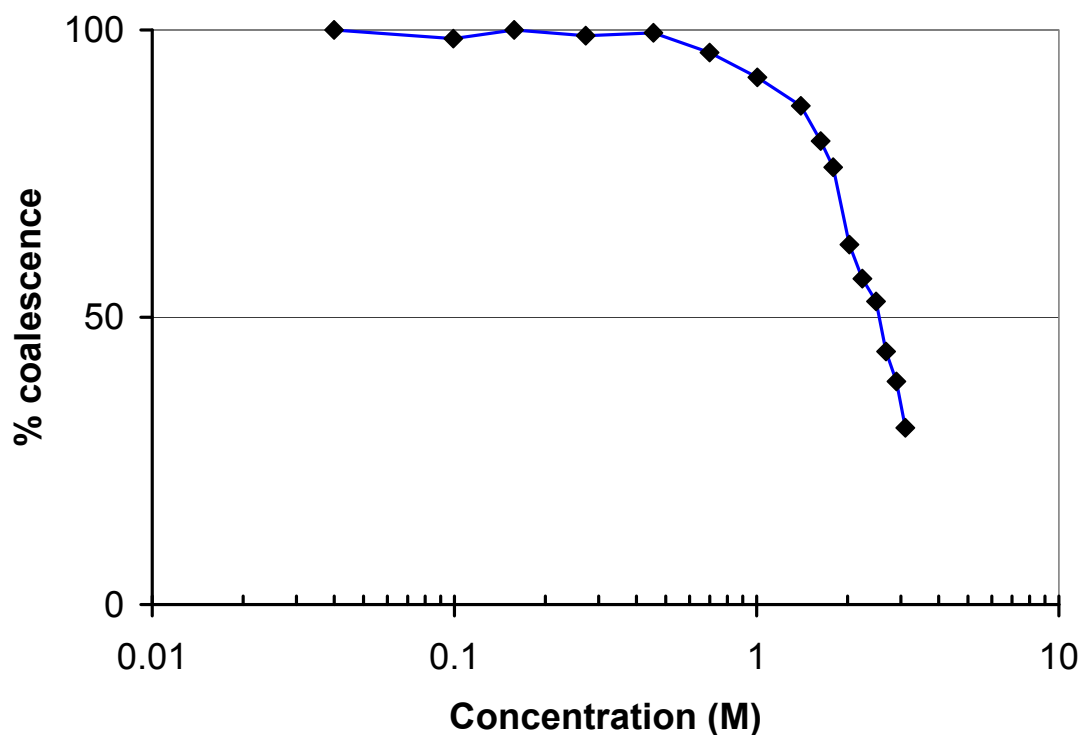


**Figure 3.10** Bubble coalescence inhibition in urea (◆) at high concentrations. 100% coalescence is defined in pure water, and the baseline (0% coalescence) is the stable low voltage value in inhibiting electrolytes. Urea shows no inhibition up to ~1M.

In equimolar mixtures of urea and electrolyte, coalescence inhibition is indistinguishable from the electrolyte solution in the absence of urea (data not shown). However, when urea is introduced at high concentrations (2-3M) before addition of electrolytes, a cooperative effect is observable in noninhibiting electrolyte  $\text{NaClO}_4$  (Figure 3.11) and inhibiting electrolyte  $\text{NaCl}$  (Figure 3.12). The results are very similar to the enhancement of electrolyte coalescence inhibition seen in the presence of sucrose.

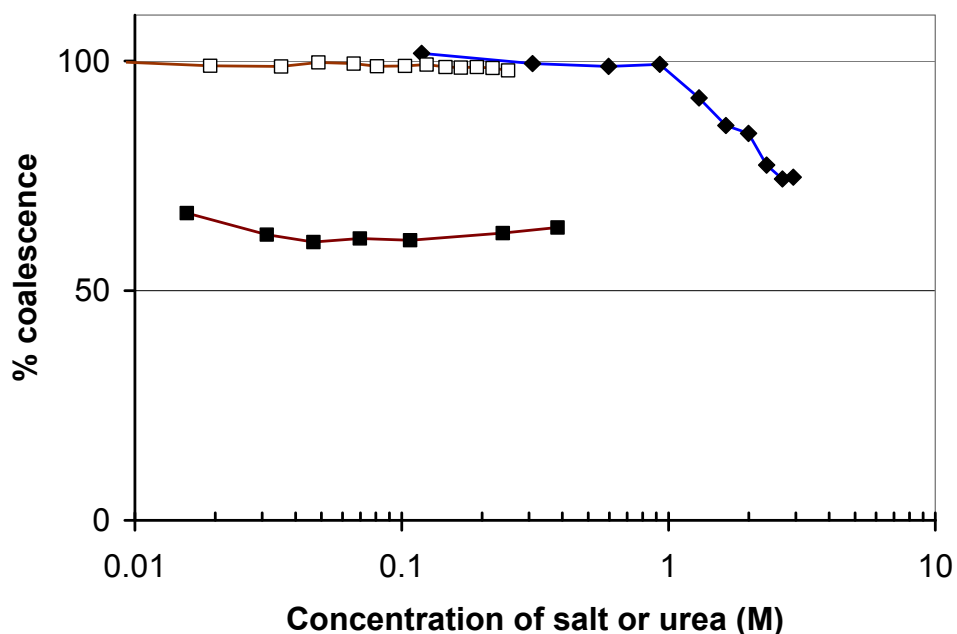


**Figure 3.11** Urea (◆) enhances the effect on bubble coalescence of  $\alpha\beta$  electrolyte  $\text{NaClO}_4$ .  $\text{NaClO}_4$  is noninhibiting, (□) but ( $\text{NaClO}_4 + 2.9\text{M}$  urea) (■) has a small effect on bubble coalescence. 100% coalescence is defined in pure water; 0% is a stable low value in inhibiting electrolytes.

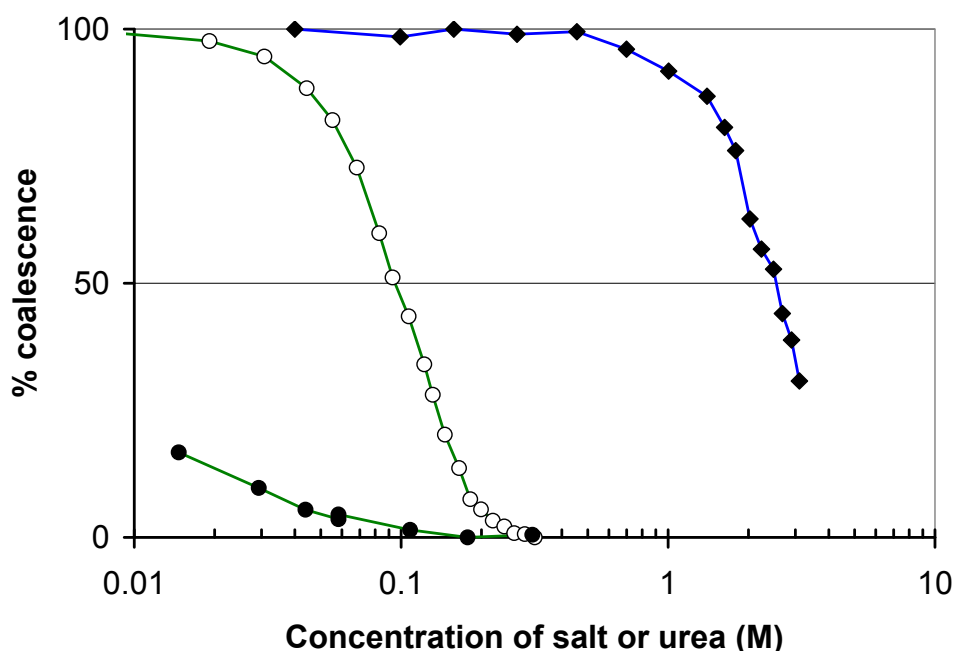


**Figure 3.12.** Urea (◆) enhances the effect on bubble coalescence of  $\alpha\alpha$  electrolyte  $\text{NaCl}$ .  $\text{NaCl}$  alone (○) requires a higher concentration for full inhibition (0% coalescence) than does ( $\text{NaCl} + 3.10\text{M}$  urea) (●). 100% coalescence is defined in pure water; 0% is a stable low value in inhibiting electrolytes.

### 3.2.5 Coalescence inhibition in sucrose and urea

We also tested the effect of mixing sucrose and urea on bubble coalescence in water. It was speculated that the “salting-in” (urea) and “salting-out” (sucrose) effects might cancel out – or, that the opposing interfacial solvation effects of the two solutes might interact in a nonlinear fashion. As shown in Figure 3.13, this hypothesis is satisfied. After urea reached 2M concentration (so that a low level of inhibition was observed), sucrose was added to the solution in the column. A higher concentration of sucrose was required, to elicit the same coalescence inhibition as observed in the absence of urea. Urea thus appears to reduce the effectiveness of sucrose as an inhibitor of bubble coalescence. This result is in contrast to the cooperative effects of urea and sucrose with electrolytes.

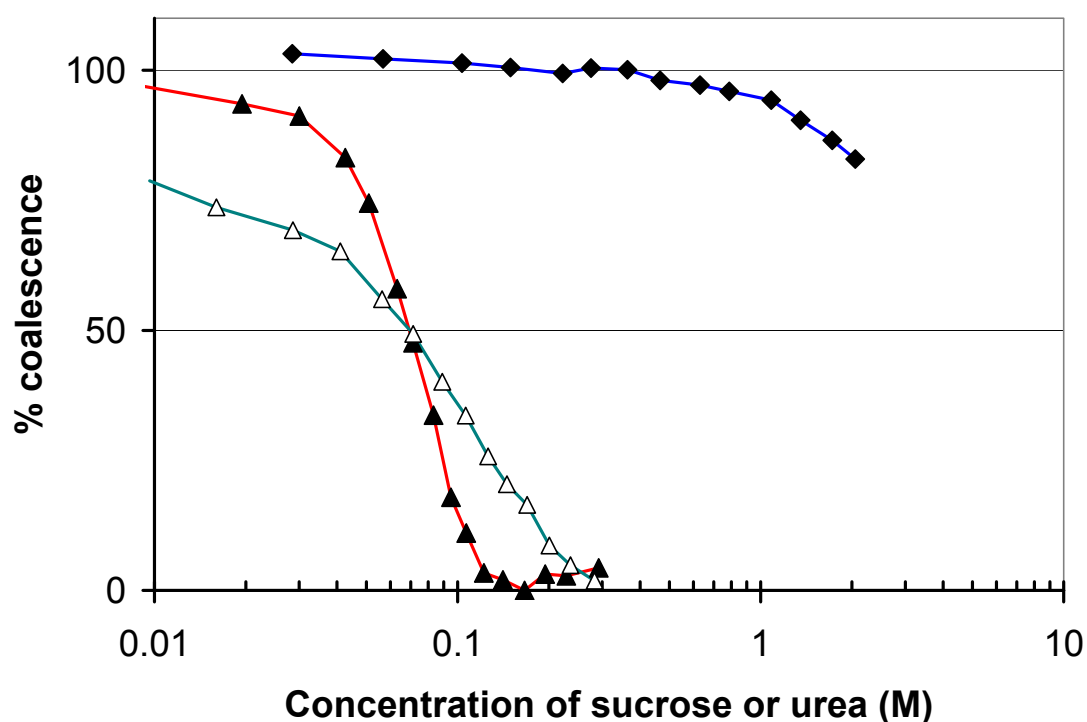


**Figure 3.13** The presence of urea reduces the effectiveness of sucrose. After urea (◆) is added to 2M concentration, (sucrose + 2M urea) (△) requires higher concentration to reach the same level of coalescence inhibition as observed in sucrose in the absence of urea (▲).

---

### 3.2.6 Discussion

We observe a difference between the effects of sucrose and urea, on bubble coalescence inhibition. Sucrose stabilises bubbles at moderate concentrations ( $\sim 0.1\text{M}$ ), over a concentration range similar to that observed in inhibiting electrolytes. Bubble coalescence inhibition takes place only at high concentrations of urea ( $>1\text{M}$ ) and coalescence inhibition does not match that in electrolytes even at  $3\text{M}$  concentration. These solutes also have opposite effects on hydrophobe solubility. Sucrose decreases solubility and stabilises protein structure, while urea increases solubility and denatures proteins. The relationship between protein stabilisation and bubble stabilisation, if any, remains unclear. It would be interesting to test the inhibition and cooperativity effects of other osmolytes. In particular, guanidinium chloride is an ionic denaturant that acts at lower concentrations than urea, and is much used in protein solubility studies.

Recent data suggest that changes to the bulk solvent structure are not the basis for urea and sucrose effects on protein solubilisation. There is a growing body of work that suggests urea manifests its protein-denaturant effect via direct interaction with the protein surface, via adsorption or hydrogen bonding.<sup>153, 166</sup> In contrast sucrose is excluded from the hydrophobic surface, which affects interfacial hydration and makes protein dissolution unfavourable.<sup>167</sup> Sucrose is also depleted from the air-water interface, as it raises the surface tension relative to pure water.<sup>168</sup>

Both urea and sucrose, when at high enough concentrations to partially inhibit bubble coalescence, appear to act to increase the effect of added electrolyte on coalescence inhibition. Notably, the addition of noninhibiting electrolyte causes a decrease in coalescence. Inhibiting salt also requires a lower concentration to elicit a given amount of coalescence inhibition. There is an opposing effect with the mixture of sucrose and urea, as urea acts to make sucrose less effective as a coalescence inhibitor. Both sucrose and urea readily form hydrogen bonds with water, and it is possible that the “turning off” of the sucrose inhibitory effect in the presence of urea, is due to association of the two species – however no information was found on other behaviour of sucrose-urea mixtures.

### 3.2.7 Conclusion

Sucrose, a kosmotrope or “salter-out” of proteins, is an inhibitor of bubble coalescence at concentrations around 0.1M – as investigated further in the next section. Urea, which increases protein solubility and is described as a chaotrope, inhibits coalescence only at very high concentrations. Both species at suitable concentration, act cooperatively to increase the effectiveness of electrolytes at inhibiting bubble coalescence; however a mixture of urea and sucrose is less effective than sucrose alone. This result demonstrates that nonelectrolytes may also be effective in bubble coalescence inhibition. It also suggests that differences in interaction with proteins may be linked with differences in bubble coalescence inhibition, although for Hofmeister ions this relationship is not straightforward. Further work is required to determine the nature of the connection between effects at biological interfaces, and effects on the air-water interface.

## 3.3 COALESCENCE INHIBITION IN SUGARS

Apart from possible solvent effects and changes to protein solubility, bubble coalescence inhibition in sugar solution is of interest in its own right. Sugars have a small effect on solution surface tension, and may increase the surface tension relative to pure water, with a concentration gradient similar to that in electrolytes.<sup>169</sup> The saccharides glucose, fructose and sucrose were shown to act to inhibit bubble coalescence inhibition to differing degrees by Craig et al.<sup>9</sup> The difference in effect between glucose and fructose, which have similar structures, raises the possibility of a “sugar specificity” in bubble coalescence inhibition. Bubble coalescence inhibition is here reported for a wider range of mono- and disaccharides.

### 3.3.1 Materials and methods

The bubble column apparatus was used for coalescence inhibition measurements, as described in Section 2.2, above. All water used in the bubble coalescence studies was purified using a Milli-Q gradient system. Water used in the surface tension studies was purified by filtering through a coarse filter, charcoal and a reverse osmosis membrane before distillation and a final purification using a Milli-Q system. Sugars were used as

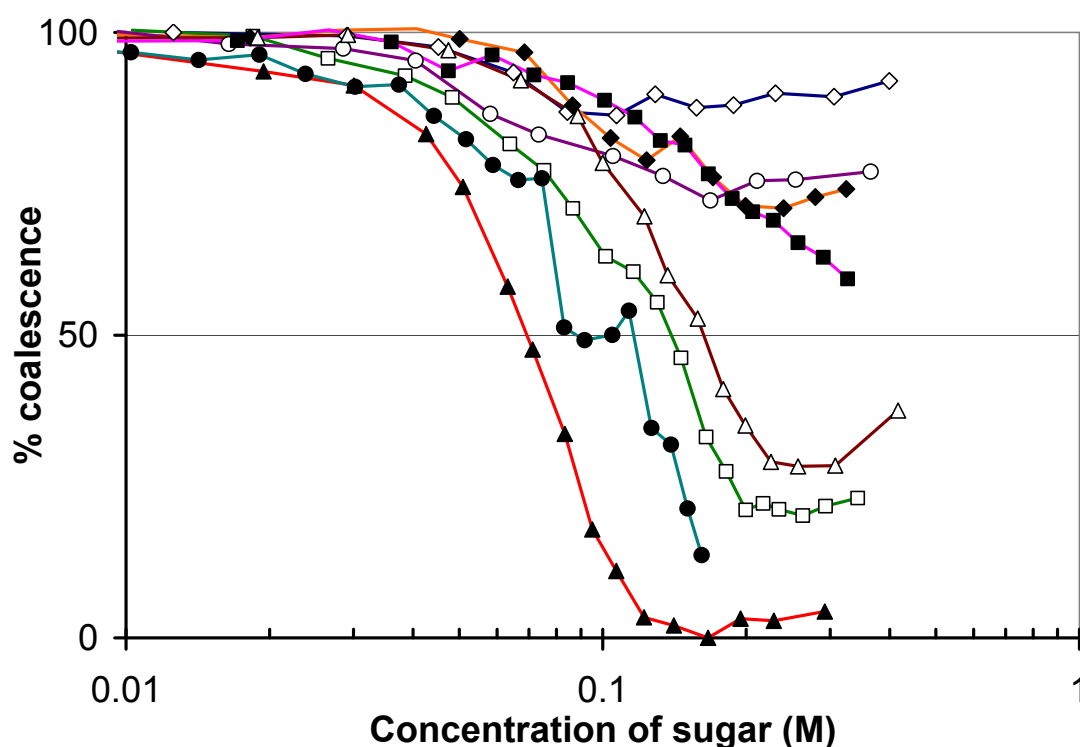


received. I used monosaccharides arabinose (Kerfoot's), fructose, galactose, mannose (all SigmaAldrich) and glucose (BDH), and disaccharides lactose (SigmaAldrich), maltose (M&B) and sucrose (Merck). Sugar structures are depicted alongside results in Table 3.1. The lactose was obtained as the monohydrate; all other sugars were anhydrous. Stock solutions were added to 41.0mL pure water.

### 3.3.2 Results

#### 3.3.2.1 Coalescence inhibition in sugars

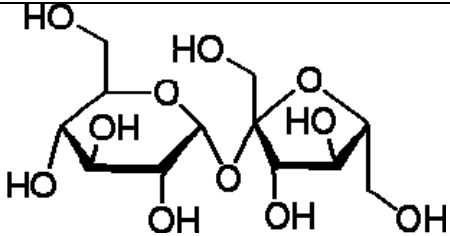
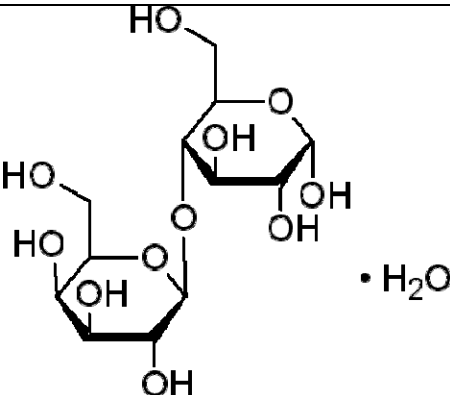
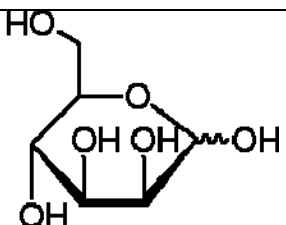
The bubble coalescence results for all sugars tested are presented in Figure 3.14. None of the sugars investigated showed surface activity (which would be indicated by high froth in the bubble column, and a very low value for transmitted light). All of them display some coalescence inhibition with increasing concentration.



**Figure 3.14** Coalescence inhibition by sugars. 0% coalescence is set by the baseline in sucrose (▲). Also shown are disaccharides lactose (●) and maltose (◆) and monosaccharide hexoses glucose (◇), galactose (○), fructose (△) and mannose (□), and pentose arabinose (■).

The relationship of coalescence inhibition to concentration, and the range of concentrations over which inhibition occurs is around 0.1M (comparable to that in inhibiting electrolytes). The transition concentration is not a meaningful measure in sugars as it is in electrolytes. All inhibiting salts reduce coalescence by (roughly) the same degree, so that the final column turbidity is roughly equivalent and hence the detector photodiode voltages are comparable across all salts. In contrast, some sugars show a sigmoidal curve of decreasing coalescence with increasing concentration to a stable coalescence value, but the lowest value of stable coalescence is not consistent across all sugars. For this reason the results in Figure 3.14 are plotted using the most inhibiting sugar, sucrose, to set the “0% coalescence” column turbidity baseline.

**Table 3.1** Bubble coalescence inhibiting power of sugars, ranked from most inhibiting to least inhibiting at a concentration of 0.15M.

Sugar	Molecular structure	Voltage change at 0.15M (V)
Sucrose		1.72
$\alpha$ -Lactose monohydrate		1.35
D-Mannose		0.96

Sugar	Molecular structure	Voltage change at 0.15M (V)
D-(-)-Fructose		0.78
$\alpha$ -Galactose		0.41
L-(+)-Arabinose		0.32 <sup>a</sup>
Maltose		0.32
D-Glucose		0.20

<sup>a</sup>Arabinose continues trending downward rather than flattening, and thus has a coalescence percentage lower than that of galactose at higher concentrations.

To make a quantitative comparison of coalescence inhibition, in Table 3.1 I have used the change in photodiode voltage for each sugar at a sugar concentration of 0.15M (chosen because all sugars have been measured at this level). A larger value of voltage change indicates a larger change in column turbidity, and is hence associated with more

powerful inhibition of bubble coalescence. The sugar structures are also given. In all sugars the initial gas flow and turbidity in water are very similar, because as the experiments were carried out over the space of a few days, with no change made to the bubble column setup. Therefore the voltage change reflecting the change in column turbidity is considered to be a valid measurement.

The transition concentration measured in sucrose was 0.075M in one run and 0.090M in the second. The reason for this discrepancy is presumed to be due to the fact that there were some months between these measurements and column set-up and gas flow probably changed a little, as discussed in the bubble column description in Section 2.2. Measurements made on the same day agree much more closely.

Some of the sugars look to contain some surface-active contamination. In particular, coalescence inhibition in lactose showed changes over time after each addition of stock solution. This is a behaviour that commonly indicates the presence of a surface-active contaminant that is being carried to the top of the glass column as the system self-cleans. In such cases it may not be practical to allow equilibration at each concentration change, and so the intermediate inhibition values in lactose must be treated with caution. At the final concentration the solution is left for a long time to ensure that a stable coalescence regime is reached. Adhikari et al. also noted the presence of a surface active contaminant in commercially available lactose.<sup>170</sup> Some of the solutions appear to show a slight upturn in coalescence (decrease in inhibition) at high sugar concentrations. The change is generally small and is attributed to natural variation in coalescence and to decrease in gas flow as the mass of solution in the column increases on the frit, but it is possible that it represents a real effect on bubble coalescence.

### 3.3.2.2 *Disaccharides and their components*

Inhibition in the disaccharides has been compared with inhibition in their monosaccharide components, alone and as an equimolar mixture. Sucrose, for instance, is comprised of one glucose and one fructose monomer, and it is of interest to compare the bubble coalescence inhibition in sucrose with glucose and fructose, and with a

1:1 (glucose+fructose) mixture, as shown in Figure 3.15. Results are also shown for lactose (glucose+galactose) in Figure 3.16, and for maltose (a diglucose) in Figure 3.17.

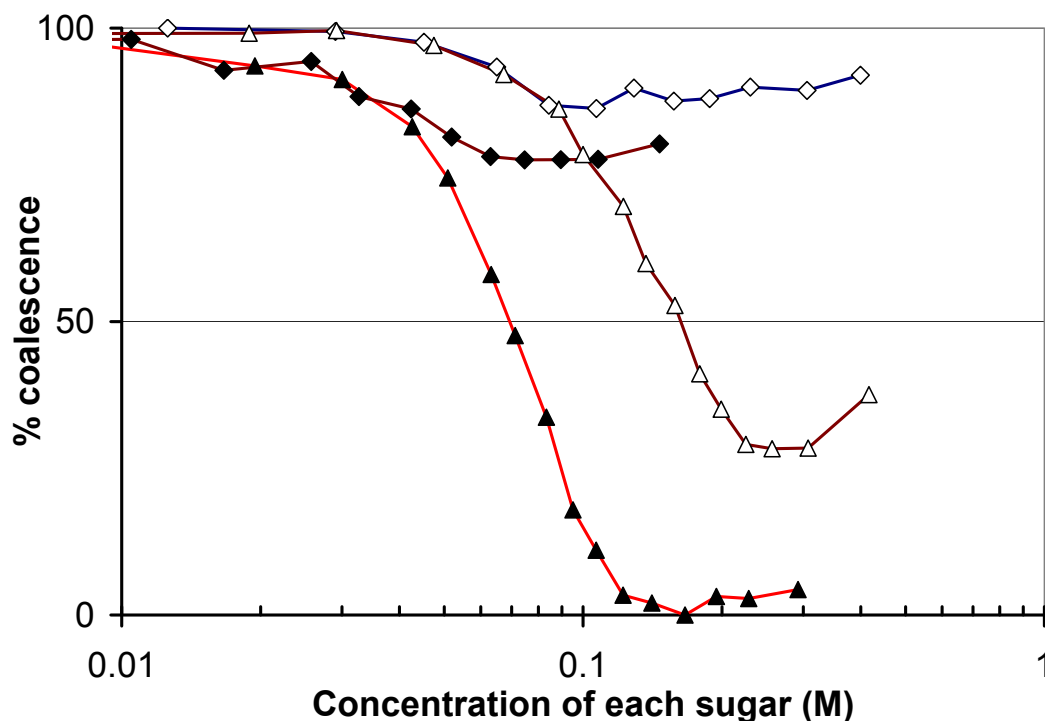


**Figure 3.15** Coalescence inhibition by sucrose ( $\blacktriangle$ ); its component monosaccharides glucose ( $\diamond$ ) and fructose ( $\triangle$ ); and an equimolar mixture of glucose+fructose ( $\blacklozenge$ ). The mixture is graphed as the concentration of each monosaccharide so it can be compared directly to sucrose. 0% coalescence is set at a stable low coalescence value in sucrose. Sucrose is stronger than each of its monomers and the equimolar mixture of them.

Both sucrose and lactose are significantly better inhibitors than their component monomers, and maltose is a somewhat stronger inhibitor than glucose. The disaccharides are stronger than an unbonded equimolar mixture of their two separate components, which indicates that there is some additional inhibition arising from the formation of the larger molecule.

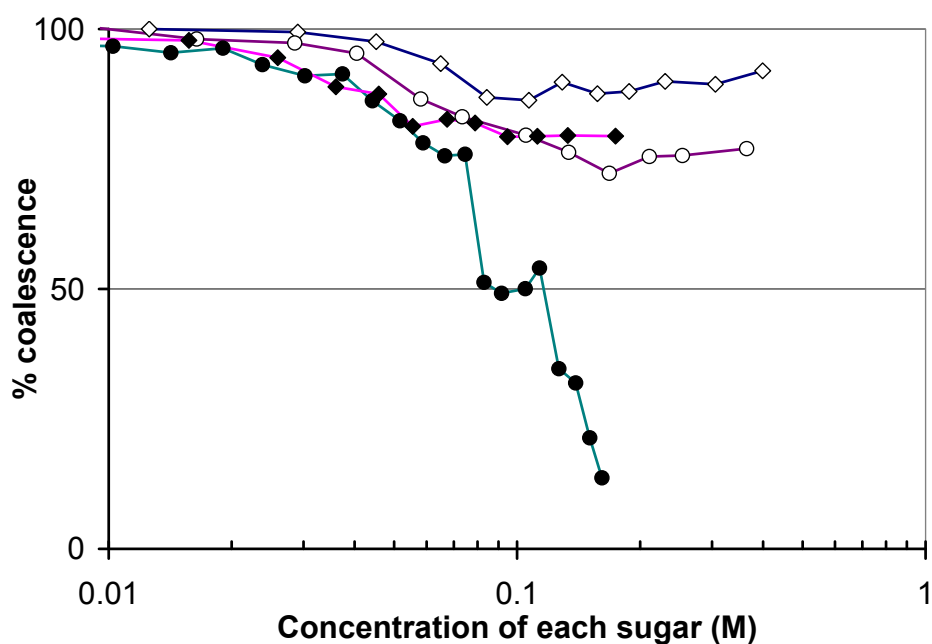


**Figure 3.16** Coalescence inhibition by lactose (●); its component monosaccharides glucose (◇) and galactose (○); and an equimolar mixture of glucose+galactose (◆). The mixture is graphed as the concentration of each monosaccharide so it can be compared directly to lactose. 0% coalescence is set at a stable low coalescence value in sucrose. Lactose is noticeably impure and the coalescence changes with time as the solution self-cleans.

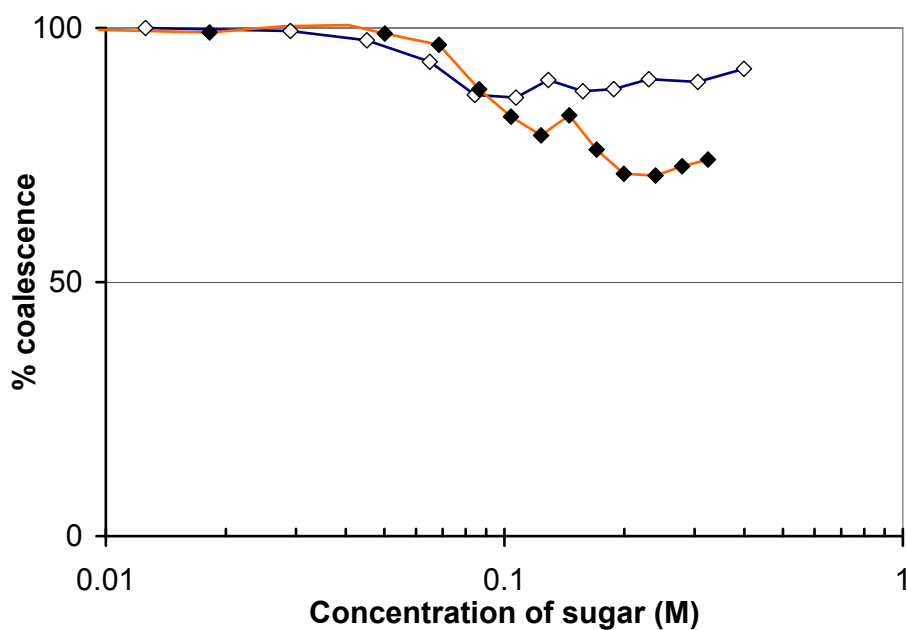


**Figure 3.17** Coalescence inhibition by maltose (◆), a disaccharide of glucose (◇). 0% coalescence is set at a stable low coalescence value in sucrose.

### 3.3.3 Discussion

Sugars can act to inhibit bubble coalescence in water, and the inhibition is “sugar specific”. A range of behaviours is observed between sucrose, which inhibits bubble coalescence to a degree comparable with 1:1 inhibiting electrolytes and a transition concentration  $<0.1\text{M}$ ; and glucose, which has only a small effect on coalescence inhibition and shows a fairly level and high coalescence up to  $0.4\text{M}$ . Sugar molecules with very similar structures can have significantly different effects on coalescence. We must consider here the same questions as arise in electrolyte bubble coalescence inhibition: how do these non-surface active solutes stabilise bubbles against coalescence? And what causes the differences between very similar molecules? A third point that arises is whether the mechanism is the same for electrolyte and sugar coalescence inhibition.

#### 3.3.3.1 *Surface affinity of sugars*

Sucrose and other sugars are not surface active and have little effect on the surface tension of water. Some data are given in Table 3.2, along with a repeat of the results data presented as voltage change in the photodiode detector at  $0.15\text{M}$  for each sugar.

However these values should be treated with caution. The literature data available for sugar surface tensions is inconsistent. Sucrose surface tension gradients reported include:  $+3\text{mN/m/M}$ ;<sup>171</sup>  $+1.8\text{mN/m/M}$ ;<sup>168</sup>  $+1.47\text{mN/m/M}$ ;<sup>163</sup>  $+1.1\text{mN/m/M}$ ;<sup>169</sup> and negative.<sup>172</sup> Hoorfar et al. report that the gradient is non-linear.<sup>173</sup>

Other sugars show similar variation. There would appear to be considerable problems associated with obtaining these data, which may be due to contamination, temperature sensitivity or other instrumental problems. Sucrose is one of the most pure sugars obtainable, so any other measurements will likely be even more difficult. It was decided that one more measurement of sucrose surface tension would not resolve the problem. More, and more precise, measurements of surface tension in sugar solutions, would certainly be of use to further investigate the possibility of a link between surface tension gradient and coalescence inhibition – and this work is planned for the future, but it is expected to require some time and the appropriate instruments.

It can be concluded that the effect of sucrose on surface tension is low, and most likely positive (indicating a depletion in the interfacial region). What data is available would suggest that there is no definite correlation between  $(d\gamma/dc)$  (or  $(d\gamma/dc)^2$ ) and bubble coalescence inhibition in sugars. For instance, glucose and sucrose have very similar surface tension gradients (from the same method in the same reference<sup>169</sup>) and yet their effect on bubble coalescence is very different.

**Table 3.2** Bubble coalescence inhibiting power of sugars

Sugar	Voltage change at 0.15M (V)	$d\gamma/dc$ (where known) (mN/m/M)
Sucrose	1.72	1.1 <sup>a</sup>
Lactose	1.35	3.24 <sup>b</sup>
Mannose	0.96	
Fructose	0.78	1.19 <sup>c</sup>
Galactose	0.41	
Arabinose	0.32	
Maltose	0.32	
Glucose	0.20	1.21 <sup>a</sup>

<sup>a</sup> From Matubayashi and Nishiyama, measured from 0-0.6 mol kg<sup>-1</sup>.<sup>169</sup>

<sup>b</sup> Value calculated from data in International Critical Tables<sup>163</sup>

<sup>c</sup> Adhikari et al. find surface tension change of +5.13mN in 60%w/w solution;<sup>170</sup> solution density 1.29g mL<sup>-1</sup> from Mettler-Toledo International Inc.<sup>174</sup>

Sugars are highly soluble in water, and can engage in hydrogen bonding through their -OH groups.<sup>175</sup> However the organic backbone also gives a partially hydrophobic character.<sup>176, 177</sup> Increased hydrophobicity may be associated with greater affinity for the air-water interface. The relative hydrophobicity of some of the sugars has been investigated.

Koga et al. probe hydrophobicity and hydrophilicity of sugars based on changes to 1-propanol interaction with water. The relative hydrophobicity increases in the order:



---

glucose < fructose < sucrose.<sup>177</sup> This order does correlate with increased bubble coalescence inhibition.

In contrast, Janado and Yako investigated hydrophobicity of monosaccharides by their partitioning in aqueous solution and a polystyrene gel. The hydrophobicity was found to increase in the order galactose < glucose < mannose < arabinose. These results do not correlate with bubble coalescence inhibition.

As with surface tension gradient, there is simply too little known about sugar interactions with hydrophobic interfaces to enable us to determine whether this is a relevant factor in bubble coalescence inhibition.

#### 3.3.3.2 *Sugar characteristics and specificity*

The bubble coalescence inhibition data suggest “sugar specificity”, with the degree of coalescence inhibition dependent upon the sugar molecule present. Some attempts have been made to consider possible differences between sugars that may explain the different abilities to stabilise bubbles in solution. It is hoped that such a correlating characteristic, if found, may also shed light upon the ion specific bubble coalescence inhibition.

The three disaccharides tested (sucrose, lactose and maltose) all inhibit coalescence more strongly than do their component monosaccharides. In addition, equimolar mixtures of the monomers of sucrose and lactose appear to inhibit somewhere midway between the two individual components. In the case of sucrose components fructose and glucose, there may even be a slight reduction in the efficacy of fructose, in the presence of glucose – suggesting possible competition effects. These results suggest that the bonding of the two monosaccharides, or the formation of a larger molecule, may be important in coalescence inhibition. The disaccharide maltose is less powerful an inhibitor than many of the monosaccharides, showing that absolute size of the molecule is not always significant.

The results of comparing disaccharides and their components, as well as the general difference in inhibiting effect amongst sugars that have very similar structures, together indicate that relatively subtle changes in solute properties may have large effect on bubble coalescence inhibition. An example is presented in Figure 3.18 of the small differences in structure that may change coalescence inhibition. Galactose and mannose are monosaccharides that differ only in the arrangement of attachment around two (chiral) carbon centres. However their effect on coalescence differs substantially.

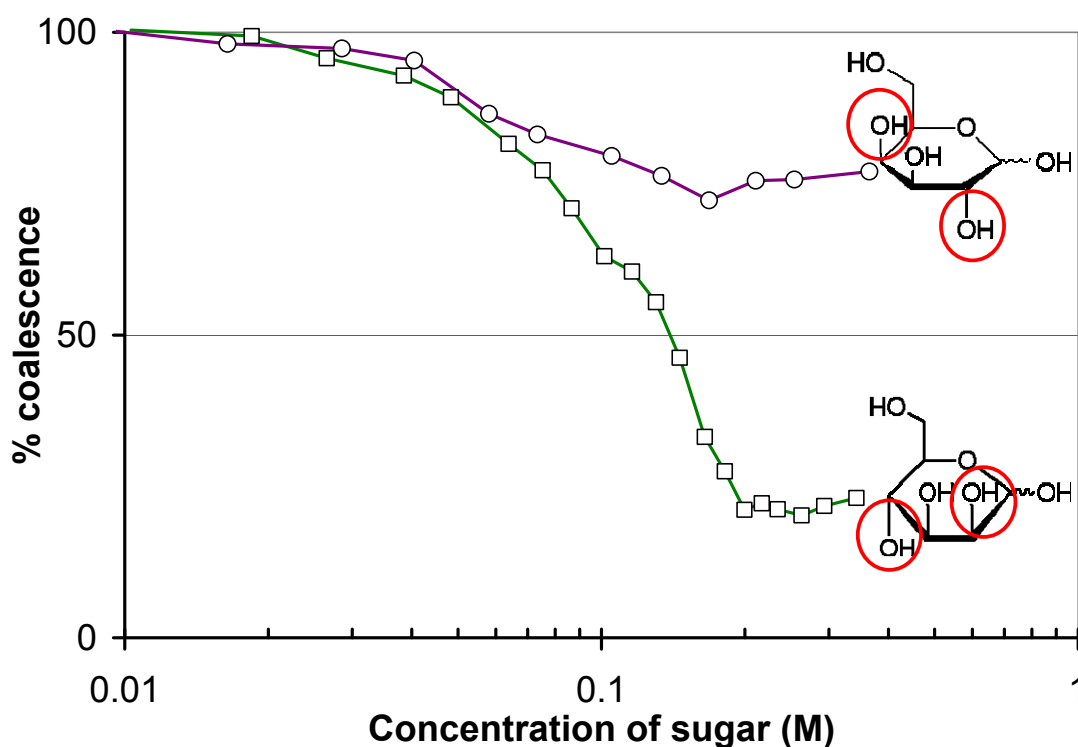


**Figure 3.18** Sugar specific coalescence inhibition in monosaccharides galactose (○) and mannose (□). The structure of each sugar is given – these two differ only in the geometry of attachment of two hydroxyl groups (circled) to their carbon centres. 100% coalescence is in pure water, 0% is a stable value in strongly inhibiting sugar sucrose.

This result suggests that molecule hydrophobicity (discussed above) is not significant – these sugars have the same chemical moieties and so are predicted to have very similar hydrophobic character. Sugars do hydrogen-bond intramolecularly and intermolecularly with water, and this bonding may be affected by small changes in the hydroxyl environment as shown between mannose and galactose.<sup>178</sup> Hydrogen bonding helps control the molecule's preferred conformation, and will also affect the local water

---

structure in the solvation shell.<sup>175, 178</sup> Both of these factors might change the effective molecular size (which is related to diffusion) or preference for the interface. It is possible that further analysis of the preferred conformation of sugars in the presence of hydrogen-bonding with water, may reveal a correlation with bubble coalescence inhibition.

Another aspect of sugar behaviour one may consider is the tendency of many of the molecules to tautomerise – to exist in different forms in aqueous solution. It was hypothesised that such a property might be important if, as in electrolytes, the combination of two different solute species was relevant to bubble coalescence inhibition. Fructose, for instance, exists as fructofuranose (5-membered ring) and fructopyranose (6-membered ring) in the ratio 30:70 at equilibrium.<sup>179</sup> However, there is no correlation between the number (or prevalence) of tautomers and the bubble coalescence inhibition here observed, for available data.<sup>179</sup>

### 3.3.4 Conclusion

The mono- and disaccharides here investigated are non-surfactants that inhibit bubble coalescence relative to pure water. They vary in their degree of effectiveness, but stabilise bubbles at about the same concentration as inhibiting electrolytes. There is not a strong correlation of coalescence inhibition with surface tension gradient, nor with solute hydrophobicity.

Disaccharides are more effective than their individual components, and more effective than equimolar mixtures of those components – indicating that size effects may be important. Subtle changes in the molecular structures of sugars can lead to significant differences in bubble coalescence in their solutions. This result is consistent with the different assignments of similar ionic species, such as  $\alpha$  anion  $\text{IO}_3^-$  and  $\beta$  anion  $\text{ClO}_3^-$ . It is possible that solvation of the solute may be implicated, and that this may change surface affinity and the size of the hydrated species.

There is no direct evidence that the mechanism of coalescence inhibition and thin film stabilisation in nonelectrolytes is the same as that in inhibiting salts. However the similarity in coalescence degree and the concentration range, as well as the existence of solute specificity, suggests the possibility of a like mechanism. Under that assumption, the charge on the ions is not important in stabilising thin films. This argues against an inhibition via a change in electrostatic surface forces. Rather, if charge on the solute is not important then an osmotic-type mechanism is suggested, that is driven by concentration gradients of solute species irrespective of charge.

---

## **Chapter 4 Bubble Coalescence Inhibition by Electrolytes in Nonaqueous Solvents**

---

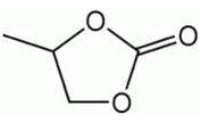
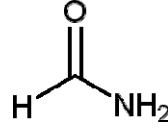
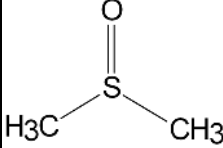
### **4.1 INTRODUCTION**

This chapter reports an investigation of the influence of electrolytes on bubble coalescence in a range of nonaqueous solvents. The use of nonaqueous solvents allows us to vary the solvent structure and physical properties. Solvent physical properties are expected to influence bubble stability and the coalescence mechanism. Thin film drainage is related to the viscosity; the surface tension is related to the intramolecular interactions of the solvent molecules; the change in surface tension is influenced by the propensity of the solute for the interface; the electrostatic component of the surface forces is influenced by the dielectric constant; and the magnitude of the interfacial charge and its electrodynamic component are governed by the absorption spectra. The chemical interactions of ions and solvent, both in bulk and at the interface, are also expected to vary between solvents.

I measured the effect of increasing electrolyte concentration on bubble coalescence in various solvents, using the bubble column apparatus. We have investigated electrolyte inhibition of coalescence in nonaqueous solvents methanol, formamide, propylene carbonate and dimethylsulfoxide (DMSO). Ideally more solvents would be studied but the choice of solvent is limited by the inability of most nonaqueous solvents to dissolve a range of electrolytes at sufficiently high concentrations, as well as by consideration of chemical stability and safety. Pertinent physical properties of the pure solvents are presented in Table 4.1. We aimed to elicit the importance of solvent structure in bubble coalescence inhibition by determining: if electrolytes inhibit coalescence in nonaqueous solvents; if this coalescence inhibition behaviour shows ion-specificity that can be

rationalized by combining rules; and if so, whether the ion empirical assignments (i.e.  $\alpha$  and  $\beta$  ion groups) differ in different solvents.

**Table 4.1.** Comparison of solvent properties<sup>a</sup>

	Water <sup>b</sup>	Methanol	Propylene carbonate	Formamide	Dimethyl-sulfoxide (DMSO)
Formula	H <sub>2</sub> O	CH <sub>3</sub> OH	C <sub>4</sub> H <sub>6</sub> O <sub>3</sub> 	HCONH <sub>2</sub> 	(CH <sub>3</sub> ) <sub>2</sub> SO 
Molecular Weight (g mol <sup>-1</sup> )	18.02	32.04	102.10	45.04	78.13
Protic	Yes	Yes	No	Yes	No
Dielectric Constant (20°C)	80.20	33.0	66.14	110.0	47.24
Polarity (Debye) (20°C)	1.85	1.70	4.94 <sup>c</sup>	3.73	3.96
Viscosity (mPa s) (25°C)	0.890	0.544	2.5 <sup>d</sup>	3.30	1.987
Density (g mL <sup>-1</sup> ) (20°C)	0.9982	0.7914	1.2047	1.133	1.1014
Surface tension (mN m <sup>-1</sup> ) (25°C)	71.99	22.07	41.9 <sup>c</sup> (20°C)	57.03	42.92
Vapour pressure (kPa) (25°C)	3.17	16.9	0.017 (20°C) <sup>e</sup>	0.011 (20°C) <sup>f</sup>	0.08

<sup>a</sup>All data taken from the CRC Handbook of Chemistry and Physics<sup>57</sup> except where otherwise referenced.

<sup>b</sup>Results reported in Craig et al.<sup>10</sup>

<sup>c</sup>Data from <http://macro.lsu.edu/howto/solvents/Dipole%20Moment.htm><sup>180</sup>

<sup>d</sup>Data from Barthel et al.<sup>181</sup>

<sup>e</sup>Data from MSDS.<sup>182</sup>

<sup>f</sup>Data from MSDS.<sup>183</sup>

---

## 4.2 MATERIALS AND METHODS

The bubble column apparatus was described in section 2.2, above. The gas flow of N<sub>2</sub> through the frit into the bubble column was measured for these experiments as 12 mL/s. In some instances this was varied to confirm independence of the transition concentration on gas flow. All experiments were done at room temperature (~23°C). The apparatus was altered to minimise exposure of the bubble column to the atmosphere during experiments in nonaqueous solvents. All the nonaqueous solvents used are hygroscopic, and so the uptake of atmospheric water was a concern. The Perspex box containing the apparatus was made nearly airtight and N<sub>2</sub> gas was passed through the chamber so formed for ~1 hour before experiments began, to reduce humidity. In some cases a vacuum line was used to extract vapour-loaded gas from the chamber. For some experiments a blanket of N<sub>2</sub> gas was used to cover the top of the burette containing stock solution; alternatively the burette was covered when not in use to minimize uptake of atmospheric H<sub>2</sub>O by the stock solution.

All water used was purified using a MilliQ gradient system. The solvents propylene carbonate (anhydrous, purity 99.7%); methanol (anhydrous, purity 99.8%); and DMSO (anhydrous, purity 99.9%) were used as received from Sigma Aldrich. Formamide (>99% purity) was used as received from Fluka and from BDH. Salts were roasted or freeze-dried to remove water; in some cases salts were used as received. Concentrated aqueous acids were used as received, as were methanolic HCl (Sigma Aldrich) and methanolic H<sub>2</sub>SO<sub>4</sub> (Sigma Aldrich). Propylene carbonate and DMSO stock solutions were made up under N<sub>2</sub> in a glove bag, and methanol and formamide stock solutions were made up in a fumehood. Stock solutions varied between 0.15 M and 1 M depending on the solubility of the salt being investigated. The effect of contaminating water on bubble coalescence was investigated by measuring bubble coalescence as a function of added water volume, in the absence and presence of electrolytes.

Solubilities were found in the literature where available, and for some electrolytes they were tested. The electrolyte solubilities in these solvents were not quantitatively measured; rather I checked whether an electrolyte-solvent combination could be used for bubble column measurements. A complete test of an electrolyte's inhibition effect

requires a minimum solubility of 0.25M, in order that the stock solution can be added to pure solvent in such a volume as to fit in the bubble column, and also reach high enough final concentration that the coalescence inhibiting nature of the electrolyte (and preferably its transition concentration) can be determined. (In some cases salts of lower solubility were used for the purposes of comparing across solvents.) If, therefore, a further study of inhibition in nonaqueous systems were to be carried out using some different technique, the arsenal of potential salt/solvent combinations has the potential to be a little extended. A list of solubility (and ion-pairing) references that were found useful for the range of solvents used is here provided.<sup>184-194</sup>

## 4.3 RESULTS

### 4.3.1 The influence of atmospheric humidity

All solvents used are hygroscopic. It was impractical to conduct the bubble coalescence experiments in a manner such that the solutions would at no stage be exposed to atmospheric humidity. This was a concern because of the possibility that the presence of even small amounts of water might affect bubble coalescence and electrolyte inhibition – either by direct surface activity, or by preferential solvation of ions in solution.

This problem was addressed by determining the effect added water has on bubble coalescence in nonaqueous solvents. We added increasing volumes of water to the solvents from a burette, and measuring coalescence inhibition as a function of water volume fraction. Results are presented for the four nonaqueous solvents in Figure 4.1.

Bubble coalescence in both propylene carbonate and formamide is relatively insensitive to added water. The photodiode signal is little affected up to ~5% v/v (~2mL in 41mL solvent). Porras and Kenndler also studied the effect of water impurities in formamide and found that a small amount of water in formamide does not greatly affect the bulk diffusion or ion mobility.<sup>195</sup> In DMSO, the effect of water becomes significant at 1.2% (v/v), and at ~5% (v/v) water the signal had decreased from 2.5V to 2.0V. This corresponds to a bubble coalescence change of 25%. The atmospheric humidity in the laboratory is around 30%, and the level of water uptake by the solvents will be well



below 1% by volume (equivalent to 0.4mL in the 41.0mL neat solvent). Under those conditions the water contribution to the observed coalescence inhibition is expected to be very small and distinguishable from the electrolyte contribution in formamide, propylene carbonate and DMSO. However the presence of trace water levels may mean that transition concentration values for electrolytes are slightly underestimated. The values observed are stable over time, indicating that uptake of atmospheric moisture is not significant in the bubble column.

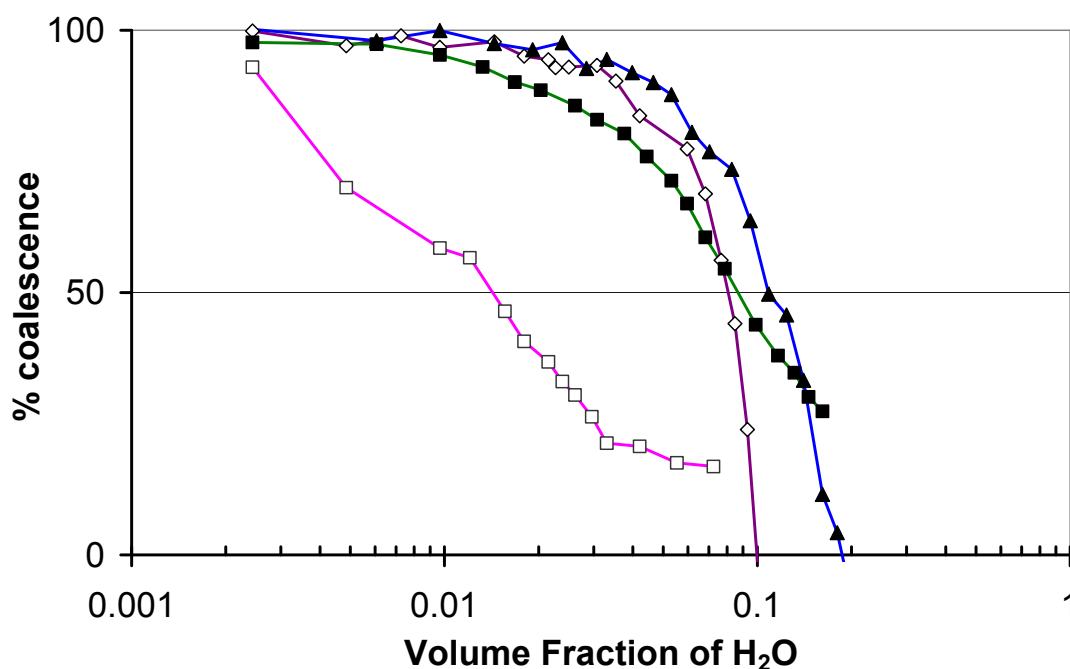


**Figure 4.1** Effect of water on coalescence in each solvent tested, as a function of log of volume ratio in methanol ( $\square$ ), DMSO ( $\blacksquare$ ), formamide ( $\blacktriangle$ ) and propylene carbonate ( $\diamond$ ). 100% coalescence is defined in the pure solvent in each case; 0% coalescence is a stable, low, voltage signal in inhibiting electrolytes. Methanol shows greatest sensitivity to small amounts of added water.

Methanol bubble stability shows the greatest sensitivity to dissolved H<sub>2</sub>O. There is an immediate decrease in photodiode signal (increase in inhibition) on addition of even 0.1mL (~0.2% v/v) water. In order to observe the effect of a smaller amount of water, a solution of 1% H<sub>2</sub>O in methanol by weight was used as stock (data not shown). The final concentration of H<sub>2</sub>O was then ~0.4% by weight. The observed signal was slightly lower (<5% coalescence) than in pure methanol. This indicates that, while water does

act to inhibit bubble coalescence even at this low concentration, the effect is likely to be dominated by the electrolyte coalescence inhibition, at any reasonable level of contaminating H<sub>2</sub>O. It was also observed that bubbling for one to two hours (the course of an experiment) in an undisturbed methanol solution led to a small decrease in photodiode voltage, or increase in bubble coalescence inhibition (~ 5% coalescence). This may be due to absorption of water from the atmosphere. Also, because methanol is volatile, it readily evaporates and condenses on the outside of the bubble column. This may influence the experiment in two ways – first, the concentration of contaminant (and electrolyte) will increase slightly during an experiment; and secondly, the N<sub>2</sub> atmosphere could not be maintained, as it was necessary to wipe the column to avoid laser scattering by external condensation, and this meant briefly opening the experiment to ambient conditions.

Tests in propylene carbonate and in methanol on the effect of water in the presence of electrolyte (not shown) demonstrated that the effects of water and of electrolyte are essentially additive and independent (within the sensitivity of the instrument). These results therefore provide confidence that coalescence effects in nonaqueous solvents can be attributed to the added electrolyte.

#### **4.3.2 Bubble coalescence inhibition in methanol**

Methanol is a protic solvent with a hydrogen-bonding network somewhat weaker than that of water, and it tends to solvate ions less strongly.<sup>196</sup> Despite having the lowest dielectric constant of all the solvents studied, methanol dissolves a wide range of electrolytes.<sup>189</sup> Thirteen different electrolytes were investigated, and all electrolytes studied were found to inhibit bubble coalescence over a relatively narrow concentration range (as seen in Figure 4.2). Transition concentrations (corresponding to 50% coalescence inhibition) for all electrolytes tested are reported in Table 4.4 along with the data from other solvents. These data demonstrate that the ability of electrolytes to inhibit bubble coalescence is not confined to aqueous systems. However, methanol shows little difference between salts, and none of the salts tested act as ‘non-inhibitors’. It is also noteworthy that electrolytes in methanol show no correlation between

transition concentration and ionic strength, whereas a strong correlation was found amongst inhibiting salts in aqueous solution.<sup>9</sup> The transition concentration for electrolytes in methanol is more than 50% lower than that typically found in water. The value of the photodiode detector voltage at high salt concentrations is much lower than observed in other solvents (0.05V compared to around 0.5V). This indicates that the laser scattering is greater and bubbles are much smaller and indeed, the column presents an opaque, frothy appearance to the eye in high concentrations of electrolyte in methanol.

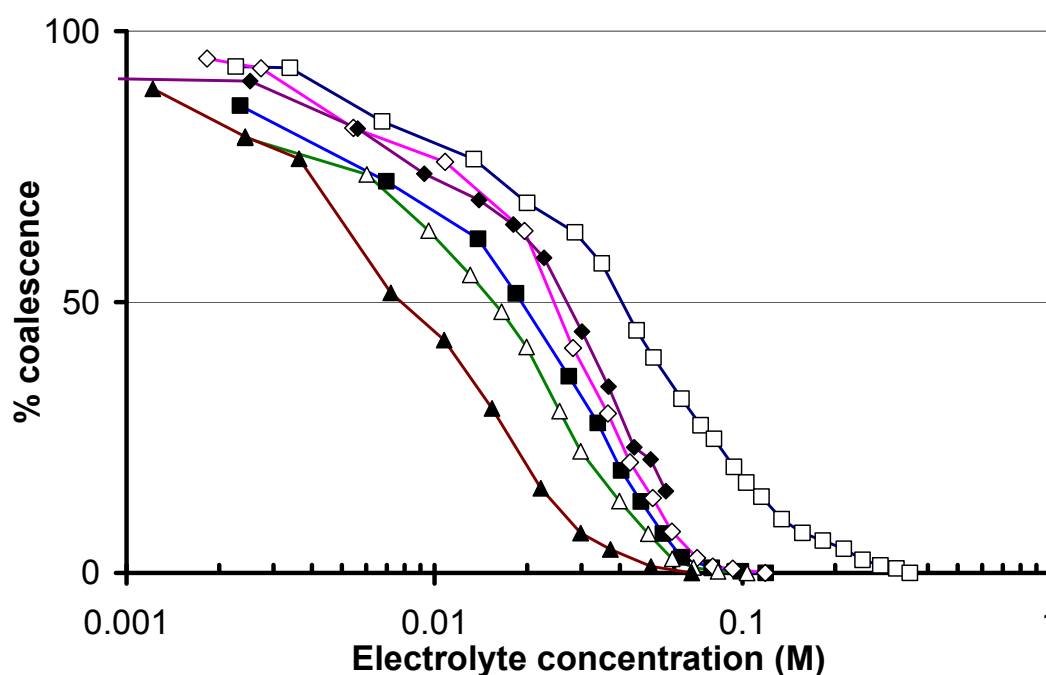


**Figure 4.2** Inhibition of bubble coalescence by selected electrolytes in methanol solutions as a function of concentration. Electrolytes shown are NH<sub>4</sub>SCN (▲), MgCl<sub>2</sub> (△), H<sub>2</sub>SO<sub>4</sub> (■), NaClO<sub>4</sub> (◇), NaCl (◆), HCl (□). 100% coalescence is defined in pure methanol, 0% coalescence is a stable low voltage signal in inhibiting electrolytes.

### 4.3.3 Bubble coalescence inhibition in formamide

Formamide is used in electrophoresis as a solvent of organic ions.<sup>195</sup> It is polar and has a strong three-dimensional hydrogen-bonding network even more pronounced than that of water.<sup>195</sup> The effects of electrolytes on bubble coalescence in formamide are shown in Figure 4.3. Coalescence inhibition trends are remarkably similar to those seen in water.

Some salts tested show strong inhibiting character, at concentrations similar to those seen in inhibiting salts in water. Others show no effect or need a much higher concentration to elicit an equivalent inhibition in coalescence. If these latter two categories (less inhibiting and non-inhibiting) are grouped, then the combining rules and designations can be determined for the effects of salts in formamide, as shown in Table 4.2. The ion  $\alpha$  and  $\beta$  assignments match those found in water.

**Table 4.2** Ion assignments in formamide

Ions		Li <sup>+</sup>	Na <sup>+</sup>	NH <sub>4</sub> <sup>+</sup>	(CH <sub>3</sub> ) <sub>4</sub> N <sup>+</sup>
Assignment		$\alpha$	$\alpha$	$\alpha$	$\beta$
Cl <sup>-</sup>	$\alpha$	✓			
Br <sup>-</sup>	$\alpha$				✗
I <sup>-</sup>	$\alpha$	✓	✓		
ClO <sub>4</sub> <sup>-</sup>	$\beta$	✗			
CH <sub>3</sub> COO <sup>-</sup>	$\beta$		✗ ✗	✗ ✗	✗ <sup>a</sup>

✓ indicates bubble coalescence inhibition.  $\alpha\alpha$  and  $\beta\beta$  salts = ✓.

✗ and ✗✗ indicate partial inhibition and no inhibition, respectively, relative to pure formamide.  $\alpha\beta$  and  $\beta\alpha$  salts = ✗ or ✗✗.

<sup>a</sup>Tetramethylammonium acetate is believed to be affected by contamination.

Tetramethylammonium acetate (data not shown) produces an inconsistent result – it is predicted to be (as in water) a  $\beta\beta$  salt that inhibits bubble coalescence relative to pure formamide. Instead, addition of the concentrated solution to the bubble column increases photodiode signal, which generally indicates lower laser scattering and increased coalescence relative to the pure solvent. This belies observations that tetramethylammonium acetate does act to inhibit bubble coalescence. Evidence for this lies in the (qualitative) “swirl test” – the generation of bubbles by a single swirl of the stock solution yields significant differences visually between inhibiting salts, which generate a slight foam that exists for several seconds after swirling, and non-inhibitors in which no long-lived bubbles are seen. Tetramethylammonium acetate is a highly hygroscopic and unstable solid, and so the results recorded are possibly influenced by

contamination. Porras and Kenndler note that formamide “as received” contains around 0.02M of the dissociation products ammonia and formic acid.<sup>195</sup> It is possible that reaction can take place with added tetramethylammonium acetate. In non-reacting conditions the dissociation products form ionic ammonium formate, and at 0.02M this electrolyte is expected to have little effect on bubble coalescence.

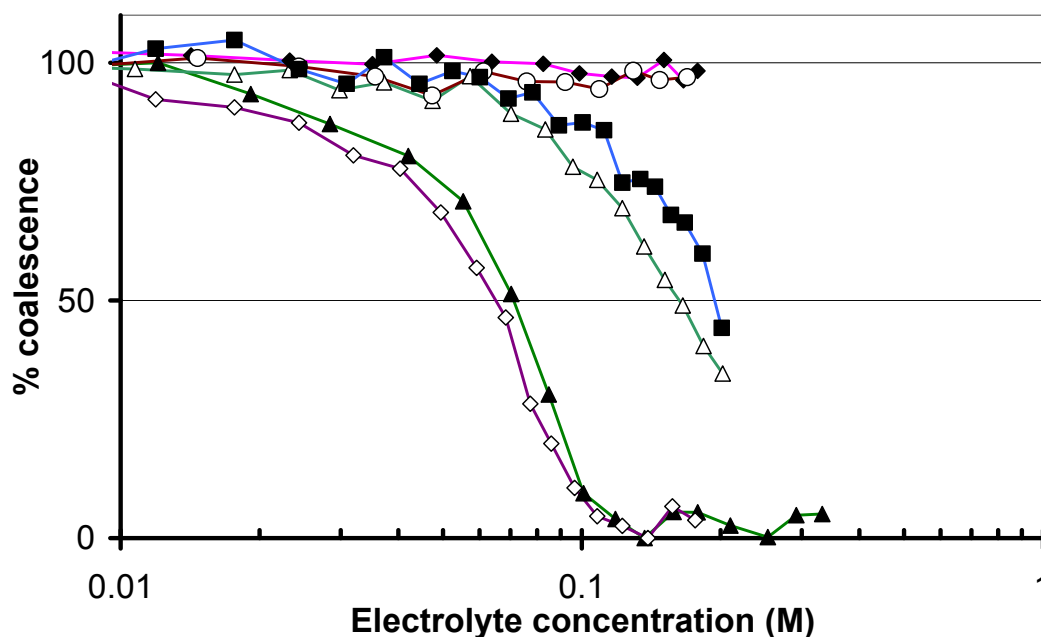


**Figure 4.3.** Inhibition of bubble coalescence by selected electrolytes in formamide solutions as a function of concentration. Electrolytes shown are NaI ( $\diamond$ ), LiCl ( $\blacktriangle$ ), LiClO<sub>4</sub> ( $\triangle$ ), (CH<sub>3</sub>)<sub>4</sub>NBr ( $\blacksquare$ ), CH<sub>3</sub>COONa ( $\blacklozenge$ ), CH<sub>3</sub>COONH<sub>4</sub> ( $\circ$ ). 100% coalescence is defined in pure formamide, 0% coalescence is a stable, low, voltage signal in inhibiting electrolytes. Electrolytes can be grouped into two categories of “inhibiting” and “less inhibiting” salts.

#### 4.3.4 Bubble coalescence in propylene carbonate

Propylene carbonate is shown in Figure 4.4. It is a high dielectric constant solvent, and therefore much in demand as a solvent for batteries.<sup>187</sup> It is aprotic and described as a “relatively unstructured” solvent by Jansen and Yeager.<sup>197</sup>

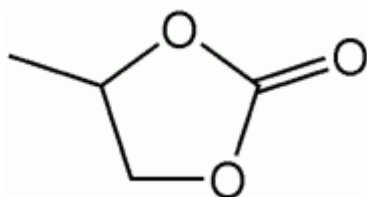


**Figure 4.4** Structure of propylene carbonate. The molecule is polar with the electronegative region over the three oxygens.<sup>192</sup>

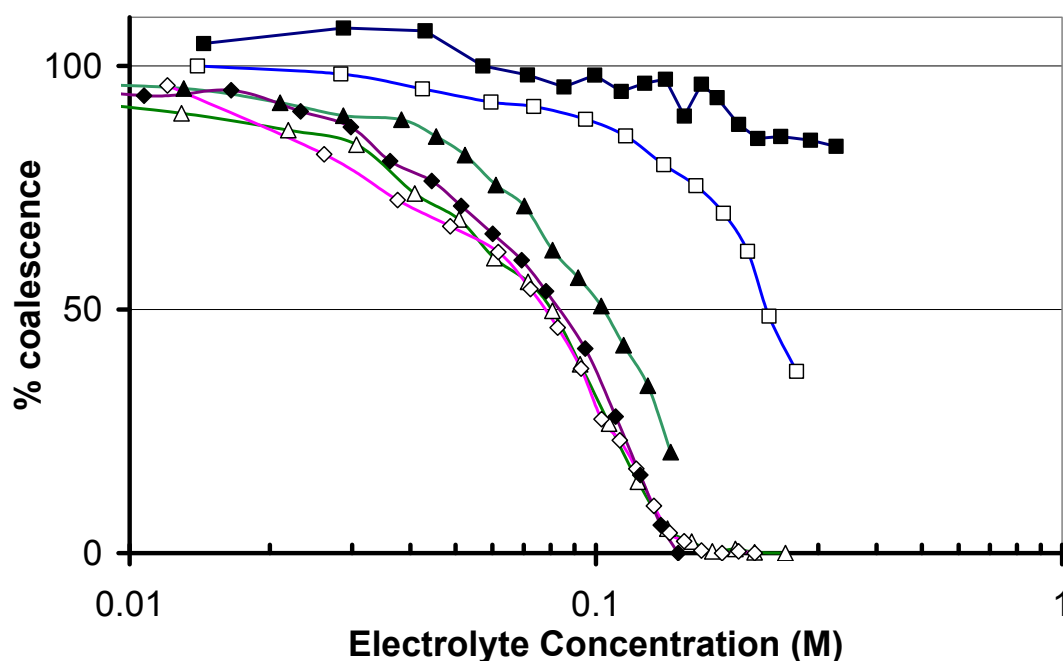


**Figure 4.5.** Inhibition of bubble coalescence by selected electrolytes in propylene carbonate solutions plotted against log of concentration. Shown are  $\text{NaClO}_4$  ( $\diamond$ ),  $\text{LiClO}_4$  ( $\triangle$ ),  $\text{NaSCN}$  ( $\blacklozenge$ ),  $\text{LiBr}$  ( $\blacktriangle$ ),  $\text{HBr}$  ( $\square$ ) and  $\text{HCl}$  ( $\blacksquare$ ). 100% coalescence is defined in pure propylene carbonate, 0% coalescence is a stable, low, voltage signal in inhibiting electrolytes. Acids are added as concentrated aqueous solutions. Two categories of electrolytes can be distinguished as “inhibiting” and “less inhibiting”.

The influence of six different electrolytes on bubble coalescence in propylene carbonate solutions was investigated (Figure 4.5). Electrolytes can inhibit bubble coalescence in propylene carbonate, and bimodal ion-specificity is observed. Four alkali metal salts tested all inhibited bubble coalescence relative to the pure solvent, over a fairly uniform concentration range.  $\text{HCl}$  and  $\text{HBr}$  (added as concentrated aqueous solutions) showed

no coalescence inhibition up to significantly higher concentrations, upon which the volume of non-propylene carbonate solvent becomes important – here, the inhibition may be partly due to water rather than electrolyte effects. Methanolic HCl was also used (data not shown) and its behaviour was consistent with the aqueous acid, suggesting that the nature of the other solvent is not important. These acids are categorized as “less-inhibiting” than the other electrolytes used.

We therefore observe in propylene carbonate two groups of electrolytes – as seen in water. A set of combining rules for cations and anions can be created that is analogous to that seen in water, for the electrolytes used here (see Table 4.3). Using comparable definitions to water,  $\text{Na}^+$  and  $\text{Li}^+$  would be  $\alpha$  cations and  $\text{H}^+$  a  $\beta$  cation. All anions used here ( $\text{Cl}^-$ ,  $\text{Br}^-$ ,  $\text{ClO}_4^-$  and  $\text{SCN}^-$ ) would be in one class, as  $\alpha$  anions. This indicates that ion assignments in nonaqueous solvents may disagree from those in water: aqueous  $\text{ClO}_4^-$  and  $\text{SCN}^-$  are in a different class ( $\beta$  anions) to  $\text{Cl}^-$  and  $\text{Br}^-$ , and  $\text{LiClO}_4$ ,  $\text{NaClO}_4$  and  $\text{NaSCN}$  have no effect on aqueous bubble coalescence.

**Table 4.3.** Ion assignments in propylene carbonate

Ions		$\text{Li}^+$	$\text{Na}^+$	$\text{H}^+$
Assignment		$\alpha$	$\alpha$	$\beta$
$\text{Cl}^-$	$\alpha$			$\times$
$\text{Br}^-$	$\alpha$	✓		$\times$
$\text{SCN}^-$	$\alpha$		✓	
$\text{ClO}_4^-$	$\alpha$	✓	✓	

✓ indicates bubble coalescence inhibition.  $\alpha\alpha$  and  $\beta\beta$  salts = ✓.

$\times$  indicates partial inhibition relative to pure propylene carbonate.  $\beta\alpha$  salts =  $\times$ .

#### 4.3.5 Bubble coalescence in dimethylsulfoxide

Dimethylsulfoxide (DMSO) is, like propylene carbonate, a polar, aprotic solvent. Four electrolytes were studied in DMSO, and all were found to inhibit coalescence over a narrow concentration range, as shown in Figure 4.6. Low salt solubility and high

reactivity prevent a wider selection of salts being used. We note one difference between DMSO and water - sodium perchlorate does not inhibit bubble coalescence in aqueous solutions, but here acts as an inhibiting salt.

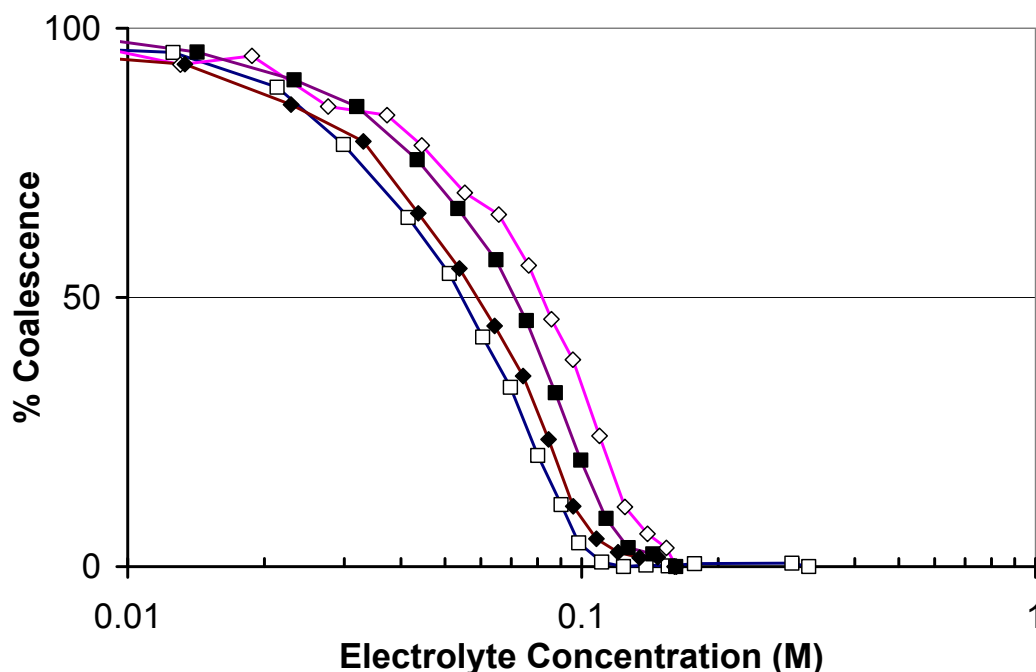


**Figure 4.6.** Inhibition of bubble coalescence by electrolytes in dimethylsulfoxide (DMSO) solutions plotted against log of concentration. Shown are KI ( $\square$ ), NaBr ( $\blacklozenge$ ), KBr ( $\blacksquare$ ) and NaClO<sub>4</sub> ( $\diamond$ ). 100% coalescence is defined in pure DMSO, 0% coalescence is a stable, low, voltage signal in inhibiting electrolytes.

#### 4.3.6 Weak inhibitors at high concentrations in water

In both propylene carbonate and formamide the distinction between salt classes is less clear than in water. It may make be more accurate to distinguish salts by their relative strength as inhibitors: “inhibiting” versus “less-inhibiting” rather than the description commonly used to describe the latter class in water, as having “no effect”.<sup>9, 58</sup> This is particularly so in light of other studies suggesting that “non-inhibiting” salts in aqueous solutions may inhibit coalescence at concentrations above 0.5M.<sup>2, 198</sup> I investigated whether coalescence inhibition is seen in the bubble column at high concentrations of aqueous solutions of two  $\alpha\beta$  electrolytes, CH<sub>3</sub>COONH<sub>4</sub> and NaClO<sub>4</sub>, and  $\beta\alpha$  electrolyte



HCl – all previously described as non-inhibiting. The results of this experiment are shown in Figure 4.7.

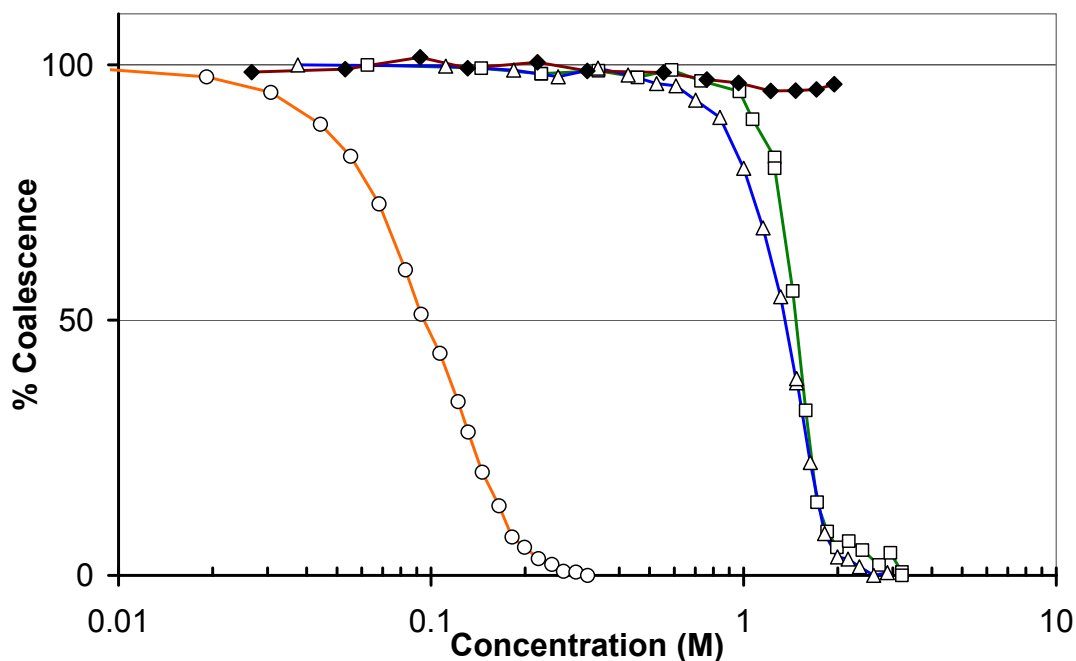


**Figure 4.7** Coalescence inhibition in  $\alpha\beta$  aqueous electrolytes  $\text{NaClO}_4$  ( $\Delta$ ) and  $\text{CH}_3\text{COONH}_4$  ( $\square$ ) and  $\beta\alpha$  electrolyte  $\text{HCl}$  ( $\blacklozenge$ ) as a function of concentration. Typical univalent inhibiting electrolyte  $\text{NaCl}$  ( $\circ$ ) is included for comparison. Percentage coalescence is plotted against concentration. Transition concentration occurs at 50% coalescence.

We report that some “non-inhibiting” electrolytes do inhibit coalescence at sufficiently high concentrations. The transition concentration of  $\text{NaClO}_4$  is 1.36M and that of  $\text{CH}_3\text{COONH}_4$  is 1.47M. Christenson et al. report transition concentrations of 1.7 and 1.1M, respectively.<sup>198</sup> They used a two-bubble experiment, so these results are reasonably consistent given the difference in methods. Hydrochloric acid shows no major effect on coalescence even up to 2M concentration. Hence bubbles may be unstable in some electrolyte solutions regardless of concentration.

At concentrations greater than 1M, it is very difficult to exclude all contamination from the system. This was one of the key reasons to reproduce the experiments of Christenson et al.<sup>56</sup> with a different technique, because two-bubble systems are more

susceptible to organic contamination. It would appear that organic contamination is not a major cause of the coalescence inhibition observed, because the bubble column is self-cleaning and no change in the photodiode voltage was observed over time when the same electrolyte concentration was measured. It is also possible that salt contamination plays some part. Minimal amounts of other cations and anions are present in most electrolytes as received. We note that even if an inhibiting ion were present at a high estimate of 2% of total electrolyte, inhibiting electrolyte would be present at  $<0.05\text{M}$  for the concentration range of  $\alpha\beta$  electrolyte here investigated. This is insufficient to cause the observed large effect on bubble coalescence inhibition. It is noted that HCl, which is obtained as the concentrated (37% w/w) aqueous solution, will be less susceptible to both organic and salt contamination.

Karakashev et al. have measured thin film drainage in  $\alpha\alpha$  and  $\alpha\beta$  electrolytes up to saturation.<sup>86</sup> In  $\alpha\beta$  electrolytes  $\text{CH}_3\text{COONa}$  and  $\text{NaClO}_3$  they find no stable films up to saturation ( $>5\text{M}$ ) in contrast to the coalescence-inhibiting electrolytes  $\text{NaCl}$  and  $\text{LiCl}$ ; however, it is stated that films at the higher concentrations of  $\alpha\beta$  electrolytes take several seconds to drain, in contrast to dilute solutions where films last less than one second. These results suggest a stabilisation over the lifetime of a bubble collision by “non-inhibiting” electrolytes, and are therefore consistent with our data. The thin film drainage measurements also indicate that there is a persistent difference in thin film stability between inhibiting and non-inhibiting electrolytes, even at high concentrations.

## 4.4 DISCUSSION

### 4.4.1 Bubble coalescence inhibition in different solvents

We have shown that thin film stabilisation by electrolytes is not unique to aqueous solutions. Methanol, formamide, propylene carbonate and DMSO solutions all exhibit coalescence inhibition by electrolytes. The data for all four solvents are presented in Table 4.4, together with previously obtained data for coalescence inhibition in water.

**Table 4.4.** Transition concentrations<sup>a</sup> for electrolytes in nonaqueous solvents and water

Electrolyte	Transition concentration (mol L <sup>-1</sup> )					
	Solvent	H <sub>2</sub> O <sup>b</sup>	Methanol	Formamide	Propylene Carbonate	DMSO
HCl		NI	0.04		NI	
HBr		NI			NI	
H <sub>2</sub> SO <sub>4</sub>		NI	0.019			
LiCl		0.095		0.072		
LiBr					0.105	
LiI		0.34		0.079		
LiClO <sub>4</sub>		NI		0.16	0.081	
NaCl		0.095	0.023			
NaBr		0.13	0.023			0.059
NaI		0.30		0.065		
NaNO <sub>3</sub>		0.101	0.025			
NaClO <sub>4</sub>		NI (1.36)	0.024		0.078	0.082
NaOOCCH <sub>3</sub>		NI	0.031	NI		
NaSCN		NI	0.0162		0.084	
KBr		0.083				0.071
KI		0.29				0.055
K <sub>2</sub> CO <sub>3</sub>			0.012			
NH <sub>4</sub> SCN		NI	0.008			
NH <sub>4</sub> OOCCH <sub>3</sub>		NI (1.47)		NI		
(CH <sub>3</sub> ) <sub>4</sub> NBr		NI	0.014	0.19		
(CH <sub>3</sub> ) <sub>4</sub> NOOCCH <sub>3</sub>		0.125		NI <sup>c</sup>		
MgCl <sub>2</sub>			0.016			
Ca(NO <sub>3</sub> ) <sub>2</sub>		0.04	0.017			

<sup>a</sup>Transition concentrations (in mol L<sup>-1</sup>) refer to the concentration at which 50% coalescence is observed. 'NI' indicates that the salt is non-inhibiting to ~0.5M; no entry indicates that the electrolyte was not tested in the given solvent, or reacted.

<sup>b</sup> Some of the results in water are taken from Craig et al.<sup>9</sup>

<sup>c</sup>(CH<sub>3</sub>)<sub>4</sub>NOOCCH<sub>3</sub> in formamide is believed to be contaminated.

In all solvents, coalescence inhibition in inhibiting electrolytes is dependent upon salt concentration over a narrow – and similar – range. The concentrations at which an

---

inhibiting effect is first observed are in the range 0.01 – 0.1M. These concentrations are typical of non-surface active species, and they are far higher than those at which surfactants stabilise thin films, which may be as low as  $10^{-6}$  M.<sup>65</sup>

Propylene carbonate and formamide both show bimodal ion-specificity, with electrolytes describable as “inhibiting” or “less-inhibiting”. Both solvents also show coalescence inhibition consistent with the existence of combining rules analogous to the  $\alpha$  and  $\beta$  assignments in water. In formamide the  $\alpha$  and  $\beta$  assignments match those in water for each ion tested, while in propylene carbonate the anion assignments differ. In methanol and DMSO all electrolytes tested inhibit coalescence relative to the pure solvent.

It is not possible for the bubble coalescence in pure solvents to be directly compared, using this particular bubble column method. The photodiode signal is a function of the amount of gas flow as well as the positioning of the bubble column, and both of these factors changed upon introducing different solvents. In addition, the baseline signal will be influenced by differences in bubble production in different solvents. Figure 4.8 shows coalescence versus concentration curves for typical inhibiting electrolytes in each solvent. Comparisons in specific salts can also be made in some cases from the transition concentrations in Table 4.4, above; however solubility and reactivity constraints prevented use of any one common electrolyte in all the solvents. The transition concentrations can be affected by even small amounts of contaminant (particularly water) as well as by changes in bubble column position, as discussed in the instrument overview in Chapter 2. Therefore only a qualitative comparison is appropriate. Overall we observe that the concentration of typical inhibiting electrolyte required for a given coalescence level, increases in the order: Methanol < DMSO < formamide < propylene carbonate < H<sub>2</sub>O. That is, bubbles in methanol are most strongly stabilized by salt. This sequence agrees with none of the solvent physical properties in Table 4.1. I have not measured physical properties (such as surface tension) of nonaqueous electrolyte solutions. The benefit was doubtful given the lack of strong correlation between physical properties of aqueous solutions and their bubble stability.

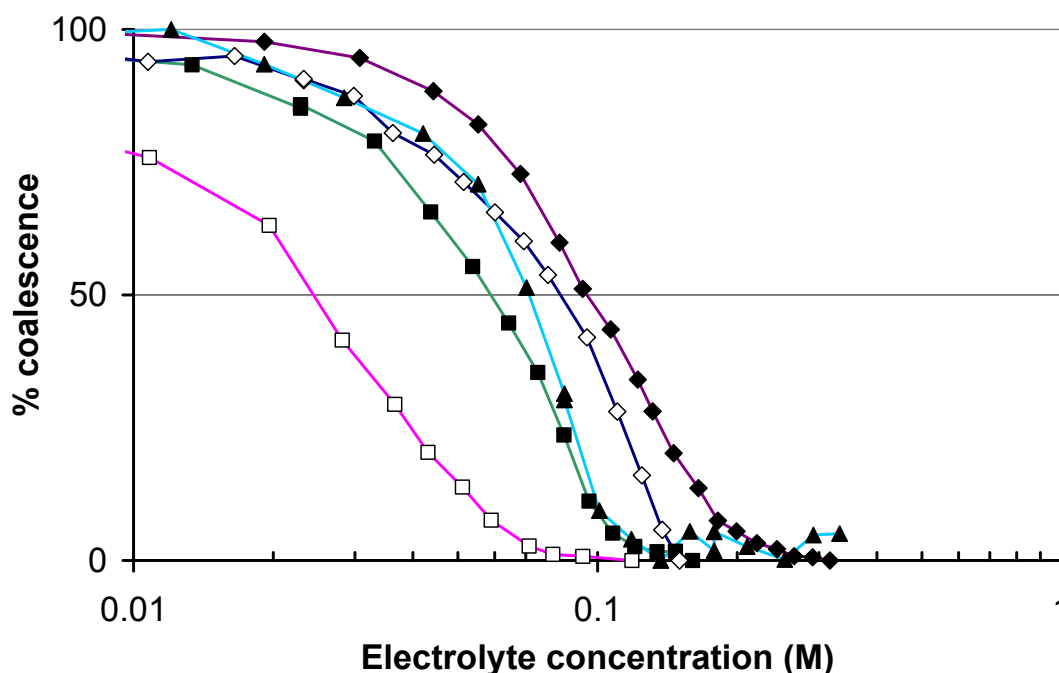


**Figure 4.8** Comparison of typical univalent salt coalescence inhibition in each solvent tested, as a function of log of electrolyte concentration. NaClO<sub>4</sub> in methanol (□), NaBr in DMSO (■), LiCl in formamide (▲), NaSCN in propylene carbonate (◇), NaCl in H<sub>2</sub>O (◆). 100% coalescence is defined in the pure solvent in each case; 0% coalescence is a stable, low, voltage signal in inhibiting electrolytes for each solvent.

#### 4.4.2 Ion specificity in different solvents

Bimodal ion specific electrolyte effects are observed in formamide and propylene carbonate, as well as in water. In propylene carbonate the ion assignments vary from those in water. In particular the anions SCN<sup>-</sup> and ClO<sub>4</sub><sup>-</sup> fall into the ‘α’ category alongside Cl<sup>-</sup> and Br<sup>-</sup>, whereas in water they behave differently and are classified ‘β’ anions. In formamide the same assignments as those made for water apply across the salts tested.

There is no obvious link between ion specific electrolyte inhibition of bubble coalescence and bulk solvent properties. Formamide, like water, is a protic solvent but so is methanol, and these behave very differently. Propylene carbonate and methanol have hydrophobic groups but again these solvents demonstrate different electrolyte

---

effects. The phenomenon of ion specific behaviour is observed in most high-salt systems, and no universal basis or mechanism has been found. The ‘combining rules’ found in the water-vapour system are not observed in other systems that exhibit ion-specificity, such as biological surfaces.<sup>143, 158</sup> It is, therefore, significant that we have produced examples of other systems that exhibit analogous behaviours. This result suggests that the vapour interface itself may be important.

Recent advances have shown that at the gas-aqueous solution interface some ions have a non-uniform distribution and an enhanced surface concentration relative to the bulk liquid, even when there is overall interfacial depletion (see Chapter 2 for a discussion).<sup>125, 137, 141</sup> It has been hypothesised that bubble coalescence inhibition may be related to the arrangement of ions at the interface. Studies in nonaqueous solvents have also shown that ions may inhabit the surface, and it is of interest to determine if the ion surface propensities in different solvents can be related to their coalescence inhibition effects. The assignment of ions to the surface and subsurface layers of the solution-vapour interface has not been consistent among different techniques and different applications of the same technique.<sup>139</sup> Nevertheless, we can compare our coalescence inhibition results in nonaqueous solvents with interfacial ion positioning data in those same solvents – data obtained using techniques of molecular dynamics simulations and surface-selective investigative techniques such as VSFG, SHG and ion-scattering.<sup>199</sup> Of the solvents tested here, research using such techniques has been done for methanol and for formamide.

#### 4.4.2.1 *Surface propensities of ions in methanol*

In molecular dynamics simulations of aqueous sodium iodide, the  $I^-$  shows a distinct preference for the water-vapour interface while  $Na^+$  exists subsurface. Dang<sup>200</sup> reports that in methanolic NaI, iodide is also stable at the interface and will inhabit the interface more than sodium ion, so there is some ion separation. However the preference relative to the bulk is not particularly strong. It is suggested that iodide subsurface positioning is driven by the ordering of interfacial methanol, with hydrophobic methyl groups at the surface and the hydroxyl group towards the bulk liquid.<sup>199</sup> This contrasts with water which shows ‘dangling OH groups’ exposed to the vapour phase. Höfft et al.<sup>201, 202</sup> also

compared aqueous and methanolic solution interfaces, using simulations as well as MIES (metastable impact electron spectroscopy) and ultraviolet photoelectron spectroscopy to study CsI and CsF at the surface of amorphous solid water and methanol. In these studies the iodide segregation seen at the water-vapour interface is not observed in methanol, but they found that iodide lies closer to the methanol surface than do  $\text{Na}^+$  and  $\text{Cs}^+$ . We note that this study (consistent with other work on aqueous interfaces<sup>148, 203, 204</sup>) found no surface preference of the fluoride ion for either solvent interface.

Electrospray ion mass spectrometry was found to be remarkably insensitive to solvent composition in a methanol-water system.<sup>205</sup> Mixtures of anions with a sodium counterion were evaluated for surface propensity by measuring concentration in small fissioned droplets. Cheng et al. find increased surface enhancement with increasing crystalline radius, and this propensity changes little as the solvent ratio of water:methanol changes.<sup>205</sup> They interpret this finding as an indication that ion position is driven by preference for the interface, rather than being controlled by solvent structure. This is consistent with our results showing similar electrolyte effects on bubble coalescence in a range of solvents.

#### 4.4.2.2 *Surface propensities of ions in formamide*

Recent work by Andersson and coworkers<sup>206, 207</sup> uses molecular dynamics simulations and neutral impact collision ion scattering spectroscopy (NICISS) to look at the formamide/vapour interface, with salts NaI, LiI and LiCl. A distinct enhancement of iodide at the interface was found, using ion backscattering. Chloride shows significantly weaker surface enhancement than iodide. The enhancement of iodide at the interface is less than that observed for equivalent concentrations in water, according to NICISS experiments and to simulations. In both solvents the cation (lithium or sodium) shows no surface enhancement, and solution surface tension increase indicates overall depletion of electrolytes from the surface region, despite the iodide positioning at the interface. Breslow and Guo have shown that the surface tension gradient of LiCl solutions in formamide is  $1.2 \text{ mN m}^{-1} \text{ M}^{-1}$ ,<sup>146</sup> similar to the gradient in aqueous solutions of  $1.98 \text{ mN m}^{-1} \text{ M}^{-1}$ .<sup>60</sup> These results suggest that ion interfacial positioning in

---

formamide is qualitatively similar to positioning in H<sub>2</sub>O. That is, the halides show some surface preference that increases for more polarisable anions, and the alkali metal ions show no surface propensity relative to the bulk.

On the basis of these reports, if there is a connection between interfacial ions and bubble coalescence then we might expect the electrolyte effect to be similar in H<sub>2</sub>O and formamide, and less so in methanol. Our results are consistent with this prediction, but any link between ion separation at the interface, and coalescence inhibition, is far from clear. Methanol demonstrates little ion-separation and a high degree of coalescence inhibition, and at the formamide interface, only inhibiting salts have been investigated by simulation and spectroscopic studies.

#### 4.4.2.3 *Ion pairing*

It had been hypothesised that ion-specific electrolyte effects in low-dielectric solvents might be affected by some degree of ion-pairing or ion association. This is more likely at high concentrations.<sup>199</sup> Where data were available in the literature I used electrolytes that show minimal ion-pairing, as electrolyte inhibition in water is known to take place in the presence of dissociated ions, and ion association may produce undesired changes to diffusion, solvation and ion position at the interface.<sup>208, 209</sup> In extreme cases of covalent association a neutral species is formed that may act as a surfactant, as in the case of aqueous acetic acid, which shows foaming behaviour. Also in water, Minofar et al. find that there is some interfacial ion pairing in magnesium acetate at 0.5M, and none in magnesium nitrate at the same concentration.<sup>209</sup> Mg(OOCCH<sub>3</sub>)<sub>2</sub> is a noninhibitor at these concentrations, while Mg(NO<sub>3</sub>)<sub>2</sub> inhibits coalescence relative to pure water. It therefore appears that increased ion pairing does not necessarily produce surface-activity or coalescence inhibition. d'Aprano suggests that in methanol, perchlorates exhibit a greater degree of ion pairing than do halides with a common cation, yet sodium perchlorate sits in the middle of the range of transition concentrations in this solvent; also, the degree of association is still low.<sup>210</sup>

Hanna<sup>211</sup> measured conductance in some dilute propylene carbonate solutions, and found a slight ion association in alkali metal perchlorates but not in iodides. The



---

coalescence inhibition in these two systems is very similar over the concentration range here investigated. Note, however, that little evidence of ion association was found in perchlorates and in potassium iodide in propylene carbonate, by other workers.<sup>197, 212</sup>

#### 4.4.3 The importance of the solvent in coalescence inhibition

The mechanism by which electrolytes inhibit coalescence is unknown even in water. The structure of the solvent in bulk has been implicated in many ion-specific systems, with ions defined as structure-makers and structure-breakers.<sup>11</sup> Alternatively it has been suggested that coalescence inhibition is related to changes in interfacial solvent structure caused by interfacial ion arrangement.<sup>58</sup> Changes in surface forces have also been suggested as a mechanism of coalescence inhibition.<sup>9</sup> Solution properties such as surface tension and viscosity will also affect the film drainage, and we hypothesised that the differences among solvents might lead to large differences in bubble coalescence behaviour.

Different solvents in fact demonstrate quite similar behaviour in the presence of electrolytes. The ability of electrolytes to inhibit bubble coalescence is not confined to aqueous systems but rather seems to be a general property. Bubble coalescence inhibition in nonaqueous solvents suggests that electrolytes stabilise thin films in a way that is not strongly dependent upon equilibrium surface forces or bulk solvent structure, which vary widely with the solvent. However the ion specificity and the effect of any particular electrolyte, can be controlled by solvent properties.

Water and formamide show very similar ion specific bubble coalescence inhibition, with ions fitting into the same  $\alpha$  and  $\beta$  categories. Therefore it is useful to consider whether these solvents show similarities in the presence of other solutes and in their surface properties. No measurements could be found for the surface potential and surface charge at the bare formamide-air interface or in electrolyte solution, to compare with water. Indeed, it is not entirely certain that such a value would be useful given the considerable controversy associated with charge and potential at the water-air surface.<sup>91, 141, 213</sup> However it is known that the dielectric constant differs between the

two solvents and so the propagation of charge will not be the same. These solvents show very different behaviours in the presence of surface active molecules and proteins. Abu-Lail and Camesano showed that biopolymer extension correlates with solvent polarity, in comparing methanol, water and formamide effects.<sup>214</sup> Surfactant surface excess and micellization are also found to differ between the two solvents. SDS<sup>215</sup> and CTAB<sup>216</sup> in formamide have distinctly different behaviour to that observed in water, with surface tension gradient, surface excess and micellization following different trends. These results provide some indication that the solvents are not equivalent, and that addition of ions and of surface active species to the two solvents does not always result in similar behaviour.

The relative independence of coalescence inhibition on solvent structure and surface forces is support for the hypothesis that electrolytes act on the dynamic film thinning process. Further, the similarity between the bubble coalescence inhibition concentration range and ion specificity in different solvents may indicate that inhibition is related to the gas-liquid interface.

## 4.5 CONCLUSIONS

Electrolytes can inhibit bubble coalescence in nonaqueous systems. Coalescence inhibition was observed in all solvents tested: methanol, formamide, propylene carbonate and DMSO. Coalescence inhibition in formamide and propylene carbonate shows bimodal ion specificity. As in water, electrolytes can be categorized as ‘inhibiting’ or ‘less inhibiting’, depending on the concentration required to elicit coalescence inhibition. We report that ion combining rules are not unique to the water-gas system. Formamide shows cation and anion assignments consistent with those in water, while propylene carbonate assignments are analogous but distinct. Methanol and DMSO show no bimodal ion specificity, with all electrolytes tested inhibiting coalescence relative to the pure solvent.

While the nature of the solvent has some effect on electrolyte coalescence inhibition and on ion specificity, the similarity of results suggests that surface forces and solvent

---

structure are not important in bubble coalescence inhibition and thin film stabilisation, as these properties are expected to vary widely between solvents. This strongly suggests that the mechanism of coalescence inhibition is related to the process of film drainage between gas interfaces.

---

## Chapter 5 Thin Film Drainage in Nonaqueous Electrolyte Solutions

---

### 5.1 INTRODUCTION

While bubble column coalescence inhibition measurements are useful for measuring electrolyte effects in a wide range of conditions and with minimal contamination, they do not reveal much about the process of thin film drainage and rupture. We therefore followed the nonaqueous measurements reported in Chapter 4 with a series of experiments designed to probe the thin film behaviour in propylene carbonate and formamide electrolyte solutions. Thin-film interferometry was used to record film drainage and lifetime in an isolated thin film. Aqueous thin film behaviour is also of interest, and is being researched by our collaborators on this project.<sup>86</sup>

It was hoped that the measurements would reveal first, how inhibiting electrolyte affects thin film lifetime, drainage and rupture thickness; and second, how thin films differ in inhibiting and noninhibiting electrolyte solutions. We also wished to ascertain how the drainage observed in electrolyte solutions compares to theories of drainage rate developed to explain surfactant systems.

#### 5.1.1 Microinterferometry and the thin film balance

The principle behind microinterferometry is that light will reflect off both surfaces of a thin film, and produce interference patterns that vary in intensity as the film thickness changes.<sup>217</sup> The thickness of the film can then be calculated at any point as a function of light intensity.<sup>84</sup> If the thin film interference is recorded via video microscopy, we can determine the drainage velocity of a thin film, from the thickness at which the planar film is formed (200-300nm), to the point of rupture.<sup>107</sup> In larger non-planar films the

variation of colour (intensity) across the film can reveal the draining pattern of the film and its propensity for distortion (see Figure 5.1).<sup>31</sup>

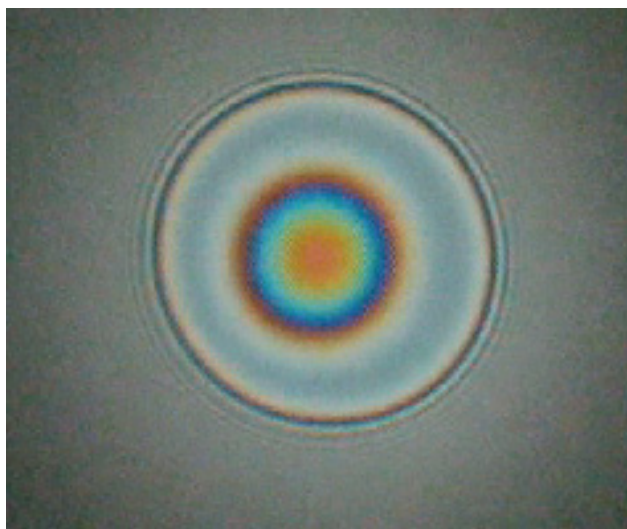


**Figure 5.1** Reflectance fringes in a non-planar thin film. The centre of the film has greatest thickness, indicating that a dimple has been formed during drainage. The grey ring surrounding it shows the thinnest part of the film,  $\sim 100\text{nm}$ . The edges of the film increase in thickness as the surfaces curve. This film is about  $130\mu\text{m}$  in radius. The solution is  $0.1\text{M CH}_3\text{COONa}$  in formamide.

The thin film balance method to study free-standing foam films has traditionally been used on long-standing surfactant or polymer films.<sup>32, 84, 218, 219</sup> The instrument was so named because the film could be held between porous walls, under a pressure of gas that could balance the disjoining pressure within the thin film under equilibrium conditions.<sup>85</sup> An alternative cell known as the Scheludko (or Sheludko) cell consists of a non-porous glass ring cell-holder with a single capillary outlet to withdraw fluid from a droplet until a thin film is formed.<sup>84</sup>

### 5.1.2 Drainage of free-standing electrolyte films

In pure liquid rupture is so rapid that often no interference fringes are observed and the technique provides no data.<sup>86</sup> Electrolyte solutions change the film behaviour enough that one can record film thinning and drainage using video at high enough capture

---

speeds. However the results are highly susceptible to surfactant contamination. Despite this problem, some previous attempts have been made to study films formed from electrolyte solutions using interferometry measurements.

Cain and Lee used interferometry to study two bubbles held on the ends of capillaries and pushed against each other. It was found that the film ruptured at 55-75nm in 1.0M KCl, and at 75-95nm in 0.5M KCl.<sup>18</sup> Film lifetime was in each case hundreds of milliseconds, and drainage was more rapid than Reynolds theory (based on planar immobile interfaces) would predict. The thin film balance was used to study aqueous films with very low surfactant concentrations, as it is expected that these would behave similarly to films in pure water.<sup>107</sup> It was found that film thickness decreased with increasing added electrolyte in accordance with DLVO theory.

Karakashev et al. studied film drainage in aqueous electrolyte solution in a similar set-up to the one used in the current experiments.<sup>86</sup> Most of their results are reported in an open cell, meaning that the gas phase was not saturated, and that the films were more exposed to contamination and to evaporative effects. Under those conditions, increasing concentration of inhibiting electrolytes NaCl and LiCl led to metastable films with lifetimes of minutes. Increasing the concentration of non-inhibiting  $\alpha\beta$  electrolytes NaClO<sub>3</sub> and CH<sub>3</sub>COONa also led to films with longer lifetimes than in pure water but in these electrolytes the increase was on the order of seconds.<sup>86</sup> It is noted that if the cell is closed and the atmosphere is allowed to saturate, then in inhibiting electrolytes thin films are produced that drain continually to rupture thickness on the order of 50nm, with a lifetime of tens of seconds – much reduced compared to the unsaturated case.<sup>86</sup> The experiments reported in this chapter were carried out in a closed Scheludko cell.

The dependence of film lifetime on film radius was also studied by Karakashev et al. for electrolyte thin films.<sup>86</sup> It is found that lifetime increases with increasing film size. In particular, a critical radius of 30 $\mu$ m is reported. In small films below this size, the film ruptures with a lifetime <1s in all salt concentrations, while above this size film lifetime increases very rapidly with size and then becomes nearly independent of radius for films with  $R \geq 80\mu$ m.

## 5.2 MATERIALS AND METHODS

### 5.2.1 Thin film balance

Thin films in nonaqueous solvents in the presence of electrolyte were studied using a microinterferometric set-up. This apparatus is shown in Figure 5.2. The film is formed in a Scheludko cell<sup>84</sup> connected via capillary to a gas-tight microsyringe pump. A metallurgical inverted microscope (Nikon, Japan) is used for illuminating and observing the film and reflected interference fringes. A CCD (charge-coupled device) video camera records images at 30fps. The records are stored to computer and analysed.

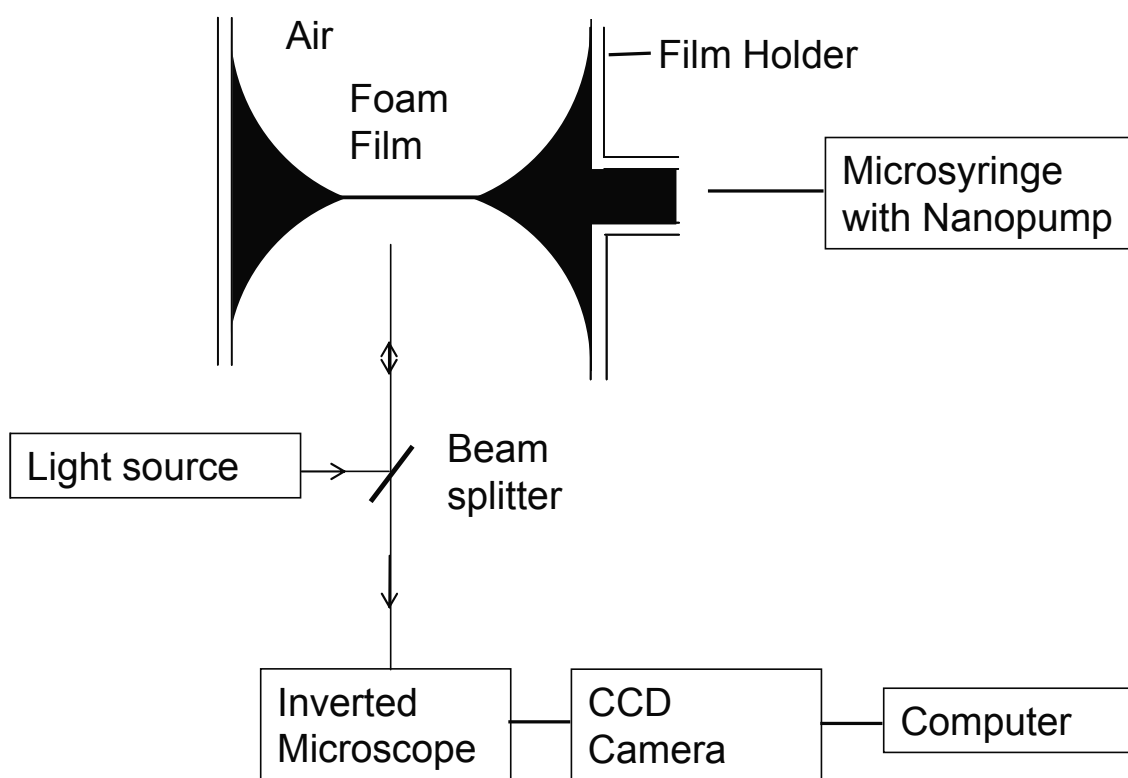


**Figure 5.2** Thin film balance apparatus. A planar film (not to scale) is formed in the Scheludko cell film holder<sup>84</sup> (4mm internal diameter) by withdrawing liquid using a microsyringe. The interferometric data is obtained using an inverted microscope and recorded to computer using a CCD camera.

The thin film is created by injecting the liquid of interest into the film-holder (radius 4mm) and then withdrawing liquid using a microsyringe pump. When the planar film is formed (interference fringes are observed) the pumping is stopped and the film is left to

---

drain until rupture. At least 20 film drainage events were recorded in each solution. In between each drainage and rupture event, liquid is pumped back into the film holder to form a stable double-concave film, from which liquid is then withdrawn to form a new film. The withdrawal rate was varied (between 20nL/s and 1000nL/s) to obtain films of different radius. Film lifetime data (the time from the formation of a planar film with visible interference fringes, until film rupture) were collected for films with  $20\mu\text{m} \leq R \leq 300\mu\text{m}$ . In some cases film thickness was measured so that drainage kinetics could be determined; the analysis required for determination of film thickness and drainage kinetics is discussed in section 5.3.4 below.

### 5.2.2 Cleaning and solutions

The thin films contain a small solution volume and have surfaces exposed for some time. The system is thus extremely susceptible to low levels of surfactant contamination, and cleaning of the Scheludko cell is important. The cell (film-holder and capillary) are rinsed many times using a mixture of ethanol:water:KOH (84:16:12.5). Sometimes RCA solution<sup>a</sup> (made up as 50mL H<sub>2</sub>O / 10mL 28% NH<sub>3</sub> / 10mL 30% H<sub>2</sub>O<sub>2</sub>) at  $\geq 70^\circ\text{C}$  was employed. After rinsing, the cleanness of the cell was checked in pure water. In a system free of organic contaminant the film is very unstable and no interference fringes are observed. Water was removed from the cell by rinsing with absolute ethanol and drying with N<sub>2</sub> gas. The solvent (formamide or propylene carbonate) was then used to rinse the film-holder and capillary. A small amount of solvent was put in the base of the closed Scheludko cell, to create a saturated atmosphere when the cell was sealed.

Thin films were measured in inhibiting and noninhibiting electrolytes, as found in bubble coalescence measurements (see Chapter 4). In propylene carbonate, inhibiting salts LiBr and NaSCN, and noninhibiting electrolyte HCl (as the 35%w/w aqueous solution) were used. Their coalescence inhibition is shown in Figure 5.3. In formamide, inhibiting electrolyte LiCl and noninhibiting electrolyte CH<sub>3</sub>COONa were used;

---

<sup>a</sup> RCA solution is so named because it was developed in the RCA (Radio Corporation of America) laboratories in the 1960s as a method for organic contaminant removal.<sup>220</sup>



coalescence inhibition is shown in Figure 5.4. Some salts used were oven-roasted to remove water and/or organic contaminants; others were used as received. Electrolytes were added to cover the range of concentrations used in bubble column measurements (0.01M to 0.3M); however for low concentrations in some cases the films were very unstable and no interference fringes were observed. Solutions were diluted from a concentrated stock solution. For stock solutions of  $\text{CH}_3\text{COONa}$  and  $\text{LiCl}$  in formamide, an additional cleaning step was used. The solutions underwent sparging for one hour with  $\text{N}_2$  gas, following a method outlined by Brandon et al.<sup>221</sup> The sparging bubbles clean the solution by collecting any surface active contaminant and depositing it on the surface of the liquid and on the glass sides of the sparging vessel – which become noticeably non-wetting during the cleaning process. The fluid is removed from the bulk with a syringe, without touching the contaminated liquid interface. The prepared solutions were kept at room temperature ( $\sim 20^\circ\text{C}$ ). The  $\text{NaSCN}$  solutions were kept wrapped in aluminium foil because the thiocyanate is light-sensitive.

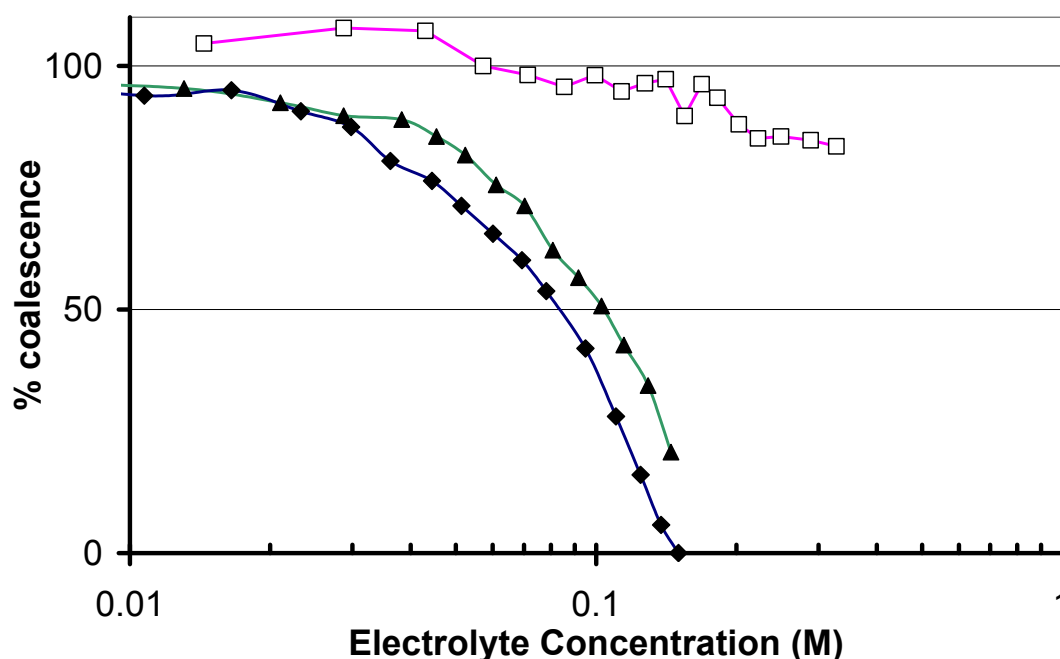


**Figure 5.3** Electrolytes used in propylene carbonate thin film drainage: inhibiting electrolytes  $\text{NaSCN}$  (◆) and  $\text{LiBr}$  (▲), and non-inhibiting electrolyte  $\text{HCl}$  (□). 100% coalescence is defined in the pure solvent; 0% coalescence is a stable, low, voltage signal in inhibiting electrolytes. These results were reported in Chapter 4.

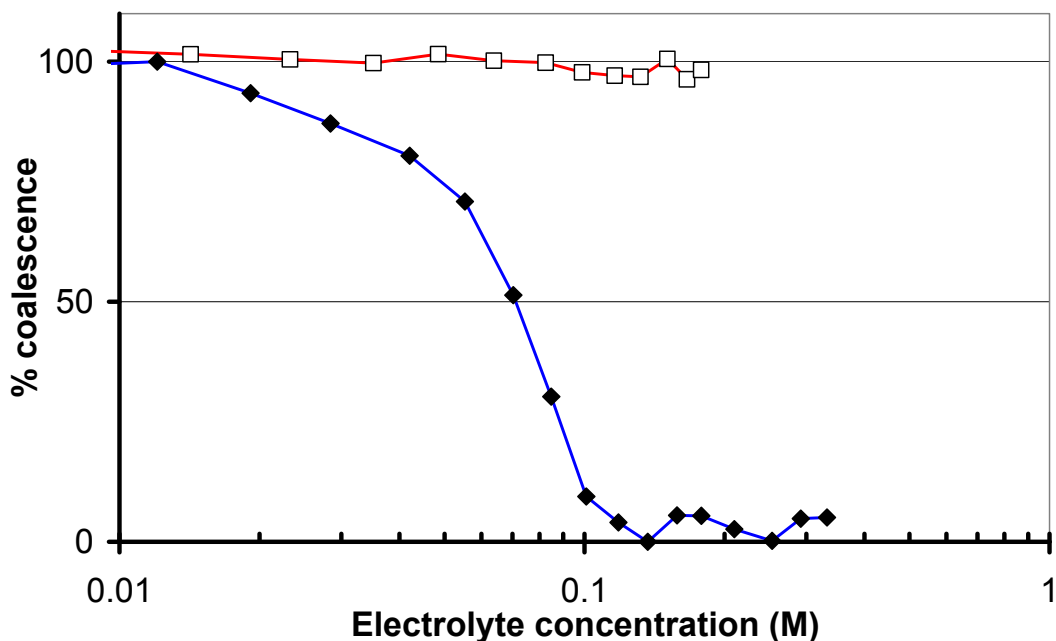


**Figure 5.4** Electrolytes used in formamide thin film drainage: inhibiting electrolyte LiCl ( $\blacklozenge$ ) and non-inhibiting electrolyte  $\text{CH}_3\text{COONa}$  ( $\square$ ). 100% coalescence is defined in the pure solvent; 0% coalescence is a stable, low, voltage signal in inhibiting electrolytes. These results were reported in Chapter 4.

In each electrolyte concentration, at least twenty films were recorded for lifetime measurements. During an experiment the solution in the film holder was replaced at least once, in order to keep to a minimum the contamination of the surface. After each such flushing of the film-holder the Scheludko cell was left sealed for at least 5 minutes to allow the cell atmosphere to equilibrate. The interval between the time when fresh solution was collected and the cell was closed, and the time at which a film measurement was taken, was recorded. This interval is defined as the *droplet age* because it is a measure of the time for which that solution droplet has been present in the cell holder of the thin film balance. As discussed below, we observed a dependence of film lifetime (film stability) on droplet age, in the case of some of the formamide solutions.

## 5.3 RESULTS AND DISCUSSION

### 5.3.1 Examples of thin film drainage

The drainage of each film is recorded on CCD camera to computer for later analysis. As well as the lifetime measurements and drainage and rupture kinetics reported here, the recordings of film drainage contain a wealth of information about the process of film thinning and the liquid movement within the film. There are clear fluctuations in film thickness in all systems except the very small plane parallel films. Films deform with time in various ways. I have presented examples of film drainage over time in two similar, coalescence-inhibiting solutions: 0.20M NaSCN in propylene carbonate (Figure 5.5) and 0.30M LiBr in propylene carbonate (Figure 5.6).

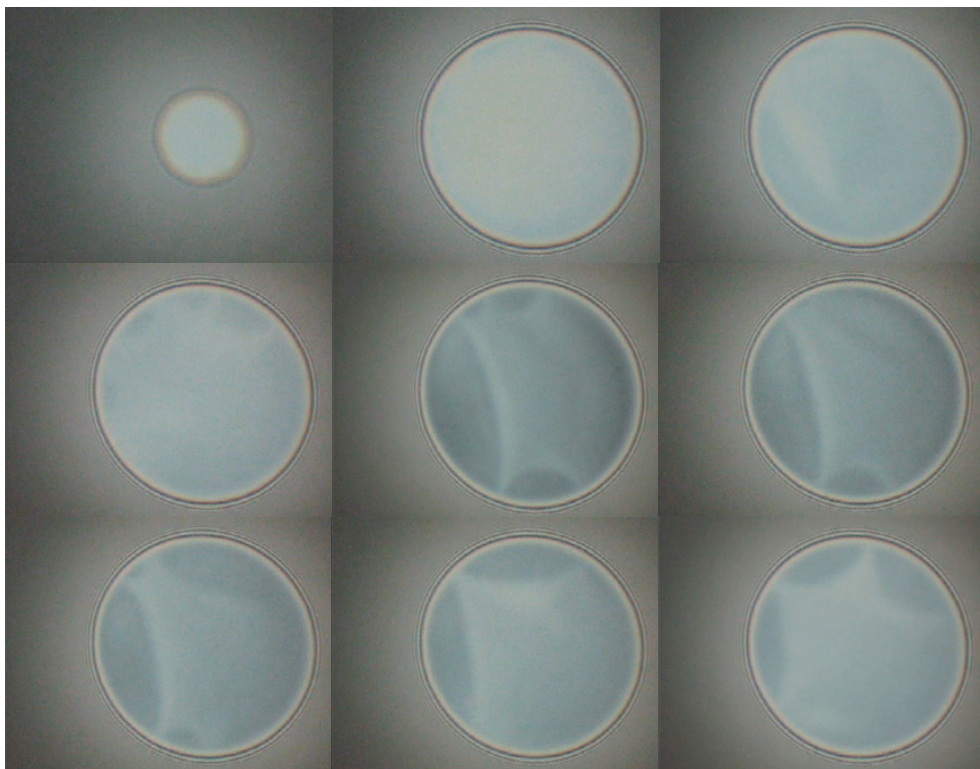


**Figure 5.5** Time series of drainage in 0.20M NaSCN in propylene carbonate. Images are at 1 second intervals (from left to right and top to bottom); 0.8s separates the last two images, the latter of which is immediately before rupture. Film lifetime was 7.8 seconds. Film radius is  $\sim 250\mu\text{m}$ . Darker regions indicate thinner parts of the film. This film's scalloped appearance is believed to show drainage through thicker (whiter) channels at multiple points on the boundary.

These two similar systems show distinct differences in drainage pattern. Figure 5.5 is an example of film drainage that shows multiple drainage points at the film meniscus. The lighter regions of the film are thicker than the darker background regions and can be considered as channels through which the liquid escapes the film. Film lifetime in this system is 7.8 seconds; the image interval is one second. Figure 5.6 also shows a time-dependent variation in thickness across the film, with a development of thin regions of vorticity. Between the twin vortices is a thicker (white) drainage channel. The film lifetime is 24.7 seconds (note the image interval is 3 seconds, rather than one second as it was in the previous series).

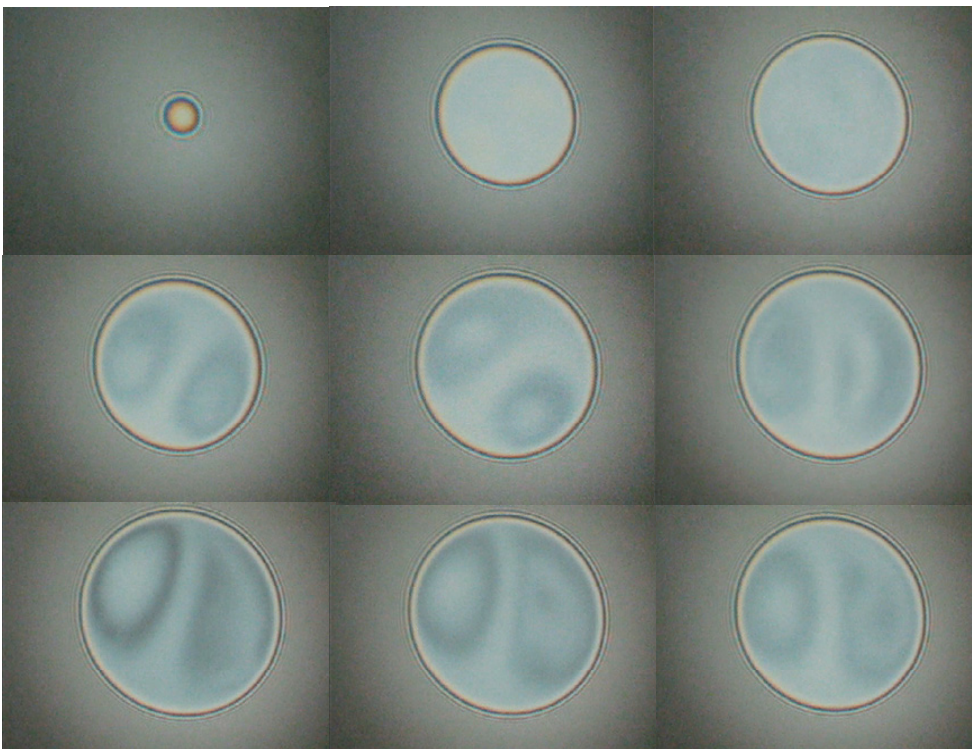


**Figure 5.6** Time series of drainage in 0.30M LiBr in propylene carbonate. Images are at 3 second intervals (from left to right and top to bottom). Film lifetime was 24.7 seconds. Final film radius is  $\sim 200\mu\text{m}$ . Darker regions indicate thinner parts of the film. Note the moving twin vortices associated with drainage.

Other films show a range of drainage behaviour, including dimpling and mobile instabilities (“black spots”). A deeper investigation of such phenomena is, unfortunately, beyond the scope of the present work. Analysing and modelling such

dynamic drainage behaviour would be a thesis-worth of work in itself. Such analysis would yield much of use to bubble coalescence inhibition study, such as velocity profiles and viscosity gradients through the thickness of the film. Therefore it is hoped that this additional information, beyond the simple lifetime measurements and kinetics studies here reported, may at some time find further use.

### 5.3.2 Thin film lifetimes in propylene carbonate solutions

The effects on propylene carbonate film drainage of inhibiting electrolytes NaSCN and LiBr, and noninhibiting electrolyte HCl (added as concentrated aqueous solution) were measured at several concentrations.

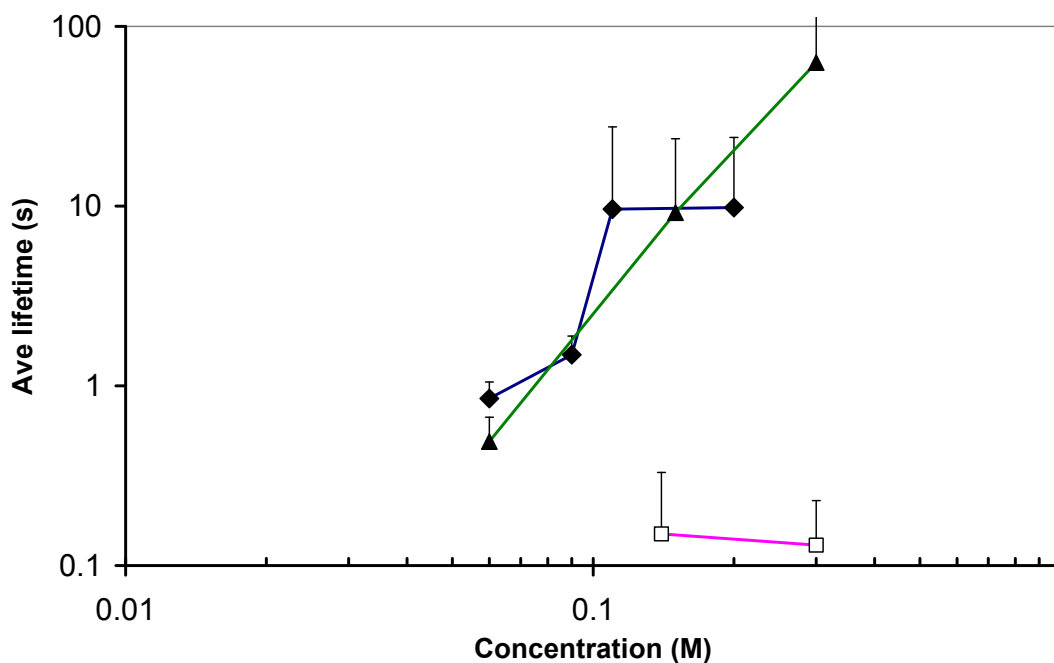


**Figure 5.7** Average lifetime of thin films as a function of concentration in inhibiting electrolytes NaSCN (◆) and LiBr (▲), and non-inhibiting electrolyte HCl (□) plotted on a log-log plot. Lifetime increases with increasing inhibiting salt. Lower concentrations showed no visible fringes and hence have a film lifetime of 0 seconds. Lifetime error bars are set at 1 standard deviation for  $21 \leq n \leq 47$ . Only the positive error is shown, for clarity and because the negative value drops below zero. Film radius is varied among and within solutions.

---

Bubble coalescence inhibition in the bubble column occurs when the duration of a bubble collision is less than the time required for film drainage and rupture processes. It is hypothesised that this will be reflected in an increase of average film lifetime with increasing inhibiting electrolyte concentration, in single thin films. In pure propylene carbonate no stable film was observed, as predicted for pure liquids,<sup>27</sup> and in most cases no interference fringes could be seen before the film ruptured. This indicates rupture occurred rapidly before the film had drained below 200nm. The average lifetimes as a function of electrolyte concentration for the three electrolytes, are shown in Figure 5.7. Increasing the concentration of inhibiting electrolyte leads to longer-lived films, whereas increasing HCl even to 0.3M, has little effect.

Histograms showing film lifetime variability for two intermediate concentrations of inhibiting salt NaSCN in propylene carbonate, are shown in Figure 5.8. At 0.06M NaSCN coalescence is a little reduced relative to the pure solvent in bubble column measurements. Thin films are stabilised relative to pure solvent but rapidly drain and rupture, with an average lifetime of  $0.86 \pm 0.21$ s for this sample (n=25). Coalescence is more inhibited at 0.11M NaSCN, and this is consistent with increase in film average lifetime to  $9.6 \pm 17$ s (n=25) as well as the existence of some long-lived films of over 60s. However the increased average film lifetime at higher concentrations is not simply a product of a few very long-lasting films: even the minimum lifetime of small films was shown to increase in increasing inhibiting electrolyte.

It will be observed in Figure 5.7 that there is a difference in lifetime at the higher concentrations of inhibiting electrolyte, with LiBr continuing to increase in film lifetime while NaSCN shows no significant change on increasing concentration from 0.11M to 0.20M solution. The behaviour in this high concentration regime is not available for comparison in the bubble column experiments, because once the conditions are such that film lifetime is longer than bubble collision lifetime, coalescence is inhibited and little further variation can be seen. It would certainly be of interest to ascertain whether higher concentrations lead to increasingly stable films or whether a maximum lifetime is reached. In aqueous solutions in a closed cell Karakashev et al. report that films even

at 4M NaCl rupture with a lifetime of tens of seconds, suggesting that lifetime does not continue to increase; however few results are given for the closed cell system.<sup>86</sup>

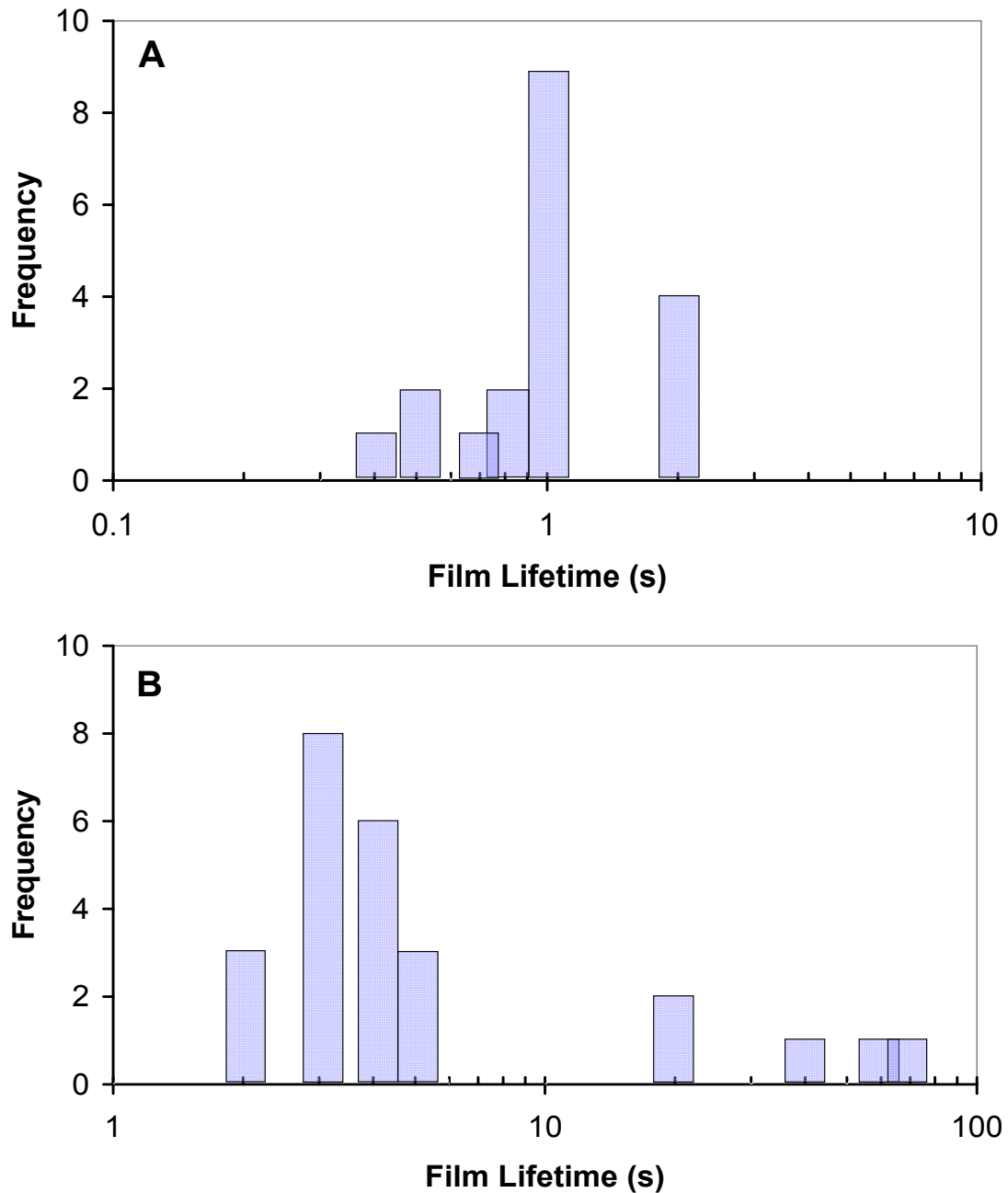


**Figure 5.8** Variation in film lifetime in two partially inhibiting electrolyte solutions. (A) 0.06M NaSCN in propylene carbonate (25 films) and (B) 0.11M NaSCN in propylene carbonate (25 films). Note the difference in timescales between (A) and (B). The minimum film lifetime, average film lifetime and maximum film lifetime all increase at the higher concentration.

### 5.3.3 Thin film lifetimes in formamide solutions

Thin film drainage was measured in inhibiting electrolyte LiCl and non-inhibiting electrolyte CH<sub>3</sub>COONa in formamide solutions. The average film lifetimes are shown in Figure 5.9. Average lifetime in lithium chloride is seen to be higher at all concentrations than in the noninhibiting sodium acetate. This result supports a difference between films in inhibiting and non-inhibiting salts. However there is an increase in film lifetime with increasing sodium acetate concentration, despite the fact that no difference in bubble coalescence was observed in the bubble column over the concentration range used here of 0M to 0.3M (see Figure 5.4).

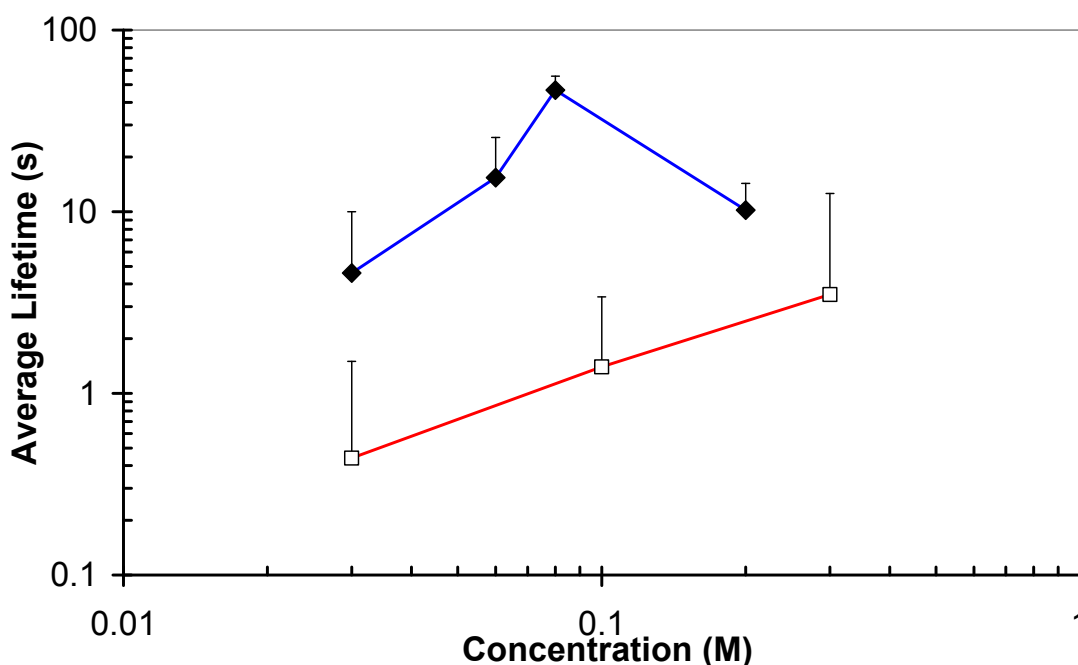


**Figure 5.9** Average lifetime of thin films as a function of concentration in inhibiting electrolyte LiCl (◆), and non-inhibiting electrolyte CH<sub>3</sub>COONa (□) as a log-log plot. Lifetime is higher in inhibiting than in non-inhibiting salt. Error bars (given as positive only for clarity) are set at 1 standard deviation;  $13 \leq n \leq 25$ . Film radius is varied among and within solutions. Films formed over 20 minutes after the introduction of fresh solution become very long-lived in all cases and are not included in these averages.

#### 5.3.3.1 Film lifetime dependence on age of solution droplet

In formamide, I observed a time-dependence of film stability. In all solutions (and in formamide as the neat solvent) leaving a droplet of solution in the sealed cell for more



than about twenty minutes, leads to much more stable thin films with lifetimes of tens of seconds or even minutes (Figure 5.10). Thus, the film lifetime was found to depend upon the droplet age, or the length of time the droplet of solution was in the thin film cell holder. This result casts doubt upon the reliability of results in this solvent. The results shown in Figure 5.9 do not include the films formed in droplets older than 20 minutes, as after this droplet aging stable films are formed that can last for greater than two minutes and skew the results.

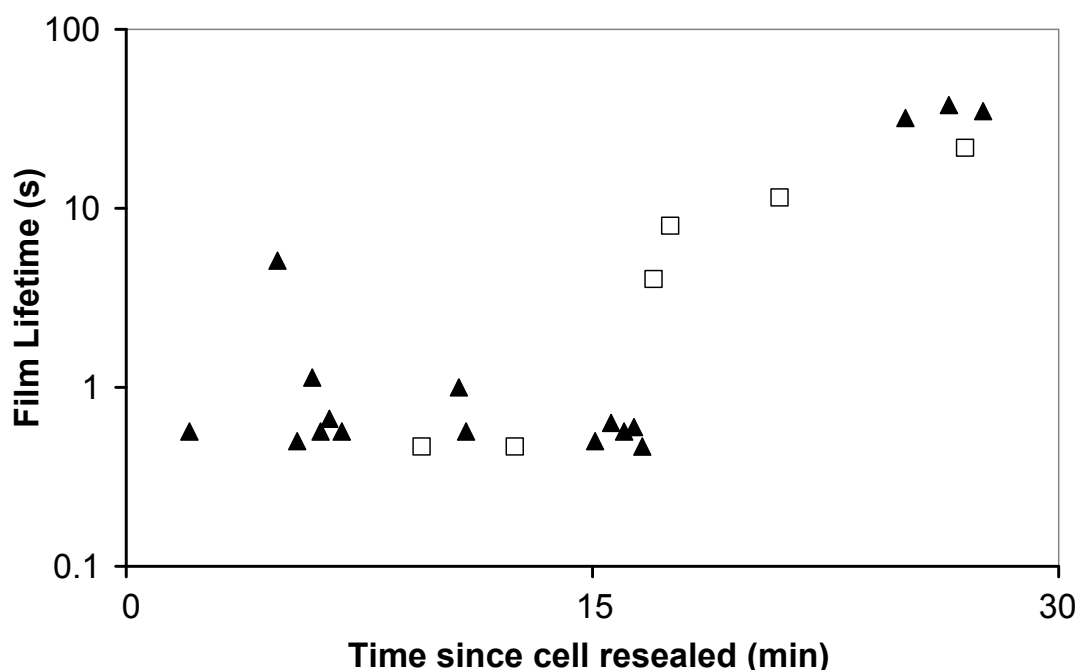


**Figure 5.10** Droplet age-dependence of film lifetime in formamide solution of non-inhibiting electrolyte 0.10M  $\text{CH}_3\text{COONa}$ . Individual film lifetimes (with initial drainage of 100 or 200nL/s) begin to increase with the length of time since fresh solution was added to the film holder. Two different uptakes of fresh solution are shown (▲ and □) and behave reproducibly. Other solutions also show this dependence on droplet age.

In neat solvent it was possible to see highly unstable films (lifetime  $\sim 0.1\text{s}$ ) for 10-15 minutes after a fresh solvent droplet was put into the cell holder. For droplet ages longer than 15 minutes the film lifetime increases. We attempted to locate the source of this droplet age-dependency of film stability. One possibility considered was that the very stable films are in fact a true reflection of film stability in saturated atmosphere, and that this solvent with its low vapour pressure took 15 minutes to saturate the cell. The

---

vapour pressure of formamide at room temperature is 0.011kPa<sup>183</sup> compared to 3.17kPa for H<sub>2</sub>O.<sup>57</sup> However propylene carbonate, which has a similarly low vapour pressure (0.017 kPa at 20°C<sup>182</sup>) shows no dependence of measurements on droplet age. Also, opening the cell and re-sealing it without using fresh solution, does not lead to unstable films. Theoretically, films in pure solvent should never be stable.<sup>27</sup> Therefore contamination of some sort seems more likely. The three possibilities are contamination by atmospheric or absorbed water; contamination by dissociation products of formamide itself; or extraneous surface active contamination.

Porras and Kenndler conducted a rigorous check on atmospheric water uptake of formamide and found to be negligible it in an open system (from 0.03% to 0.22% in low humidity after 8 hours).<sup>195</sup> However, the formamide that I was using had been previously exposed to the atmosphere during earlier experiment preparation so it is possible that water concentration was higher. I tested the effect of small amounts of added water on film stability by adding 2% and 4% by volume to neat solvent, as shown in Figure 5.11. This did produce an increase in film stability, with lifetimes of tens of seconds in the formamide+H<sub>2</sub>O mixtures. It is therefore possible that absorbed water is at least partly responsible for the increase in film lifetime with droplet age in the film holder.

Porras and Kenndler also note that the hydrolysis products of formamide (formic acid and ammonia, forming ammonium formate in solution) are present in analytical grade solvent at a concentration of ~0.02M.<sup>195</sup> This concentration would have a minimal effect on bubble coalescence if considered as a normal electrolyte. Nonetheless, the presence of these species may affect film stability.

Under the conditions in which pure solvent could not form a stable thin film – that is, for droplet ages of 5-20 minutes – there is reason to believe that the data recorded may be reliable. However, all of the thin film results in this solvent need to be treated with caution. The effect seen in thin films will not affect the bubble column data reported in Chapter 4 above, as in that case there is continual fresh interface being created and saturation and contamination are not a problem.

Because of the droplet age-dependence of formamide thin film stability, the emphasis of the kinetics and rupture analysis below is on the propylene carbonate system.

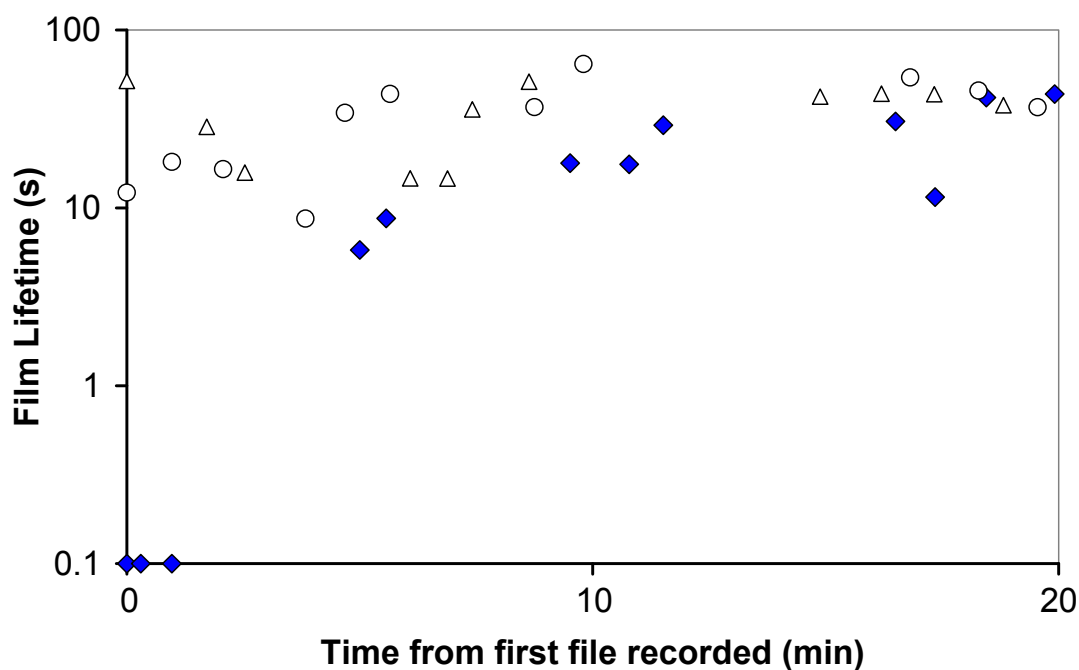


**Figure 5.11** Effect of added water on formamide film lifetime. Lifetime of individual films on a log scale (with initial drainage at 200nL/s) is plotted against the time since measurement was started in that solution. Note that the droplet was aged five minutes before measurements started, to allow the cell atmosphere to saturate with formamide vapour. Neat solvent (◆) shows an increase in film lifetime with droplet age in the film holder. With 2% v/v (○) or 4% v/v (△) H<sub>2</sub>O, unstable films are not observed.

### 5.3.4 Film drainage and rupture: Background

The lifetime data reported above is consistent with bubble column coalescence measurements, and confirms a difference between thin film stabilities in inhibiting and noninhibiting electrolyte solutions. It is possible to obtain further information about the kinetics of film drainage and the rupture thickness, for a subset of these films. Small films (those with  $R \leq 40\mu\text{m}$ ) can be modelled using theories of drainage between plane parallel surfaces (larger films show regions of deformation and non-uniform thickness,<sup>31</sup> and are not suitable for this analysis). Such analysis is time-consuming, and so was performed on only 1-2 plane parallel films in each concentration here seen. The analysis

was done by Dr Stoyan Karakashev at the University of Queensland, as part of our collaboration.

In some of the electrolyte concentrations no suitable films were obtained, either because at all drainage rates tested the films produced were too large and non-planar, or because the films were too unstable and no interference fringes were recorded for analysis before film rupture. In some cases film radius changed during drainage, and this also cannot be fit using existing models that assume a constant film radius. The majority of the results presented in this section are from the propylene carbonate system because formamide films showed some evidence of contamination (see section 5.3.3 above). However where possible, data for formamide solutions are presented.

#### 5.3.4.1 Film thickness determination

The film is illuminated with white coherent light (150W). This light is reflected off both film surfaces creating an interference pattern (Newton rings) with colour dependent upon the film thickness. To determine the film thickness, the interferometric images were processed by a digital filtration procedure using software for digital processing (*Optimas 6.1*, Optimas, USA) and a digital green filter with wavelength  $\lambda = 546$  nm.<sup>222</sup> This procedure converted the polychromatic into monochromatic interferograms suitable for calculating the film thickness. The film thickness,  $h$ , is calculated using the interferometric equation:<sup>84, 223</sup>

$$h = \frac{\lambda}{2\pi n} \left[ l\pi \pm \arcsin \sqrt{\frac{\Delta(1+r^2)}{(1-r^2) + 4r^2\Delta}} \right] \quad (5.1)$$

In equation 5.1, the Fresnel reflection coefficient,  $r = (n - 1)^2 / (n + 1)^2$ , for the air-solution interface is a function of the refractive index,  $n$ , of the film solution;  $l = 0, 1, 2, \dots$ , is the order of interference; and  $\Delta = (I - I_{\min}) / (I_{\max} - I_{\min})$ , where  $I$  is the instantaneous intensity of the photocurrent and  $I_{\min}$  and  $I_{\max}$  are its minimum and maximum values. The refractive index used was that for the neat solvents (1.42 for propylene carbonate;<sup>57</sup> 1.447 for formamide<sup>183</sup>) as it was assumed that any refractive index change due to added electrolyte at  $\leq 0.3$ M will be small and have minimal effect on the film thickness calculation.

### 5.3.4.2 Theories of film drainage

A single film thickness measurement in the last collected image before film rupture tells us the rupture thickness of the film. By measuring film thickness for a single film as a function of time across several images, drainage kinetics can be determined and compared with theory. The theory for drainage velocity between immobile planar interfaces is that of Reynolds drainage, which for thin films is given by the Stefan-Reynolds equation.<sup>224</sup>

$$V_{Re} = \frac{2h^3}{3\eta R^2} (P_\sigma - \Pi) \quad (5.2)$$

Here  $V_{Re}$  is velocity from Reynolds theory,  $h$  is the film thickness,  $\eta$  is solution viscosity,  $R$  is film radius,  $P_\sigma$  is the capillary pressure and  $\Pi$  is the total of the disjoining pressure including van der Waals, electrostatic and non-DLVO components.<sup>225</sup>

Karakashev and Nguyen have developed a model for drainage allowing partial mobility of the interfaces – under which conditions drainage velocity will exceed that predicted by the Reynolds theory.<sup>225</sup> This theory and its derivation are presented in the literature and are not discussed here in any detail. Important assumptions are made to simplify the calculations in the case of electrolyte solutions here considered.

1) We make the assumption the electrostatic component of the disjoining pressure can be ignored as a factor controlling drainage at these film thicknesses. The dielectric constants are 66.14 and 110.0 for propylene carbonate and formamide, respectively.<sup>57</sup> Therefore for 0.01M 1:1 electrolyte the Debye length can be calculated as 2.8nm in propylene carbonate solutions and 3.6nm in formamide solutions. All of the films here observed rupture at thicknesses  $>20$ nm, at which thickness the surfaces are screened from each other.

2) Non-DLVO components of the disjoining pressure are likewise ignored. Steric forces due to solvation are only observed at small surface separation ( $\sim 5$ nm),<sup>30</sup> and so will not affect films more than 20nm thick. The hydrophobic force is a controversial long-range force that attracts two hydrophobic surfaces across water. A term for hydrophobic

attraction is included by Karakashev and Nguyen in their model for film drainage.<sup>225</sup> However because the nature of the force, its strength and its distance-dependence are hotly debated, and because its existence in nonaqueous systems and at fluid interface is unclear, it has not been included.

These two assumptions mean that disjoining pressure  $\Pi$  consists of the attractive van der Waals force only, which can be calculated with knowledge of the Hamaker constant for the solvent. The Hamaker constant  $A(h, \kappa)$  is derived from Hamaker-Lifshitz theory and includes weak dependence on electrolyte concentration and film thickness. The relevant equations for deriving  $A(h, \kappa)$  and for its use to determine the van der Waals component of disjoining pressure, are equations (7) and (6), respectively, from Karakashev and Nguyen's paper.<sup>225</sup>

3) The Marangoni number is assumed to be zero. The Marangoni number,  $Ma$ , is given by:

$$Ma \equiv ER/(D_s \eta) \quad (5.3)$$

Where  $E$  is Gibbs elasticity,  $R$  is film radius,  $D_s$  is surface diffusivity of species, and  $\eta$  is solution viscosity.<sup>225</sup> Gibbs elasticity  $E$  is in turn proportional to  $(d\gamma/dc)^2$ , the square of surface tension gradient,<sup>56</sup> which will be very small in non-surface active species.

In analysis using the Karakashev-Nguyen model, we obtain a value for the fitting parameter *surface shear viscosity*,  $\eta_s$ . An increase in the value of surface viscosity with which the experimental data are fit, indicates a decrease in film drainage rate. I emphasise, however, that we do not necessarily ascribe this drainage velocity change to surface viscosity alteration; it is simply a convenient means to compare drainage rates between solutions, at varying film thickness and radius.

In determining the surface shear viscosity fit, we have used the values for the neat solvent for such parameters as surface tension. This means that any differences due to the addition of electrolyte will also be subsumed within the surface shear viscosity parameter. However the change in these values is expected to be very small at the electrolyte concentrations used. Relevant solution properties are presented in Table 5.1.

**Table 5.1** Parameters used in thin film drainage calculations

	Refractive Index, n	Surface tension (mN/m)	Bulk Viscosity (mPa s)
Propylene Carbonate	1.42	41.9	2.5
Formamide	1.447	57.03	3.3

### 5.3.5 Film drainage and rupture: Results

The experimental drainage data can be compared to the drainage velocity predicted by the Stefan-Reynolds equation (equation 5.2 above) for immobile interfaces. This theory is expected to provide a “lower bound” on drainage velocity. By setting the surface viscosity to a low value ( $6 \times 10^{-8}$  Pa s m), the “upper bound” drainage velocity between fully mobile planar interfaces can also be predicted, and compared with our results. An example of the comparison between experimental data and the two limiting cases (mobile interfaces and Reynolds) is given in Figure 5.12 for a typical plane parallel film – in this case in a system with partial coalescence inhibition, 0.15M LiBr in propylene carbonate.

In this example and in all solutions for which measurement was done, the film drainage fell between the two theoretical limits – that is, drainage is more rapid than predicted by Reynolds theory for planar immobile surfaces, but less rapid than plug flow between fully mobile low-viscosity interfaces. One film in 0.30M HCl in propylene carbonate followed Reynolds drainage before rupturing at 137nm. However, a second film in this solution as well as a film in 0.14M HCl in propylene carbonate, show the more rapid drainage equivalent to partially mobile interfaces. The aberrant film ruptured at a very high thickness and was very unstable. The surface shear viscosities, as well as rupture thicknesses, are presented in Table 5.2 for all files analysed.

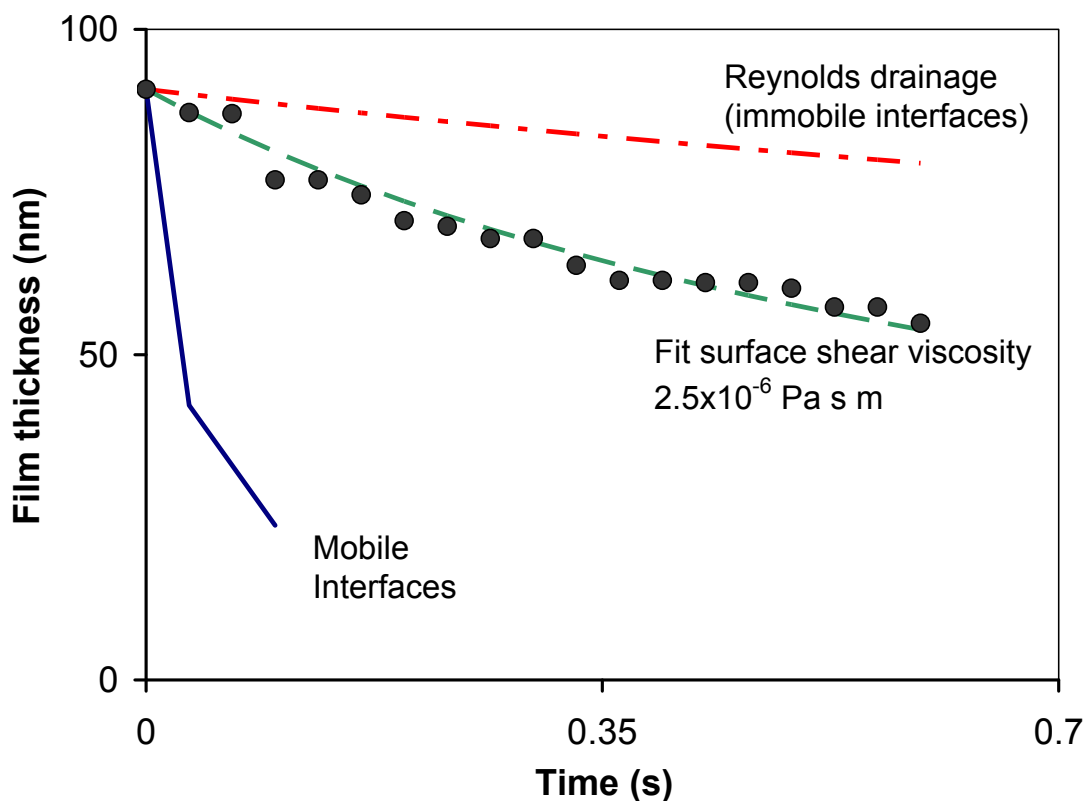


**Figure 5.12** Comparison of experimental film drainage data (●) with theoretical drainage in Reynolds (---) and mobile interface (—) cases. The experiment data are fit with a surface shear viscosity of  $2.5 \times 10^{-6}$  Pa s m (---). The film here is in 0.15M LiBr in propylene carbonate. Film rupture occurs at a thickness of 55nm.

**Table 5.2** Rupture thickness and fit surface shear viscosity in plane parallel films

Solvent	Electrolyte	Conc. (M)	Lifetime (s)	Rupture radius ( $\mu\text{m}$ )	Rupture thickness (nm)	Surface Shear Viscosity ( $\times 10^{-7}$ Pa s m)
Propylene Carbonate	HCl	0.14	0.066	20	102	3.37
		0.3	0.1	23	137	7990
		0.3	0.067	20	97	3.48
Propylene Carbonate	NaSCN	0.06	0.4	28	29.9	4.94
		0.09	0.67	20	23.6	10.8
		0.2	1.36	17	34	51.4
Propylene Carbonate	LiBr	0.06	0.198	38	38.4	2.30
		0.15	0.594	20	53.8	25.0
		0.3	7	34	34	136



Solvent	Electrolyte	Conc. (M)	Lifetime (s)	Rupture radius ( $\mu\text{m}$ )	Rupture thickness (nm)	Surface Shear Viscosity ( $\times 10^{-7}$ Pa s m)
Formamide	CH <sub>3</sub> COONa	0.03	0.132	31	46.5	2.80
		0.1	0.396	35	28	3.95
		0.3	0.066	28	31.9	1.44
Formamide	LiCl	0.03	2.36	19	36.4	63.1
Formamide	NEAT	0.02 <sup>a</sup>	0.066	20	47.8	3.91

<sup>a</sup> Ionic strength of dissociation products ammonium and formate in formamide.<sup>195</sup>

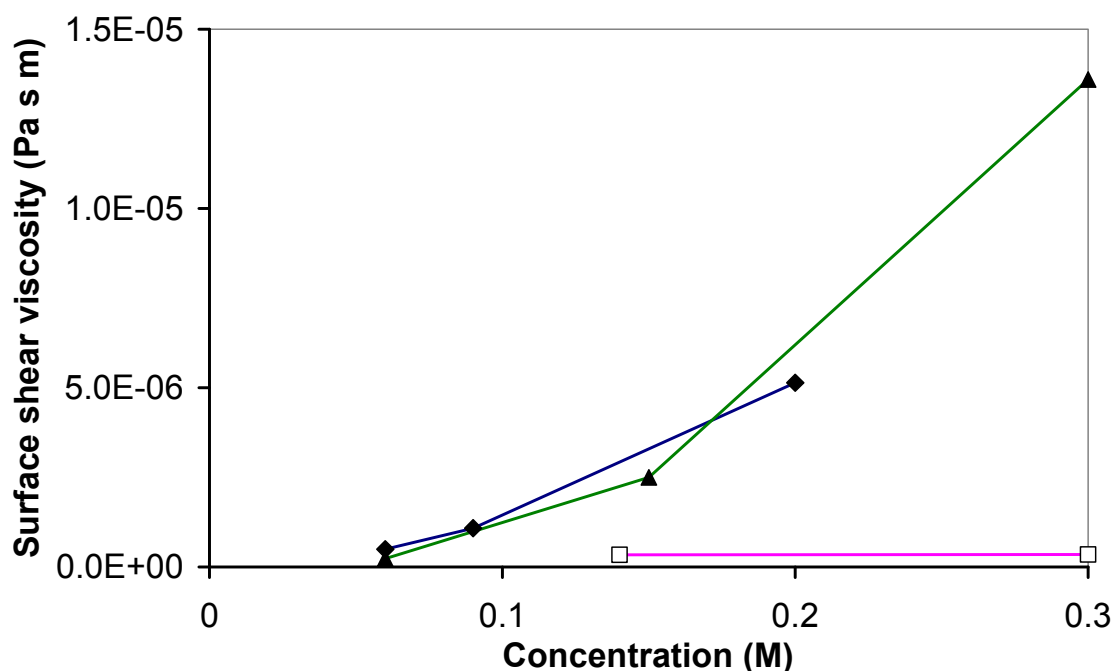


**Figure 5.13** Surface shear viscosity as a function of electrolyte concentration in propylene carbonate, for plane parallel films in solutions of inhibiting electrolytes NaSCN (◆) and LiBr (▲) and non-inhibiting electrolyte HCl (□). Higher surface shear viscosity fit reflects slower film drainage. There is a strong correlation between bubble coalescence inhibition and drainage retardation.

In Figure 5.13 the surface shear viscosity, which is a parameter that increases with slower film drainage rate, is plotted as a function of electrolyte concentration in propylene carbonate solutions. There is a strong link between increasing concentration of inhibiting electrolyte, and decrease in drainage rate (as reflected in higher surface

shear viscosity fit). The increase in surface shear viscosity matches closely with increasing film lifetime (Figure 5.7 above), indicating that decreased drainage rate, as reflected in increased surface shear viscosity, is a likely cause of bubble coalescence inhibition.

For the noninhibiting electrolyte sodium acetate in formamide, the surface shear viscosity does not show a monotonic trend with concentration. However the formamide solutions are suspected to be contaminated, and there is insufficient data to investigate a correlation with inhibiting electrolyte LiCl in formamide.

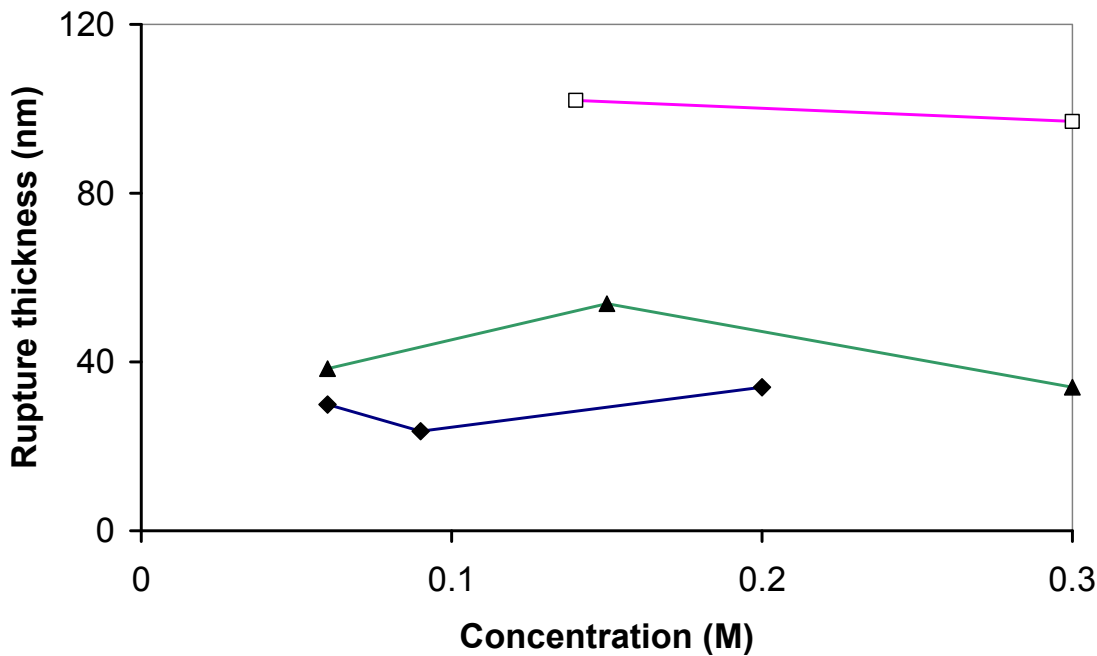


**Figure 5.14.** Film rupture thickness as a function of electrolyte concentration in propylene carbonate, for plane parallel films in solutions of inhibiting electrolytes NaSCN (◆) and LiBr (▲) and non-inhibiting electrolyte HCl (□). The thickness does not correlate with concentration in the films analysed, but rupture thickness is reduced in inhibiting electrolytes.

Figure 5.14 shows film rupture thickness in propylene carbonate solutions. The film drains to smaller thicknesses before rupturing in inhibiting electrolytes NaSCN and LiBr, in which rupture takes place at film thicknesses between 23-53nm, than in noninhibiting electrolyte HCl, in which films rupture at around 100nm. No film was

---

recorded in pure solvent, which is in itself an indication that rupture thickness is large. If the noninhibiting case is taken as comparable then we can conclude that electrolytes inhibit coalescence in part by allowing the thin film to drain to thinner bubble separations without rupture and coalescence occurring – *in addition to* retarding film drainage. There is no correlation between rupture thickness and concentration of inhibiting electrolyte in the propylene carbonate data (Figure 5.14). This lack of correlation is consistent with the idea that rupture is a stochastic process that can occur with increasing probability once the film drains to below a certain thickness.<sup>223</sup>

### 5.3.6 Discussion

The results of single film drainage measurements are generally consistent with the bubble column measurements reported in Chapter 4 for these systems. In both formamide and propylene carbonate solutions, average thin film lifetimes were measured for thin films at a range of film sizes. The average lifetime of thin films increases with increasing inhibiting electrolyte concentration. In propylene carbonate films are highly unstable in concentrations of the noninhibiting electrolyte HCl, up to the maximum tested (0.30M). (In formamide an increase in film lifetime in a noninhibiting electrolyte is measured, but it is believed that this system has some contamination.)

As well as determining film lifetimes, we measured drainage kinetics and film rupture in a subset of small, plane parallel films. The drainage was fit using a theory developed by Karakashev and Nguyen to produce the fitting parameter surface shear viscosity, which increases with decreased drainage rate. Shear viscosity remains low in noninhibiting HCl, but increases with increasing concentrations of inhibiting electrolytes NaSCN and LiBr in propylene carbonate. The data match well with the average lifetime measurements, as shown in Figure 5.15 where both average lifetime and surface shear viscosity are presented together.

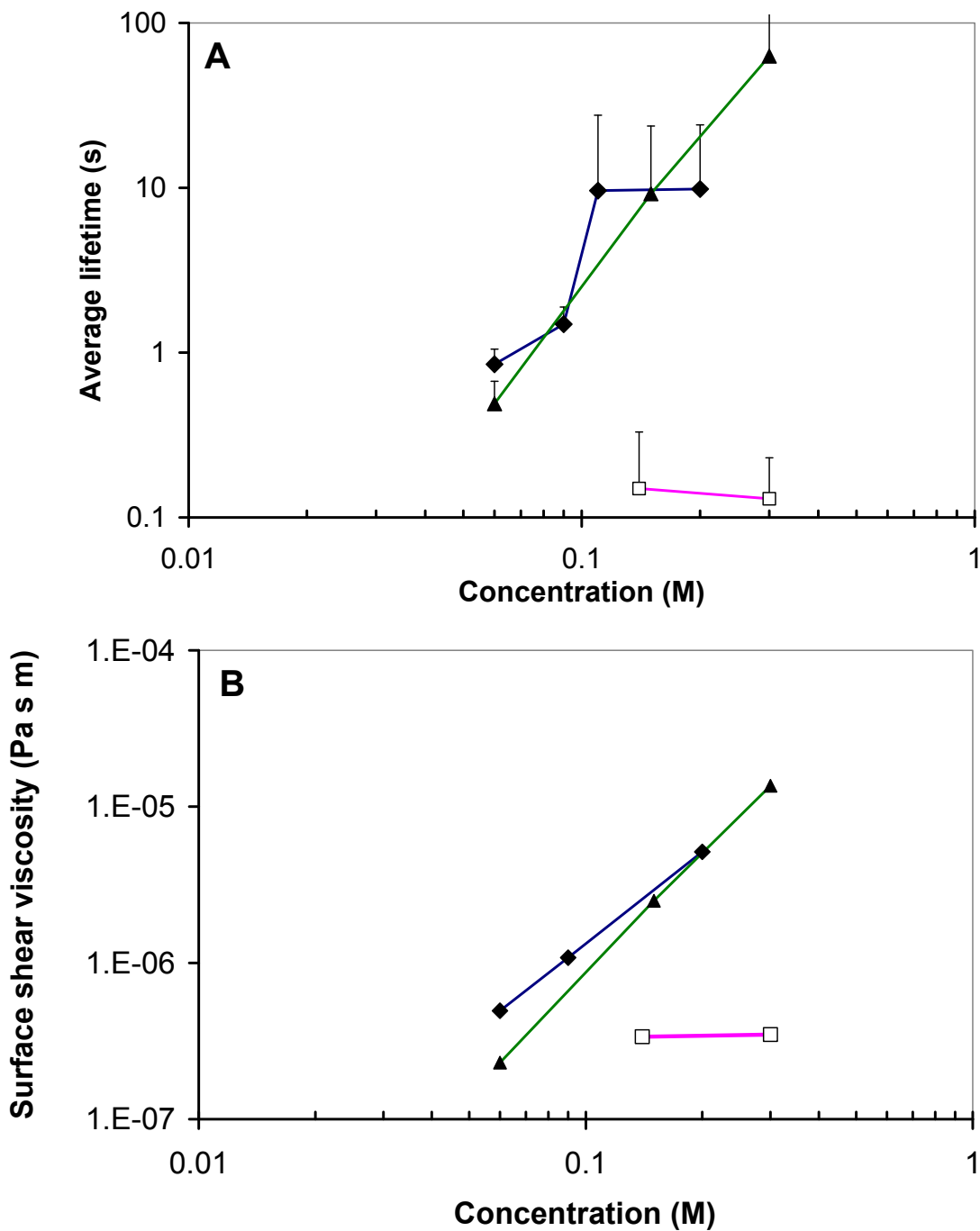


**Figure 5.15** (A) Average lifetime (taken from Figure 5.7) and (B) surface shear viscosity (taken from Figure 5.13) as a function of the log of electrolyte concentration in propylene carbonate, for plane parallel films in solutions of inhibiting electrolytes NaSCN (◆) and LiBr (▲) and non-inhibiting electrolyte HCl (□).

This is not a trivial result, because it links analysis of a particular, easily modelled case (plane parallel interfaces) with the general case of thin film stability at any film size and

---

in the presence of deformation. The correlation between surface shear viscosity and bubble coalescence inhibition is strong evidence for the argument that electrolytes inhibit coalescence relative to pure solvent (or noninhibiting electrolytes) in part by a retardation of film drainage. This is not necessarily by a change to the surface shear viscosity – no direct information about the mechanism by which electrolytes slow drainage, has been obtained. Our findings indicate that deeper probing of the thin film drainage process at a molecular level, may yield much useful data.

We observed that films rupture at a lower thickness in the presence of inhibiting electrolytes in propylene carbonate. The rupture thickness showed no trend with electrolyte concentration, however. We can conclude that electrolytes inhibit coalescence by affecting both the drainage rate and the rupture thickness of the bubble coalescence process.

Given that the films analysed have short lifetimes, one may question whether the drainage kinetics are influenced by the presence of an external force from the microsyringe pump. Once a planar film with interference fringes is visible, the pumping is arrested manually. In films with lifetime  $<1$ s, the film drainage by pumping and the independent drainage coincide. It has previously been found that the pumping velocity mainly controls film radius, with more rapid fluid withdrawal creating a larger planar film.<sup>226</sup> The films analysed for drainage and rupture thickness are chosen for their similar (small) size and so the drainage rate should not be significant. Indeed, we observed no correlation between either film rupture or surface shear viscosity and pumped drainage rate, over a range between 100 and 400nL/s in our analysed films (data not shown).

It is not possible to draw from the thin film analysis alone, conclusions about the molecular-scale mechanism by which electrolytes inhibit coalescence. A retardation of film drainage may be caused by dynamic effects such as Marangoni stresses at the air-water surface or changes in interfacial viscosity.<sup>31</sup> It may also arise from a change in the static surface forces involving either an increase in surface repulsion or a decrease in surface attraction.<sup>16, 111</sup> A closer analysis of the drainage kinetics, with more accurate

initial parameters (such as surface tension gradient and Hamaker constant for the electrolyte solutions) may enable us to eliminate one or more of these possible drainage retardation mechanisms. Similarly, a decrease in the film rupture thickness might be caused by hydrodynamics (damping of interfacial deformations, for example) or by a net decrease in any repulsive surface force, enabling the surfaces to approach more closely.

## 5.4 CONCLUSIONS

We have shown that increased inhibiting electrolyte concentration stabilises thin films in thin film drainage experiments. The results are largely consistent with bulk bubble coalescence measured in bubble column experiments, for propylene carbonate and formamide electrolyte solutions. Inhibiting electrolytes act both to reduce thin film drainage rate and to reduce the rupture thickness, relative to pure solvent. Both of these effects are expected to stabilise bubbles against coalescence over the lifetime of a collision. The film drainage velocity in plane parallel films lies between the two theoretical bounds for immobile, planar interfaces (Reynolds drainage) and for low-viscosity surfaces.

---

## Chapter 6 Surface Mobility of Bubbles in Electrolyte Solutions

---

### 6.1 INTRODUCTION

We have determined the effect of electrolytes on bubble interfacial mobility by measuring the terminal rise velocity of single, small bubbles. Much of the work here presented has been previously published.<sup>227</sup>

The stabilization mechanism of bubbles in electrolytes is unclear.<sup>41</sup> Any mechanism for bubble coalescence inhibition should be consistent with the difference in effects between inhibiting and non-inhibiting salts. It has been hypothesised that inhibiting electrolytes may alter the hydrodynamic boundary condition at the liquid-gas interface from slip to no-slip, or immobility.<sup>21, 25, 58, 94, 228</sup> In pure liquids the gas-liquid interface cannot support a surface stress, and the interface is fully mobile. This mobility leads to rapid drainage of a thin film between two bubbles, which enhances coalescence over the lifetime of a bubble collision in pure water.<sup>27</sup> The presence of a third component makes it feasible that a shear stress in the interface may be established and the mobility of the interface reduced.<sup>23</sup> During the drainage of a film in the presence of surfactant, gradients in surface tension across the thin film are established. This creates a surface shear stress and retards surface mobility via Marangoni effects that oppose film drainage – one factor that contributes to bubble stabilization in surfactants.<sup>17</sup>

Early models of electrolyte bubble coalescence inhibition predicted that electrolytes give rise to dynamic increases in interfacial tension and similarly retard the surface flow of thin liquid films via Marangoni effects, leading to immobile or partially mobile interfaces.<sup>21, 25, 73, 228</sup> Weissenborn and Pugh, however, calculated that the small gradients in electrolyte solution are too small to immobilise the interface.<sup>60</sup> An

alternative suggestion was made by our group<sup>58</sup> in light of findings that some ions inhabit the interfacial layers of water.<sup>124, 139</sup> In the sub-nanometre interface the granularity of the solution becomes important, and it was hypothesised that ions at the interface may alter interfacial water structure so as to change the surface mobility.

We here test the hypothesis of an immobile interface in electrolyte solution by determining the boundary condition of a single bubble in electrolyte solution. In order to find the electrolyte effect on the surface mobility alone, the measurement is divorced from actual bubble collision and coalescence, which is a complex and imperfectly-understood process even in pure water, with interrelated steps of film drainage and rupture.<sup>17, 41</sup> The boundary condition is instead determined via its effect on the terminal rise velocity,  $U_t$  of a single bubble rising under its own buoyancy in a quiescent liquid. Terminal rise velocity is reached when a bubble's buoyancy is balanced by the drag. In larger bubbles, these forces cause asymmetry of the flow field from top to bottom, or physical deformation of the bubble from sphericity.<sup>229</sup> The models involved become complex. For a gas bubble of  $\sim 100\mu\text{m}$ , rising at terminal velocity in water, typically Reynolds number  $< 1$ , allowing the inertial component of hydrodynamic drag to be neglected. Reynolds number,  $\text{Re}$ , is the ratio of inertial to viscous forces and for a spherical bubble is given by,

$$\text{Re} = \frac{2vr\rho}{\eta} \quad (6.1)$$

where  $v$  is bubble velocity for a bubble far from an interface,  $\rho$  is fluid density,  $r$  is sphere radius and  $\eta$  is the fluid viscosity. For  $\text{Re} < 1$ , the bubble can be considered as an undeformed sphere. For immobile interfaces terminal rise velocity  $U_t$  is then given by Stokes' Law,

$$U_{t(ST)} = \frac{2r^2\Delta\rho g}{9\eta} \quad (6.2)$$

where  $r$  is sphere radius,  $\Delta\rho$  is the difference in density between the sphere and the surrounding fluid,  $g$  is gravitational acceleration and  $\eta$  is the fluid viscosity.



An interface between gas and a pure liquid cannot support a shear stress, and therefore the interface is fully mobile.<sup>27</sup> Terminal rise velocity is then given by the Hadamard-Rybczynski equation,<sup>230, 231</sup>

$$U_{t(H-R)} = \frac{2r^2 \Delta \rho g}{3\eta} \frac{\eta + \eta'}{2\eta + 3\eta'} \quad (6.3)$$

where  $\eta'$  is the internal viscosity of the fluid drop. Where  $\eta' \ll \eta$ , as is the case for the gas-water system, this equation can be simplified so that:

$$U_{t(H-R)} = \frac{3}{2} U_{t(ST)} \quad (6.4)$$

Thus, for a spherical bubble in the low-Reynolds regime, the terminal rise velocity observed for a mobile gas-liquid interface is 1.5 times greater than that generated by an immobile interface.

We used electrolyte solutions that span the concentration range from no effect on bubble coalescence in the bubble column to strong inhibition of bubble coalescence, and measured the terminal rise velocity. The capability to do such measurements using single, reproducible microbubbles has only recently been acquired.<sup>232</sup> In addition, a very clean system is required to observe interface mobility. It has been shown that  $<10^{-7}$ M surfactant can alter the boundary condition from slip to no-slip for these small bubbles.<sup>221, 232</sup>

## 6.2 METHODS AND MATERIALS

The experimental set-up is shown in Figure 6.1 and has been described by Parkinson et al.<sup>232</sup> A bubble of clean N<sub>2</sub> is released from a fine glass capillary (internal diameter 0.5-4 $\mu$ m) into the centre of a closed cylindrical chamber (38mm internal diameter) containing 12mL solution. A microscope with attached CCD camera is used to record bubble rise at 1000 frames per second. The bubble is ~15mm above the capillary when recording starts. At this height terminal velocity has been reached. Bubble rise velocity and bubble diameter are then determined, with associated errors estimated at  $\pm 15\mu$ m/s and  $\pm 4\mu$ m, respectively. Bubbles with diameter from 40-100 $\mu$ m were used for

measurements. A variation from the previous work is the addition of a sparging chamber to clean the solution of surface active contaminants before measurement, following the results of Brandon et al.<sup>221</sup> Clean N<sub>2</sub> gas was sparged through ~ 600mL solution for at least one hour. The sparging bubbles collect surface active contaminant and deposit it on the glass above the liquid interface – which, indeed, becomes noticeably hydrophobic as evidenced by dewetting of the aqueous solution. Clean solution is extracted via glass and high-grade silicone rubber tubing (driven by a peristaltic pump) from the bottom of the sparging vessel, and the top contaminated surface is not disturbed.

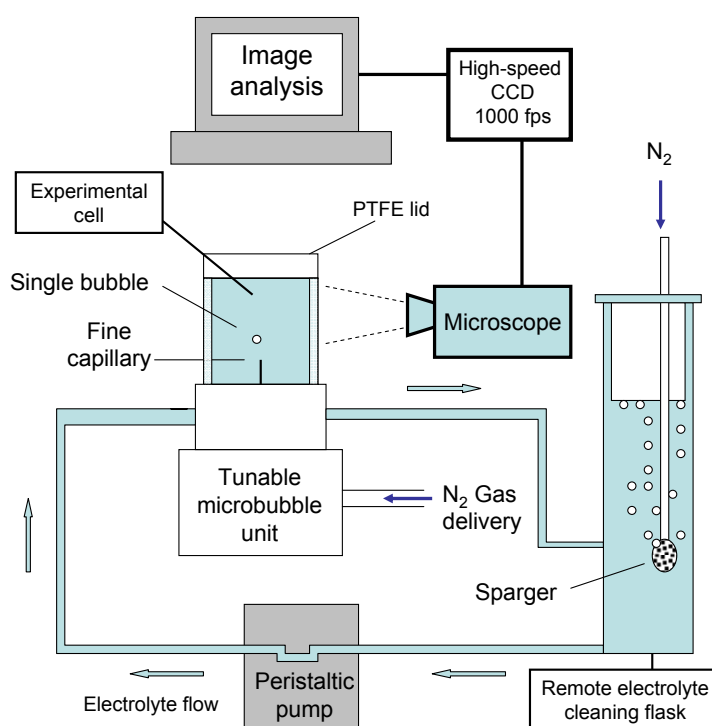


**Figure 6.1** Experimental setup for bubble terminal rise velocity measurement. (Diagram created by Luke Parkinson, reproduced from Henry et al.<sup>227</sup>)

All water used was from a MilliQ system, with resistivity  $\geq 18.2 \text{M}\Omega \text{ cm}^{-1}$ . The electrolytes used were KCl, NaCl and HClO<sub>4</sub>, which inhibit bubble coalescence; and CH<sub>3</sub>COONa, NaClO<sub>4</sub> and (CH<sub>3</sub>)<sub>4</sub>NBr, in which bubble coalescence is unchanged from pure water (at the concentrations employed). Where salts do inhibit coalescence in bubble column experiments, the inhibition is concentration dependent, with a change from no inhibitory effect at 0.01M, to complete inhibition by around 0.2M.<sup>63</sup> This range

---

of concentrations was covered for all electrolytes investigated. All electrolytes were obtained from SigmaAldrich. The perchloric acid was used as received and diluted with milliQ water. NaCl and KCl were roasted at 500°C for several hours. NaClO<sub>4</sub> and CH<sub>3</sub>COONa were freeze-dried in liquid nitrogen under vacuum for several hours to remove excess moisture. (CH<sub>3</sub>)<sub>4</sub>NBr was dried at 300°C for several hours.

For each electrolyte, bubble rise velocity was first measured in pure water, to confirm the system was free from contamination. The concentration was then increased by adding either solid salt or, in the case of the acid, stock solution. After each addition of material the solution was cleaned by sparging with nitrogen for at least one hour.

### 6.3 RESULTS

For each electrolyte, the terminal velocity and diameter of at least eight bubbles of varying size (from 40-100μm) were measured at each concentration.

Bubble size was altered via fine adjustments to the gas release mechanism of the apparatus. The bubbles produced showed a variation in size that did not appear to be correlated in any way to the electrolyte used. Results for two electrolytes are given in Figure 6.2. Perchloric acid inhibits coalescence at the concentration shown, 0.11 molal. Sodium perchlorate has no effect on coalescence. In both cases the terminal rise velocity agrees with the theoretical prediction from the Hadamard-Rybczynski equation (fully mobile interface) and is significantly different from the rise velocity predicted for a bubble with immobile interface by the Stokes model. That is, the rise velocity is the same as in pure water.

By rearrangement of equations (6.2) and (6.3) above, it can be seen that the terminal rise velocity normalized by the bubble radius squared is a constant. We chose to plot the data in this manner as we could then average results at each concentration across the range of bubble sizes, and any variation in the boundary condition with electrolyte concentration would lead to a change in the agreement of data and theory. Results from all electrolytes tested are shown in Figure 6.3. Here the terminal rise velocity is

normalized by  $r^2$ , and the average across bubbles of all sizes ( $n \geq 8$ ) is plotted as a function of concentration, for a selection of electrolytes. This normalized velocity,  $U_t/r^2$ , shows minimal dependence on the value of radius  $r$  in the range of bubble sizes tested. Also shown are the theoretical values corresponding to the Hadamard-Rybczynski terminal rise velocity, and Stokes terminal rise velocity, for pure water. (Changes in viscosity and density do change these predictions at the higher salt concentrations, but this alters the values shown by less than 3%.)

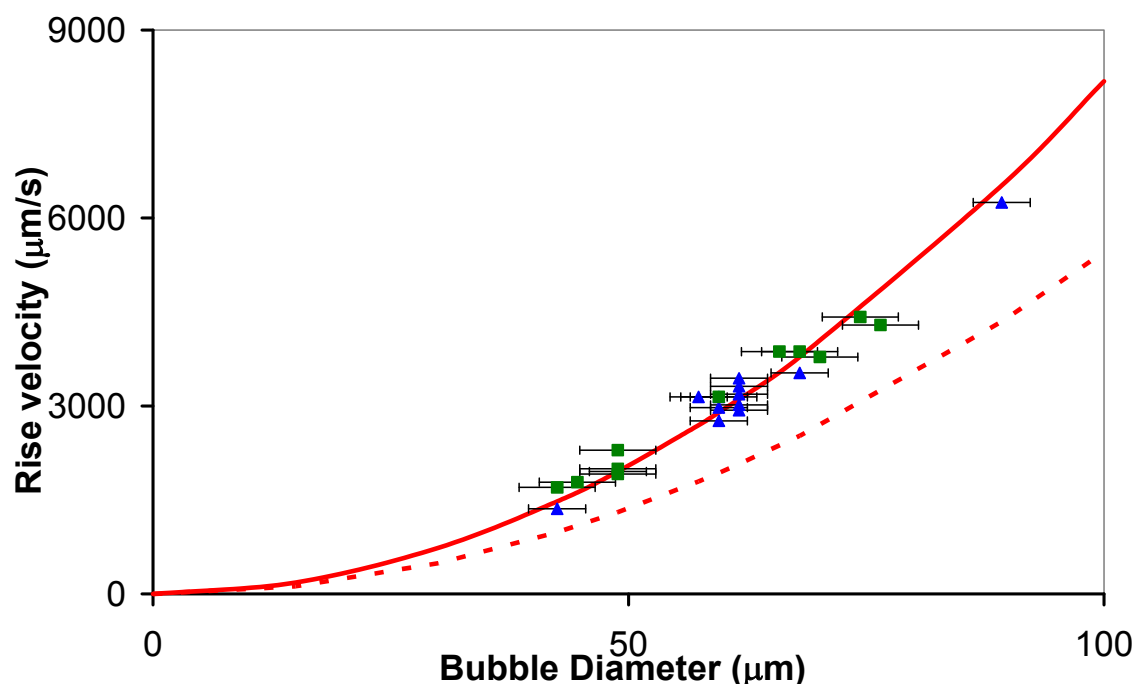


**Figure 6.2** Terminal rise velocity  $U_t$  as a function of bubble size in electrolyte solutions. Bubble coalescence-inhibiting electrolyte  $\text{HClO}_4$  (0.11 molal,  $\blacksquare$ ) and non-inhibiting  $\text{NaClO}_4$  (0.23 molal,  $\blacktriangle$ ) are compared with theoretical Stokes (broken line) and Hadamard-Rybczynski (solid line) predictions. The Stokes prediction is for an immobile interface and the Hadamard-Rybczynski prediction is for a fully mobile interface. Both electrolytes show rise velocities consistent with a fully mobile interface (slip boundary condition). Uncertainty in bubble diameter is  $\pm 4 \mu\text{m}$ .

## 6.4 DISCUSSION

All the electrolytes tested had no effect on the interfacial mobility. This finding is consistent with the idea that a higher surface tension gradient than that induced by

electrolytes, is required to retard bubble motion.<sup>60</sup> Electrolytes in general have a small effect on surface tension, and the change with concentration can be positive or negative – although most simple electrolytes increase surface tension, corresponding to net depletion in the interfacial region. In addition, surface diffusion of ions is likely to be rapid,<sup>30</sup> and so any surface tension gradient created as the bubble rises and fresh interface is created, is likely to be rapidly dissipated.

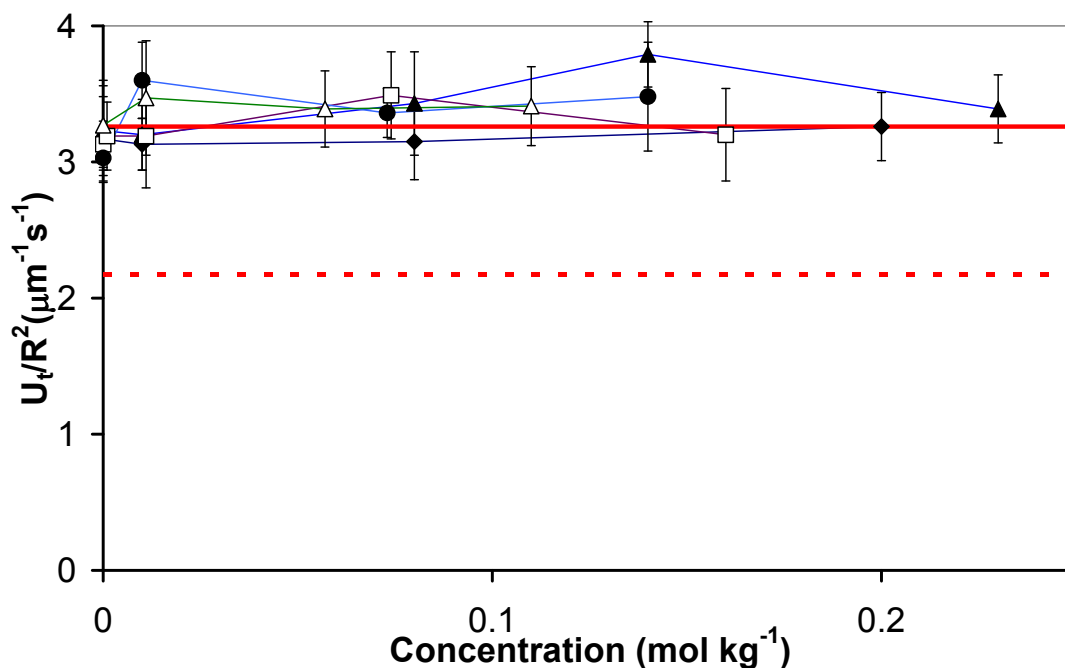


**Figure 6.3** Mean terminal rise velocity  $U_t$ , normalized by the square of bubble radius, as a function of concentration for bubble coalescence-inhibiting electrolytes KCl (□) and HClO<sub>4</sub> (△) and non-inhibiting electrolytes NaClO<sub>4</sub> (▲), CH<sub>3</sub>COONa (◆) and (CH<sub>3</sub>)<sub>4</sub>NBr (●). Also shown are theoretical values from Stokes (broken line) and Hadamard-Rybczynski (solid line) predictions for immobile and mobile interfaces respectively. Error bars at  $\pm 1$  standard deviation,  $n \geq 8$ .

Immobile fluid surfaces have been found in pure liquid or dilute salt solutions, in the absence of added surfactant.<sup>233, 234</sup> We suggest that most of these observations can be attributed to trace surfactant contamination, as Brandon et al. found that even  $10^{-7}$ M added surfactant was sufficient to immobilise the interface of a small bubble.<sup>221</sup> These low levels of contamination are undetectable by many conventional measurements of solution purity such as surface tension measurement. Manor et al. recently found gas

bubbles in supposedly clean electrolyte solution to have a partially mobile interface, and could explain this partial mobility by a small amount of surface contaminant.<sup>89</sup> Many of the works on bubble rise acknowledge the difficulty of obtaining a truly contaminant-free system.<sup>235</sup> The system used here is shown to be free of contaminants in pure water, after N<sub>2</sub> gas sparging, because the bubble rise velocity agrees with the theory for a mobile, clean interface.

It must be acknowledged that there are differences between a single bubble rising in a quiescent fluid and the thinning of a film between two colliding bubbles. Diffusion of electrolyte between bulk and interface is likely to be different, particularly if the film is very thin. Additionally, the presence of surface forces may influence the distribution of ions in a thin film. The larger bubbles in most coalescence studies will undergo surface deformation<sup>76</sup> and this is expected to affect electrolyte concentration gradients. However we can state that the presence of electrolyte per se does not change interfacial mobility. This is an important, if negative, result in the bid to determine the mechanism behind ion-specific electrolyte inhibition of bubble coalescence. It had been hypothesised that ions positioned in the surface layer of solvent, might change the liquid structure so as to induce immobility at the boundary.<sup>58</sup> While the importance of interfacial ion preferences is still a matter for study, this particular mechanism can now be rejected. Many of the early theories proposed for electrolyte inhibition of bubble coalescence relied upon an immobilisation of the thin film boundary to reduce drainage and so inhibit bubble coalescence.<sup>25, 61, 228</sup> This hypothesis supposes that the Marangoni effects that occur with adsorbed surfactant, are also relevant to electrolyte coalescence inhibition – although this was refuted by Weissenborn and Pugh.<sup>60</sup> Such Marangoni effects would, if present, also act to create a shear gradient at the surface of a single rising bubble, and so the results reported here support the view that electrolytes do not inhibit via this mechanism.

We note that in reference to Figure 6.3 we are unable to rule out completely a terminal rise velocity above the theoretical prediction for a completely mobile interface at some concentrations of some electrolytes. The increase is small and does not correlate with concentration, and therefore we attribute this to experimental error. A more substantial

---

small increase was seen in earlier work on the terminal rise velocity of CO<sub>2</sub> bubbles in water.<sup>232</sup>

## 6.5 CONCLUSION

In all electrolytes tested, the terminal rise velocity fits the Hadamard-Rybczynski equation and does not change relative to pure water. Hence, the aqueous electrolyte- gas interface is fully mobile, and a slip boundary condition is appropriate, in both bubble coalescence-inhibiting and non-inhibiting electrolytes.

---

## Chapter 7 Electrolyte Coalescence Inhibition: A New Model

---

### 7.1 OVERVIEW OF FINDINGS

The starting point for the study of bubble coalescence inhibition in electrolytes is that some electrolytes inhibit bubble coalescence in aqueous solution at concentrations on the order of 0.1M, while other electrolytes have no effect up to 0.5M and beyond. In addition, the effect of the electrolyte depends on the combination of cation and anion present. Cations and anions each fit into two categories, designated  $\alpha$  and  $\beta$ , with  $\alpha$  and  $\beta$  ions having different effects on bubble coalescence in the presence of a given counterion.<sup>9,10</sup>

Electrolytes also show ion specificity in their effect on solution surface tension.<sup>11</sup> In single electrolytes, those salts that have a larger (positive or negative) effect on surface tension are more likely to inhibit bubble coalescence.<sup>59, 60, 62</sup> In Chapter 2 it was shown that this relationship did not hold for mixed electrolyte solutions: The surface tension gradient of mixtures does not correlate with the bubble coalescence inhibition. We can therefore conclude that bubble coalescence inhibition does not occur via any effect dependent upon the equilibrium surface tension – such as changes to surface Gibbs Elasticity.

Chapter 2 also used mixed electrolytes to test the hypothesis that electrolytes manifest their effect via ion separation within the interfacial region<sup>126</sup> – a hypothesis arising from the finding that some ions have a non-uniform distribution at the air-water interface.<sup>125</sup> Electrolyte mixtures were shown to be consistent with different surface positions of  $\alpha$  and  $\beta$  cations and anions. In addition the  $\alpha$  and  $\beta$  ion assignments are shown to predict the coalescence inhibition behaviour of electrolyte mixtures, with all mixtures tested inhibiting coalescence except for  $(\alpha\beta + \alpha\beta)$  and  $(\beta\alpha + \beta\alpha)$  salt combinations.



---

The ion separation mechanism was not supported by bubble coalescence inhibition in alkali metal halides. Iodide is enhanced at the surface to a greater extent than bromide, chloride and fluoride,<sup>141</sup> but in the presence of sodium – which has little to no surface enhancement – the iodide salt is the least powerful inhibitor. This indicates that while ions at the interface may be important, ion separation is not required for coalescence inhibition.

Electrolytes are not the only non-surface active species that transiently stabilise thin liquid films. In Chapter 3 it was shown that some osmolytes that affect protein stability in a way similar to Hofmeister salts, can also inhibit bubble coalescence in a way similar to inhibiting electrolytes. While urea – a salting-in agent of proteins – only inhibits coalescence at greater than 1M concentration, salting-out cosolute sucrose shows coalescence inhibition at around 0.1M – a concentration similar to inhibiting electrolytes. Moreover, sucrose and salts have a cooperative effect.

A review of recent literature suggests that electrolytes and other cosolutes do not, as traditionally thought, change bulk water structure and the hydrogen-bonding network.<sup>117</sup> Rather, their interaction is local and limited to the water molecules in the solvation shell. Thus, the differing effects of salt, sucrose and urea on protein stability are related to the direct interactions with protein surfaces.<sup>156</sup> If sucrose is assumed to inhibit bubble coalescence via the same mechanism as electrolytes, then this supports the importance of the air-water interface in the inhibition mechanism, rather than bulk water structure. If we do assume a similar mechanism of coalescence inhibition in sugars and in electrolytes, then we can conclude that the charged nature of the ions may not be determinative. The coalescence inhibition observed in sugars is thus a strong argument against an electrostatic force causing coalescence inhibition. This finding may instead point towards an osmotic-type mechanism whereby the solute distribution and concentration are important.

We also report “sugar specificity” – different mono- and disaccharides at concentrations on the order of 0.1M, may act as strong or weak inhibitors of bubble coalescence. The sugar specificity is not currently understood. It is demonstrated that the difference in

inhibition may be associated with minor structural changes in the sugar molecule, from which it can be concluded that small differences in the solute (and its hydration shell) can affect thin film stability. Disaccharides are stronger inhibitors than the sum of their two individual monosaccharides, so size or the particular orientation of the monosaccharides may be implicated.

Ion specific bubble coalescence inhibition in nonaqueous electrolyte solutions (Chapter 4) is confirmation that solvent structure is not crucial in the film stabilisation mechanism. Electrolytes inhibit coalescence in four polar solvents investigated: methanol, dimethylsulfoxide (DMSO), propylene carbonate and formamide. In methanol no bimodal ion specificity is observed over a wide range of electrolytes, with all electrolytes tested showing inhibition. In both formamide and propylene carbonate, electrolytes can be classed as “inhibiting” or “less inhibiting” based on the concentration at which their effect manifests. Some electrolytes (like NaSCN and LiClO<sub>4</sub>) inhibit coalescence in propylene carbonate but do not do so in water. Thus, ion assignments differ between the two solvents, which points to some role for the solvent properties in the ion specificity of electrolyte coalescence inhibition. In formamide ion combining rules and  $\alpha$  and  $\beta$  assignments can be made that are identical to those in water, for the salts tested. This result is strong evidence against the importance of solvent structure. It is also strong evidence against a surface forces explanation for electrolyte coalescence inhibition. While little information is available on the surface charge properties of formamide, it is expected to have a surface charge and potential that vary from those of water, and the change in dielectric constant of the solvent means that charge will propagate differently. An electrostatic model for coalescence inhibition would be strongly dependent on the solvent, which is not consistent with our results. A model of coalescence inhibition based on the dynamic process of thin film drainage and solute concentration gradients (in accordance with results in aqueous sugar solutions) is to be preferred.

The film drainage and rupture process was studied for an individual thin film between air interfaces using a microinterferometric technique, as described in Chapter 5. Solutions in propylene carbonate and in formamide were chosen to cover inhibiting and

---

noninhibiting electrolytes, on the basis of the bubble column experiments in Chapter 4. It was found that average film lifetimes (for a range of film sizes) agree very well with the bubble column coalescence inhibition data, with inhibiting electrolytes increasing film lifetime at higher concentrations, and noninhibiting electrolyte showing no effect or smaller effects on film stability. Coalescence inhibition is expected when the film lifetime is longer than the lifetime of a bubble collision. Further analysis of the kinetics of drainage and rupture in small films with planar interfaces in propylene carbonate solution, shows that inhibiting electrolyte reduces film drainage rate with increasing concentration, relative to pure solvent. In addition, films drain to lower thickness before rupturing. It can be concluded that inhibiting electrolyte acts on two of the steps of coalescence – both retarding film drainage, and stabilising thinner films. Thus, any mechanism proposed should include an explanation for both of these effects.

It was shown in Chapter 6 that the surface of a single, small, non-deformed bubble is mobile in electrolyte solution. The single bubble terminal rise measurements enable us to conclude that the presence of electrolyte does not immobilise the air-water interface. In the context of the conclusion derived from the previous chapters – that electrolytes inhibit bubble coalescence inhibition by changing the dynamics of the interface during film drainage – this result has further implications. Surfactants affect the rheology of the air-water interface both by changing surface mobility and by changing surface deformation.<sup>17</sup> If electrolyte solution interfaces are mobile (for small, spherical bubbles) then the dynamic process affected in thin film stabilisation is likely to be the surface deformability.

In the literature review of Chapter 1, I described three broad (and not incompatible) categories of hypotheses concerning the mechanism by which electrolytes can inhibit bubble coalescence in water. An inhibiting electrolyte could affect equilibrium surface forces between gas interfaces; it could change the solvent properties of the entire thin liquid film (like the hydrogen-bonding network); or it could act on the dynamic film drainage and change the non-equilibrium properties of the interface.

As shown above, electrolytes are likely to inhibit coalescence by changing the dynamic process of film drainage. There is experimental evidence against the importance of surface forces and against that of bulk solvent structure. Furthermore, coalescence inhibition in non-electrolytes like the sugars shows that at a molecular level, this mechanism may not be related to the charged nature of the ions. Rather, then, osmotic qualities of the electrolyte as solute are implicated. The most likely way in which this osmotic effect will come into play, is in the concentration variation at the interface. There is an equilibrium concentration gradient between the bulk and the interfacial region, which is associated with a positive or negative surface excess and a related surface tension gradient.<sup>236</sup> There are also transient concentration gradients created during dynamic drainage, due to interfacial deformations.<sup>55</sup>

In Section 7.2 I will describe a link between equilibrium ion concentration gradients at the air-water interface, in terms of the ion partitioning coefficients, and  $\alpha$  and  $\beta$  assignments from coalescence inhibition. The key to the correlation is a new thermodynamic model for ion partitioning.<sup>237</sup> Section 7.3 describes how ion partitioning at the air-water interface might be related to thin film stabilisation, through non-equilibrium concentration gradients induced at the interface by surface deformation. Section 7.4 describes a link between ion partitioning at the gas-solution interface and ion partitioning at the protein interface, which is implicated in Hofmeister-type ion specific effects.<sup>143</sup> This therefore relates ion specific bubble coalescence inhibition to the wider realm of specific ion effects.

## 7.2 ELECTROLYTE INHIBITION AND SURFACE PARTITIONING

### 7.2.1 The Solute Partition Model

Pegram and Record have recently developed the thermodynamic Solute Partitioning Model for surface partitioning of individual ions at the air-water interface.<sup>143, 236-238</sup> The model uses electrolyte surface tension gradients to derive surface partitioning of each ion present. Ion contributions to electrolyte surface tension gradients are independent and additive (at least up to 1 mol kg<sup>-1</sup> concentration).<sup>236</sup> A lower surface affinity of a

single species is associated with a larger positive contribution to surface tension, in accordance with Gibbs adsorption isotherm.

Pegram and Record assume that the two ions that make up the electrolyte with the highest surface tension gradient used,  $\text{Na}_2\text{SO}_4$ , are both completely excluded from the air-water surface.<sup>237</sup> The values of the ion partition coefficients of all other ions can then be calculated relative to these. Ion surface affinities are presented in terms of an ion surface partition coefficient,  $K_{p,i}$ , which can be thought of as a ratio of surface to bulk concentration. Completely surface-excluded species such as  $\text{Na}^+$  and  $\text{SO}_4^{2-}$  will have a partition coefficient of  $K_{p,i} = 0$ . Species with neutral surface affinity relative to the bulk have  $K_{p,i} = 1$ , and an enhancement at the surface is indicated by  $K_{p,i} > 1$  (see Figure 7.1 for a diagram of ion positions). The average partition coefficient of any ion can be determined using an average from the surface tension gradients of its different salts.

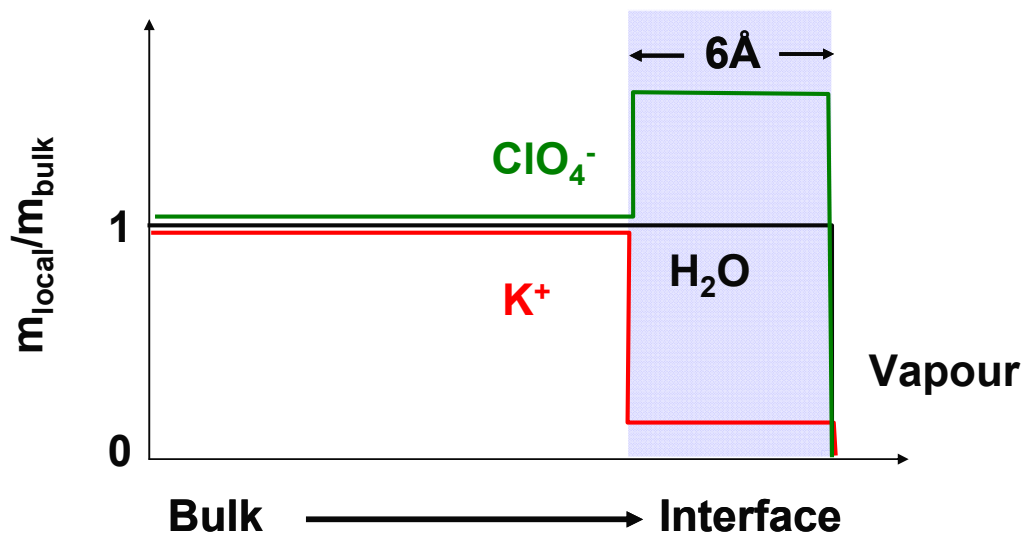


**Figure 7.1** An example of ion surface partitioning according to the Solute Partitioning Model.<sup>237</sup> The ratio of local concentration to bulk concentration is plotted as a function of position. The interfacial region is set at  $6\text{\AA}$  in depth. Potassium is excluded from the surface and has low concentration in the interfacial region relative to the bulk ( $K_{p,i} = 0.12$ ). Perchlorate anion has higher surface concentration than in bulk ( $K_{p,i} = 1.77$ ). The water concentration is constant through the solution. Diagram based on Pegram and Record.<sup>238</sup>

The equation used to relate surface tension gradient (as a function of molality rather than molarity) and the ion partitioning coefficients, is given by:<sup>237</sup>

$$\frac{d\gamma}{dm_2} = -\frac{RTb_1^\sigma \nu}{m_1^\bullet} (1 + \varepsilon_\pm^b) \left[ \left( \frac{\nu_+ K_{p,+} + \nu_- K_{p,-}}{\nu} \right) - 1 \right] \quad (7.1)$$

where  $(d\gamma/dm_2)$  is the surface tension gradient as a function of electrolyte concentration in moles  $m_2$ ,  $R$  is ideal gas constant,  $T$  is temperature,  $b_1^\sigma \equiv n_1^\sigma/A$  is the number of moles of water molecules per unit surface area,  $\nu \equiv \nu_+ + \nu_-$  is the number of ions per formula unit of electrolyte, and  $m_1^\bullet$  is the solvent molality,  $55.5 \text{ mol kg}^{-1}$  for  $\text{H}_2\text{O}$ .  $(1 + \varepsilon_\pm^b)$  reflects nonideality and conversion from activity to concentration,  $(1 + \varepsilon_\pm^b) = \nu^{-1} (dOsm/dm_2)$  where  $(dOsm/dm_2)$  is the osmolality gradient. The ion partition coefficients  $K_{p,+}$  and  $K_{p,-}$  are related to the overall electrolyte surface partitioning by  $\nu K_{p,2} = \nu_+ K_{p,+} + \nu_- K_{p,-}$ . Using the assumption that  $\text{Na}^+$  and  $\text{SO}_4^{2-}$  are excluded from the interface and that therefore the surface of  $\text{Na}_2\text{SO}_4$  contains only water molecules, the surface water concentration  $b_1^\sigma$  can be used to obtain a thickness for the interfacial layer. Using a value for  $b_1^\sigma$  of  $0.19$  water molecules per  $\text{\AA}^2$ , the interfacial layer thickness is calculated as  $6 \text{\AA}$ .<sup>237</sup>

The air-water surface partition coefficients for the ions investigated are given in Table 7.1 (cations) and Table 7.2 (anions) together with the ion's  $\alpha$  or  $\beta$  assignment.

**Table 7.1** Cation partition coefficients at the air-water interface, ranked from most excluded to most accumulated at the air-water surface

Ion	$K_{p,i} \pm \text{s.d.}^a$	Ion assignment
$\text{Na}^+$	0.00 (defined)	$\alpha$
$\text{Cs}^+$	$0.01 \pm 0.04$	$\alpha$
$\text{Li}^+$	$0.08 \pm 0.21$	$\alpha$
$\text{K}^+$	$0.12 \pm 0.08$	$\alpha$
$\text{NH}_4^+$	$0.25 \pm 0.07$	$\alpha$
$\text{H}^+$	$1.50 \pm 0.04$	$\beta$

<sup>a</sup> Data taken from Pegram and Record.<sup>237</sup>

**Table 7.2** Anion partition coefficients at the air-water interface, ranked from most excluded to most accumulated at the air-water surface

Ion	$K_{p,i} \pm \text{s.d.}^a$	Ion assignment
$\text{SO}_4^{2-}$	0.00 (defined)	$\alpha$
$\text{F}^-$	$0.53 \pm 0.02$	$\alpha$
$\text{OH}^-$	$0.58 \pm 0.04$	$\alpha$
$\text{Cl}^-$	$0.69 \pm 0.04$	$\alpha$
$\text{Br}^-$	$0.86 \pm 0.08$	$\alpha$
$\text{NO}_3^-$	$0.98 \pm 0.09$	$\alpha$
$\text{I}^-$	$1.18 \pm 0.12$	$\alpha$
$\text{CH}_3\text{COO}^-$	$1.30 \pm 0.05$	$\beta$
$\text{ClO}_3^-$	$1.44 \pm 0.03$	$\beta$
$\text{SCN}^-$	1.64	$\beta$
$\text{ClO}_4^-$	$1.77 \pm 0.04$	$\beta$

<sup>a</sup> Data taken from Pegram and Record.<sup>237</sup>

The trend in ion surface partition coefficients aligns with bubble coalescence inhibition  $\alpha$  and  $\beta$  assignments for all ions tested.  $\alpha$  cations and  $\alpha$  anions are more excluded from the interface than, respectively,  $\beta$  cations and  $\beta$  anions. Note in particular that although iodide is classified as an  $\alpha$  anion its alkali metal salts are poor coalescence inhibitors relative to other univalent electrolytes. This is consistent with iodide's position at the boundary of  $\alpha$  and  $\beta$  surface partition coefficients.

The correlation revealed here between ion surface partitioning and  $\alpha$  and  $\beta$  assignments leads to the conclusion that interfacial ion positioning is related to bubble coalescence inhibition, and that (see Figure 7.2):

- Two subsurface ions inhibit coalescence, as an  $\alpha\alpha$  electrolyte;
- Two surface-enhanced ions inhibit coalescence, as a  $\beta\beta$  electrolyte; and
- One surface-excluded ion and one surface-accumulated ion do not inhibit coalescence. This is the category of  $\alpha\beta$  and  $\beta\alpha$  electrolytes.

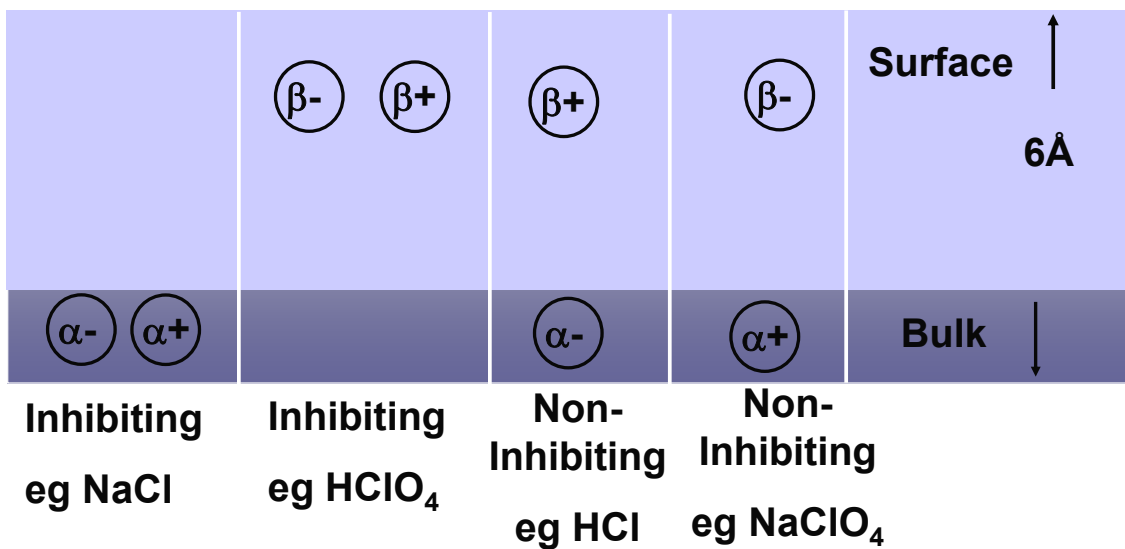


**Figure 7.2** Ion partitioning and ion assignments from bubble coalescence.  $\alpha$  cations and  $\alpha$  anions are both excluded from the interface;  $\beta$  cations and  $\beta$  anions are accumulated at the interface.  $\alpha\alpha$  and  $\beta\beta$  electrolytes inhibit coalescence;  $\alpha\beta$  and  $\beta\alpha$  electrolytes are less-inhibiting. Interfacial layer width of  $6\text{\AA}$  from Pegram and Record.<sup>237</sup>

Note that this is the antithesis of the interfacial ion hypothesis first put forward, which supposed that bubble coalescence inhibition depends upon the separation of ions at the interface.<sup>126</sup> Possible bubble coalescence mechanisms that are consistent with this view of ions at the surface are discussed below, but first the Solute Partitioning Model is considered further.

### 7.2.2 Ion partitioning and mixed electrolytes

We are able to test the validity of ion partitioning coefficients at the air-water interface by using the partition coefficients of Pegram and Record to derive surface tension gradients for electrolyte mixtures (using equation (7.1)), and comparing to our experimental values.<sup>58</sup> We have done this for mixtures for which individual ion partitions and surface tension gradients are available. The osmolality change, ( $d\text{Osm}/dm$ ), was calculated as the average of two individual electrolyte osmolality values<sup>239</sup> as reported by Pegram and Record.<sup>237</sup> The results of the comparison are presented in Figure 7.3.



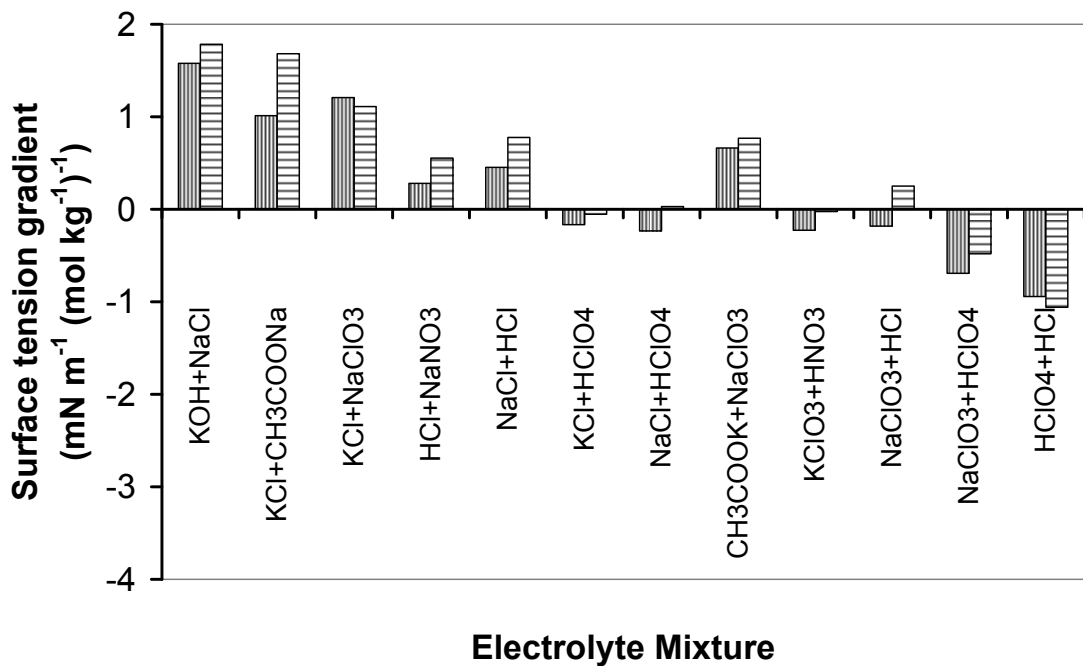


**Figure 7.3** Comparison of mixed electrolyte surface tension gradients from experiment (left column, vertical stripes) and as predicted using surface partition model individual ion partition coefficients (right column, horizontal stripes). Experimental values are as reported in Chapter 2,<sup>58</sup> and ion partition coefficients are from Pegram and Record.<sup>237</sup> The agreement is reasonably consistent, showing that individual ion contributions can predict mixed electrolyte surface tensions.

The predictions from the Solute Partitioning Model in general agree well with experimental measurements of surface tension gradient, given the assumptions employed. This result supports the use, at least to a first approximation, of the assumptions of independence and additivity of ion contributions to solution surface tension. However some of the differences in surface tension gradient of mixtures are out by as much as 200%, so the model should be treated with caution. It is also worth pointing out that some of the experimental results for mixed electrolytes were measured using only one (equimolar) concentration. It is assumed that mixed electrolyte concentration gradients will be linear, but this has not been substantiated for all cases.

### 7.2.3 Solute Partitioning Model coefficients and interfacial ion data

In developing the Solute Partitioning Model, Pegram and Record derived ion partition coefficients from static surface tension values of electrolytes.<sup>236</sup> One of the principles behind the Solute Partitioning Model is the concept that some ions can show enhanced concentration at the air water surface, even in an electrolyte that raises the overall surface tension.<sup>125, 137, 240</sup> A non-uniform distribution at the solution interface has been found for some ions in molecular dynamics simulations and surface-selective spectroscopy experiments.<sup>124, 125, 137, 142</sup>

It is possible to check partition coefficients against available experimental and simulation data for ion enhancement at the solution surface. The trend in anion surface partition constants calculated by Pegram and Record, shown in Table 7.2, is consistent with the experimental study of ion surface affinities conducted by Cheng et al.<sup>205, 241</sup> Electrospray ionization mass spectrometry was used to measure anion concentrations in fissioning droplets from a solution containing six anions with a sodium counterion. The droplets fissioned first from the main droplet surface will be from the surface layers and so contain higher concentrations of ions that favour the surface.<sup>241</sup> The ion surface affinity increases in the order  $\text{Br}^- < \text{NO}_3^- < \text{I}^- < \text{SCN}^- < \text{ClO}_4^-$ , which matches the increasing surface partition coefficients of these anions. Incidentally, Cheng et al. also note a correlation between anion surface enhancement and crystalline ionic radius (a better correlation than with polarisability or ion volume).<sup>241</sup> It is suggested that the driving force for interfacial ions is the release of water from the solvation shell to take part in the bulk network. This is consistent with a later study in which ion surface affinities were shown to be insensitive to the ratio of water:methanol in solution – indicating that the exact solvent interactions are not as important as ion exclusion in general.<sup>205</sup>

Ion surface or subsurface enhancements are not consistent across all theoretical and experimental techniques. This is perhaps not surprising – these are, after all, attempts to measure to sub-nanometre resolution the position of mobile species at a dynamic interface; a difficult task made more so by an interface prone to contamination.<sup>133, 242</sup>

In general, molecular dynamics simulations and surface-selective spectroscopy predict that large, polarisable ions will show a surface preference while smaller, harder, more easily solvated ions exist away from the surface. Thus, ions like sodium and fluoride are prefer the subsurface as determined by several techniques.<sup>124, 142, 203, 204</sup> The halide surface preference will increase with increasing size from  $F^-$  to  $I^-$ , as predicted by ion partition coefficients.<sup>124, 148, 243</sup> Some studies do find surface enhancement of  $Br^-$  and  $Cl^-$  at the air-water interface,<sup>137, 244</sup> while the partition coefficient prediction is for depleted concentration relative to the bulk.<sup>237</sup> This finding is perhaps explained by the fact that different techniques probe different surface depths.<sup>213</sup> Other work has found that nitrate,<sup>136, 209</sup> thiocyanate<sup>245</sup> and acetate<sup>246</sup> anions all show surface enhancement, consistent with the ion partition coefficients.

Hydrogen – or hydronium,  $H_3O^+$  - is also predicted to have an enhanced surface concentration, in agreement with its high surface partitioning coefficient.<sup>91, 213</sup> The hydronium surface enhancement is attributed to the ion asymmetry which means that it causes less disruption of the water hydrogen-bonding network by partitioning to the surface.<sup>141</sup>

The Solute Partitioning Model uses a thermodynamic method to derive ion partitioning constants from electrolyte surface tension gradients. The forces that determine an ion's preference for or exclusion from the solution surface are not particularly relevant to the application of the model. It is worth noting however that a variety of theoretical developments have also shown enhancement of some ions at the surface. The traditional Onsager-Samaras model<sup>132</sup> states that an image-charge repulsion makes interfacial ions energetically unfavourable: there is an equivalent 'charge' in the low-dielectric vapour region repulsing ions. A series of works have since demonstrated that ion surface enhancement and electrolyte surface tension gradients can be obtained if short-range attractive dispersion forces are included in calculations.<sup>39, 247</sup> In a separate approach, the molecular dynamics of Jungwirth and coworkers show enhancement of ions at the interface only if polarisability of water by the ions is taken into account.<sup>124, 204, 244</sup> Thus, the partitioning of ions to the air-water interface can be supported by sufficiently complex models of the system.

One of the contradictions between Solute Partitioning Model and the molecular dynamics simulations and spectroscopy measurements of interfacial ion concentration, is the assumption of independence of ion position. Molecular dynamics simulations show that an ion's concentration gradient is affected by the presence of oppositely charged species, such that a subsurface ion such as sodium can be dragged towards the surface by a surface-enhanced anion like iodide.<sup>125</sup> Many of the simulations, however, are done at higher concentrations where it is more likely that ion association will start to occur. In using the surface-selective spectroscopy technique sum frequency generation spectroscopy (SFG) Petersen and Saykally assume that detectable ions can be used to deduce the position of non-detectable species – thus, a greater enhancement in surface I<sup>-</sup> in HI but not NaI is attributed to presence of H<sup>+</sup> at the surface.<sup>91</sup>

It is suggested that the variation seen by Pegram and Record in an ion's surface partitioning coefficient in the presence of different counterions (which is reflected in the standard deviation associated with the average partition coefficient in Table 7.1 and Table 7.2 above), as well as the errors in some of the mixed electrolyte surface tension gradient predictions, can in part be attributed to the dependence of ion distribution on other species.<sup>237</sup> Overall, however, the surface partitioning coefficients of different ions are in agreement with the available experimental and simulation evidence for ion surface enhancement.

### **7.3 IONS AT THE INTERFACE AND SURFACE RHEOLOGY**

Ion  $\alpha$  and  $\beta$  assignments from bubble coalescence inhibition are correlated with ion surface partitioning coefficients. In general  $\alpha$  cations and  $\alpha$  anions partition away from the air-water surface, while  $\beta$  cations and  $\beta$  anions show enhanced concentration at the interface relative to the bulk. The question then becomes how ion surface partitioning affects bubble coalescence inhibition, and why electrolytes with one ion at the surface and one subsurface, fail to inhibit coalescence.

---

One possibility might be that the link between bubble coalescence inhibition and ion partitioning is simply through the net effect that the electrolyte has on surface tension gradient. The electrolytes with the smaller effect on surface tension are those with one surface-enhanced and one surface-depleted species because these have opposite and additive contributions to solution surface tension, and so have a lower magnitude surface tension gradient overall. However, our experimental results in Chapter 2 showed that the square of the surface tension gradient (as  $(d\gamma/dc)^2$ ) does not correlate with bubble coalescence inhibition in mixed electrolytes.<sup>58</sup> The ion partition coefficients have been shown to be valid in predicting mixed electrolyte surface tensions (Section 7.2.2). This, combined with the bubble coalescence inhibition data in mixed electrolytes, shows that ions at the interface do not manifest their effect via changes to the macroscopic, equilibrium surface tension.

### **7.3.1 Hypothesis: Thin film stability is driven by non-equilibrium ion interfacial gradients**

Rather than equilibrium surface tension, I propose that the important process in inhibiting electrolytes is the development of, and response to, non-equilibrium surface tension gradients. These gradients are driven by the kilohertz-range deformation of the interface during the dynamic film drainage process.

As the gas-solution interface deforms during a bubble collision, transient ion concentration gradients are set up along the thin film interface and between the interface and the bulk. These concentration gradients will affect surface tension and drive a restoring ion diffusion from interface to bulk or vice versa. I propose that the effect is to counter film deformation so as to reduce film drainage and disfavour film rupture. This model for electrolyte inhibition is analogous to recent observations on surfactant effects on the surface rheology of thin films, and is explored further below.<sup>248</sup>

In qualitative terms, and as will be discussed in more detail below, the model of surface-subsurface equilibration is consistent with the observed difference in inhibition between  $\alpha\alpha$  and  $\beta\beta$ , and  $\alpha\beta$  and  $\beta\alpha$  electrolytes. Inhibiting electrolytes of  $\alpha\alpha$  or  $\beta\beta$  type have

both ions in bulk or both at the interface, and the concentration gradients, restoring forces and relative timescales to restore surface-subsurface equilibrium are expected to be larger than in noninhibiting electrolytes. With one ion at the surface and one in bulk there is overall a more even solute distribution, and hence a smaller impact of surface deformation on solute concentration. Equilibration is likely to be more rapid than the inhibiting electrolyte distribution. Thus, under this model the equilibrium ion partitioning in the interface determines the degree of the local surface stresses and the rate of surface response.

### 7.3.2 Dilational surface modulus

The hypothesis outlined above holds that inhibiting electrolytes alter the response of the air-water surface to a change in surface area during deformation. In particular, the concentration gradients caused will alter the local surface tension. The rate of change of surface tension as a film deforms is a surface rheological quantity, known as the surface elastic dilational (or dilatational) shear modulus,  $\varepsilon$ .<sup>249</sup> The surface dilational modulus shows how the local surface tension changes for a relative change in local surface area.<sup>248</sup>

$$\Delta\gamma = \varepsilon(\omega) \frac{\Delta A}{A} \quad (7.2)$$

where  $\Delta\gamma$  is the change in surface tension,  $\varepsilon(\omega)$  is the frequency-dependent surface dilational shear modulus, and  $\Delta A/A$  is the relative change in surface area for a surface deformation. The dilational modulus is thus a measure of the system's ability to adjust surface tension with application of stress.<sup>250</sup> Note that when the surface does not exchange with the bulk (for example, when there is an insoluble monolayer of surfactant) then  $\varepsilon$  is equivalent to the surface Gibbs Elasticity,  $E$ .<sup>249</sup> The response to deformation is then purely elastic. When surface and subsurface are not at equilibrium then surface excess changes with diffusion towards or away from the bulk, and this drives a surface viscosity represented by the imaginary component of  $\varepsilon(\omega)$ .<sup>251</sup>

Because thin film surfaces undergo rapid deformations<sup>76</sup> and changes in area during drainage, the dilational modulus is expected to be a relevant quantity for thin film

---

stability in electrolyte solutions. After a deformation, ions will migrate to or away from the interface in order to restore equilibrium. Thus, dilational modulus is found to depend upon the concentration of solute and the bulk and surface diffusion parameters.

### 7.3.2.1 *Dilational shear modulus and surfactant film stabilisation*

Dilational shear modulus is dependent on the relative timescales of surface deformation and system response. Traditionally the limit on measurements on oscillating bubble surfaces has been around 1Hz, and many non-equilibrium effects were not observable.<sup>250</sup> The technique of capillary pressure tensiometry is well-suited to probing the dynamics of surfactant-covered interfaces.<sup>252</sup> The pressure difference across the interface of a bubble oscillated by a piezo is measured and the amplitude and phase response can be used to give information on dynamics of adsorption kinetics and diffusion between the interface and bulk.<sup>250</sup> The technique can probe the frequency range 1-500Hz. This is mid-range for surfactants, covering low-frequency cases where the system is always at equilibrium and there is no surface elasticity, to high-frequency cases where there is no diffusion from bulk and the surface behaves like a non-diffusing monolayer.<sup>253</sup>

It has been shown that in surfactant films a stabilisation of the foam film over long timescales is correlated with the frequency-dependence of the dilational surface modulus in the frequency range 1-500Hz.<sup>251</sup> The dilational modulus  $\varepsilon(\omega)$  has elastic and viscous (dissipative) components, with the dilational surface viscosity sometimes defined as  $\kappa$ . Foam film lifetime does not correlate with the elastic component; but increased stability is associated with the viscous component of the dilational surface response.<sup>248</sup> Intrinsic surface viscosity is observed as a frequency-dependence of the dilational surface modulus, and it appears at high surfactant concentrations (for some species). Koelsch and Motschmann attribute the foam stabilisation to increased damping of surface waves in the presence of a surface viscosity.<sup>251</sup>

Note that this dilational surface viscosity is related to, but cannot be directly compared with, the surface viscosity measured in thin film drainage experiments<sup>55, 225</sup> and used as a fitting parameter in the drainage kinetics experiments of Chapter 5. The surface

viscosity used in thin film drainage models is valid under certain limiting conditions – local equilibrium between bulk and surface is commonly assumed, for example<sup>129</sup> – which do not apply in the frequency regime at which dilational viscosity is observed. As Ivanov et al. point out in a thorough review of surface viscosity, dilational viscosity is only one component of the measured surface viscosity which can also, in the case of surfactants, include a “true” surface viscosity change because of the adsorbed surfactant.<sup>254</sup>

Recent work has linked the surface viscosity to a non-equilibrium diffusion process between a sublayer and the surface.<sup>250</sup> Notably, some surfactant species show a purely elastic surface response, attributed to more rapid solute exchange between the surface and the subsurface surfactant populations that allows the solute to equilibrate on a faster timescale than the surface deformations. Thus, slower equilibration between a sub-layer and a surface layer is associated with dilational surface viscosity and longer film lifetimes, in ionic surfactant solutions.<sup>250</sup>

### **7.3.3 Dilational shear modulus in electrolyte-stabilised thin films: future experiments**

It is hypothesised that the relationship observed in surfactant films between film stability and equilibrium-restoring concentration gradients in the surface layers, is also present in electrolyte solutions.

The need for diffusion between bulk and surface layers is consistent with the link between ion partitioning and coalescence inhibition. Under this model, where ions are both excluded from or both enhanced at the air surface then concentration gradients will be relatively high. Restoration of equilibrium between interface and bulk will be slower than in the case of electrolytes where one ion is enhanced and one is depleted at the interface. In the latter case the overall solute gradients will be smaller during deformation and diffusion processes may be less important, so the interface dilational modulus will have only a small viscous dissipation component. This is an explanation for why noninhibiting electrolytes do not stabilise thin films.



---

The surface dilational viscosity will depend physically on surface to sub-surface concentration gradients, but it will also be related to the nature of the surface deformations, and to ion diffusion in the bulk and at the surface. Diffusion is complex and can depend upon solvated ion size and interaction with the solvent, but also on the presence of other solute species and so concentration will also control this process.<sup>129</sup> Therefore a theoretical model of surface concentration, diffusion, deformation and viscosity effects would be very complex indeed.

It is hoped that in the future the dilational surface modulus of electrolyte solutions can be measured at relevant timescales. It is expected that equilibration processes in ionic solutions will be more rapid than for larger surfactant molecules, and so the study of bubble surfaces in electrolyte may well require a development of this technique beyond its current limits to probe the appropriate higher-frequency range. (For instance, it is known that bubble surfaces in water undergo deformations at a rate exceeding 1000Hz.<sup>76</sup>) Such experiments would in the future be beneficial to establishing the mechanism of bubble coalescence inhibition in electrolytes. It is also possible (currently at lower frequencies only) to combine dilational modulus studies with the surface-specific spectroscopy method second harmonic generation (SHG).<sup>250, 253</sup> By this means the identity and orientation of interfacial species can be probed – suggesting that with further expansion of instrumental capabilities, it may be possible to determine the surface rheology of bubbles in electrolyte solution, and the individual ion surface concentrations.

### **7.3.4 Evidence for a deformation-based mechanism**

#### *7.3.4.1 Existence of deformations at the bubble surface*

One important piece of support for the deformation-driven electrolyte effect is that bubbles in water are observed to undergo rapid surface deformations that could drive non-equilibrium ion concentration gradients. Krzan et al. used high-speed video to record bubbles rising towards a free surface in pure water, and showed that the surface of a 1.5mm-diameter bubble oscillates with a frequency greater than 1000Hz.<sup>76</sup> A surface-active species, 1-pentanol, reduces pulsation amplitude. Tse et al. used high-

speed video to observe bubble coalescence and break-up in a bubble column. They observe a similar high-speed deformation of bubbles in pure water, and report qualitatively increased rigidity of bubbles in solutions of inhibiting electrolyte  $\text{MgSO}_4$ .<sup>49</sup>

Such increased rigidity is what would be predicted if the electrolyte is reducing deformability of the surface (via increases in dilational surface viscosity). Increased rigidity will reduce thin film drainage and reduce growth of surface waves that lead to rupture.<sup>255</sup> These results therefore support the existence of a rapid deformation of the air-water surface, which is reduced by inhibiting electrolyte.

The existence of low-amplitude thermal fluctuations of the free water surface on a rapid timescale has been modeled by Sharma and Ruckenstein<sup>44</sup> and can be observed at frequencies on the order of  $10^5$  Hz or higher.<sup>256</sup> During thin film drainage mechanical fluctuations will also occur, and the interplay of surface deformations can be complex. It is not my aim in this discussion to suggest the precise origin of the surface deformations that drive concentration gradients at the thin film surface, but the high frequency thermal fluctuations may be thought of as an upper limit of the possible frequency range to be probed.

#### 7.3.4.2 *Bubble size-dependence of coalescence inhibition*

If electrolyte coalescence inhibition is driven by surface deformation, then it is predicted that the effect will decrease in bubbles of smaller size that are less deformable.

Struthwolf and Blanchard measured lifetime against a planar free surface of small bubbles in the diameter range  $40\text{-}400\mu\text{m}$ .<sup>79</sup> In pure water, large bubbles ( $>100\mu\text{m}$  diameter) are very unstable and rapidly coalesce with the free surface. In seawater and NaCl they found increasing surface lifetime (decreased coalescence) with increasing bubble size, indicating that the salt becomes more effective with increasing bubble size. Below  $80\mu\text{m}$  diameter, bubbles are unstable and coalescence occurs within 10 milliseconds even in the presence of electrolyte. (It is noted that in distilled water coalescence increases for the smallest bubbles; this is attributed to the presence of small

---

amounts of contamination.) Thus, for very small bubbles electrolyte has no stabilising effect. It is in this sub-100 $\mu\text{m}$  bubble size range that a spherical non-deformed geometry is expected, because of the very high Laplace pressure.<sup>229</sup> Therefore these results support the importance of bubble deformation for electrolyte bubble coalescence inhibition.

Our measurements of terminal rise velocity in Chapter 6 were also done on bubbles with diameter <100 $\mu\text{m}$ . This size range was chosen so that the bubbles would be non-deformed and spherical, and hence easily modeled. The results are still relevant as ruling out immobilization of the interface by electrolyte via a Marangoni effect (in contrast to surfactants<sup>221</sup>); however they do not tell us anything about the proposed deformation-based mechanism.

At sizes greater than around 100 $\mu\text{m}$  diameter, the Laplace pressure is lowered sufficiently that the bubble surface can deform.<sup>229</sup> Bubble size is still found to have an effect on electrolyte inhibition of coalescence; however it is noted that many mechanisms for electrolyte coalescence inhibition will show a dependence on bubble size, and so little can be gained (from a mechanistic standpoint) from these studies. Thin films of larger radius will drain more slowly if Reynolds theory for static planar surfaces is applied ( $V \propto R^{-2}$ ).<sup>112</sup> However large films can deform,<sup>255</sup> and films that deform allow more rapid drainage – so the relationship between size and bubble stability becomes complex and model-dependent. For instance, Manev et al.<sup>255</sup> use a model for deformable mobile interfaces with differently deformed domains, and show that drainage velocity should be proportional to  $R^{-4/5}$ . Other drainage models show different proportionality.

Tsang et al. measured bubble size dependence of coalescence in  $\text{MgSO}_4$  using two bubbles on neighbouring capillaries. The bubbles used were on the order of 1-5mm diameter. Transition concentration  $c_t$  was found to decrease with increasing bubble size, with  $c_t \propto d^{-1.2}$  where  $d$  is some mean bubble diameter.<sup>66</sup> Thus, electrolyte has a greater effect in stabilising larger bubbles. A model is proposed for this relationship whereby

bubbles are stabilised by repulsive hydration forces even at large separations;<sup>257</sup> however there is no other evidence for such a surface repulsion.

Ribeiro and Mewes in an elegant series of experiments used downward-flowing liquid to alter relative velocity of bubble approaches in what were essentially two-dimensional collisions between flat glass walls.<sup>20</sup> They find that for a given bubble approach velocity, bubbles above a certain critical size are less likely to coalesce – in both water and partially-inhibiting NaCl solutions. The approach velocity required for bubble bouncing (non-coalescence) decreases with increasing bubble size up to a critical radius (in their case, 2.3mm) and is then independent of bubble radius. Ribeiro and Mewes hypothesise that interface deformability increases coalescence inhibition. However interfaces are expected to be freely deformable well below 4.6mm bubble diameter, so this explanation seems unlikely. It is possible that bubble size increases the bubble interaction time.

### **7.3.5 Ion partitioning and surface viscoelasticity model, and bubble coalescence experiments**

The proposed model for electrolyte inhibition of bubble coalescence is that inhibiting electrolytes are those that have a large exclusion or a large accumulation of total solute at the interface. This partitioning creates transient concentration gradients during the deformation of the air-solution surface as it drains, and these gradients set up a process to restore equilibrium that involves diffusion between bulk and surface layers of the interface, in a way similar to surfactants. The dis-equilibrium creates a surface dilational viscosity that acts against the film deformations to retard film drainage and to stabilise the film against rupture.

In this section I briefly discuss whether such a mechanism is consistent with the bubble coalescence results reported in this thesis.

#### *7.3.5.1 Single electrolytes*

Inhibiting electrolytes stabilize bubbles against coalescence. One point that needs to be addressed is the bimodal nature of the coalescence inhibition. With some exceptions

---

such as the iodide salts, all univalent inhibiting electrolytes have about the same transition concentration. It might be expected on the basis of the partition coefficients that NaF, NaCl and NaBr would have differing transition concentrations. It is suggested that in determining concentration effects on dilational modulus and surface partitioning, the assumption of independence can be challenged. Equilibration at the surface will depend upon the positioning of the ions as well as their diffusion – their change in position – in the bulk and at the solution surface. These parameters are expected to depend on the surrounding ions, and so the average partition coefficients are a poor guide to precise transition concentrations of any given electrolyte, while still having predictive value in determining whether a salt will or will not inhibit coalescence.

#### 7.3.5.2 *Mixed electrolytes*

In electrolyte mixtures the single ion surface partition coefficients provide a reasonably good prediction of surface tension gradient, suggesting that they correctly show the ion positioning. However the surface tension gradient does not provide a good prediction of bubble coalescence inhibition in comparison to single electrolytes. It is suggested that in the presence of more ions the equilibrium, static surface tension will be a poorer indicator of the dynamic ion diffusion processes related to interfacial deformation and the dilational shear modulus. It is also expected that the surface exclusion or accumulation of different ions will not be truly independent, and so the partitioning and ion diffusion will be more complex in electrolyte mixtures.

#### 7.3.5.3 *Sugars and non-electrolytes*

There is no direct evidence that coalescence inhibition by sucrose and electrolytes is via the same mechanism. However there is a similar effect at a similar concentration for a species having a similar effect on surface tension, so a like mechanism can be considered a possibility. Because the dilational shear modulus is driven by non-equilibrium concentration gradients and diffusion processes it can be applied to any solute, and does not depend upon the ion charge. Thus, the proposed mechanism is entirely consistent with a similar coalescence inhibition by non-electrolytes. We can also explain the difference in inhibition between sugar molecules with similar structures – small differences in molecular configuration, water solvation and intermolecular hydrogen-bonding are expected to affect the solute diffusion and surface preference.

Disaccharides are in all cases stronger inhibitors than their component monosaccharides, which is consistent with the larger molecules having slower diffusion and slower equilibration.

The solute partition model can be used to determine the surface partitioning of non-ionic substances at the interface as well as electrolytes.<sup>238</sup> Most sugars raise the surface tension of water<sup>169</sup> and so will have a surface partitioning coefficient  $K_{p,i} < 1$ . It would be useful in the future to determine surface tension gradients and partition coefficients for the sugars studied here, and see if a correlation exists with their coalescence inhibiting effects.

#### 7.3.5.4 *Nonaqueous solvents*

It may at first appear that ion partitioning will depend on the solvent, and that therefore one would expect ion  $\alpha$  and  $\beta$  assignments to alter a great deal between solvents if surface partitioning is the relevant parameter. However ion surface enhancement is in fact interpreted largely as an osmotically-driven process, with the exclusion of an ion from the solvent being the driving process. This means that many polarisable liquids will have very similar ion-partitioning.<sup>199, 207</sup> Evidence that ion interfacial enhancement is not solvent-specific, comes from molecular dynamics simulations and from surface-selective experimental methods. For example, iodide (as sodium iodide) is shown to have a surface concentration peak in polarisable solvents water, formamide, ammonia and ethylene glycol.<sup>141</sup> Cheng et al. showed that the relative surface enhancement of anions remained approximately constant in all compositions of water/methanol mixtures.<sup>205</sup> Different solvents are expected to change dilational surface modulus because there will be variations in surface and bulk ion diffusion and association, and these factors would have to be compared in any application of the suggested model to nonaqueous solvents.

The link between ion surface partitioning and bubble coalescence inhibition could be tested in nonaqueous solvents, but only after experiments to determine surface tension gradients and nonideality (osmolality) factors in these solutions. This is suggested as a possible future project.

### 7.3.5.5 *Thin film drainage*

The thin film drainage study in propylene carbonate and formamide solutions shows that electrolytes affect both film drainage and the stable film thickness. This is consistent with a deformation-based mechanism, because drainage is increased with surface corrugations<sup>255</sup> and rupture is believed to occur through contact of deformations at each thin film surface.<sup>42</sup>

The electrolyte inhibition effect is seen in plane parallel films, which show no evidence of variations in thickness. However the creation and drainage of the thin film is in itself a surface deformation, and during drainage the film stretches and concentration gradients may be introduced.<sup>112</sup> It may also be that there are oscillations on the planar film with a very high frequency and these deformations are not observable at the resolution and data collection speed (30Hz) used in our thin film balance experiments. Alternatively, deformations occurring in the meniscus around the thin film may affect film stability – as is suggested for some surfactant films.<sup>23</sup> A future experiment to probe the existence and electrolyte-dependence of surface deformations of a thin film, would be useful. A technique such as laser speckle measurement has the temporal and spatial resolution necessary.<sup>258</sup>

## 7.4 SURFACE PARTITIONING, BUBBLE COALESCENCE INHIBITION AND HOFMEISTER EFFECTS

In Section 7.2 we reported a correlation between ion partitioning coefficients and the ion  $\alpha$  or  $\beta$  assignment in bubble coalescence inhibition. Pegram and Record have previously linked ion partitioning at the air-water interface with partitioning at hydrophobic surfaces, and thus with Hofmeister ion effects on protein solubility and stabilisation. Therefore, it is now possible to link ion specificity in Hofmeister and biological systems, with bubble coalescence inhibition.

The solute partitioning model works for any surface, not just the air-water interface.<sup>143,</sup>  
<sup>238</sup> By the use of some assumptions, it is possible to derive partitioning coefficients for hydrophobic and polar protein moieties. Although the partition coefficients differ for

each surface (as expected), those for hydrocarbon align reasonably closely with those for the hydrophobic air-water surface.<sup>143</sup> It is found that hydrocarbons are “salted in” more (solubility is increased) by those ions that accumulate at the hydrophobic surface, and that this effect is stronger for anions. By modelling the exposed protein surface as a mixture of hydrophobic and polar amide areas, and using partition coefficients for each of these areas proportionally, Pegram and Record have had some success at modelling Hofmeister ion effects on protein solubility for various proteins.<sup>143, 238</sup> The ion specificity tends to be dominated by ion partitioning to the hydrophobic surface.

The connection between Hofmeister-type ion specificity and ion specific bubble coalescence inhibition is thus derived: Ion accumulation at the hydrophobic protein interface controls the stabilisation of proteins, and ion accumulation at or depletion from the hydrophobic air-water interface also controls the stabilisation of bubbles. In both cases the partition coefficients can be used to predict stability of a protein or a bubble, respectively, in solution.

Despite this common basis in interfacial ion partitioning, the  $\alpha$  and  $\beta$  ion assignments from bubble coalescence inhibition do not align with Hofmeister series of cations and anions. One reason for this lack of agreement is that the partition coefficients of the ions will vary between the air/water and protein/water interfaces (and they will also vary among protein surfaces).<sup>143, 238</sup>

An additional point of difference is the difference in the relevant timescale of interactions at each interface. Ion association (or exclusion from) with protein surfaces is largely an equilibrium effect governed by thermodynamic principles.<sup>143</sup> In contrast the bubble coalescence inhibition has been shown to be a dynamic effect, probably driven by non-equilibrium interfacial concentration gradients.

#### **7.4.1 Surfactant-free emulsions and ion partitioning**

The fact that some ions partition to hydrocarbon interfaces while some are excluded<sup>238</sup> allows us to propose a mechanism for another related colloidal phenomenon. It is



---

suggested that a dynamic stabilisation based on ion partitioning, analogous to the bubble coalescence inhibition hypothesis, is behind the stabilisation of some surfactant-free emulsions by high salt concentrations, observed by Nandi et al. and by Stevens et al. (see Chapter 1).<sup>94, 95</sup> Oil-water interfaces will deform on a longer timescale than the air-water case, but this deformation can still drive concentration gradients of the electrolyte in the interfacial region. An investigation of the surfactant-free emulsion system is suggested as a possible future project. To establish this correlation it would be necessary to measure oil droplet coalescence in a wider range of electrolyte solutions, as previous studies have been limited to  $\alpha\alpha$  electrolytes only and little ion specificity was observed.<sup>94, 95</sup> It would also be necessary to determine partition coefficients of ions for specific polar and non-polar oils, as the nature of the hydrophobic phase was found to determine emulsion response to high electrolyte.

Correlating different oil partition coefficients with emulsion stability would be a further check upon the relationship between thin film drainage, ion interfacial partitioning, and interface deformability.

## 7.5 CONCLUSIONS

Electrolytes inhibit bubble coalescence in water, and the inhibition is ion specific. To date there has been no consistent explanation for this phenomenon that could describe all of the observations. I have considerably extended the experimental observations to show ion specificity in mixed electrolytes, and coalescence inhibition and ion combining rules in nonaqueous solvents. Nonelectrolyte solutes, sugars, can also inhibit bubble coalescence. Experiments on thin film drainage in electrolyte solution showed that electrolyte affects both film drainage rate and film rupture thickness, while single bubble terminal rise measurements showed that interfacial mobility is not affected. The results have enabled us to conclude that electrolytes do not inhibit coalescence via a change in equilibrium surface forces, nor do they act upon the bulk structure of the solvent. Rather, electrolyte coalescence inhibition is a nonequilibrium effect that acts upon the dynamic film drainage process, through ion specific interfacial partitioning.

In this chapter a mechanism has been proposed by which electrolytes affect interfacial dynamics. Inhibiting electrolytes are predicted to reduce surface deformations of bubbles and thin films, which will both reduce thin film drainage and stabilise the film against rupture. Surface deformations are damped in the presence of a dilational surface viscosity which arises when the equilibration of non-equilibrium concentration gradients caused by surface deformations, is on the same timescale as those deformations.<sup>250</sup> While the timescale for deformation and equilibration is believed to be in the sub-millisecond range for electrolytes, this transient effect can lead to film stabilisation over timescale of seconds or longer – as observed in surfactant films.<sup>251</sup> Noninhibiting electrolytes have more even ion distribution between bulk and surface layers and so will have more rapid equilibration of solute, so that the gas-solution surface has a purely elastic response to deformation. Under these circumstances deformation is not damped and film drainage and rupture are not inhibited.<sup>248</sup>

The Solute Partitioning Model of Pegram and Record<sup>237</sup> was used to show that  $\alpha$  anions and  $\alpha$  cations are excluded from the surface layer of solution, while  $\beta$  cations and  $\beta$  anions show surface enhancement at the air-water interface. Thus, electrolytes with two excluded or two accumulated ions inhibit coalescence, but those with a more even total ion distribution between interface and bulk, show no inhibiting effect.

The Solute Partitioning Model has also been used to explain Hofmeister ion effects, with ions that partition to the hydrophobic surface increasing hydrocarbon solubility.<sup>143</sup> We can therefore link ion specificity in biological systems with ion specific bubble coalescence inhibition on the basis of ion partitioning. Differences in ion effects between the two systems are explained by different partitioning at the air-water and hydrocarbon-water interfaces, and by the observation that while protein interaction is an equilibrium thermodynamic effect, bubble coalescence inhibition involves dynamic film drainage and solute equilibration processes.

It is perhaps no less significant that the proposed hypothesis can relate the mechanism of action of electrolytes and surfactants at the air-water surface. Surface activity is a continuum, and yet traditional models of surfactant coalescence inhibition have failed to

---

explain coalescence inhibition by electrolytes. While thin film lifetimes in surfactants are controlled by a complex array of effects,<sup>259</sup> including Marangoni effects at the film surface, both soluble surfactants and electrolytes are hypothesized to stabilise thin films by an increased surface dilational viscosity, driven by equilibrium processes between the surface and the subsurface regions of the interface. Both surfactants and inhibiting electrolytes will reduce film surface deformations to reduce film drainage velocities and inhibit film rupture.

---

## Chapter 8 Summary

---

Bubble coalescence in pure water is stabilised by the addition of salt. The effect is ion specific: some electrolytes inhibit coalescence at around 0.1M, while others show no effect up to 0.5M and higher. The coalescence inhibition of any single electrolyte is predicted by ion combining rules. While the mechanism for ion specific bubble coalescence inhibition by electrolyte remains to be validated, this thesis has presented several experiments to investigate coalescence inhibition by electrolytes that have increased our understanding of the problem. This progress has culminated in a proposed mechanism for coalescence inhibition that has consolidated several different approaches. Experimental results and the hypothesised mechanism of thin film stabilisation, are here summarised.

- Mixed electrolyte coalescence can be predicted from the single electrolyte  $\alpha$  and  $\beta$  assignments, with all mixtures inhibiting coalescence except those of two like non-inhibiting single electrolytes ( $\alpha\beta+\alpha\beta$  and  $\beta\alpha+\beta\alpha$  mixtures). Mixed electrolyte coalescence inhibition shows an agreement with predictions from a hypothesis based on ion positioning within the interfacial region. However the suggested mechanism, which relies on ion separation at the interface, is not supported by coalescence in the alkali metal halides. Sodium iodide is a poorer inhibitor than the other halides despite the fact that sodium is subsurface and iodide shows surface enhancement.
- Mixed electrolyte bubble coalescence inhibition is not correlated with surface tension gradient. In single electrolytes a correlation was observed between electrolyte inhibition and square of surface tension gradient,  $(d\gamma/dc)^2$ . Surface tension gradients were measured for electrolyte mixtures and there is found to be no correlation with coalescence inhibition. This shows that the equilibrium

---

surface tension gradient is not a controlling parameter in coalescence inhibition. In addition coalescence inhibition is not controlled by an increase in Gibbs Elasticity in inhibiting electrolytes.

- Non-electrolyte solutes can inhibit bubble coalescence in water. Urea has no effect on coalescence inhibition below 1M. However sucrose inhibits coalescence over a similar concentration range to that in inhibiting electrolytes. There is a cooperative effect with electrolytes, in both sucrose and urea, while in contrast urea has an antagonistic effect on sucrose coalescence inhibition.
- Mono- and disaccharides can inhibit bubble coalescence, but vary in the degree of inhibition and thus exhibit “sugar specificity”. Small differences between molecular structures can lead to significant differences in coalescence inhibition. Disaccharides are more powerful than the sum of their individual monosaccharide components. The mechanism of coalescence inhibition by non-surfactants is charge-independent, suggesting an osmotic pressure-driven process.
- Electrolytes can also inhibit coalescence in nonaqueous solvents. Methanol and dimethylsulfoxide show no bimodal ion specificity, with all electrolytes tested inhibiting coalescence. Formamide shows ion-specific salt effects in a way dependent upon ion combining rules that match those in water. Propylene carbonate also demonstrates ion specificity of coalescence inhibition, but the ion assignments vary from those in water.

The similarity between solvents indicates that the mechanism of coalescence inhibition does not depend on surface forces across the thin liquid film, nor does it depend on solvent structure – as both of these effects are strongly solvent dependent. Rather, an effect on the dynamic film drainage process is implicated.

- Inhibiting electrolytes act by reducing the rate of thin film drainage and by lowering the thin film rupture thickness. Solutions of inhibiting and

noninhibiting electrolytes in formamide and in propylene carbonate were used to investigate thin film drainage and rupture between gas interfaces, using microinterferometry in the thin film balance. Both drainage retardation and stabilisation of films against rupture will inhibit coalescence over the lifetime of a bubble collision.

- The gas-solution interface is not immobilised by the addition of electrolyte. Measurements of terminal rise velocity of single small bubbles through electrolyte solution, show that the gas-solution interface is fully mobile and therefore electrolytes do not act via Marangoni-type interface immobilisation.
- Ion  $\alpha$  and  $\beta$  assignments from bubble coalescence can be related to the ion partitioning at the air-water interface.  $\alpha$  cations and  $\alpha$  anions are excluded from the interface, while  $\beta$  cations and  $\beta$  anions accumulate at the gas surface. The partition coefficients have been used to predict surface tension gradients in mixed electrolytes.
- Interfacial ion partitioning also drives Hofmeister ion specificity, because accumulation at the hydrophobic surface stabilises proteins. There is, therefore, a link between ion specificity in bubble coalescence inhibition and ion specificity in biological systems.
- It is hypothesised that bubble coalescence inhibition is related to surface deformation. During dynamic film drainage, inhibiting electrolytes induce a surface viscosity that dampens high-frequency surface deformation, thus retarding drainage and inhibiting thin film rupture over the lifetime of a bubble collision. Noninhibiting electrolytes have more evenly distributed interfacial ions and more rapid surface equilibration under deformation. The surface deformation mechanism is supported by literature showing high-speed surface deformation in bubbles, and a lack of coalescence inhibition in small non-deforming bubbles.

---

This hypothesised model is consistent with the results of various bubble coalescence inhibition experiments. Several new approaches to investigate the dynamic interfacial processes that occur during coalescence, have been suggested. Ultimately, an investigation of the dynamic drainage of thin films in electrolyte solution should not only lead to greater understanding of the role that ions play in bubble coalescence inhibition, but it will improve our understanding of ion interfacial effects in colloids and biological systems, and also expand our knowledge of the dynamics and rheology of deformable interfaces generally.

---

## References

---

1. Winkel, E. S.; Ceccio, S. L.; Dowling, D. R.; Perlin, M., Bubble-size distributions produced by wall injection of air into flowing freshwater, saltwater and surfactant solutions. *Experiments in Fluids* **2004**, 37, 802-810.
2. Hofmeier, U.; Yaminsky, V. V.; Christenson, H. K., Observations of Solute Effects on Bubble Formation. *J. Colloid Interface Sci.* **1995**, 174, 199-210.
3. Slauenwhite, D. E.; Johnson, B. D., Bubble shattering: differences in bubble formation in fresh water. *J. Geophys. Res. - Oceans* **1999**, 104, (C2), 3265-3275.
4. Quinn, J. J.; Kracht, W.; Gomez, C. O.; Gagnon, C.; Finch, J. A., Comparing the effect of salts and frother (MIBC) on gas dispersion and froth properties. *Miner. Eng.* **2007**, 20, 1296-1302.
5. Linek, V.; Beneš, P.; Holeček, O., Correlation for volumetric mass transfer coefficient in mechanically agitated aerated vessel for oxygen absorption in aqueous electrolyte solutions. *Biotechnol. Bioeng.* **1988**, 32, 482-490.
6. Kristof, P.; Pritzker, M., Effect of electrolyte composition on the dynamics of hydrogen gas bubble evolution at copper microelectrodes. *J. Appl. Electrochem.* **1997**, 27, 255-265.
7. Tanaka, Y.; Kikuchi, K.; Saihara, Y.; Ogumi, Z., Bubble visualization and electrolyte dependency of dissolving hydrogen in electrolyzed water using Solid-Polymer-Electrolyte. *Electrochim. Acta* **2005**, 50, 5229-5236.
8. Horozov, T. S.; Binks, B. P.; Gottschalk-Gaudig, T., Effect of electrolyte in silicone oil-in-water emulsions stabilised by fumed silica particles. *Phys. Chem. Chem. Phys.* **2007**, 9, (48), 6398-6404.
9. Craig, V. S. J.; Ninham, B. W.; Pashley, R. M., The effect of electrolytes on bubble coalescence in water. *J. Phys. Chem.* **1993**, 97, 10192-10197.
10. Craig, V. S. J.; Ninham, B. W.; Pashley, R. M., Effect of electrolytes on bubble coalescence. *Nature* **1993**, 364, 317-319.
11. Collins, K. D.; Washabaugh, M. W., The Hofmeister effect and the behaviour of water at interfaces. *Quart. Rev. Biophys.* **1985**, 18, 323-422.
12. Leontidis, E., Hofmeister anion effects on surfactant self-assembly and the formation of mesoporous solids. *Curr. Opin. Colloid Interface Sci.* **2002**, 7, (1-2), 81-91.
13. Franks, G. V., Zeta potentials and yield stresses of silica suspensions in concentrated monovalent electrolytes: Isoelectric point shift and additional attraction. *J. Colloid Interface Sci.* **2002**, 249, 44-51.



- 
14. Kunz, W.; Lo Nostro, P.; Ninham, B. W., The present state of affairs with Hofmeister effects. *Curr. Opin. Colloid Interface Sci.* **2004**, 9, 1-18.
  15. Stover, R. L.; Tobias, C. W.; Denn, M. M., Bubble coalescence dynamics. *AIChE J.* **1997**, 43, (10), 2385-2392.
  16. Bergeron, V., Forces and structure in thin liquid soap films. *J. Phys. : Condens. Matter* **1999**, 11, R215-R238.
  17. Ivanov, I. B., *Thin Liquid Films*. CRC Press: 1988.
  18. Cain, F. W.; Lee, J. C., A technique for studying the drainage and rupture of unstable liquid films formed between two captive bubbles: Measurements on KCl solutions. *J. Coll. Interface Sci.* **1985**, 106, (1), 70-85.
  19. Kazakis, N. A.; Mouza, A. A.; Paras, S. V., Coalescence during bubble formation at two neighbouring pores: An experimental study in microscopic scale. *Chem. Eng. Sci.* **2008**, 63, 5160-5178.
  20. Ribeiro, C. P.; Mewes, D., The effect of electrolytes on the critical velocity of bubble coalescence. *Chem. Eng. J.* **2007**, 126, 23-33.
  21. Lee, J. C.; Hodgson, T. D., Film flow and coalescence-I Basic relations, film shape and criteria for interface mobility. *Chem. Eng. Sci.* **1968**, 23, 1375-1397.
  22. Machon, V.; Pacek, A. W.; Nienow, A. W., Bubble sizes in electrolyte and alcohol solutions in a turbulent stirred vessel. *Trans. I.Chem.E.* **1997**, 75, (A3), 339-348.
  23. Danov, K. D.; Valkovska, D. S.; Ivanov, I. B., Effect of surfactants on the film drainage. *J. Colloid Interface Sci.* **1999**, 211, 291-303.
  24. Coons, J. E.; Halley, P. J.; McGlashan, S. A.; Tran-Cong, T., Bounding film drainage in common thin films. *Colloids and Surface A: Physicochem. Eng. Aspects* **2005**, 263, 197-204.
  25. Marrucci, G., A theory of coalescence. *Chem. Eng. Sci.* **1969**, 24, 975-985.
  26. Gibbs, J. W., The Collected Works. In *The Collected Works*, Longmans, Green and Co.: New York, 1928; Vol. I, pp 300-315.
  27. Li, D.; Liu, S., Coalescence between small bubbles or drops in pure liquid. *Langmuir* **1996**, 12, 5216-5220.
  28. Horn, R. G.; Asadullah, M.; Connor, J. N., Thin film drainage: Hydrodynamic and disjoining pressures determined from experimental measurements of the shape of a fluid drop approaching a solid wall. *Langmuir* **2006**, 22, 2610-2619.
  29. Oolman, T. O.; Blanch, H. W., Bubble coalescence in stagnant liquids. *Chem. Eng. Comms* **1986**, 43, 237-261.

- 
30. Israelachvili, J. N., *Intermolecular and Surface Forces*. Academic Press: London, 1992.
  31. Manev, E. D.; Nguyen, A. V., Critical thickness of microscopic thin liquid films. *Adv. Colloid Interface Sci.* **2005**, 114-115, 133-146.
  32. Stubenrauch, C.; Von Klitzing, R., Disjoining pressure in thin liquid foam and emulsion films - new concepts and perspectives. *J. Phys. : Condens. Matter* **2003**, 15, R1197-R1232.
  33. Angarska, J. K.; Dimitrova, B. S.; Danov, K. D.; Kralchevsky, P. A.; Ananthapadmanabhan, K. P.; Lips, A., Detection of the hydrophobic surface force in foam films by measurements of the critical thickness of the film rupture. *Langmuir* **2004**, 20, (5), 1799-1806.
  34. Lyklema, J.; Fleer, G. J.; van Leeuwen, H. P., *Fundamentals of Interface and Colloid Science*. Academic Press: 2000.
  35. Derjaguin, B. V.; Landau, L., Theory of the stability of strongly charged lyophobic sols and of the adhesion of strongly charged particles in solution of electrolytes. *Acta. Physicochem. URSS* **1941**, 14, 633.
  36. Verwey, E. G. W.; Overbeek, J. T. G., *Theory of the stability of lyophobic colloids*. Elsevier: Amsterdam, 1948.
  37. Evans, E. A.; Parsegian, V. A., Thermal-mechanical fluctuations enhance repulsion between bimolecular layers. *Proc. Natl Acad. Sci. USA* **1986**, 83, 7132-7136.
  38. Marcelja, S., Short-range forces in surface and bubble interaction. *Curr. Opin. Colloid Interface Sci.* **2004**, 9, 165-167.
  39. Ninham, B. W.; Yaminsky, V., Ion binding and ion specificity: The Hofmeister effect and Onsager and Lifshitz theories. *Langmuir* **1997**, 13, 2097-2108.
  40. Boström, M.; Williams, D. R. M.; Ninham, B. W., Specific ion effects: Why DLVO theory fails for biology and colloidal systems. *Phys. Rev. Lett.* **2001**, 87, (16), 8103.
  41. Craig, V. S. J., Bubble coalescence and specific-ion effects. *Curr. Opin. Colloid Interface Sci.* **2004**, 9, 178-184.
  42. Coons, J. E.; Halley, P. J.; McGlashan, S. A.; Tran-Cong, T., A review of drainage and spontaneous rupture in free standing thin films with tangentially immobile interfaces. *Advances Coll. Interface Sci.* **2003**, 105, 3-62.
  43. Ivanov, I. B.; Radoev, B.; Manev, E.; Scheludko, A., Theory of the critical thickness of rupture of thin liquid films. *Trans. Faraday Soc.* **1970**, 66, 1262-1273.
  44. Sharma, A.; Ruckenstein, E., Stability, critical thickness, and the time of rupture of thinning foam and emulsion films. *Langmuir* **1987**, 3, (5), 760-768.

- 
45. Aarts, D. G. A. L.; Schmidt, M.; Lekkerkerker, H. N. W., Direct visual observation of thermal capillary waves. *Science* **2004**, 304, 847-850.
  46. Ruckenstein, E.; Jain, R. K., Spontaneous Rupture of Thin Liquid Films. *J. Chem. Soc., Faraday Trans. II* **1973**, 70, 132-147.
  47. Mahnke, J.; Schulze, H. J.; Stöckelhuber, K. W.; Radoev, B., Rupture of thin wetting films on hydrophobic surfaces. Part II: fatty acid Langmuir-Blodgett layers on glass surfaces. *Colloids and Surfaces A* **1999**, 157, 11-20.
  48. Müller, H.-J.; Balinov, B. B.; Exerowa, D. R., Black foam and emulsion films from nonionic surfactant solutions: rupture by hole formation. *Colloid Polym. Sci.* **1988**, 266, 921-925.
  49. Tse, K. L.; Martin, T.; McFarlane, C. M.; Nienow, A. W., Small bubble formation via a coalescence dependent break-up mechanism. *Chem. Eng. Sci.* **2003**, 58, 275-286.
  50. Sagert, N. H.; Quinn, M. J., The coalescence of gas bubbles in dilute aqueous solutions. *Chem. Eng. Sci.* **1978**, 33, (8), 1087-1095.
  51. Chesters, A. K.; Hofman, G., Bubble coalescence in pure liquids. *Appl. Sci. Res.* **1982**, 38, 353-361.
  52. Doublez, L., Capillary instability of a fast-draining film. *Colloids Surf.* **1992**, 68, 17-23.
  53. Pashley, R. M.; Karaman, M. E., *Applied Colloid and Surface Chemistry*. John Wiley & Sons, Ltd.: 2004.
  54. Ribeiro, C. P.; Mewes, D., On the effect of liquid temperature upon bubble coalescence. *Chem. Eng. Sci.* **2006**, 61, 5704-5716.
  55. Valkovska, D. S.; Danov, K. D., Influence of ionic surfactants on the drainage velocity of thin liquid films. *J. Coll. Interface Sci.* **2001**, 241, 400-412.
  56. Christenson, H. K.; Yaminsky, V. V., Solute effects on bubble coalescence. *J. Phys. Chem.* **1995**, 99, 10420.
  57. CRC, *Handbook of Chemistry and Physics*. 80th ed.; CRC Press: 1999-2000.
  58. Henry, C. L.; Dalton, C. N.; Scruton, L.; Craig, V. S. J., Ion-specific coalescence of bubbles in mixed electrolyte solutions. *J. Phys. Chem. C* **2007**, 111, 1015-1023.
  59. Weissenborn, P. K.; Pugh, R. J., Surface tension and bubble coalescence phenomena of aqueous solutions of electrolytes. *Langmuir* **1995**, 11, 1422-1426.
  60. Weissenborn, P. K.; Pugh, R. J., Surface tension of aqueous solutions of electrolytes: relationship with ion hydration, oxygen solubility and bubble coalescence. *J. Colloid Interface Sci.* **1996**, 184, 550-563.

- 
61. Foulk, C. W., A theory of liquid film formation. *Ind. Eng. Chem.* **1929**, 21, 815-817.
  62. Marrucci, G.; Nicodemo, L., Coalescence of gas bubbles in aqueous solutions of inorganic electrolytes. *Chem. Eng. Sci.* **1967**, 22, 1257-1265.
  63. Lessard, R. R.; Zieminski, S. A., Bubble coalescence and gas transfer in aqueous electrolytic solutions. *Ind. Eng. Chem. Fundam.* **1971**, 10, (2), 260-269.
  64. Zahradnik, J.; Fialova, M.; Linek, V., The effect of surface-active additives on bubble coalescence in aqueous media. *Chem. Eng. Sci.* **1999**, 54, 4757-4766.
  65. Muruganathan, R. M.; Krastev, R.; Müller, H.-J.; Möhwald, H., Foam films stabilized with dodecyl maltoside. 2. Film stability and gas permeability. *Langmuir* **2006**, 22, 7981-7985.
  66. Tsang, Y. H.; Koh, Y.-H.; Koch, D. L., Bubble-size dependence of the critical electrolyte concentration for inhibition of coalescence. *J. Coll. Interface Sci.* **2004**, 275, 290-297.
  67. Tse, K. L.; Martin, T.; McFarlane, C. M.; Nienow, A. W., Visualisation of bubble coalescence in a coalescence cell, a stirred tank and a bubble column. *Chem. Eng. Sci.* **1998**, 53, (23), 4031-4036.
  68. Foulk, C. W., Foaming of boiler water. *Ind. Eng. Chem.* **1924**, 16, (11), 1121-1126.
  69. Foulk, C. W.; Miller, J. N., Experimental evidence in support of the balanced-layer theory of liquid film formation. *Ind. Eng. Chem.* **1931**, 23, 1283.
  70. Zieminski, S. A.; Whittemore, R. C., Behavior of gas bubbles in aqueous electrolyte solution. *Chem. Eng. Sci.* **1971**, 26, 509-520.
  71. Kim, J. W.; Chang, J. H.; Lee, W. K., Inhibition of bubble coalescence by the electrolytes. *Korean J. of Chem. Eng.* **1990**, 7, (2), 100-108.
  72. Radoev, B.; Scheludko, A.; Manev, E., Critical thickness of thin liquid films: Theory and experiment. *J. Colloid Interface Sci.* **1983**, 95, 254-265.
  73. Lee, J. C.; Meyrick, D. L., Gas-liquid interfacial areas in salt solutions in an agitated tank. *Trans. I.Chem.E.* **1970**, 48, T37.
  74. Prince, M. J.; Blanch, H. W., Transition electrolyte concentrations for bubble coalescence. *AIChE J.* **1990**, 36, (9), 1425-1429.
  75. Spyridopoulos, M. T.; Simons, S. J. R., Effect of natural organic matter on the stability of a liquid film between two colliding bubbles. *Colloids and Surfaces A: Physicochem. Eng. Aspects* **2004**, 235, (25-34).

- 
76. Krzan, M.; Lunkenheimer, K.; Malysa, K., Pulsation and bouncing of a bubble prior to rupture and/or foam film formation. *Langmuir* **2003**, 19, 6586-6589.
77. Tsao, H.-K.; Koch, D. L., Collisions of slightly deformable, high Reynolds number bubbles with short-range repulsive forces. *Phys. Fluids* **1994**, 6, (8), 2591-2605.
78. Ghosh, P., Coalescence of air bubbles at air-water interface. *Chem. Eng. Res. Des.* **2004**, 82, (A7), 849-854.
79. Struthwolf, M.; Blanchard, D. C., The residence time of air bubbles < 400 $\mu$ m diameter at the surface of distilled water and seawater. *Tellus Ser. B* **1984**, 36B, 294-299.
80. Deschenes, L. A.; Barrett, J.; Muller, L. J.; Fourkas, J. T.; Mohanty, U., Inhibition of bubble coalescence in aqueous solutions. I. Electrolytes. *J. Phys. Chem. B* **1998**, 102, 5115-5119.
81. Ribeiro Jr., C. P.; Mewes, D., The influence of electrolytes on gas hold-up and regime transition in bubble columns. *Chem. Eng. Sci.* **2007**, 62, 4501-4509.
82. Alves, S. S.; Maia, C. I.; Vasconcelos, J. M. T.; Serralheiro, A. J., Bubble size in aerated stirred tanks. *Chem. Eng. J.* **2002**, 89, 109-117.
83. Kellermann, H.; Juttner, K.; Kreysa, G., Dynamic modelling of gas hold-up in different electrolyte systems. *J. Appl. Electrochem.* **1998**, 28, 311-319.
84. Sheludko, A., Thin liquid films. *Adv. Colloid Interface Sci.* **1967**, 1, 391-464.
85. Mysels, K. J.; Jones, M. N., Direct measurement of the variation of double-layer repulsion with distance. *Disc. Faraday Soc.* **1966**, 42, 42-50.
86. Karakashev, S. I.; Nguyen, P. T.; Tsekov, R.; Hampton, M. A.; Nguyen, A. V., Anomalous ion effects on rupture and lifetime of aqueous foam films formed from monovalent salt solutions up to saturation concentration. *Langmuir* **2008**.
87. Carnie, S. L.; Chan, D. Y. C.; Lewis, C.; Manica, R.; Dagastine, R. R., Measurement of dynamical forces between deformable drops using the atomic force microscope. I. Theory. *Langmuir* **2005**, 21, 2912-2922.
88. Vakarelski, I. U.; Lee, J.; Dagastine, R. R.; Chan, D. Y. C.; Stevens, G. W.; Grieser, F., Bubble colloidal AFM probes formed from ultrasonically generated bubbles. *Langmuir* **2008**, 24, (3), 603-605.
89. Manor, O.; Vakarelski, I. U.; Tang, X.; O'Shea, S. J.; Stevens, G. W.; Grieser, F.; Dagastine, R. R.; Chan, D. Y. C., Hydrodynamic boundary conditions and dynamic forces between bubbles and surfaces. *Phys. Rev. Letts* **2008**, 101, 024501-1-4.
90. Beattie, J. K.; Djerdjev, A. M., The pristine oil/water interface: Surfactant-free hydroxide-charged emulsions. *Angew. Chem. Intl Ed.* **2004**, 43, 3568-3571.

- 
91. Petersen, P. B.; Saykally, R. J., Is the liquid water surface basic or acidic? Macroscopic vs. molecular-scale investigations. *Chem. Phys. Letts* **2008**, 458, 255-261.
92. Neumann, B.; Vincent, B.; Krustev, R.; Müller, H.-J., Stability of various silicone oil/water emulsion films as a function of surfactant and salt concentration. *Langmuir* **2004**, 20, 4336-4344.
93. Maeda, N.; Rosenberg, K. J.; Israelachvili, J. N.; Pashley, R. M., Further studies on the effect of degassing on the dispersion and stability of surfactant-free emulsions. *Langmuir* **2004**, 20, 3129-3137.
94. Nandi, A.; Agterof, W. G. M.; van den Ende, D.; Mellema, J., Investigation of the effect of a simple salt on the kinetics of gravity induced coalescence for a viscosity matched emulsion system. *Colloids and Surface A: Physicochem. Eng. Aspects* **2003**, 213, 199-208.
95. Stevens, G. W.; Pratt, H. R. C.; Tai, D. R., Droplet coalescence in aqueous electrolyte solutions. *J. Colloid Interface Sci.* **1990**, 136, 470-479.
96. Chen, C.-T.; Maa, J.-R.; Yang, Y.-M.; Chang, C.-H., Effects of electrolytes and polarity of organic liquids on the coalescence of droplets at aqueous-organic interfaces. *Surf. Sci.* **1998**, 406, 167-177.
97. Clasohm, L. Y.; Vakarelski, I. U.; Dagastine, R. R.; Chan, D. Y. C.; Stevens, G. W.; Grieser, F., Anomalous pH dependent stability behavior of surfactant-free nonpolar oil drops in aqueous electrolyte solutions. *Langmuir* **2007**, 23, 9335-9340.
98. Blake, T. D.; Kitchener, J. A., Stability of aqueous films on hydrophobic methylated silica. *J. Chem. Soc, Faraday Trans. I* **1972**, 68, 1435-1442.
99. Diakova, B.; Fliliatre, C.; Platikanov, D.; Foissy, A.; Kaisheva, M., Thin wetting films from aqueous electrolyte solutions on SiC/Si wafer. *Adv. Colloid Interface Sci.* **2002**, 96, 193-211.
100. Yoon, R.-H.; Yordan, J. L., The critical rupture thickness of thin water films on hydrophobic surfaces. *J. Colloid Int. Sci.* **1991**, 146, (2), 565-572.
101. Somasundaran, P.; Simpson, S.; Jain, R. K.; Ivanov, I. B.; Raghuraman, V., Investigation of thin aqueous films on silica using a modified interferometric technique. *J. Colloid Interface Sci.* **2000**, 225, 243-246.
102. Deschenes, L. A.; Zilaro, P.; Muller, L. J.; Fourkas, J. T.; Mohanty, U., Quantitative measure of hydrophobicity: experiment and theory. *J. Phys. Chem. B* **1997**, 101, 5777-5779.
103. Miklavcic, S. J., Deformation of fluid interfaces under double-layer forces stabilizes bubble dispersions. *Phys. Rev. E* **1996**, 54, 6551-6556.

- 
104. Craig, V. S. J.; Ninham, B. W.; Pashley, R. M., Comment on "Deformation of fluid interfaces under double-layer forces stabilizes bubble dispersions". *Phys. Rev. E* **1998**, *57*, 7362-7363.
105. Shubin, V. E.; Kékicheff, P., Electrical double layer structure revisited via a surface force apparatus: Mica interfaces in lithium nitrate solutions. *J. Colloid Interface Sci.* **1993**, *155*, 108-123.
106. Pashley, R. M., Hydration forces between mica surfaces in aqueous electrolyte solutions. *J. Colloid Interface Sci.* **1981**, *80*, 153-162.
107. Pugh, R. J.; Yoon, R. H., Hydrophobicity and rupture of thin aqueous films. *J. Colloid Interface Sci.* **1994**, *163*, 169-176.
108. Craig, V. S. J.; Ninham, B. W.; Pashley, R. M., Study of the long-range hydrophobic attraction in concentrated salt solutions and its implications for electrostatic models. *Langmuir* **1998**, *14*, 3326-3332.
109. Meyer, E. E.; Rosenberg, K. J.; Israelachvili, J. N., Recent progress in understanding hydrophobic interactions. *Proc. Natl Acad. Sci. USA* **2006**, *103*, (43), 15739-15746.
110. Wang, L.; Yoon, R. H., Stability of foams and froths in the presence of ionic and non-ionic surfactants. *Miner. Eng.* **2004**, *19*, 539-547.
111. Wang, L.; Yoon, R. H., Hydrophobic forces in thin aqueous films and their role in film thinning. *Colloids and Surface A: Physicochem. Eng. Aspects* **2005**, *263*, 267-274.
112. Ivanov, I. B.; Dimitrov, D. S., Hydrodynamics of thin liquid films: Effect of surface viscosity on thinning and rupture of foam films. *Colloid Polym. Sci.* **1974**, *252*, 982-990.
113. Kunz, W., Specific ion effects in liquids, in biological systems, and at interfaces. *Pure Appl. Chem.* **2006**, *78*, (8), 1611-1617.
114. Lo Nostro, P.; Lo Nostro, A.; Ninham, B. W.; Pesavento, G.; Fratoni, L.; Baglioni, P., Hofmeister specific ion effects in two biological systems. *Curr. Opin. Colloid Interface Sci.* **2004**, *9*, 97-101.
115. Kunz, W.; Henle, J.; Ninham, B. W., Franz Hofmeister's historical papers. *Curr. Opin. Colloid Interface Sci.* **2004**, *9*, (1-2), 19-37.
116. Lo Nostro, P.; Fratoni, L.; Ninham, B. W.; Baglioni, P., Water absorbency by wool fibers: Hofmeister effect. *Biomacromolecules* **2002**, *3*, (6), 1217-1224.
117. Ball, P., Water as an active constituent in cell biology. *Chem. Rev.* **2008**, *108*, (1), 74-108.

- 
118. Collins, K. D.; Neilson, G. W.; Enderby, J. E., Ions in water: Characterizing the forces that control chemical processes and biological structure. *Biophys. Chem.* **2007**, *129*, 95-104.
119. Hribar, B.; Southall, N. T.; Vlachy, V.; Dill, K. A., How ions affect the structure of water. *J. Am. Chem. Soc.* **2002**, *124*, 12302-12311.
120. Marcus, Y., A simple empirical model describing the thermodynamics of hydration of ions of widely varying charges, sizes, and shapes. *Biophys. Chem.* **1994**, *51*, 111-127.
121. Zhang, Y.; Cremer, P. S., Interactions between macromolecules and ions: the Hofmeister series. *Curr. Opin. Chem. Biol.* **2006**, *10*, 658-663.
122. Pashley, R. M.; Craig, V. S. J., Effects of electrolytes on bubble coalescence. *Langmuir* **1997**, *13*, 4772-4774.
123. Rumpf, B.; Xia, J.; Maurer, G., Solubility of carbon dioxide in aqueous solutions containing acetic acid or sodium hydroxide in the temperature range from 313 to 433 K and at total pressures up to 10MPa. *Ind. Eng. Chem. Res.* **1998**, *37*, (5), 2012-2019.
124. Jungwirth, P.; Tobias, D. J., Ions at the air/water interface. *J. Phys. Chem. B* **2002**, *106*, (25), 6361-6373.
125. Garrett, B. C., Ions at the air/water interface. *Science* **2004**, *303*, 1146-1147.
126. Marcelja, S., Selective coalescence of bubbles in simple electrolytes. *J. Phys. Chem. B* **2006**, *110*, 13062-13067.
127. Dalton, C. N. The effect electrolyte mixtures have on bubble coalescence. Masters, University of Southern Queensland, 2005.
128. Pollock, J. A., The origin of the small bubbles of froth. *Philos. Mag.* **1912**, *24*, 189-196.
129. Stoyanov, S. D.; Denkov, N. D., Role of surface diffusion for drainage and hydrodynamic stability of thin liquid films. *Langmuir* **2001**, *17*, (4), 1150-1156.
130. Fainerman, V. B.; Miller, R., Maximum bubble pressure tensiometry- an analysis of experimental constraints. *Adv. Colloid Interface Sci.* **2004**, *108-09*, 287-301.
131. Ikeda, S.; Ozeki, S., The Gibbs adsorption equation for aqueous solutions containing a weak base. *Bull. Chem. Soc. Japan* **1980**, *53*, 1837-1841.
132. Onsager, L.; Samaras, N. N. T., The surface tension of Debye-Hückel Electrolytes. *J. Chem. Phys.* **1934**, *2*, 528-536.
133. Viswanath, P.; Motschmann, H., Oriented thiocyanate anions at the air-electrolyte interface and its implications on interfacial water - a vibrational sum frequency spectroscopy study. *J. Phys. Chem. C* **2007**, *111*, (12), 4484-4486.



- 
134. Hu, J. H.; Shi, Q.; Davidovits, P.; Worsnop, D. R.; Zahniser, M. S.; Kolb, C. E., Reactive uptake of Cl<sub>2</sub>(g) and Br<sub>2</sub>(g) by aqueous surfaces as a function of Br<sup>-</sup> and I<sup>-</sup> ion concentration: The effect of chemical reaction at the interface. *J. Phys. Chem.* **1995**, *99*, 8768-8776.
135. Jungwirth, P.; Curtis, J. E.; Tobias, D. J., Polarizability and aqueous solvation of the sulfate dianion. *Chem. Phys. Lett.* **2003**, *367*, 704-710.
136. Salvador, P.; Curtis, J. E.; Tobias, D. J.; Jungwirth, P., Polarizability of the nitrate anion and its solvation at the air/water interface. *Phys. Chem. Chem. Phys.* **2003**, *5*, 3752-3757.
137. Ghosal, S.; Hemminger, J. C.; Bluhm, H.; Mun, B. S.; Hebenstreit, E. L. D.; Ketteler, G.; Ogletree, D. F.; Requejo, F. G.; Salmeron, M., Electron spectroscopy of aqueous solution interfaces reveals surface enhancement of halides. *Science* **2005**, *307*, 563-566.
138. Levering, L. M.; Sierra-Hernandez, M. R.; Allen, H. C., Observation of hydronium ions at the air-aqueous acid interface: Vibrational spectroscopic studies of aqueous HCl, HBr and HI. *J. Phys. Chem. C* **2007**, *111*, 8814-8826.
139. Petersen, P. B.; Saykally, R. J., On the nature of ions at the liquid water surface. *Annu. Rev. Phys. Chem.* **2006**, *57*, 333-364.
140. Vrbka, L.; Mucha, M.; Minofar, B.; Jungwirth, P.; Brown, E. C.; Tobias, D. J., Propensity of soft ions for the air/water interface. *Curr. Opin. Colloid Interface Sci.* **2004**, *9*, 67-73.
141. Jungwirth, P.; Winter, B., Ions at aqueous interfaces: From water surface to hydrated proteins. *Annu. Rev. Phys. Chem.* **2008**, *59*, 343-366.
142. Petersen, P. B.; Saykally, R. J.; Mucha, M.; Jungwirth, P., Enhanced concentration of polarizable anions at the liquid water surface: SHG spectroscopy and MD simulations of sodium thiocyanide. *J. Phys. Chem. B* **2005**, *109*, 10915-10921.
143. Pegram, L. M.; Record, M. T., Jr., Thermodynamic origin of Hofmeister ion effects. *J. Phys. Chem. B* **2008**, *112*, 9428-9436.
144. Street, T. O., A molecular mechanism for osmolyte-induced protein stability. *Proc. Natl Acad. Sci. USA* **2006**, *103*, 13997-14002.
145. Bolen, D. W., Effects of naturally occurring osmolytes on protein stability and solubility: issues important in protein crystallization. *Methods* **2004**, *34*, 312-322.
146. Breslow, R.; Guo, T., Surface tension measurements show that chaotropic salting-in denaturants are not just water-structure breakers. *Proc. Natl Acad. Sci. USA* **1990**, *87*, 167-169.

- 
147. Cacace, M. G.; Landau, E. M.; Ramsden, J. J., The Hofmeister series: salt solvent effects on interfacial phenomena. *Quart. Rev. Biophys.* **1997**, 30, (3), 241-277.
148. Raymond, E. A.; Richmond, G. L., Probing the molecular structure and bonding of the surface of aqueous salt solutions. *J. Phys. Chem. B* **2004**, 108, 5051-5059.
149. Nucci, N. V.; Vanderkooi, J. M., Effects of salts of the Hofmeister series on the hydrogen bond network of water. *J. Molec. Liquids* **2008**, 143, 160-170.
150. Omta, A. W.; Kropman, M. F.; Woutersen, S.; Bakker, H. J., Negligible effect of ions on the hydrogen-bond structure in liquid water. *Science* **2003**, 301, 347-349.
151. Mancinelli, R.; Botti, A.; Bruni, F.; Ricci, M. A.; Soper, A. K., Hydration of sodium, potassium, and chloride ions in solution and the concept of structure maker/breaker. *J. Phys. Chem. B* **2007**, 111, 13570-13577.
152. Näslund, L.-Å.; Edwards, D. C.; Phillippe, W.; Bergmann, U.; Ogasawara, H.; Pettersson, L. G. M.; Satish, M.; Nilsson, A., X-ray absorption spectroscopy study of the hydrogen bond network in the bulk water of aqueous solutions. *J. Phys. Chem. A* **2005**, 109, 5995-6002.
153. Rezus, Y. L. A.; Bakker, H. J., Effect of urea on the structural dynamics of water. *Proc. Natl Acad. Sci. USA* **2006**, 103, 18417-18420.
154. Lo Nostro, P.; Ninham, B. W.; Milani, S.; Fratoni, L.; Baglioni, P., Specific anion effects on the optical rotation of glucose and serine. *Biopoly.* **2006**, 81, 136-148.
155. Batchelor, J. D.; Olteanu, A.; Tripathy, A.; Pielak, G. J., Impact of protein denaturants and stabilizers on water structure. *J. Am. Chem. Soc.* **2004**, 126, 1958-1961.
156. Moreira, L. A.; Boström, M.; Ninham, B. W.; Biscaia, E. C.; Tavares, F. W., Hofmeister effects: Why protein charge, pH titration and protein precipitation depend on the choice of background salt solution. *Colloids and Surface A: Physicochem. Eng. Aspects* **2005**, 282-283, 457-463.
157. Walrafen, G. E., Raman spectral studies of the effects of urea and sucrose on water structure. *J. Chem. Phys.* **1996**, 104, (10), 3726-3727.
158. Collins, K. D., Ions from the Hofmeister series and osmolytes: effects on proteins in solution and in the crystallization process. *Methods* **2004**, 34, 300-311.
159. Soper, A. K.; Benmore, C. J., Quantum differences between heavy and light water. *Phys. Rev. Letts* **2008**, 101, 065502.
160. Jorgensen, W. L.; Madura, J. D., Temperature and size dependence for Monte Carlo simulations of TIP4P water. *Mol. Phys.* **1985**, 56, 1381-1392.
161. Liu, Y.; Bolen, D. W., The peptide backbone plays a dominant role in protein stabilization by naturally occurring osmolytes. *Biochemistry* **1995**, 34, 12884-12891.

- 
162. Soper, A. K.; Castner, E. W.; Luzar, A., Impact of urea on water structure: a clue to its properties as a denaturant? *Biophys. Chem.* **2003**, 105, 649-666.
163. Washburn, E. D., *International Critical Tables of numerical data, physics, chemistry and technology*. McGraw-Hill: New York, 1930.
164. Bian, L.-J.; Yang, X.-Y., Effect of denaturant concentration on hen-egg white lysozyme renaturation. *Chin. J. Chem.* **2006**, 24, 653-659.
165. Marti, D. N., Apparent pKa shifts of titratable residues at high denaturant concentration and the impact on protein stability. *Biophys. Chem.* **2005**, 118, 88-92.
166. O'Brien, E. P.; Dima, R. I.; Brooks, B.; Thirumalai, D., Interactions between hydrophobic and ionic solutes in aqueous guanidinium chloride and urea solutions: Lessons for protein denaturation mechanism. *J. Am. Chem. Soc.* **2007**, 129, 7346-7353.
167. Lee, J. C.; Timasheff, S. N., The stabilization of proteins by sucrose. *J. Biol. Chem.* **1981**, 256, 7193-7201.
168. Söderlund, T.; Alakoskela, J.-M. I.; Pakkanen, A. L.; Kinnunen, P. K. J., Comparison of the effects of surface tension and osmotic pressure on the interfacial hydration of a fluid phospholipid bilayer. *Biophys. J.* **2003**, 85, 2333-2341.
169. Matubayasi, N.; Nishiyama, A., Thermodynamic quantities of surface formation of aqueous electrolyte solutions VI. Comparison with typical nonelectrolytes, sucrose and glucose. *J. Colloid Interface Sci.* **2006**, 298, 910-913.
170. Adhikari, B.; Howes, T.; Shrestha, A.; Bhandari, B. R., Effect of surface tension and viscosity on the surface stickiness of carbohydrate and protein solutions. *J. Food Eng.* **2007**, 79, (4), 1136-1143.
171. Mathlouthi, M.; Reiser, P., *Sucrose: Properties and Applications*. Blackie Academic and Professional: 1995.
172. Mathlouthi, M.; Hutteau, F.; Angiboust, J. F., Physicochemical properties and vibrational spectra of small carbohydrates in aqueous solution and the role of water in their sweet taste. *Food Chemistry* **1996**, 56, (3), 215-221.
173. Hoorfar, M.; Kurz, M. A.; Policova, Z.; Hair, M. L.; Neumann, A. W., Do polysaccharides such as dextran and their monomers really increase the surface tension of water? *Langmuir* **2006**, 22, 52-56.
174. Mettler-Toledo International, I. D-Fructose Density Concentration Table (+20°C). [http://us.mt.com/mt/ed/appEdStyle/D\\_Fructose\\_de\\_e\\_0x000248e10002599200075141.jsp](http://us.mt.com/mt/ed/appEdStyle/D_Fructose_de_e_0x000248e10002599200075141.jsp) (26 November 2008),
175. Suzuki, T., The hydration of glucose: the local configurations in sugar-water hydrogen bonds. *Phys. Chem. Chem. Phys.* **2008**, 10, 96-105.

- 
176. Janado, M.; Yano, Y., Hydrophobic nature of sugars as evidenced by their differential affinity for polystyrene gel in aqueous media. *J. Soln Chem.* **1985**, 14, (12), 891-902.
177. Koga, Y.; Nishikawa, K.; Westh, P., Relative hydrophobicity/hydrophilicity of fructose, glucose, sucrose and trehalose as probed by 1-propanol: A differential approach in solution thermodynamics. *J. Phys. Chem. B* **2007**, 111, 13943-13948.
178. Macleod, N. A.; Johannessen, C.; Hecht, L.; Barron, L. D.; Simons, J. P., From the gas phase to aqueous solution: Vibrational spectroscopy, Raman optical activity and conformational structure of carbohydrates. *Intl J. Mass Spec.* **2006**, 253, 193-200.
179. David, S., *The Molecular and Supramolecular Chemistry of Carbohydrates*. Oxford University Press: 1997.
180. Polymer Analysis Laboratory, L. S. U. How-to Guide: Solvent Properties. <http://macro.lsu.edu/howto/solvents/Dipole%20Moment.htm> (17 February 2008),
181. Barthel, J.; Neueder, R.; Roch, H., Density, relative permittivity, and viscosity of propylene carbonate + dimethoxyethane mixtures from 25°C to 125°C. *J. Chem. Eng. Data* **2000**, 45, 1007-1011.
182. SigmaAldrich Propylene Carbonate MSDS No. 82226 [online]. <http://www.sigmaaldrich.com/cgi-bin/hsrun/Suite7/Suite/HAHTpage/Suite.HsSigmaAdvancedSearch.formAction> (17 February 2008),
183. SigmaAldrich Formamide MSDS No. F7503 [online]. <http://www.sigmaaldrich.com/cgi-bin/hsrun/Suite7/Suite/HAHTpage/Suite.HsSigmaAdvancedSearch.formAction> (17 February 2008),
184. Arnett, E. M.; McKelvey, D. R., Enthalpies of transfer from water to dimethyl sulfoxide for some ions and molecules. *J. Am. Chem. Soc.* **1966**, 88, (11), 2598-2599.
185. Bunakova, L. V.; Khanova, L. A.; Krishtalik, L. I., Energies of transport of individual ions out of water into aprotic solvents: special features of acetate ion transport. *Russian J. Electrochem.* **2005**, 41, (3), 287-293.
186. Kloss, A. A.; Fawcett, W. R., ATR-FTIR studies of ionic solvation and ion-pairing in dimethylsulfoxide solutions of the alkali metal nitrates. *J. Chem. Soc., Faraday Trans.* **1998**, 94, (11), 1587-1591.
187. Muhuri, P. K.; Ghosh, S. K.; Hazra, D. K., Solubilities of some alkali-metal salts, tetraphenylarsonium chloride and tetraphenylphosphonium bromide in propylene carbonate at 25°C using the ion-selective electrode technique. *J. Chem. Eng. Data* **1993**, 38, 242-244.

- 
188. Harner, R. E.; Sydnor, J. B.; Gilreath, E. S., Solubilities of anhydrous ionic substances in absolute methanol. *J. Chem. Eng. Data* **1963**, 8, (3), 411-412.
189. Stenger, V. A., Solubilities of various alkali metal and alkaline earth metal compounds in methanol. *J. Chem. Eng. Data* **1996**, 41, 1111-1113.
190. Stenger, V. A.; Van Effen, R. M., Solubilities of alkali metal bromates and iodates in methanol at room temperature. *J. Chem. Eng. Data* **1999**, 44, 173-174.
191. Stenger, V. A.; Van Effen, R. M.; Frawley, N. N., Solubilities of alkaline earth metal bromates and iodates in methanol at room temperature. *J. Chem. Eng. Data* **2000**, 45, 1160-1161.
192. Salomon, M., Thermodynamics of lithium chloride and lithium bromide in propylene carbonate. *J. Phys. Chem.* **1969**, 73, (10), 3299-3306.
193. Pinho, S. P.; Macedo, E. A., Solubility of NaCl, NaBr, and KCl in water, methanol, ethanol, and their mixed solvents. *J. Chem. Eng. Data* **2005**, 50, 29-32.
194. Labban, A. K. S.; Marcus, Y., The solubility and solvation of salts in mixed nonaqueous solvents. 1. Potassium halides in mixed aprotic solvents. *J. Solution Chem.* **1991**, 20, (2), 221-232.
195. Porras, S. P.; Kenndler, E., Formamide as solvent for capillary zone electrophoresis. *Electrophoresis* **2004**, 25, 2946-2958.
196. Johnsson, M.; Persson, I., Determination of heats and entropies of transfer for some univalent ions from water to methanol, acetonitrile, dimethylsulfoxide, pyridine and tetrahydrothiophene. *Inorg. Chim. Acta* **1987**, 127, 25-34.
197. Jansen, M. L.; Yeager, H. L., A conductance study of 1-1 electrolytes in propylene carbonate. *J. Phys. Chem.* **1973**, 77, (26), 3089-3092.
198. Christenson, H. K.; Bowen, R. E.; Carlton, J. A.; Denne, J. R. M.; Lu, Y., Electrolytes that show a transition to bubble coalescence inhibition at high concentrations. *J. Phys. Chem. C* **2008**, 112, 794-796.
199. Cwiklik, L.; Andersson, G.; Dang, L. X.; Jungwirth, P., Segregation of inorganic ions at surfaces of polar nonaqueous liquids. *ChemPhysChem* **2007**, 8, 1457-1463.
200. Dang, L. X., Ions at the liquid/vapor interface of methanol. *J. Phys. Chem. A* **2004**, 108, (42), 9014-9017.
201. Höfft, O.; Borodin, A.; Kahnert, U.; Kempter, V.; Dang, L. X.; Jungwirth, P., Surface segregation of dissolved salt ions. *J. Phys. Chem. B* **2006**, 110, 11971-11976.
202. Höfft, O.; Kahnert, U.; Bahr, S.; Kempter, V., Interaction of NaI with solid water and methanol. *J. Phys. Chem. B* **2006**, 110, 17115-17120.

- 
203. Mucha, M.; Frigato, T.; Levering, L. M.; Allen, H. C.; Tobias, D. J.; Dang, L. X.; Jungwirth, P., Unified molecular picture of the surfaces of aqueous acid, base and salt solutions. *J. Phys. Chem. B* **2005**, 109, 7617-7623.
204. Jungwirth, P.; Tobias, D. J., Molecular structure of salt solutions: A new view of the interface with implications for heterogeneous atmospheric chemistry. *J. Phys. Chem. B* **2001**, 105, 10468-10472.
205. Cheng, J.; Hoffmann, M. R.; Colussi, A. J., Anion fractionation and reactivity at air/water:methanol interfaces. Implications for the origin of Hofmeister effects. *J. Phys. Chem. B* **2008**, 112, 7157-7161.
206. Andersson, G.; Krebs, T.; Morgner, H., Angle resolved ion scattering spectroscopy reveals the local topography around atoms in a liquid surface. *Phys. Chem. Chem. Phys.* **2005**, 7, 2948-2954.
207. Andersson, G.; Morgner, H.; Cwiklik, L.; Jungwirth, P., Anions of alkali halide salts at surfaces of formamide solutions: concentration depth profiles and surface topography. *J. Phys. Chem. C* **2007**, 111, 4379-4387.
208. Chorny, I.; Dill, K. A.; Jacobson, M. P., Surfaces affect ion pairing. *J. Phys. Chem. B* **2005**, 109, 24056-24060.
209. Minofar, B.; Vácha, R.; Wahab, A.; Mahiuddin, S.; Kunz, W.; Jungwirth, P., Propensity for the air/water interface and ion pairing in magnesium acetate vs magnesium nitrate solutions: molecular dynamics simulations and surface tension measurements. *J. Phys. Chem. B* **2006**, 110, 15939-15944.
210. d'Aprano, A., Association of alkali perchlorates in anhydrous methanol at 25°. *J. Phys. Chem.* **1972**, 76, (20), 2920-2922.
211. Hanna, E. M.; Al-Sudani, K., Conductance studies of some ammonium and alkali metal salts in propylene carbonate. *J. Solution Chem.* **1987**, 16, (2), 155-162.
212. Yeager, H. L.; Fedyk, J. D.; Parker, R. J., Spectroscopic studies of ionic solvation in propylene carbonate. *J. Phys. Chem.* **1973**, 77, (20), 2407-2410.
213. Vácha, R.; Buch, V.; Milet, A.; Devlin, J. P.; Jungwirth, P., Autoionization at the surface of neat water: is the top layer pH neutral, basic, or acidic? *Phys. Chem. Chem. Phys.* **2007**, 9, 4736-4747.
214. Abu-Lail, N. I.; Camesano, T. A., The effect of solvent polarity on the molecular surface properties and adhesion of *Escherichia coli*. *Colloids and Surface B: Biointerfaces* **2006**, 51, 62-70.
215. Inglese, A.; D'Angelo, P.; De Lisi, R.; Milioto, S., Surface tension, heat capacity, and volume of amphiphilic compounds in formamide solutions. *J. Soln Chem.* **1998**, 27, 403-424.

- 
216. Auvray, X.; Petipas, C.; Anthore, R.; Rico, I.; Lattes, A.; Ahmah-Zadeh Samii, A.; de Savignac, A., Formamide, a water substitute XIV (1) waterless microemulsions 8. Structural analysis by X-ray scattering of CTAB aggregates in formamide and in the microemulsion system (formamide, CTAB, isoctane, 1-butanol). *Colloid Polym. Sci.* **1987**, 265, 925-932.
217. Exerowa, D. R.; Kruglyakov, P. M., *Foam and Foam Films*. Elsevier: 1998.
218. Manev, E.; Scheludko, A.; Exerowa, D. R., Effect of surfactant concentration on the critical thicknesses of liquid films. *Colloid Polym. Sci.* **1974**, 252, 586-593.
219. Von Klitzing, R.; Kolarić, B.; Jaeger, W.; Brandt, A., Structuring of poly(DADMAC) chains in aqueous media: a comparison between bulk and free-standing film measurements. *Phys. Chem. Chem. Phys.* **2002**, 4, 1907-1914.
220. Kern, W., *Handbook of Semiconductor Wafer Cleaning Technology*. William Andrew Inc.: 1993.
221. Brandon, N. P.; Kelsall, G. H.; Levine, S.; Smith, A. L., Interfacial electrical properties of electrogenerated bubbles. *J. Appl. Electrochem.* **1985**, 15, 485-493.
222. Karakashev, S. I.; Nguyen, A. V.; Manev, E. D., A novel technique for improving interferometric determination of emulsion film thickness by digital filtration. *J. Colloid Interface Sci.* **2007**, 306, 449-453.
223. Nguyen, A. V.; Schulze, H. J., *Colloidal Science of Flotation*. 1 ed.; CRC Press: 2003; p 850.
224. Nguyen, A. V., Historical note on the Stefan-Reynolds Equations. *J. Colloid Interface Sci.* **2000**, 231, 195.
225. Karakashev, S. I.; Nguyen, A. V., Effect of sodium dodecyl sulphate and dodecanol mixtures on foam film drainage: Examining influence of surface rheology and intermolecular forces. *Colloids and Surfaces A: Physicochem. Eng. Aspects* **2007**, 293, 229-240.
226. Karakashev, S. I., Personal Communication. In 2008.
227. Henry, C. L.; Parkinson, L.; Ralston, J. R.; Craig, V. S. J., A mobile gas-water interface in electrolyte solutions. *J. Phys. Chem. C* **2008**, 112, 15094-15097.
228. Prince, M. J.; Blanch, H. W., Bubble coalescence and break-up in air-sparged bubble columns. *AIChE J.* **1990**, 36, (10), 1485-1499.
229. Kulkarni, A. A.; Joshi, J. B., Bubble formation and bubble rise velocity in gas-liquid systems: A review. *Ind. Eng. Chem. Res.* **2005**, 44, 5873-5931.
230. Hadamard, J., Mouvement permanent lent d'une sphere liquide et visqueuse dans un liquide visqueux. *Comptes Rendus* **1911**, 152, 1735-1752.

- 
231. Rybczynski, W., On the translatory motion of a fluid sphere in a viscous medium. *Bull. Acad. Sci. Cracow Ser. A* **1911**, 40-60.
232. Parkinson, L.; Sedev, R.; Fornasiero, D.; Ralston, J., The terminal rise velocity of 10-100 $\mu$ m diameter bubbles in water. *J. Coll. Interface Sci.* **2008**, 322, 168-172.
233. Klaseboer, E.; Chevaillier, J. P.; Gourdon, C.; Masbernat, O., Film drainage between colliding drops at constant approach velocity: Experiments and modeling. *J. Colloid Interface Sci.* **2000**, 229, (1), 274-285.
234. Manica, R.; Connor, J. N.; Carnie, S. L.; Horn, R. G.; Chan, D. Y. C., Dynamics of interactions involving deformable drops: Hydrodynamic dimpling under attractive and repulsive electrical double layer interactions. *Langmuir* **2007**, 23, 626-637.
235. Sam, A.; Gomez, C. O.; Finch, J. A., Axial velocity profiles of single bubbles in water/frother solutions. *Int. J. Miner. Process* **1996**, 47, 177-196.
236. Pegram, L. M.; Record Jr., M. T., Partitioning of atmospherically relevant ions between bulk water and the water/vapor interface. *Proc. Natl Acad. Sci.* **2006**, 103, (39), 14278-14281.
237. Pegram, L. M.; Record Jr., M. T., Hofmeister salt effects on surface tension arise from partitioning of anions and cations between bulk water and the air-water interface. *J. Phys. Chem. B* **2007**.
238. Pegram, L. M.; Record, M. T., Jr., Quantifying accumulation or exclusion of H<sup>+</sup>, OH<sup>-</sup>, and Hofmeister salt ions near interfaces. *Chem. Phys. Letts* **2008**, 467, 1-8.
239. RxKinetics, I. Calculating Osmolarity of an IV Admixture. [http://www.rxkinetics.com/iv\\_osmolarity.html](http://www.rxkinetics.com/iv_osmolarity.html) (6 January 2009),
240. Jungwirth, P.; Tobias, D. J., Specific ion effects at the air/water interface. *Chem. Rev.* **2006**, 106, 1259-1281.
241. Cheng, J.; Vecitis, C. D.; Hoffmann, M. R.; Colussi, A. J., Experimental anion affinities for the air/water interface. *J. Phys. Chem. B* **2006**, jp066197k.
242. Bian, H.-t.; Feng, R.-r.; Xu, Y.-y.; Guo, Y.; Wang, H.-f., Increased interfacial thickness of the NaF, NaCl and NaBr salt aqueous solutions probed with non-resonant surface second harmonic generation (SHG). *Phys. Chem. Chem. Phys.* **2008**, 10, 4920-4931.
243. Padmanabhan, V.; Daillant, J.; Belloni, L.; Mora, S.; Alba, M.; Konovalov, O., Specific ion adsorption and short-range interactions at the air aqueous solution interface. *Phys. Rev. Letts* **2007**, 99, 086105-1 - 086105-4.
244. Tůma, L.; Jeniček, D.; Jungwirth, P., Propensity of heavier halide for the water/vapor interface revisited using the Amoeba force field. *Chem. Phys. Letts* **2005**, 411, 70-74.



- 
245. Viswanath, P.; Motschmann, H., Effect of interfacial presence of oriented thiocyanate on water structure. *J. Phys. Chem. C* **2008**, 112, 2099-2103.
246. Minofar, B.; Jungwirth, P.; Das, M. R.; Kunz, W.; Mahiuddin, S., Propensity of formate, acetate, benzoate and phenolate for the aqueous solution/vapor interface: Surface tension measurements and molecular dynamics simulations. *J. Phys. Chem. C* **2007**, 111, 8242-8247.
247. Boström, M.; Williams, D. R. M.; Ninham, B. W., Surface Tension of electrolytes: Specific Ion Effects Explained by Dispersion Forces. *Langmuir* **2001**, 17, 4475-4478.
248. Fruhner, H.; Wantke, K.-D.; Lunkenheimer, K., Relationship between surface dilational properties and foam stability. *Colloids and Surface A: Physicochem. Eng. Aspects* **2000**, 162, 193-202.
249. Langevin, D., Influence of interfacial rheology on foam and emulsion properties. *Adv. Colloid Interface Sci.* **2000**, 88, 209-222.
250. Andersen, A.; Oertegren, J.; Koelsch, P.; Wantke, D.; Motschmann, H., Oscillating bubble SHG on surface elastic and surface viscoelastic systems: New insights in the dynamics of adsorption layers. *J. Phys. Chem. B* **2006**, 110, 18466-18472.
251. Koelsch, P.; Motschmann, H., Relating foam lamella stability and surface dilational rheology. *Langmuir* **2005**, 21, 6265-6269.
252. Fruhner, H.; Wantke, K.-D., A new oscillating bubble technique for measuring surface dilational properties. *Colloids and Surface A: Physicochem. Eng. Aspects* **1996**, 114, 53-59.
253. Oertegren, J.; Wantke, K.-D.; Motschmann, H.; Möhwald, H., A study of kinetic molecular exchange processes in the medium frequency range by surface SHG on an oscillating bubble. *J. Colloid Interface Sci.* **2004**, 279, 266-276.
254. Ivanov, I. B.; Danov, K. D.; Ananthapadmanabhan, K. P.; Lips, A., Interfacial rheology of adsorbed layers with surface reaction: On the origin of the dilatational surface viscosity. *Adv. Colloid Interface Sci.* **2005**, 114-115, 61-92.
255. Manev, E.; Tsekov, R.; Radoev, B., Effect of thickness non-homogeneity on the kinetic behaviour of microscopic foam films. *J. Disp. Sci. Tech.* **1997**, 18, 769-788.
256. Earnshaw, J. C.; McGivern, R. C., Photon correlation spectroscopy of thermal fluctuations of liquid surfaces. *J. Phys. D: Appl. Phys.* **1987**, 20, 82-92.
257. Chan, B. S.; Tsang, Y. H., A theory on bubble-size dependence of the critical electrolyte concentration for inhibition of coalescence. *J. Coll. Interface Sci.* **2005**, 286, 410-413.

- 
258. Rabal, H. J.; Braga Jr., R. A., *Dynamic Laser Speckle and Applications*. CRC Press: 2008.
259. Malysa, K.; Lunkenheimer, K., Foams under dynamic conditions. *Curr. Opin. Colloid Interface Sci.* **2008**, 13, 150-162.
260. Abramzon, A. A.; Gaukhberg, R. D., Surface tension of salt solutions. *Russian J. App. Chem.* **1993**, 66, (6), 1139-1146.
261. Abramzon, A. A.; Gaukhberg, R. D., Surface tension of salt solutions. *Russian J. App. Chem.* **1993**, 66, (7), 1315-1320.
262. Abramzon, A. A.; Gaukhberg, R. D., Surface tension of salt solutions. *Russian J. App. Chem.* **1993**, 66, (8), 1473-1480.

## Appendix      Surface Tension in Single Electrolytes

**Table A.1** Surface tension gradient and bubble coalescence inhibition in single electrolyte solutions with increasing magnitude of  $(d\gamma/dc)^2$ .

Salt	$d\gamma/dc$ (mN/m/M)	Pearson Correlation Coefficient	W&P <sup>a</sup>	Litera- ture <sup>260-262</sup>	$(d\gamma/dc)^2$ (mN/m/M) <sup>2</sup>	Coalescence Inhibition <sup>b</sup>	Transition Concentration <sup>b</sup> (mol/L)
HCl	-0.25	0.9747	-0.27	-0.29	0.06	✘	-
HNO <sub>3</sub>	-0.45	0.9898	-0.83	-0.70	0.21	✘	-
HBr	-0.46	0.9952			0.21	✘	-
H <sub>2</sub> SO <sub>4</sub>	0.59	0.9973	0.44	0.64	0.34	✘	-
NaClO <sub>4</sub>	0.62	0.9981	0.22	0.73	0.39	✘	-
(CH <sub>3</sub> COO) <sub>2</sub> Ca	0.70	0.4637 <sup>c</sup>			0.49	✘	-
KClO <sub>3</sub>	0.72	0.9977			0.51	✘	-
NaClO <sub>3</sub>	0.72	0.9924	0.89	0.57	0.52	✘	-
CH <sub>3</sub> COOK	0.75	0.9803	0.76	0.45	0.56	✘	-
Mg(ClO <sub>4</sub> ) <sub>2</sub>	0.99	0.9947			0.97	✘	-
NH <sub>4</sub> NO <sub>3</sub>	1.17	0.9963	1.15	2.06	1.38	✓	0.140
Ca(ClO <sub>4</sub> ) <sub>2</sub>	1.25	0.9961			1.57	✘	-
NaNO <sub>3</sub>	1.35	0.997			1.82	✓	0.101
CH <sub>3</sub> COONa	1.41	0.9881	0.93	0.54	1.99	✘	-
KCl	1.68	0.9993	1.85	1.60,1.65	2.82	✓	0.120
HClO <sub>4</sub>	-1.70	0.9985	-2.15	-1.64	2.89	✓	0.070
NaBr	1.71	0.9970	1.83	1.97	2.93	✓	
KBr	1.74	0.9877			3.04	✓	0.083
KOH	1.75	0.9916	1.98	1.77	3.06	✓	0.053
NaCl	1.76	0.9995	2.08		3.09	✓	0.078
NH <sub>4</sub> Cl	1.78	0.9989	1.59		3.17	✓	0.100
NaOH	2.03	0.9374			4.12	✓	
MgSO <sub>4</sub>	2.37	0.9927	2.44	2.24	5.60	✓	0.020
Ca(NO <sub>3</sub> ) <sub>2</sub>	2.64	0.9948	2.47		6.98	✓	0.040

Salt	$d\gamma/dc$ (mN/m/M)	Pearson Correlation Coefficient	W&P <sup>a</sup>	Litera- ture <sup>260-262</sup>	$(d\gamma/dc)^2$ (mN/m/M) <sup>2</sup>	Coalescence Inhibition <sup>b</sup>	Transition Concentration <sup>b</sup> (mol/L)
Na <sub>2</sub> SO <sub>4</sub>	2.99	0.9999	2.90	2.96	8.95	✓	
CaCl <sub>2</sub>	3.64	0.9966	4.02	3.22	13.22	✓	0.037
MgCl <sub>2</sub>	3.73	0.9988	4.06	3.14	13.89	✓	
CH <sub>3</sub> COOH <sup>d</sup>	-12	0.8975 <sup>c</sup>	-38		144	✓	0.02

<sup>a</sup> Weissenborn and Pugh.<sup>60</sup>

<sup>b</sup> Craig et al.<sup>9</sup>

<sup>c</sup> Acetate salts yield a non-linear surface tension gradient.

<sup>d</sup> Incomplete dissociation will result in uncharged species that are surface active.